

https://dspace.org/

A study of the finite element method, with reference to the Adina finite element package

Constancon, Charles Peter

1983

University of the Witwatersrand, Johannesburg

http://hdl.handle.net/10539/16963

Constancon, Charles Peter. (1983). A study of the finite element method, with reference to the Adina finite element package. [Master's dissertation, University of the Witwatersrand, Johannesburg]. WIReDSpace. http://hdl.handle.net/10539/16963

Downloaded from a DSpace repository. https://dspace.org/

A STUDY OF THE FINITE ELEMENT METHOD, *with reference to the ADINA finite element package*

C P CONSTANCON

A dissertation submitted to the Faculty of Engineering, University of the Witwatersrand, Johannesburg in fulfillment of the requirements for the Degree of Master of Science

Johannesburg 1983

DECLARATION

I hereby certify that this thesis is my own work and has not been submitted for a Masters degree to any other University

C P CONSTANCON

ABSTRACT

This dissertation presents a theoretical and practical study of the finite element method using the ADINA finite element program. The package was applied to the analysis of three different problems, namely: A nonlinear static analysis; a free vibration analysis and a thermal analysis. The first two analyses were supplemented with experimental results for the purpose of comparison whilst the last was compared with a closed form analytic solution.

The first problem consisted of a materially nonlinear static analysis of a cast iron sheave wheel. The sheave was physically loaded with a rope up to failure of the rim. Strain gauges monitored strain at twenty four locations. In order to simulate the nonlinear properties of the cast iron, a Drucker Prager yield criterion was utilised and accordingly, a subroutine describing the elasto-plastic constitutive laws was interfaced with the ADINA package. Owing to self imposed limitations on computer resources, the sheave was modelled as a two dimensional body. The results correlated well in the linear region but deviated when plastic deformation was pronounced. It is suspected that this was due to a combination of approximations in modelling the geometry and the material.

In the free vibration analysis a simple portal frame was built in order to compare its natural mode shapes and frequencies with those obtained from a finite element simulation. This comparison proved satisfactory.

The thermal analysis was executed primarily to test and gain first hand experience with the ADINAT package. A two dimensional flat plate subjected to a sinusoidal temperature load was simulated. Although the application was simple, the accuracy of the FEM results confirmed that the package was operating correctly.

In all these excercises the ADINA package performed satisfactorily. Experience showed that the programme was not user-friendly, however this is not considered a drawback in a research environment.

ACKNOWLEDGEMENTS

The author acknowledges assistance received from the following people:

- Professor C Dimitriou for his unfailing support and stimulation during the course of this study

- Mr W Leong of the Computer Centre for assistance with the control of the ADINA programme

- Dr C Wright for providing an informative discussion course relating to the mathematical aspects of the finite element method

- Mr F Bezuidenhout and the Mechanical Engineering Laboratory staff for assistance with experimental apparatus

- To students who cooperated in the progress of various undergraduate projects (specifically mentioned in Appendix A6)

- Mrs F Roxton Wiggill for typing the script

- To my parents for their moral and financial support

CONTENTS

		Page
DECLARATION		i
ABSTRACT		ii
ACKNOWLEDGEMENTS		iv
CONTENTS		v
LIST OF FIGURES		xi
LIST OF PHOTOGRAPHIC PLATES		xiv
LIST OF PLOTS		xiv
LIST OF TABLES		xvi
LIST OF NOTATION		xviii
1	INTRODUCTION	1
1.1	PURPOSE	1
1.2	BACKGROUND	1
1.3	PROCEDURE	2
2	THE FINITE ELEMENT METHOD	4
2.1	HISTORICAL DEVELOPMENT	4
2.2	THE DISPLACEMENT BASED FINITE ELEMENT FORMULATION	5
2.2.1	General Approach to the Problem	5
2.2.2	Derivation of the Displacement Based Finite Element Method	7
2.3	ELEMENT ASSEMBLY	11
2.4	THE ADINA FINITE ELEMENT PROGRAM: STATIC ANALYSIS	14
3	RESEARCH ON THE STRENGTH OF SHEAVE WHEELS	18
3.1	INTRODUCTION	18
3.2	PREVIOUS RESEARCH	19
3.3	CURRENT RESEARCH PROGRAMME	19
3.4	PRELIMINARY FINITE ELEMENT ANALYSIS	21
3.4.1	Finite Element Mesh	21
3.4.2	Material Properties	21
3.4.3	Finite Element Results	25
3.4.4	Conclusions	25
3.5	BASIS FOR A MORE DETAILED STUDY	26

		Page
4	PLASTICITY	27
4.1	INTRODUCTION	27
4.2	THE MATHEMATICAL THEORY OF PLASTICITY	28
4.2.1	The Yield Criterion	29
4.2.2	The Drucker Prager Yield Criterion	31
4.2.3	The Definition of Work Hardening	32
4.2.4	The Elastoplastic Stress Strain Relations	33
4.2.5	Matrix Formulation of the Stress Strain Relationship	35
4.2.6	The Hardening Parameter K	38
4.3	THE DRUCKER PRAGER MATERIAL MODEL	39
4.3.1	The Elastoplastic Matrix	41
4.3.2	The Parameter A	42
4.4	IMPLEMENTATION OF THE DRUCKER PRAGER CONSTITUTIVE RELATIONS	43
4.4.1	Procedures Employed in the Solution of Elastoplastic problems	44
4.4.2	The Newton Raphson Method	46
4.4.3	The Modified New Raphson Method	47
4.4.4	The BFGS Matrix Update Method	48
4.5	FINITE ELEMENT SIMULATION OF THE UNIAXIAL BEHAVIOUR OF CAST IRON	52
4.6	CONCLUDING REMARKS	58
5	TWO-DIMENSIONAL SOLID ELEMENT ANALYSIS OF THE SHEAVE	60
5.1	INTRODUCTION	60
5.2	EXPERIMENTAL PROCEDURE	60
5.2.1	Experimental Results	66
5.3	FINITE ELEMENT SIMULATION	67
5.3.1	The Finite Element Mesh	68
5.4	FINITE ELEMENT RESULTS	71
5.5	COMPARISON OF RESULTS	77
5.6	CONCLUSION	84

		Page
6	MECHANICAL VIBRATIONS	95
6.1	THE ANALYSIS OF MECHANICAL VIBRATIONS	95
6.2	DIRECT FORMULATION OF TIME DEPENDENT PROBLEMS WITH SPATIAL FINITE ELEMENT DISCRETIZATION: THE DYNAMIC BEHAVIOUR OF STRUCTURES WITH LINEAR DAMPING	95
6.2.1	Free Vibration Analysis	99
6.2.2	Forced Vibration Analysis	100
6.3	ADINA PROGRAM CAPABILITIES	102
6.3.1	Free Vibration Analysis	102
6.3.2	Forced Vibration Analysis	103
6.3.3	Linear Forced Vibration Analysis	103
6.3.4	Nonlinear Forced Vibration Analysis	103
6.4	APPLICATION OF THE METHOD: FREE VIBRATION ANALYSIS OF SIMPLE BEAM STRUCTURES	106
6.4.1	Introduction	106
6.4.2	Experimental Apparatus	109
6.4.3	Experimental Procedure	110
6.4.4	Limitations of the Measuring Technique	110
6.5	FINITE ELEMENT ANALYSIS	113
6.5.1	Finite Element Mesh	114
6.5.2	Free Vibration Analysis of a Cantilever Beam	115
6.5.3	Free Vibration Analysis of a Portal Frame	119
6.6	CONCLUSIONS	125
7	ADINAT	129
7.1	INTRODUCTION	129
7.2	ADINAT PROGRAM CAPABILITIES	129
7.3	THE GOVERNING FIELD EQUATIONS	131
7.3.1	Variational Formulation	131
7.3.2	Establishment of a Natural Variational Principle	132
7.3.3	Boundary Conditions	135
7.3.4	Finite Element Discretisation	135
7.4	TEST PROBLEM	136

		Page
7.4.1	Finite Element Analysis	137
7.4.2	Comparison with the Exact Results	138
7.5	CONCLUSIONS - GENERAL Comments	139
8	CONCLUDING CHAPTER	140
8.1	INTRODUCTION	140
8.2	ADINA	141
8.2.1	Installation	141
8.2.1.1	*Assessment of Performance*	141
8.3	ADINAT	144
8.3.1	Assessment of Performance	144
8.4	ADINA PLOT	145
8.4.1	Assessment of the ADINA-PLOT Program	145
8.5	CONCLUSIONS	
8.5.1	The Sheave Wheel Experiment	146
8.5.2	Vibration Analysis	147
8.5.4	General	147
REFERENCES		149
APPENDICES		151
A1	THE MECHANICAL PROPERTIES OF CAST IRON	151
A1.1	INTRODUCTION	151
A1.2	STANDARD TESTING PROCEDURES	151
A1.3	MATERIAL SPECIMENS	152
A1.4	STRAIN MEASUREMENT TECHNIQUE	153
A1.5	EXPERIMENTAL PROCEDURE	153
A1.6	THE CALCULATION OF THE TANGENT MODULUS AND POISSON'S RATIO	154
A1.7	ASSESSMENT OF THE BEHAVIOUR OF CAST IRON	173
A1.8	THE ELASTIC CONSTANTS OF CAST IRON	174
A1.9	CONCLUSION	174

		Page
A2	PLASTICITY	176
A2.1	EXPLICIT FORMULATION OF THE ELASTOPLASTIC MATRIX	176
A2.2	ASSOCIATED PLASTICITY	179
A2.3	NON ASSOCIATED PLASTICITY	180
A2.4	PARAMETER A	181
A2.5	THE DIMENSIONLESS STRESS RATIO R	185
A2.6	AN ALTERNATIVE FORMULATION OF PARAMETER A	189
A2.7	AN ALTERNATIVE PLASTIC POTENTIAL SURFACE	192
A3	MATERIAL MODEL SUBROUTINE	195
A3.1	INTRODUCTION	195
A3.2	INPUT DATA FORMAT	195
A3.2.1	Element Group Control Card	195
A3.2.2	Material Property Data Card	197
A3.3	SUBROUTINE EIPLA, ELPAL, MIDEP	198
A3.3.1	Soubroutine EIPLA	189
A3.3.2	Subroutine ELPAL	199
A3.3.3	Subroutine MIDEP	199
A3.4	PROGRAM LISTING	203
A4	PROPERTIES RELATING TO THE SHEAVE	214
A4.1	BEAM ELEMENT DIMENSIONS EMPLOYED IN THE PRELIMINARY ANALYSIS OF THE SHEAVE	214
A4.2	DIMENSIONS OF THE UNMACHINED SHEAVE	215
A4.3	DIMENSIONS OF THE MACHINED SHEAVE	215
A4.4	CALCULATION OF THE SECOND MOMENT OF AREA OF THE RIM SECTION	215
A4.5	GEOMETRIC PROPERTIES OF THE RIM SECTION EMPLOYED IN THE FINITE ELEMENT SIMULATION	215
A4.6	METHOD OF CONVERTING THE FINITE ELEMENT RESULTS	220
A5	ADINA/ADINAT/ADINA-PLOT PROGRAM	224
A5.1	PROGRAM EXECUTION	224
A5.2	BACK UP ROUTINES	226

		Page
A2	PLASTICITY	176
A2.1	EXPLICIT FORMULATION OF THE ELASTOPLASTIC MATRIX	176
A2.2	ASSOCIATED PLASTICITY	179
A2.3	NON ASSOCIATED PLASTICITY	180
A2.4	PARAMETER A	181
A2.5	THE DIMENSIONLESS STRESS RATIO R	185
A2.6	AN ALTERNATIVE FORMULATION OF PARAMETER A	189
A2.7	AN ALTERNATIVE PLASTIC POTENTIAL SURFACE	192
A3	MATERIAL MODEL SUBROUTINE	195
A3.1	INTRODUCTION	195
A3.2	INPUT DATA FORMAT	195
A3.2.1	Element Group Control Card	195
A3.2.2	Material Property Data Card	197
A3.3	SUBROUTINE EIPLA, ELPAL, MIDEP	198
A3.3.1	Soubroutine EIPLA	189
A3.3.2	Subroutine ELPAL	199
A3.3.3	Subroutine MIDEP	199
A3.4	PROGRAM LISTING	203
A4	PROPERTIES RELATING TO THE SHEAVE	214
A4.1	BEAM ELEMENT DIMENSIONS EMPLOYED IN THE PRELIMINARY ANALYSIS OF THE SHEAVE	214
A4.2	DIMENSIONS OF THE UNMACHINED SHEAVE	215
A4.3	DIMENSIONS OF THE MACHINED SHEAVE	215
A4.4	CALCULATION OF THE SECOND MOMENT OF AREA OF THE RIM SECTION	215
A4.5	GEOMETRIC PROPERTIES OF THE RIM SECTION EMPLOYED IN THE FINITE ELEMENT SIMULATION	215
A4.6	METHOD OF CONVERTING THE FINITE ELEMENT RESULTS	220
A5	ADINA/ADINAT/ADINA-PLOT PROGRAM	224
A5.1	PROGRAM EXECUTION	224
A5.2	BACK UP ROUTINES	226

		Page
A5.2.1	ENGPAC	226
A5.2.2	FADINA	226
A5.2.3	ADINAT/ADINAT/ADPLOT	226
A5.3	DEFINING TEMPORARY STORAGE SPACE ON THE READ/WRITE DISK FOR LARGE LISTING FILES	226
A5.4	REMOTE JOB EXECUTION	227
A6	UNDERGRADUATE PROJECTS RELEVANT TO THE DEVELOPMENT OF THE FINITE ELEMENT METHOD AT THE UNIVERSITY OF THE WITWATERSRAND	233
A6.1	REPLACING THE HUMAN KNEE JOINT	233
A6.2	PREPROCESSOR PROGRAM	235
A6.3	FINITE ELEMENT ANALYSIS OF A THIN SQUARE PLATE	235
A7	ADINA-PLOT, PROGRAM DESCRIPTION AND INSTALLATION	238
A7.1	PROGRAM DESCRIPTION	238
A7.2	INSTALLATION	239

LIST OF FIGURES

FIG	TITLE	PAGE
2.1	Finite Element Mesh	7
2.2	Finite Element Approximation of the Potential Energy of a Linear Elastic Structure	14
2.3	Flow Chart of the Static Analysis Options available in the ADINA Package	16
2.4	Flow Chart - Nonlinear Options	17
3.1	Diagramatic representation of the loaded sheave	18
3.2	Loading Rig	18
3.3	Revised Dimensions of the Rim Section	20
3.4	Finite Element Mesh of the Sheave (20 Beam Elements	22
3.5	Stress Distribution over the Inner Rim Surface (Rope Tension = 250 KN)	23
3.6	Stress Distribution over the Outer Rim Surface (Rope Tension = 250 KN)	24
4.1	The Drucker Prager and Mohr Coulomb Surfaces	32
4.2	Graphical Representation of a Non Associated Plastic Potential Surface	37
4.3	Idealized Material Behaviour	38
4.4	Alternative Modes of Expansion of the Yield Locus in Plane stress	40
4.5	The Drucker Prager Yield Surface (2-D)	41
4.6	The Dimensionless Ratio R	43
4.7	Graphical Representation of an Iterative Scheme Employed in the Solution of Non-Linear Problems	46
4.8	Iterative Schemes available in the ADINA Library	49
4.9a	Flow Chart of Elastoplastic Solution Procedures	50
4.9b	Flow Chart of the Material Model Subroutine	51
4.10	Five Noded Two-Dimensional Plane Stress Element	52
4.11	Paraboloid Plastic Potential Surfaces	54
4.12	Techniques of Modelling the Tangent Modulus	58

		Page
5.1	Strain Gauge Locations	65
5.2	Primary and Secondary Areas of Fracture of the Sheave	66
5.3	Finite Element Mesh	69
5.4	FEM Idealisation of the Rim Profile	70
5.5	Spread of Plasticity (Non Associated Simulation)	72
5.6	Deformation of the Sheave: Rope Tension = 124 KN	73
5.7a	Radial Stress Distribution	74
5.7b	Circumferential Stress Distribution	74
5.8	Vector Plot of Principal Stresses	75
5.9	Exploded View of Principal Stresses in the Spoke	76
6.1	Flow Chart Illustration of the Options Available when Executing a Free Vibration Analysis with ADINA	104
6.2	Flow Chart Illustration of the Options Available when Executing a Forced Vibration Analysis with ADINA	105
6.3	Cantilever Beam, Portal Frame Models	107
6.4	Mass Configurations	108
6.5	Electromagnetic Vibrator Attachment	109
6.6	Two-Noded Beam Element	114
6.7	Mesh Topology for Model 1	115
6.8	Mode Shapes of the Cantilever Beam	116
6.9	Mesh Topology for Model 2	119
6.10-13	Mode Shapes of the Portal Frame	121
7.1	Finite Element Simulation of a High Temperature Kiln	130
7.2	Flat Plate Subjected to a Sinusoidal Temperature Distribution	137
7.3	Finite Element Mesh Topology	137
7.4	Sinusoidal Temperature Loading	138
A1.1	Tensile Compression Test Specimens	152
A1.2	Step Size Sensitivity of the Tangent Modulus	155
A1.3	The Stress Strain Behaviour of Cast Iron	173
A1.4	Material Origin of the Test Specimens	175

		Page
A2.1	Plane Stress Element	176
A2.2	Drucker Prager Surfaces in the Principal Stress Space at Different Stages of Expansion	186
A2.3	Drucker Prager Surfaces in the Shear/Mean Stress Space at Different Stages of Expansion	186
A2.4	An Alternative Formulation of the Increment of Plastic Work, dK_0	190
A3.1	Flow Chart of the Material Model Subroutine EL2D14	196
A3.2	Flow Chart of Subroutine EPLAL	201
A3.3	Flow Chart of Subroutine MIDEP	202
A4.1	Dimensions of the Beam Elements	214
A4.2	Dimensions of the Unmachined Sheave	216
A4.3	Dimensions of the Machined Sheave	217
A4.4	Idealised Cross Section of the Rim	218
A4.5	Finite Element Simulation of the Rim Section	219
A4.6	Geometric Location of the Strain Gauges	221
A5.1	Flow Chart Illustrating ADINA/ADINAT/ADINA-PLOT Execution Procedure	224
A6.1	Analysis of a Knee Joint Prosthesis	234
A7.1	Flow Chart Illustrating the Interaction between the ADINA/ADINA-PLOT Programmes	238

LIST OF PHOTOGRAPHIC PLATES

PLATE	TITLE	PAGE
5.1	The Sheave Mounted in the Loading Rig	62
5.2	The Sheave Mounted on the Pedistal	63
5.3	The Sheave After the Destructive Test	63
5.4	Primary and Secondary Failure of the Rim Section	64

LIST OF PLOTS

PLOT	TITLE	PAGE
4.1	Specification of the Tangent Modulus as a Function of the Stress Ratio R	55
4.2	Uniaxial Tension Test	56
4.3	Uniaxial Compression Test	56
4.4	Tensile Volumetric Strain	57
4.5	Compressive Volumetric Strain	57
5.1 - 5.9	Comparison of FEM and Experimental Results for the Sheave Analysis	86
6.1	Stress Strain Curve for the Steel Rod	112
7.1	Thermal Analysis of a Flat Square Plate: Finite and Exact Results	139

		Page
A1.1	Average Tensile Strain (Tests 1,2 & 3)	163
A1.2	Average Volumetric Strain vs Stress (Tests 2, 3)	164
A1.3	Average Circumferential Strain vs Stress (Tests 2-3)	165
A1.4	Average Compressive Strain vs Stress (Tests 1-2)	166
A1.5	Average Circumferential Strain vs Stress (Test 2)	167
A1.6	Average Volumetric Strain vs Stress (Test 2)	168
A1.7	Tangent Modulus vs Tensile Stress (Tests 1, 2 & 3)	169
A1.8	Poisson's Ratio vs Tensile Stress (Tests 2,3)	170
A1.9	Tangent Modulus vs Compressive Stress (Tests 1,2)	171
A1.10	Poisson's Ratio vs Compressive Stress (Test 2)	172

LIST OF TABLES

TABLE	TITLE	PAGE
5.1	Experimental Results: First Loading (Gauges 1-9)	78
5.2a	Experimental Results: Second Loading (Gauges 1-14)	79
5.2b	Experimental Results: Second Loading (Gauges 15-	80
5.3	Finite Element Results: Associated Plasticity	81
5.4	Finite Element Results: Non-Associated Plasticity	81
5.5	Central Deflection of the Sheave (FEM Results)	84
6.1	Mechanical Properties of the Steel Rod: Experimental Results	113
6.2	Free Vibration Analysis of a Cantilever Beam: (FEM Results)	116
6.3	Discrepancy between Experimental Measurements and Finite Element Results for Mesh 3 (cantilever beam)	118
6.4	Natural Frequencies of a Cantilever Beam	118
6.5	Vibration Analysis of a Portal Frame	120
6.6	Discrepancy between Experimental Measurements and Finite Element Results (Model 2, Mesh 2)	125
7.1	Finite Element and Exact Results (Thermal Problem)	138
A1.1	Tension Test 1	155
A1.2	Tension Test 2	157
A1.3	Tension Test 3	158
A1.4	Compression Test 1	159
A1.5	Compression Test 2	160
A1.6	The Tangent Modulus and Poisson's Ratio in Tension	161
A1.7	The Tangent Modulus and Poisson's Ratio in Compression	162

		Page
A4.1	Dimensions of the Beam Elements (Rim and Spoke)	214
A4.2a	Calculation of the Centroid of the Section	218
A4.2b	Calculation of the Moment of Inertia of the Section	218
A4.3	Centroid, Moment of Inertia of the Simulated Section (FEM)	219
A4.4	Element/Integration Point Corresponding to the Gauge Location	221
A4.5a	Associated Plasticity Results	222
A4.5b	Non-Associated Plasticity Results	223
A5.1	VMS/CMS Command for Innitiating ADINA/ADINAT/ ADINA-PLOT Execution	225

LIST OF NOTATIONS

VECTOR NOTATIONS

$\{a_i\}$; $\{a\}$		nodal or global displacements
$\{q_i\}^e$		nodal force at i due to element e
$\{f_p\}^e$		nodal element force due to distributed load P
$\{R\}$		external nodal force vector
$\{R^1\}$	=	$\{R\} - \{f_p\} - \{f_{\varepsilon_0}\} - \{f_{\sigma_0}\}$
$\{p\}^e$		element distributed loads/unit area
$\{b\}^e$		element distributed loads/unit volume
$\{u\}$		displacement vector (components u, v)
$\{\sigma\}$		stress vector
$\{\varepsilon\}$		strain vector
σ_{ij}		stress component
$d\sigma_{ij}$		increment of stress
$d\varepsilon^p_{ij}$		increment of plastic strain
$d\varepsilon^e_{ij}$		increment of elastic strain
$\{d\varepsilon\}$		incremental strain vector
$\{d\varepsilon^e\}$		elastic strain vector
$\{d\varepsilon^p\}$		plastic strain vector
$\psi(a^n)$		residual load vector after the nth iteration
$P(a)$		equivalent external load vector evaluated from the internal stresses
∇^T		gradient operator = $[\frac{\partial}{\partial x}, \frac{\partial}{\partial y}, \frac{\partial}{\partial z}]$

SCALAR NOTATIONS

e	reference to element e
$f(\sigma)$	the stress component of the yield criterion
$\kappa(k)$	material parameter dependent on the work hardening parameter k
k	the work hardening parameter
$F(\sigma,k)$	the general yield criterion
Q	plastic potential
J_1	first stress invarient = $\sigma_1 + \sigma_2 + \sigma_3 = \sigma_m \times 3$
J_2	second stress invarient = $\frac{1}{2}(s_1^2 + s_2^2 + s_3^2)$
α, $c(k)$, $\phi(k)$, K	yield surface parameters
π	total potential energy
U	total strain energy
$d\lambda$	plastic multiplier
δW	increment of work performed
ζ	damping coefficient
E	Young's modulus
ν	Poisson's ratio

MATRIX NOTATION

$[N_e]$, $[N]$	matrix of element/assembled shape functions
$[B_e]$, $[B] = [L][N]$	strain shape function
$[L]$	strain operator

$[K]^e$, $[K]$	element/assembled stiffness matrix
$[K]_T^n$	tangent stiffness matrix during iteration n
$[M]^e$, $[M]$	element/assembled mass matrix
$[\zeta]^e$, $[\zeta]$	element/assembled damping matrix
$[D]$	linear elastic constitutive matrix
$[D_{ep}]$	elastoplastic constitutive matrix

Symbols used in Chapter 7 (ADINAT) are not listed above. They are defined as they occur in that Chapter.

$[K]^e$, $[K]$	element/assembled stiffness matrix
$[K]_T^n$	tangent stiffness matrix during iteration n
$[M]^e$, $[M]$	element/assembled mass matrix
$[\zeta]^e$, $[\zeta]$	element/assembled damping matrix
$[D]$	linear elastic constitutive matrix
$[D_{ep}]$	elastoplastic constitutive matrix

Symbols used in Chapter 7 (ADINAT) are not listed above. They are defined as they occur in that Chapter.

CHAPTER 1

INTRODUCTION

1.1 PURPOSE

The purpose of this study was

(i) To study the Finite Element Method (FEM) and learn how to use it in a number of relatively simple situations

(ii) To assess some aspects of the FEM package ADINA

1.2 BACKGROUND

The advent of the digital computer has made it possible to analyse continuous systems in a discrete manner. One of the mathematical approaches to this transformation is the finite element method which has become a highly sophisticated technique enveloping a broad spectrum of engineering problems. In the past the method was confined to the upper echelons of the technological and academic world. However, over the last decade it has been popularised to the extent that, to date, numerous computer packages are commercially available.

In 1981 the University of the Witwatersrand acquired the 1977 version of the ADINA finite element program and its thermal counterpart, ADINAT. Although the University had existing finite element programs (STRUDL, GENESYS, PAFEC 71) the ADINA/ADINAT package constitutes a more advanced facility in keeping with the present state of the art. This program, developed at M.I.T., is frequently viewed as a research tool which is not user friendly. Further

development is continuing and it is forseen that in the near future the program will be sufficiently well documented to afford easy access to less experienced users. It is likely to become a powerful tool for the training of both undergraduate and postgraduate students.

In March 1983 an updated 1981 version of the package was installed. This is the most recent edition available in the country. The material models applicable in the previous edition have been refined and an isoparametric beam element, as well as an alternative plate element, have been included in the existing element arsenal. This edition is complemented by a plotting routine ADINA-PLOT, which reduces the post-processing effort required in analysis.

1.3 PROCEDURE

In order to achieve the purposes of this study the ADINA package was used to solve a number of problems.

Before any finite element analysis was performed with the facility, the test programs supplied with the package were executed. This excercise confirmed that the source programmes had been installed correctly. However a few modifications in the back-up routines were required before the ADINA-PLOT program could be utilised. Further elaboration on this problem is presented in the concluding chapter.

The major project undertaken consists of a study of the strength of the rim of a cast iron sheave. This involved a finite element simulation supported by a destructive test on a 1,2 metre diameter sheave. Strains were physically measured at thirty locations on the sheave for comparison with the results of the finite element analysis. During the course of the study it became evident that the nonlinear properties of cast iron would have to be considered if the finite element simulation were to be effective. This

necessitated the development of a material model subroutine compatible with the ADINA package which would be capable of accounting for the nonlinear behaviour.

The ADINA package was later employed to obtain the natural frequencies of a simple beam structure. The results were compared with values determined from experiments performed on physical models. In this excercise the capabilities of the ADINA package to analyse dynamic conditions were investigated.

The thermal counterpart, ADINAT, of the ADINA program was briefly assessed. ADINAT may be employed to simulate linear and nonlinear steady state or transient thermal systems, however it is primarily intended to facilitate the study of thermo-elastic/plastic stress distributions. Test analyses supplied with the package were executed satisfactorily, confirming that the source program had been installed correctly. A further steady state temperature analysis was performed to gain first-hand experience in applying the package. No experimental work was carried out to confirm this analysis since a closed form solution is available.

Familiarity with the ADINA package was extended by assisting in undergraduate projects in which the package was used to analyse static problems. These projects served to stimulate interest in the technique at an undergraduate level. They are presented briefly in Appendix 6 for the purpose of completeness.

CHAPTER 2

FINITE ELEMENT METHOD

2.1 HISTORICAL DEVELOPMENT

In the early 1940's it became apparent that more sophisticated techniques of structural analysis were required to keep abreast of technological developments. Substantial research was required to develop such a technique which is today termed the finite element method and has proved to be an invaluable tool in the engineering world.

Prior to 1950 [4] virtually all structures were analysed by the so-called force method in which the internal forces were treated as the fundamental unknowns of the problem. Structural engineers were compelled to abandon this concept, which although powerful for analysing frame type structures, failed when continuum problems were encountered. This led to a careful examination of the displacement approach in which the displacements are the primary unknowns of the problem.

In the early 1940's it was shown by McHenry, Hrenikoff and Newmark that reasonably good estimates to continuum problems could be obtained by modelling the continuum as a fine mesh of elastic bars [1]. The concept of discretising the continuum into a mesh of elements together with the displacement approach, enabled Argyris and Turner *et al* to propose a more direct formulation in which the displacement field within each element behaved in a simplified manner. This marked the beginning of the displacement-based finite element method.

At a later stage it was shown that the method derived by engineers was in essence identical to contemporary techniques employed by mathematicians for obtaining approximations to problems governed by partial differential equations on geometrically complicated domains [1,4]. Although the mathematical foundations of these techniques had existed for some time (for instance the Rayleigh Ritz (1870 - 1909) and Galerkin (1915) methods), it was the unifying concept of discretising the domain into a set of elements which enabled the full potential of these techniques to be realised. Such an approach was first visualised by Courant in 1943 [1].

To date it is commonly accepted that in the context of elasticity, the finite element method is equivalent to the minimisation of the total potential energy of the system in terms of the prescribed displacement field [1]. Convergence proofs have been provided which are based on the correct selection of the displacement field. In view of this, the method is often interpreted as an extension of the well known Rayleigh-Ritz procedure which is based on a variational principle.

Variational and weighted residual procedures have extended the use of the finite element technique to a broad class of physical problems. In the majority of engineering applications it is possible to formulate a variational principle since the differential operator is positive definite self-adjoint. Where the operator is non-self-adjoint, a weighted residual technique may be applied to obtain an approximate solution.

2.2 THE DISPLACEMENT BASED FINITE ELEMENT FORMULATION

2.2.1 General Approach to the Problem

In the finite element approach, the structure is divided by imaginary lines into a discrete number of elements joined at nodal points. Associated with the nodal points are degrees of freedom which are

representative of the deformations possible in the particular continuum under consideration. These degrees of freedom represent the primary unknowns of the problem and are employed to interpolate and hence define uniquely, the deformation of the continuum within the element by specifying the displacement of any point within the element. The particular interpolation or basis (or shape) functions chosen must satisfy the following convergence criteria if convergence is to be guaranteed [1]

(i) The deformations of adjacent elements must be compatible along common boundaries

(ii) The element must be capable of modelling constant strain conditions, as well as rigid body movements

(iii) The displacement functions should be chosen so that the strains along element interfaces are finite (even though indeterminate).

Once the internal element deformations have been defined in terms of nodal point displacements, the latter can be related to equivalent nodal loads by means of energy considerations, thus ensuring overall element equilibrium. This leads to a set of simultaneous equations in which the nodal displacements are related to equivalent nodal loads by a stiffness matrix.

The equations relating the external forces to the nodal degrees of freedom are obtained by assembling the component element stiffness matrices and nodal load vectors.

The assembled equations enable the nodal point displacements and subsequently internal stresses and strains to be calculated for all elements within the structure.

2.2.2 Derivation of the Displacement Based Finite Element Method [1]

This derivation is documented in the literature [1, 3], but is presented for the purpose of defining a c stent notation which will form the basis for discussion throughout the dissertation.

The displacement function

A typical element, e , considered in isolation to the rest of the continuum (Fig 2.1) is defined by nodes i, j, m etc, and boundary lines joining the nodes

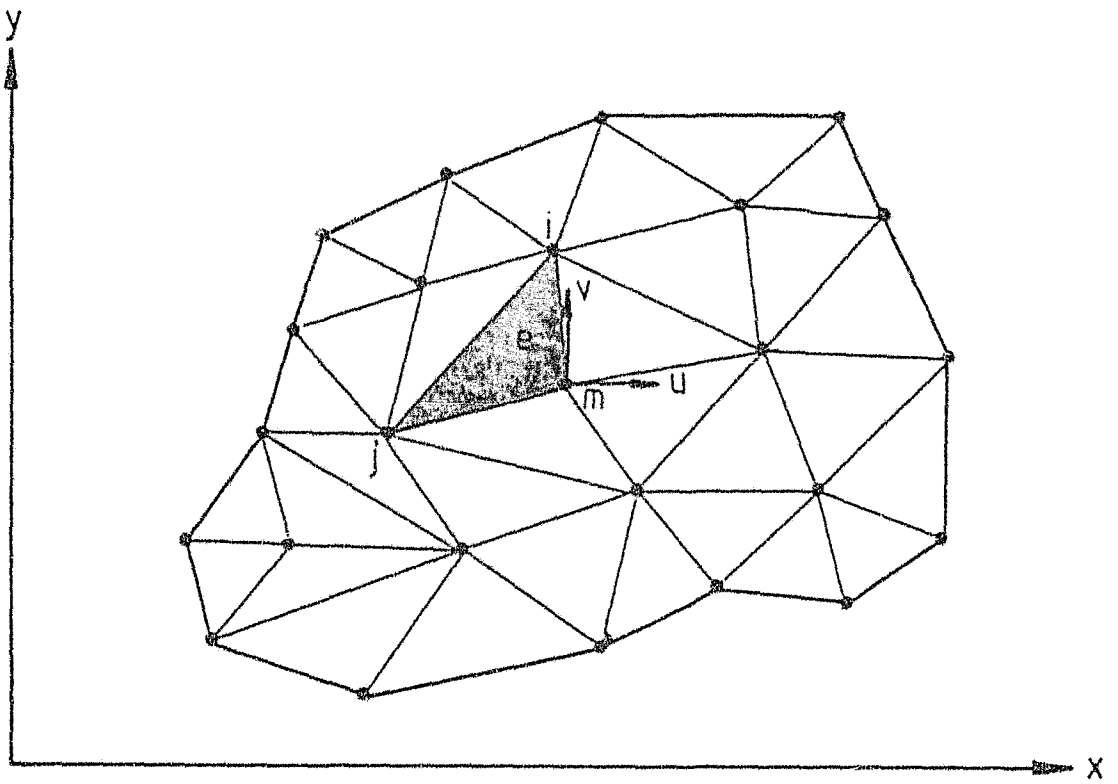

Figure 2.1 - Finite Element Mesh

The displacement field at any point within the element is approximated by a linear combination of a set of basis functions (shape functions) N_i with unknown coefficients a_i, which represent the as yet undetermined nodal point displacements

$$\{u\}^e = \Sigma N_i a_i = [N_i, N_j, \ldots] \begin{Bmatrix} a_i \\ a_j \\ \vdots \end{Bmatrix}^e = [N_e]\{a\}^e \qquad (2.1)$$

where $\{u\}^e$ represents the displacement field.

The components of $[N_e]$ are prescribed functions of position whilst $\{a\}^e$ lists the nodal displacements for the element.

Internal strains

With the displacement field eqn(2.1) defined for all points within the element, the strain at any point may be determined. This always results in a linear relationship which may be written as

$$\{\varepsilon\}^e = [L]\{u\}^e \qquad (2.2)$$

where $\{\varepsilon\}^e$ denotes the strain at any point within the element, e

ie $\{\varepsilon\}^{eT} = (\varepsilon_x, \varepsilon_y, \varepsilon_z, \gamma_{xy}, \gamma_{yz}, \gamma_{zx})$

$[L]$ represents the linear differential operator governing the relationship between the displacement field and the strain

Substituting eqn (2.1) into eqn (2.2)

$$\{\varepsilon\}^e = [L][N_e]\{a\}^e \qquad (2.3)$$

$$\{\varepsilon\}^e = [B_e]\{a\}^e \qquad (2.4)$$

where

$[B_e] = [L][N_e]$

Internal stresses

For linear elasticity, stress is related to strain by a relationship of the form

$$\{\sigma\} = [D](\{\varepsilon\}-\{\varepsilon_0\}) + \{\sigma_0\} \tag{2.5}$$

where $\{\sigma\}$ represents the components of stress

ie $\{\sigma\}^T = (\sigma_x,\sigma_y,\sigma_z,\tau_{xy},\tau_{yz},\tau_{zx})$

$\{\sigma_0\}$ represents initial stresses within the element

$\{\varepsilon_0\}$ represents initial strains within the element

$[D]$ represents the linear elastic constitutive matrix.

Equivalent nodal forces

As described by Zienkiewicz [1], the simplest technique to evaluate the equivalent nodal forces required to balance the boundary stresses and distributed loads acting on an element in isolation, is to apply the principle of virtual work. That is to impose virtual nodal displacements and subsequently equate the internal work with the external work performed during the deformation.

The argument proceeds as follows:
Let the virtual nodal displacements imposed on the element be denoted by $\{\delta a\}^e$; the resulting displacement field according to eqn (2.1) is then

$$\{\delta u\}^e = [N_e]\{\delta a\}^e \tag{2.6}$$

Consequently the internal strains are

$$\{\delta \varepsilon\}^e = [B_e]\{\delta a\}^e \tag{2.7}$$

The external work performed by the nodal forces is obtained from the scalar product of the nodal force vector with the corresponding nodal displacement vector

$$\delta W_{ext} = (\{\delta a\}^e)^T \{q\}^e \tag{2.8}$$

where $\{q\}^e$ represents the equivalent nodal forces required to maintain overall element equilibrium

The internal work performed per unit volume of material is given by

$$(\{\delta\varepsilon\}^e)^T\{\sigma\}^e - (\{\delta u\}^e)^T\{b\}^e \tag{2.9}$$

where $\{b\}^e$ represents distributed loads acting on a unit volume of material within element e , with directions corresponding to those of the displacements $\{u\}^e$ at that point.

Substituting eqn (2.7) and integrating over the volume of the element V^e

$$\delta W_{int} = \int_{V^e} [(\{\delta a\}^e)^T([B_e]^T\{\sigma\}^e - [N_e]^T\{b\}^e)]dV^e \tag{2.10}$$

The virtual work theorem holds for any set of virtual displacements $\{\delta a\}^e$. This condition is automatically satisfied on equating the internal and external virtual work terms because $\{\delta a\}^e$ is a common factor. Therefore $\{\delta a\}^e$ can be eliminated leaving

$$\{q\}^e = \int_{V^e} [B_e]^T\{\sigma\}^e dV^e - \int_{V^e} [N_e]^T\{b\}^e dV^e \tag{2.11}$$

By substituting eqn (2.3), (2.5) the equation may be written as

$$\{q\}^e = [K]^e\{a\}^e + \{f\}^e \tag{2.12}$$

where

$$\{f\}^e = \{f_b\}^e + \{f_p\}^e + \{f_{\varepsilon 0}\}^e + \{f_{\sigma 0}\}^e \tag{2.13}$$

and

$$[K]^e = \int_{V^e} [B_e]^T [D] [B_e] dV^e$$

$$\{f_b\}^e = -\int_{V^e} [N_e]^T \{b\}^e dV^e$$

$$\{f_p\}^e = -\int_{A_\Gamma^e} [N_e]^T \{p\}^e dA_\Gamma^e \qquad (2.14)$$

$$\{f_{\varepsilon 0}\}^e = -\int_{V^e} [B_e]^T [D] \{\varepsilon_0\}^e dV^e$$

$$\{f_{\sigma 0}\}^e = \int_{V^e} [B_e]^T \{\sigma_0\}^e dV^e$$

The term $\{f_p\}^e$ represents the equivalent nodal load required to balance a distributed external load $\{p\}$ acting per unit area on the element boundary Γ.

For initial strains and stresses $\{\sigma_0\}$ to exist within an element, the element displacement field must be distorted from its unstrained configuration. The nodal point displacements and nodal loads required to achieve such a distortion are represented by the last two terms in eqn (2.13) respectively. Since the overall structure must remain in equilibrium, the forces generated by the initial stress are identically zero after assembly. If however an element is removed from a mesh which contains such residual stresses/strains, then the initial stress term $\{f_{\sigma 0}\}^e$ constitutes a force imbalance generated by the element removal and hence a redistribution of forces is required to absorb and equilibrate this effect.

2.3 ELEMENT ASSEMBLY

To evaluate the overall response of the structure to external, concentrated and distributed loads, the element equilibrium equations

must be assembled and the resulting set of simultaneous equations solved. The assembly process results in a set of equations governing the overall equilibrium of the structure, which are given by

$$[K]\{a\} + \{f\} = \{R\} \tag{2.15}$$

where

$$[K] = \Sigma[K]^e$$

$$\{f\} = \{f_f\} + \{f_b\} + \{f_{\sigma 0}\} + \{f_{\varepsilon 0}\}$$

$$\{f_p\} = \Sigma\{f_p\}^e$$

$$\{f_b\} = \Sigma\{f_b\}^e$$

$$\{f_{\sigma 0}\} = \Sigma\{f_{\sigma 0}\}^e$$

$$\{f_{\varepsilon 0}\} = \Sigma\{f_{\varepsilon 0}\}^e \tag{2.16}$$

$$\{R\} = \Sigma\{q\}^e$$

$$\{a\} = \begin{Bmatrix} \{a\}^1 \\ \{a\}^2 \\ \vdots \\ \{a\}^n \end{Bmatrix}$$

In this context

$[K]$ represents the assembled stiffness matrix obtained from the assembly of the element stiffness matrices $[K]^e$

$\{f\}$ represents the assembled load vector required to balance any distributed loads acting on the structure

{R} represents the external concentrated load vector

{a} represents an assembled vector containing all the degrees of freedom defined in the discretisation process.

The principle of virtual work employed in deriving the finite element equations has been shown to be equivalent to the requirement, that the total potential energy of the structure is stationary and attains a minimum for any virtual variation of admissible displacements [1]. Thus the finite element process seeks to approximate the 'true minimum' within the constraint of the displacement pattern chosen.

Although the finite element method always minimises the potential energy of the idealised structure, it only achieves the 'true minimum' in the limit, as the number of degrees of freedom associated with the discretisation process increases. This is conceptually illustrated in Fig 2.2 for an elastic structure which is free of initial stresses and strains. In such a case it can be shown that the potential energy, π , is equal and opposite in sign to the strain energy U [1].

$$\pi + U = 0$$

The finite element method always overestimates the potential energy of the external loads π , and consequently under estimates the strain energy U , [1,12]. Thus the resulting deflections are in general under estimated and the predicted stiffness is over estimated. In an attempt to rectify this effect, it is common practice to numerically under integrate the stiffness coefficients and hence under evaluate the stiffness matrix. Although this technique is acceptable for linear analyses, it does not always apply to non-linear systems [5].

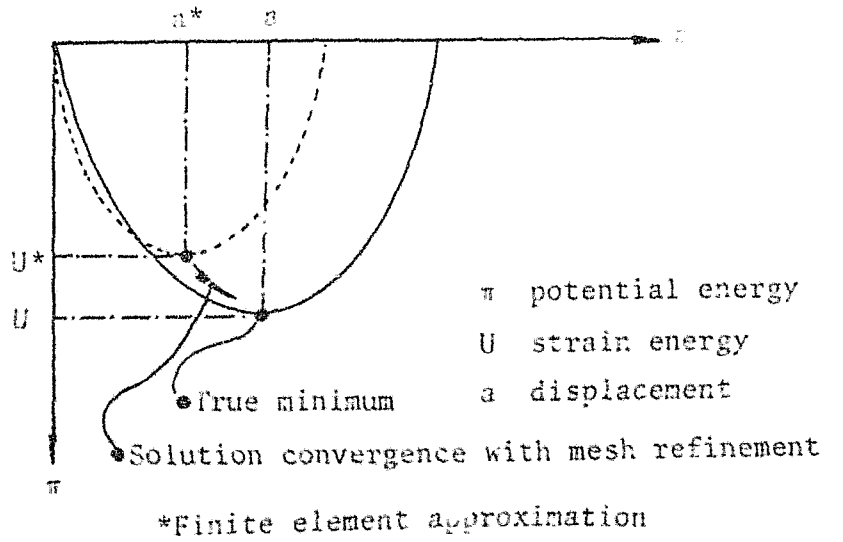

Figure 2.2 - Finite Element Approximation of the Potential Energy of a Linear Elastic Structure

Although the derivation presented concerns linear elastic structures the basic principles involved can be extended to incorporate non-linear behaviour induced by material and/or geometric effects. These formulations are based on an incremental approach and are described in detail by Zienkiewicz [1] and Bathe [3]. The method may also be extended to include temporal effects. The discussion of this formulation is deferred to Chapter 6, where a dynamic simulation of a simple structure is presented.

Continuous research has contributed towards developing elements for different types of continua, ie truss, beam, 2-dimensional, etc. Furthermore, elements have been developed making it possible to model curved boundaries more accurately. These developments are discussed in detail in Ref [1,12].

2.4 THE ADINA FINITE ELEMENT PROGRAM: *STATIC ANALYSIS*

The ADINA (Automatic Dynamic Incremental Non-linear Analysis) finite element program is capable of modelling a variety of engineering systems. These may be linear or non-linear and static or dynamic in nature. The various options available for static analysis are

summarised in Fig 2.3, whilst those applicable to dynamic systems are discussed in Chapter 6.

As illustrated, a linear or non-linear analysis may be performed. With both types, the structure may be modelled by a series of element groups. An element group defines a set of elements of the same type (ie, 2/D solid), specified by the same material model (ie, elasto plastic). It is possible however, to specify different material properties for each element in the group.

In a linear analysis, substructuring may be employed to reduce the amount of input data when there are repetitive features in the structure. Also, some degrees of freedom may be condensed out prior to solution.

Equilibrium iteration is an essential part of non-linear analysis. One of two techniques may be selected, ie Modified Newton Iteration or BFGS Method. An Aitken acceleration scheme may be employed to increase solution efficiency with Modified Newton Iteration. In all non-linear analyses, the type of non-linear formulation (non-linear material, total Lagrangian, updated Lagrangian) selected is specified at element level and is thus dependent on whether it is applicable to that element.

summarised in Fig 2.3, whilst those applicable to dynamic systems are discussed in Chapter 6.

As illustrated, a linear or non-linear analysis may be performed. With both types, the structure may be modelled by a series of element groups. An element group defines a set of elements of the same type (ie, 2/D solid), specified by the same material model (ie, elasto plastic). It is possible however, to specify different material properties for each element in the group.

In a linear analysis, substructuring may be employed to reduce the amount of input data when there are repetitive features in the structure. Also, some degrees of freedom may be condensed out prior to solution.

Equilibrium iteration is an essential part of non-linear analysis. One of two techniques may be selected, ie Modified Newton Iteration or BFGS Method. An Aitken acceleration scheme may be employed to increase solution efficiency with Modified Newton Iteration. In all non-linear analyses, the type of non-linear formulation (non-linear material, total Lagrangian, updated Lagrangian) selected is specified at element level and is thus dependent on whether it is applicable to that element.

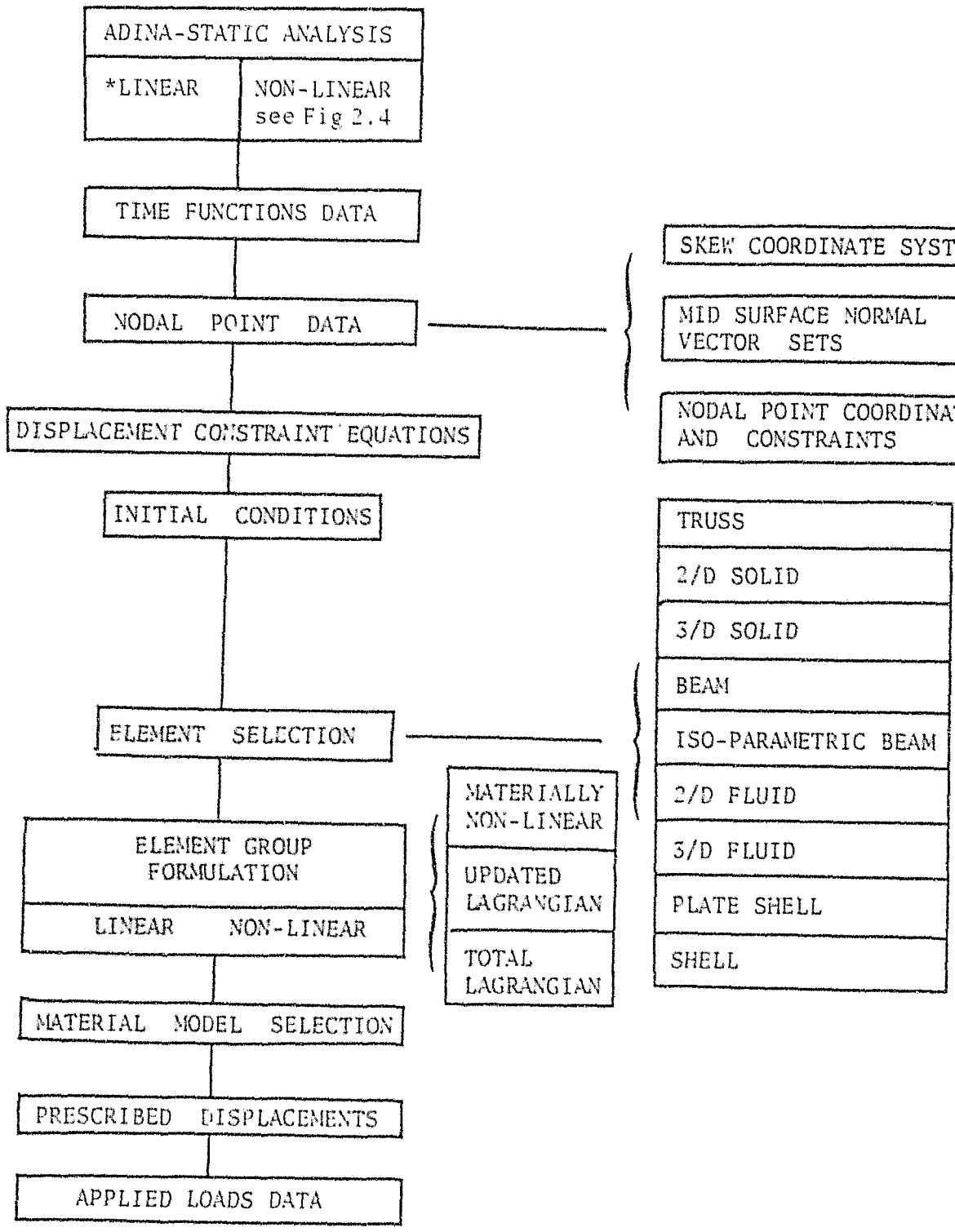

Figure 2.3 - Flow Chart of the Static Analysis Options Available with the ADINA Package

---

*If the overall analysis is linear (ie only linear element groups are defined, then a substructuring option is applicable.

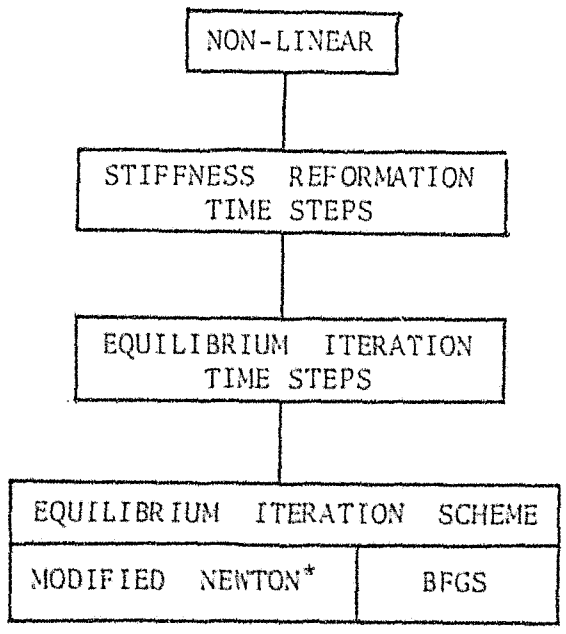

* acceleration scheme optional

Figure 2.4 - Flow Chart of Non-Linear Options

Further information on the elements available and the material models applicable to each element is documented in detail in the ADINA users manual.

CHAPTER 3

RESEARCH ON THE STRENGTH OF SHEAVE WHEELS

3.1 INTRODUCTION

The force distribution in a spoked wheel due to a concentrated load is well known [20] and the results are applicable to vehicle wheels and gears, but no information appears to be available for sheaves where the load is distributed over a fairly substantial arc of the circumference [21].

Large sheaves with many slender spokes may be analysed adequately by employing simple triangular trusses with one degree of indeterminacy [19]. This approach has been confirmed by frame analysis with programmes such as STRUDL and GENESYS. In these analyses the rope is treated as a distributed compressive radial load over the arc of contact as shown in Fig 3.1. The results show that the spokes and rim over the unloaded portion ABC are lightly stressed. Experimental confirmation of this has been obtained by loading small sheaves in the loading rig illustrated diagramatically in Fig 3.2, [17,18].

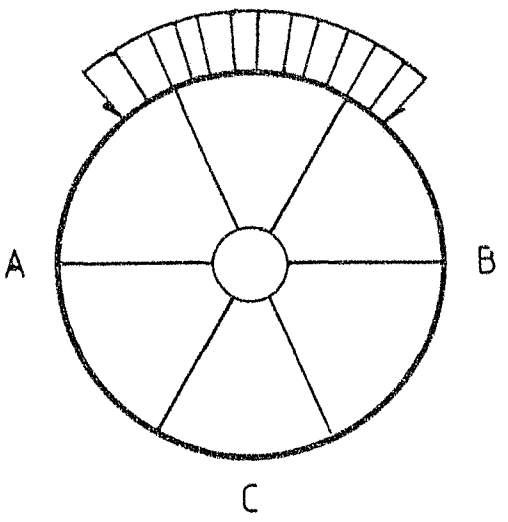

Figure 3.1 - Diagramatic Representation of the Loaded Sheave

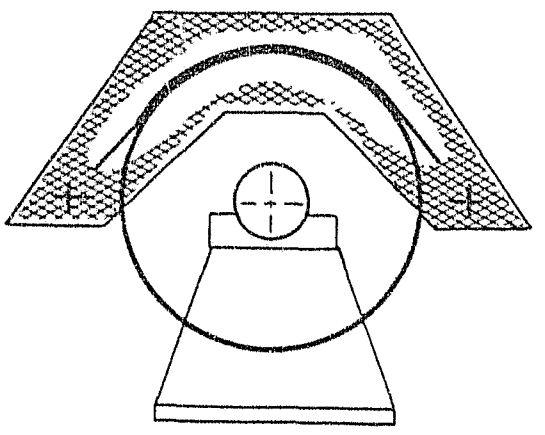

Figure 3.2 - Loading Rig

A compressive radial load is applied by the rope on inserting the assembly into an Amsler compression testing machine.

3.2 PREVIOUS RESEARCH [18]

In 1981 two cast iron[1] sheaves were acquired and prepared for testing to destruction. These had a diameter of 1 m and six integrally cast spokes.

The spokes of the first sheave were thinned and consequently buckled in a destructive test at a rope tension of 100 KN.

In order to induce failure in the rim of the second sheave, its rim section was reduced. This sheave was loaded up to a rope tension of 250 KN without producing failure and the test was thus discontinued. The average dimensions and geometric properties of this sheave are presented in Appendix 4. (Fig A4.2)

3.3 CURRENT RESEARCH PROGRAMME

It was decided to use the second sheave as a means of checking the results obtained from ADINA with particular emphasis on the non-linear behaviour of the material. To realise this purpose, it was decided

(i) to reduce the rim section in order to achieve failure without excessive rope loading

(ii) to monitor strains at some points on the sheave during the test

(iii) to simulate the behaviour of the sheave throughout its loading history with the ADINA finite element package.

---

1. Grade 17 grey cast iron, as specified by the manufacturers.

In order to implement the first objective, revised dimensions for the rim section were selected. Prior to machining, a simple finite element analysis was performed to assess whether failure would be attained (see Section 3.4).

The final dimensions selected are illustrated in Fig 3.3 below. The moment of inertia, cross sectional area and centroid, were estimated by dividing the section into elements. These calculations are presented in Appendix 4. The final outcome is a reduction in the moment of inertia and cross sectional area of 60% and 20% respectively. The average dimensions of this sheave are illustrated in Fig A4.3 in Appendix 4.

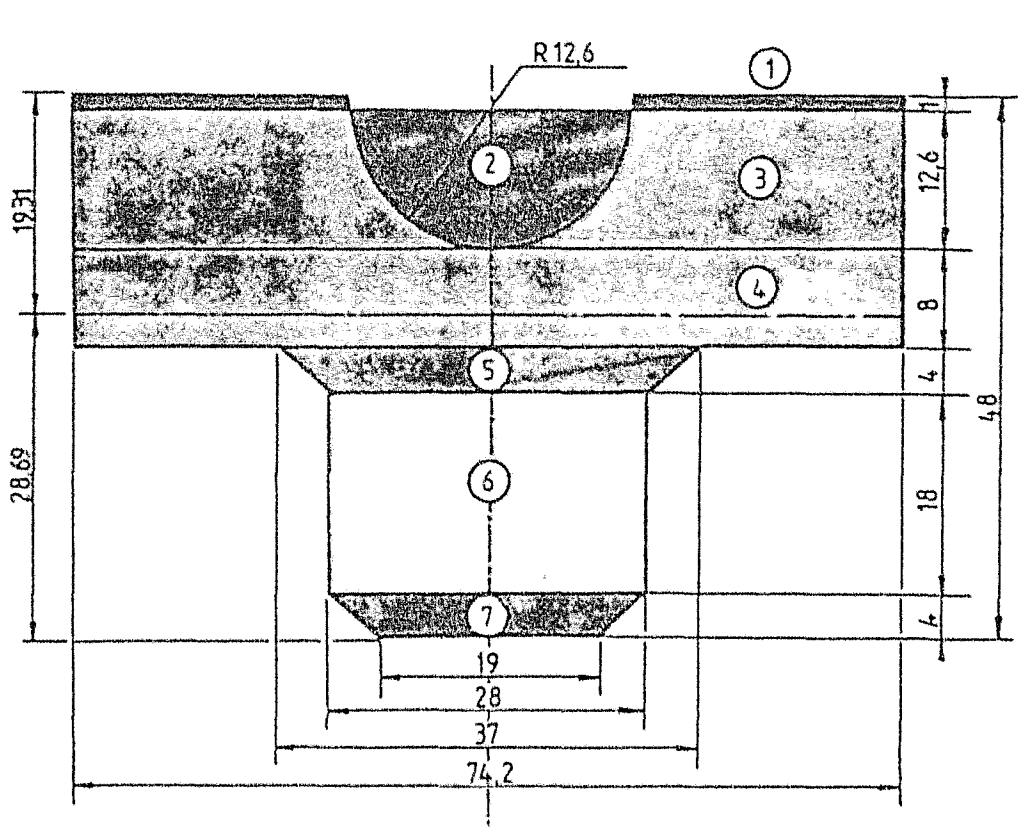

Figure 3.3 - Revised Dimensions of the Rim Section

3.4 PRELIMINARY FINITE ELEMENT ANALYSIS

The purpose of this analysis was to verify that the dimensions selected above, would be likely to cause rim failure of the sheave without excessive loading of the test rig.

It was considered necessary to use a nonlinear analysis which would simulate, to some extent, the actual behaviour of the material. In order to limit the work involved at this stage, it was decided to use beam elements rather than two dimensional solid elements.

3.4.1 Finite Element Mesh

The sheave was treated as a plane body loaded in its plane by a uniform compressive radial load over 120° arc of contact. A symmetrical half was modelled by using two-dimensional beam elements. (The mesh design is illustrated in Fig 3.4.) Since only circular or rectangular sections are applicable to beam elements, the rim and spokes were modelled by rectangular sections as specified in Appendix 4.1.

The spoke dimensions selected are representative of the actual section. Since the significant stresses in the rim are caused by bending, the dimensions selected for the rim, model the depth and moment of inertia but not the area of the section.

3.4.2 Material Properties

By this stage preliminary tensile/compression tests had been performed on specimens machined from section ABC of the first sheave tested in 1981 (see Fig 3.2). The non-linear behaviour was approximated with a bi-linear model, von Mises yield criterion and hardening. The ADINA library has such beam elements. The difference in strength between tension and compression was disregarded at this stage.

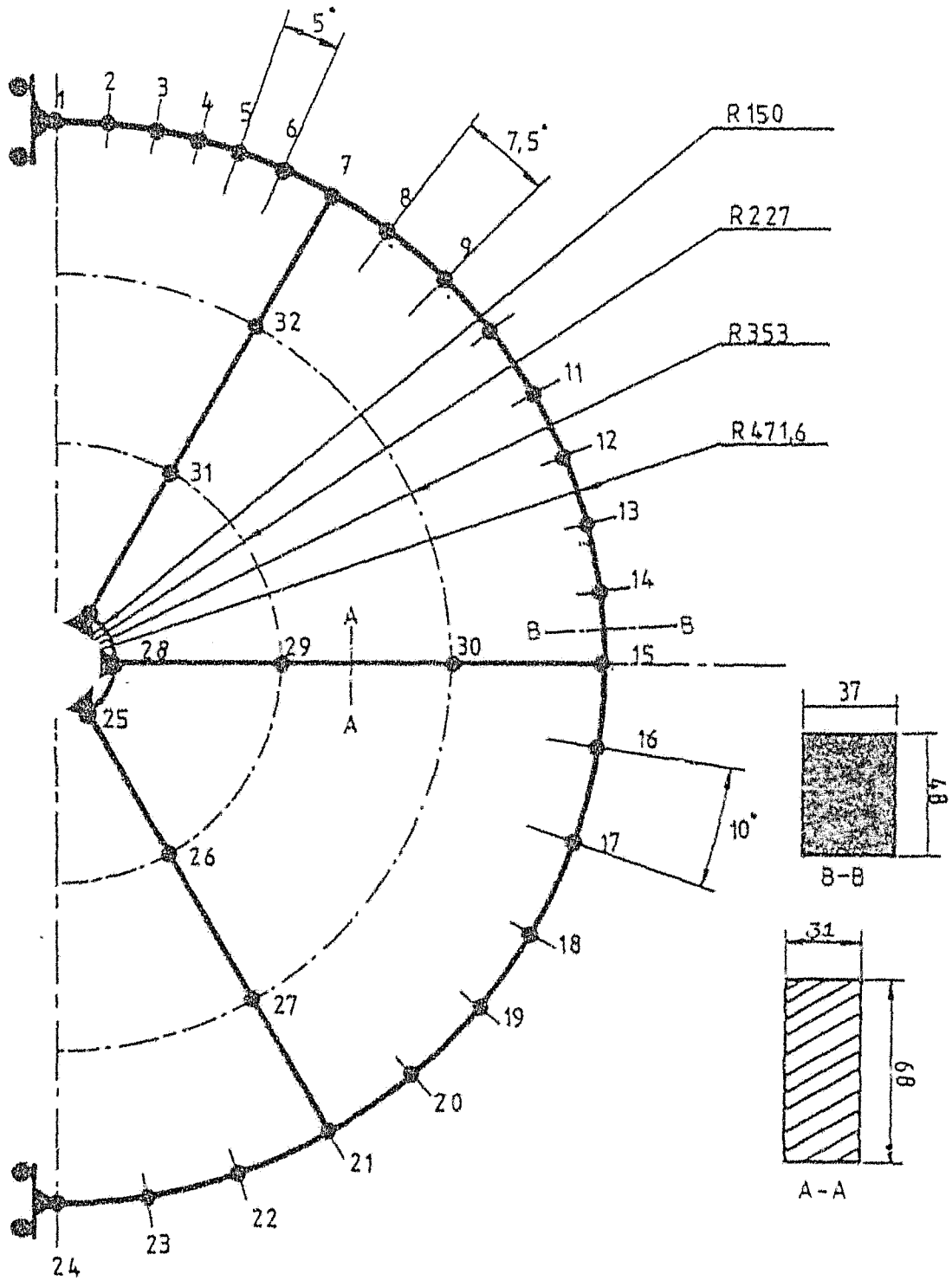

Figure 3.4 - Finite Element Mesh

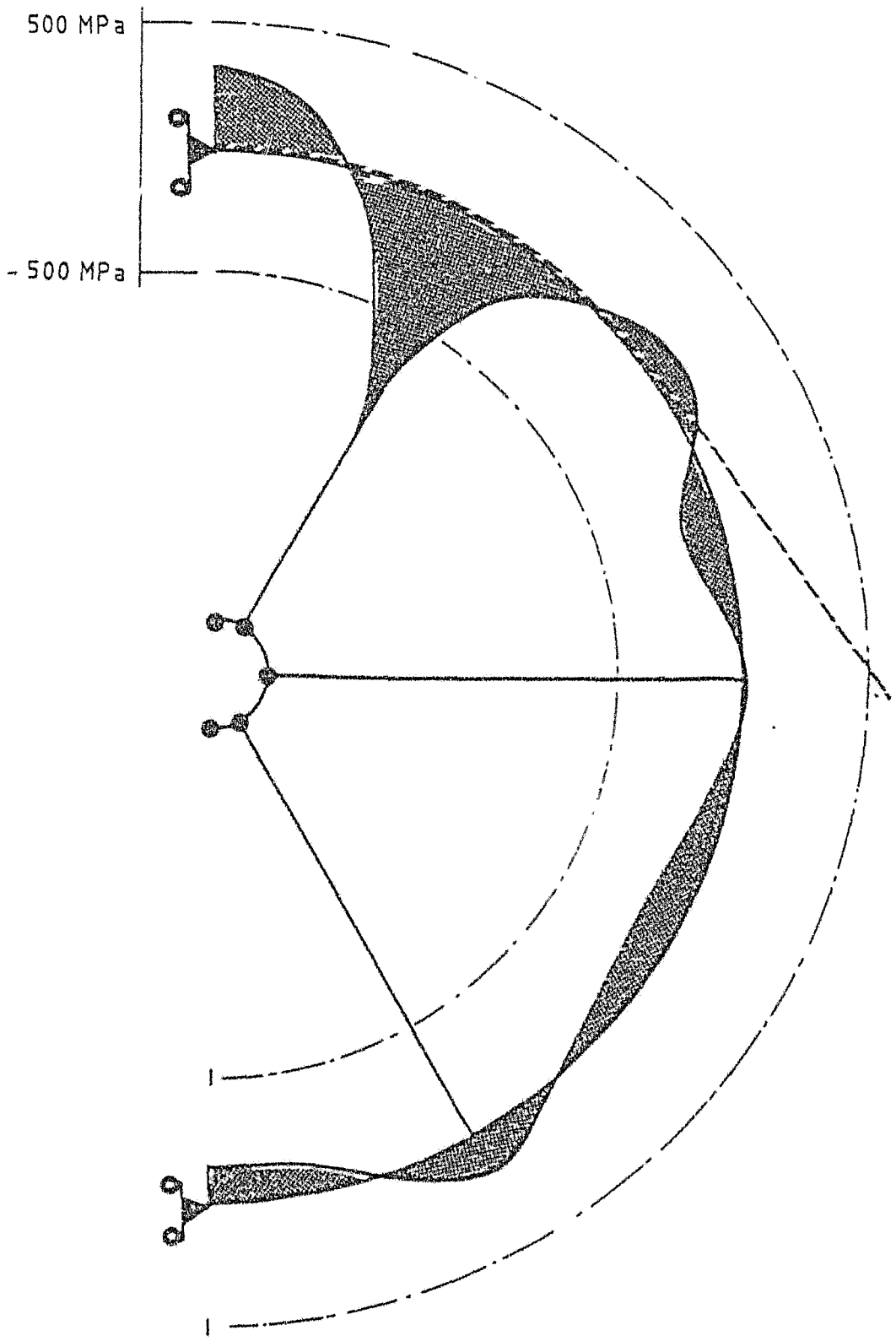

Figure 3.5 - Stress distribution over the inner rim surface
(Rope tension = 250 KN)

Author Constancon C P
Name of thesis A study of the finite element method, with reference to the Adina finite element package 1983

PUBLISHER:
University of the Witwatersrand, Johannesburg
©2013

LEGAL NOTICES:

Copyright Notice: All materials on the University of the Witwatersrand, Johannesburg Library website are protected by South African copyright law and may not be distributed, transmitted, displayed, or otherwise published in any format, without the prior written permission of the copyright owner.

Disclaimer and Terms of Use: Provided that you maintain all copyright and other notices contained therein, you may download material (one machine readable copy and one print copy per page) for your personal and/or educational non-commercial use only.

The University of the Witwatersrand, Johannesburg, is not responsible for any errors or omissions and excludes any and all liability for any errors in or omissions from the information on the Library website.

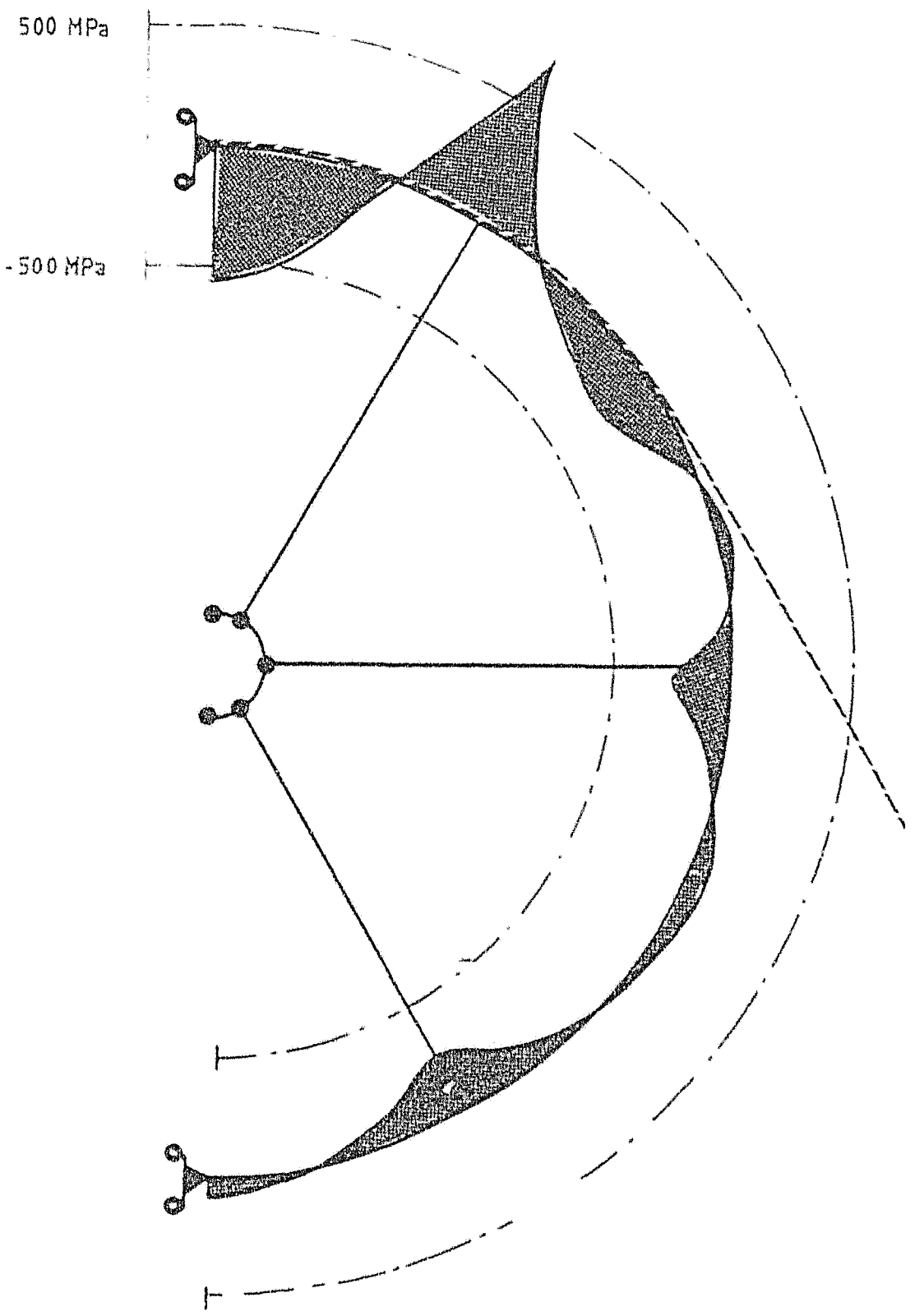

Figure 3.6 - Stress distribution over the outer rim surface
(Rope tension = 250 KN)

The particular material parameters required as input by this model and the values selected are listed below

E - Young's Modulus - 96 GPa

ν - Poisson's Ratio - 0,3

σ_y - yield stress - 180 MPa

E_T - linear strain hardening modulus - 70 GPa

3.4.3 Finite Element Results

In the finite element simulation a uniform compressive load, equivalent to that generated by a 250 KN tensile rope load, was applied in a single step. The load acted on nodes 1-11. Equilibrium iteration was employed to track the specified nonlinear behaviour.

The results of the analysis confirm that the maximum stress occurs at the centre of the arc on the line of symmetry and at the junction of the spoke to the rim. The stress distribution predicted by the analysis over the inner and outer rim surface, is illustrated in Figs 3.5 and 3.6 respectively.

The maximum tensile and compressive stresses achieved at the centre of the arc were 337 MPa and -520 MPa, whilst at the junction of the spoke to the rim, stresses of 548 MPa and -592 MPa were predicted. In both cases the tensile stress exceeds the ultimate tensile stress of the material, 220 MPa, as determined experimentally. Since compressive failure was not achieved in the compression tests (loading was discontinued when barrelling became noticible), it is likely that rim failure will be initiated by tensile cracks and hence the tensile stress will determine failure.

3.4.4 Conclusions

Although this analysis was simplistic it indicated to some extent that the reduced rim section proposed, would result in failure before reaching the maximum load which the rig could withstand.[1]

---

1. The loading frame was designed to operate up to a rope tension of 250 KN, with a safety factor of ~2, [17].

The major limitations of this analysis are listed below

- the rim was approximated grossly by a rectangular section
- the radii at the junction of the spoke to the rim were neglected
- the nonlinear material properties of the cast iron were inadequately represented.

3.5 BASIS FOR A MORE DETAILED STUDY

Ideally an accurate finite element simulation of the sheave would involve a three-dimensional analysis incorporating the nonlinear material behaviour. Limitations on computer resources prevent such an approach, however a good approximation may be achieved by modelling the sheave adequately. The approach adopted was to model the rim of the sheave with two-dimensiona plane stress elements of varying thickness in areas of high stress and with beam elements in areas where the stresses were likely to be low.

A number of nonlinear material models are available in ADINA for two dimensional solid elements. Although material model 7 (Drucker Prager yield criterion with hardening cap and tension cut off) is capable of modelling materials exhibiting higher strength in compression than tension, it predicts volumetric plastic dilatency, which is not common in metal plasticity and which was considered originally as inapplicable to cast iron.

Accordingly, it was decided to utilise the 'user supplied' material model option for developing a nonlinear material law which would account for the cast iron properties. The law adopted was similarly based on the Drucker Prager yield criterion, however initially it did not predict volumetric plastic dilatency.

The formulation of the nonlinear material law and the subsequent development of a material model subroutine based on this law, is discussed in Chapter 4.

CHAPTER 4

PLASTICITY

4.1 INTRODUCTION

The basic laws governing the elastoplastic behaviour of the cast iron material used in the manufacture of the sheave must be derived before any numerical aspects of a finite element analysis can be considered. Using existing classical hypotheses it is possible to derive a two-dimensional stress strain relationship from experimental data acquired from material tests. In order to formulate such a relationship it is necessary to postulate the existence of a yield criterion which describes the stress level at which plastic flow commences. Ideally biaxial tests are required to determine such a criterion experimentally. The facilities for performing these tests were not available hence a yield criterion had to be selected on the grounds of the uniaxial test results.

The uniaxial behaviour of the cast iron was studied by testing specimens machined from a similar sheave manufactured from the same cast (see Appendix 1). The results of these tests confirmed that the yield strength of the cast iron is higher in compression than it is in tension. This property is characteristic of a frictional material conforming to the Mohr Coulomb failure criterion or the Drucker Prager yield criterion. The latter is computationally easier to implement and it was thus postulated that it represents the yield criterion of cast iron.

In order to derive the relationship between the increments of plastic strain and stress a further assumption regarding the material behaviour must be made. Classically it is assumed that the plastic

strain component is normal to the yield surface. This is termed the normality condition which leads to an associated theory of plasticity. When applied to the Drucker Prager criterion this theory predicts material dilatancy during plastic deformation.

Initially the cast iron material was assumed to be plastically incompressible. To implement this assumption a von Mises plastic potential was defined leading to a non associated theory of plasticity. Additional experimental tests were performed on both tensile and compressive specimens to verify the above assumption. The specimens tested were machined from lightly loaded portions of the actual sheave after the destructive test. This ensured that the uniaxial test results would represent the virgin properties of the material as closely as possible. These results revealed that the cast iron dilates substantially during plastic deformation hence the initial assumption proved to be invalid. Subsequently the associated constitutive law which accounts for plastic dilatancy was formulated.

Both the associated and non associated constitutive relationships based on the Drucker Prager yield criterion are discussed and developed in subsequent sections.

4.2 THE MATHEMATICAL THEORY OF PLASTICITY,[1] [13]

'The object of the mathematical theory of plasticity is to provide a theoretical description of the relationship between stress and strain for a material which exhibits an elasto plastic response. In essence this relationship is characterized by an irreversible

---

1. It is the author's opinion that the mathematical theory of plasticity has been concisely expressed in the literature by various researchers. For this reason the author has chosen to quote directly from other literature sources where a more concise explanation could not be produced without loss of meaning.

straining which is independent of time and which can only be sustained once a certain level of stress has been reached. In order to formulate a theory which models elasto plastic material deformation three requirements have to be met'.

- An explicit constitutive relationship must be formulated to describe material behaviour under elastic conditions.
- A yield criterion must be postulated to indicate the stress level at which plastic flow commences.
- A relationship describing both elastic and plastic behaviour must be developed for post yield conditions.

The strain is linearly related to stress in the elastic region by Hookes Law. This results in a unique relationship between stress and strain which is independent of the stress level. In the plastic region however the relationship is nonlinear. Furthermore the relationship is non unique [11] since the total plastic strains are path dependent. Before presenting the theoretical derivation of the elastoplastic relationship the concept of a yield surface is examined.

4.2.1 The Yield Criterion

It is postulated that yielding can only occur if the state of stress satisfies the yield criterion [13]

$$f(\sigma) = \kappa(k) \qquad (4.1)$$

where f is a function of the stress (σ) and κ is a material parameter determined experimentally. This parameter may be a function of a hardening parameter k (refer to Section 4.2.6), which governs the expansion of the yield surface in the principal stress space. Since the yield criterion is invariant in this space it must consist of the three stress invariants, [11,13]

$$J_1 = \sigma_1 + \sigma_2 + \sigma_3 = \sigma_{ii} \quad [1]$$

$$J_2 = \frac{1}{2}\sigma_{ij}\sigma_{ij} \qquad (4.2)$$

$$J_3 = \frac{1}{3}\sigma_{ij}\sigma_{jk}\sigma_{k\ell}$$

Thus the yield criterion can be visualised as a surface in the n-dimensional stress space with the position of the surface dependent on the instantaneous value of κ .

As expressed by eqn (4.1), $f(\sigma) = \kappa$ represents plastic behaviour, whilst $f(\sigma) < \kappa$ characterises elastic behaviour. By evaluating the incremental change in the yield function f, due to an incremental stress change, it is possible to determine the type of loading occuring, ie [13]

$$df = \frac{\partial f}{\partial \sigma} d\sigma \qquad (4.3)$$

if: $df < 0$ elastic unloading occurs and the stress point returns inside the yield surface

$df = 0$ neutral loading occurs and the stress point remains on the stationary yield surface (plastic behaviour for a perfectly plastic material)

$df > 0$ plastic loading and the stress point remains on the expanding yield surface (plastic behaviour for a hardening material).

---

1. Einstein's summation convention is invoked, whereby it is implicitly assumed that a summation from 1 to 3 is performed over any index which is repeated in any term of an expression. Indices 1, 2, 3 refer to cartesian coordinates x, y, z respectively, ie $\sigma_{11} = \sigma_{xx} = \sigma_x$

$$J_1 = \sigma_1 + \sigma_2 + \sigma_3 = \sigma_{ii} \quad [1]$$

$$J_2 = \frac{1}{2}\sigma_{ij}\sigma_{ij} \qquad (4.2)$$

$$J_3 = \frac{1}{3}\sigma_{ij}\sigma_{jk}\sigma_{k\ell}$$

Thus the yield criterion can be visualised as a surface in the n-dimensional stress space with the position of the surface dependent on the instantaneous value of κ .

As expressed by eqn (4.1), $f(\sigma) = \kappa$ represents plastic behaviour, whilst $f(\sigma) < \kappa$ characterises elastic behaviour. By evaluating the incremental change in the yield function f, due to an incremental stress change, it is possible to determine the type of loading occuring, ie [13]

$$df = \frac{\partial f}{\partial \sigma} d\sigma \qquad (4.3)$$

if: $df < 0$ elastic unloading occurs and the stress point returns inside the yield surface

$df = 0$ neutral loading occurs and the stress point remains on the stationary yield surface (plastic behaviour for a perfectly plastic material)

$df > 0$ plastic loading and the stress point remains on the expanding yield surface (plastic behaviour for a hardening material).

---

1. Einstein's summation convention is invoked, whereby it is implicitly assumed that a summation from 1 to 3 is performed over any index which is repeated in any term of an expression. Indices 1, 2, 3 refer to cartesian coordinates x, y, z respectively, ie $\sigma_{11} = \sigma_{xx} = \sigma_x$

4.2.2 The Drucker-Prager Yield Criterion

The Drucker-Prager yield criterion is extensively employed in the field of soil mechanics as an approximation to the Mohr Coulomb failure criterion. The yield surface is a right circular cone inclined along the mean stress axis in the principal stress space. For this case the yield criterion expressed in eqn (4.1) is re-written as

$$F(\sigma,k) = f(\sigma) - \kappa(k) = 0 \tag{4.4}$$

where $F(\sigma,k)$ now represents a function of both the stress state and the hardening parameter k. The Drucker-Prager criterion is expressed as

$$F(\sigma,k) = \alpha J_1 + J_2^{1/2} - K \tag{4.5}$$

where α, K are material parameters determined experimentally.

In order to ensure that the Drucker-Prager criterion coincides with the outer apices of the Mohr Coulomb hexagon at any section along the mean stress axis, it can be shown that [13]

$$\alpha = \frac{2\sin\phi}{\sqrt{3}(3-\sin\phi)} \tag{4.6}$$

$$K = \frac{6\cos\phi}{\sqrt{3}(3-\sin\phi)}$$

where c and ϕ represent the cohesion and the angle of internal friction of the material respectively. Furthermore both c and ϕ may be functions of the hardening parameter k, ie $c(k)$, $\phi(k)$. A geometrical representation of both the Mohr Coulomb and Drucker-Prager yield surfaces in the principal stress space is illustrated in Fig 4.1.

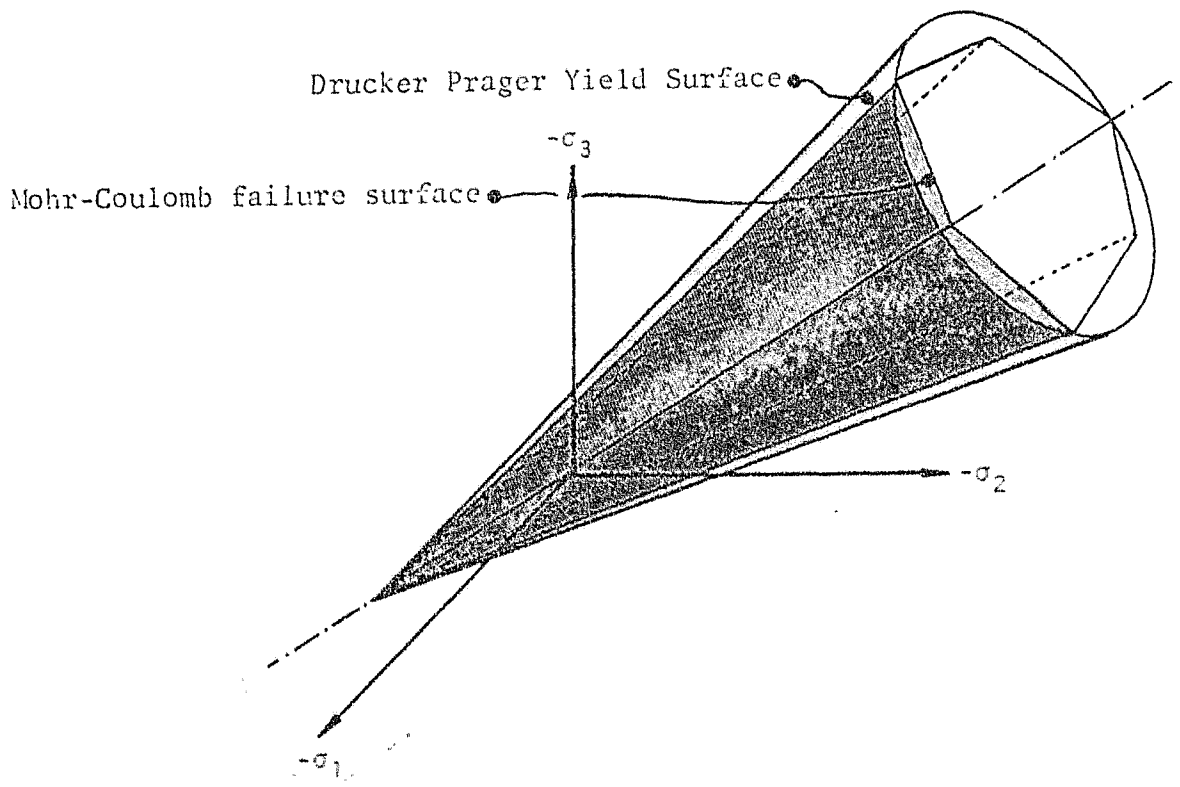

Figure 4.1 - The Drucker Prager and Mohr Coulomb surfaces

4.2.3 The Definition of Work Hardening [10]

A precise definition of work hardening was first proposed by Drucker.

Drucker postulated that for a work hardening material at a given state of stress; if an external agency slowly applied additional stresses and then slowly removed them, the material remained in equilibrium and:

1) *'Positive work is done by the external agency during the application of the added set of stresses.'*

2) *'The net work performed by the external agency over the cycle of application and removal is positive if plastic deformation occurred in the cycle. The net work is zero if and only if elastic changes in strain alone are produced.'*

These conditions may be stated in mathematical terms as

1) $$\delta W = (\sigma_{ij}-\sigma^*_{ij})d\varepsilon^p_{ij} + d\sigma_{ij}d\varepsilon^p_{ij} > 0 \qquad (4.7)$$

2) $$\delta W = d\sigma_{ij}d\varepsilon^p_{ij} > 0 \qquad (4.8)$$

where σ_{ij} represents a state of stress lying on the yield surface

σ^*_{ij} represents a state of stress lying on or inside the yield surface

$d\sigma_{ij}$ represents an increment of stress which produces a small increment of plastic strain $d\varepsilon^p_{ij}$

It has been shown by Drucker that both of these conditions are satisfied only if

(i) the yield surface is convex

(ii) the plastic strain increment is normal to the yield surface.

4.2.4 The Elasto Plastic Stress Strain relations

After initial yielding the material behaviour will be partly elastic and partly plastic. The changes of strain due to an increment of stress $d\sigma_{ij}$ exceeding the yield limit are assumed to be decomposable into elastic and plastic components

$$d\varepsilon_{ij} = d\varepsilon^e_{ij} + d\varepsilon^p_{ij} \tag{4.9}$$

where the elastic increment of strain is related to the stress increment by

$$d\varepsilon^e_{ij} = D^{-1}_{ijk\ell} d\sigma_{k\ell} \tag{4.10}$$

where $D_{ijk\ell}$ represents the elastic constitutive matrix.

The plastic increment of strain is assumed to be proportional to the gradient of a quantity termed the plastic potential, Q . ie

$$d\varepsilon^p_{ij} = d\lambda \frac{\partial Q}{\partial \sigma_{ij}} \tag{4.11}$$

where $d\lambda$ represents a positive proportionality constant; the plastic multiplier. This relationship determines the flow rule of the material since it governs plastic flow after yielding has occurred. The relation $Q \equiv F$ has special significance as it implies normality of the plastic strain increment to the yield surface and results in certain uniqueness and variational theorems, [1,3,11,13].

A further assumption that is implied in this derivation is that the increments of stress and plastic strain are linearly related.

$$d\sigma_{ij} = D^{p}_{ijk\ell} d\varepsilon^{p}_{k\ell} \tag{4.12}$$

where $D^{p}_{ijk\ell}$ represents the plastic constitutive law governing the relation between the increment of stress and plastic strain. Thus it is assumed that $D^{p}_{ijk\ell}$ is dependent only on the current stress and total strain levels but not on their increments. In the special case of a hardening material where the yield function is only dependent on the current stress level and total plastic strain no assumption is necessary, [10]. That is when

$$F(\sigma, \varepsilon^{p}) = f(\sigma) - \kappa(\varepsilon^{p})$$

differentiating gives

$$dF = 0 = \frac{\partial F}{\partial \sigma_{ij}} d\sigma_{ij} + \frac{\partial F}{\partial \varepsilon_{ij}} d\varepsilon^{p}_{ij} \quad [1]$$

In this case $\partial F/\partial \sigma_{ij}$ and $\partial F/\partial \varepsilon^{p}_{ij}$ are independent of $d\sigma_{ij}$, $d\varepsilon^{p}_{ij}$. A linear relationship between the increment of stress $d\sigma_{ij}$ and the

---

1. This is the requirement to ensure that the stress point remains on the expanding yield surface.

increment of plastic strain clearly exists, [10].

Matrix Formulation of the Stress Strain Relationship

The theoretical expressions are now converted into matrix form. In the following section vectors and matrices are denoted by { } and [ ], respectively.

As stated in equation (4.9)

$$\{d\varepsilon\} = \{d\varepsilon^e\} + \{d\varepsilon^p\} \tag{4.13}$$

where

$$\{d\varepsilon^e\} = [D]^{-1}\{d\sigma\}$$

$$\{d\varepsilon^p\} = d\lambda\left\{\frac{\partial Q}{\partial \sigma}\right\}$$

thus

$$\{d\varepsilon\} = [D]^{-1}\{d\sigma\} + d\lambda\left\{\frac{\partial Q}{\partial \sigma}\right\} \tag{4.14}$$

When plastic yield occurs the stresses remain on the expanding yield surface, ie

$$F(\sigma, k) = 0 \tag{4.15}$$

and

$$\left\{\frac{\partial F}{\partial \sigma}\right\}^T\{d\sigma\} + \frac{\partial F}{\partial k}dk = 0 \tag{4.15}$$

$$\left\{\frac{\partial F}{\partial \sigma}\right\}^T\{d\sigma\} - Ad\lambda = 0 \tag{4.16}$$

where

$$A = -\frac{\partial F}{\partial k}dk\frac{1}{d\lambda} \tag{4.17}$$

Equations (4.14) and (4.16) can be written in matrix form as, [1]

$$\begin{Bmatrix} \{d\varepsilon\} \\ 0 \end{Bmatrix} = \begin{bmatrix} [D]^{-1} & \{\frac{\partial Q}{\partial \sigma}\} \\ \{\frac{\partial F}{\partial \sigma}\}^T & -A \end{bmatrix} \begin{Bmatrix} \{d\sigma\} \\ d\lambda \end{Bmatrix}$$

The constant $d\lambda$ is eliminated resulting in an explicit expansion which determines the stress increments in terms of the imposed strain increments.

$$\{d\sigma\} = [D_{ep}]\{d\varepsilon\} \tag{4.18}$$

where

$$[D_{ep}] = [D] - \frac{[D]\{\frac{\partial Q}{\partial \sigma}\}\{\frac{\partial F}{\partial \sigma}\}^T[D]}{A + \{\frac{\partial F}{\partial \sigma}\}^T[D]\{\frac{\partial Q}{\partial \sigma}\}} \tag{4.19}$$

This matrix is symmetric only when plasticity is associated, that is, when $Q \equiv F$.

By re-examining the second condition stated when defining a work hardening material, a mathematical explanation of this restriction to symmetry is obtained, ie

$$\delta W = d\sigma_{ij} d\varepsilon^p_{ij} > 0$$

$$= 0 \quad \text{only if} \quad d\varepsilon^p_{ij} \equiv 0$$

This may be stated in vector form as

$$\{d\varepsilon^p\}^T\{d\sigma\} \geq 0 \tag{4.20}$$

From eqn (4.13)

$$\{d\varepsilon^p\} = \{d\varepsilon\} - \{d\varepsilon^e\}$$

Equation (4.20) may be restated as

$$\{d\varepsilon\}^T\{d\sigma\} \geq \{d\varepsilon^e\}^T\{d\sigma\} \tag{4.21}$$

substituting eqn (4.10), eqn (4.18) into eqn (4.20)

$$\{d\varepsilon\}^T[D_{ep}]\{d\varepsilon\} \geq \{d\varepsilon^e\}^T[D]\{d\varepsilon^e\} \tag{4.22}$$

Since the right hand side of eqn (4.22) is always real and greater than zero, unless $\{d\varepsilon^e\} \equiv 0$

$$\{d\varepsilon\}^T[D_{ep}]\{d\varepsilon\} > 0 \tag{4.23}$$

$$= 0 \quad \text{if and only if} \quad \{d\varepsilon\} \equiv 0$$

For this quantity to be real and greater than zero for any $\{d\varepsilon\}$, the elastoplastic matrix must be Hermite and hence symmetric and positive definite. Hence by deduction a nonsymmetric elastoplastic matrix implies that inequality (4.20) may be violated for certain strain paths.

This concept is illustrated in Fig 4.2 where a non associated plastic potential defines the direction of the plastic strain increment.

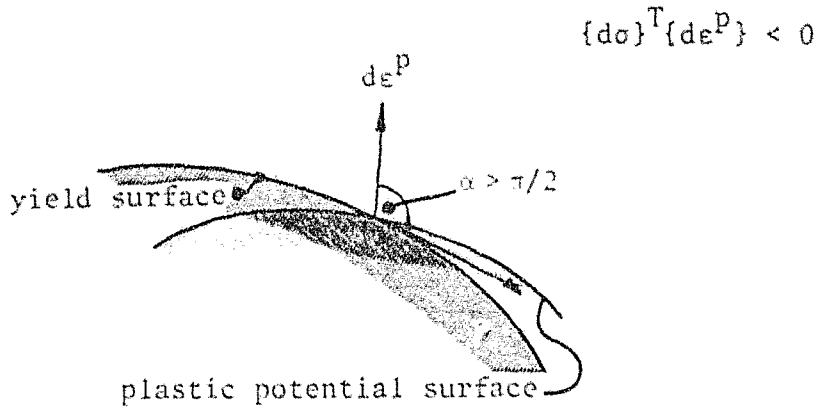

Figure 4.2 - A Graphical Representation of a Non Associated Plastic Potential Surface

The foregoing discussion illustrates that if a non associated plastic potential is employed during a cycle of loading it is possible to recover energy which would otherwise be lost. Although this is unacceptable from a thermodynamic consideration the non associated formulation is still employed in plasticity.

4.2.6 The Hardening Parameter k

A material may be idealised as behaving perfectly plastically when once the yield limit has been reached the material deforms plastically at constant stress. Alternatively it may exhibit a rising stress strain curve in the plastic region. In the latter case the material behaviour is termed work- or strain-hardening.

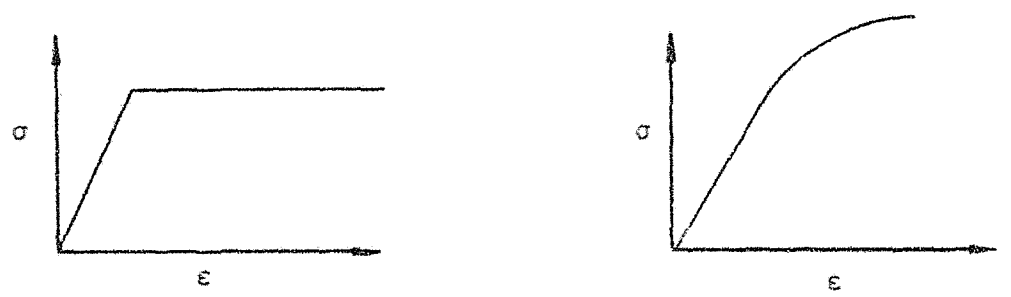

Perfectly plastic (a)

Hardening material (b)

Figure 4.3 - Idealised Material Behaviour

The degree of hardening is calculated in one of two ways. Firstly it may be postulated to be a function of the total plastic work W_p only. Hence the hardening parameter k is interpreted as

$$k = W_p \qquad (4.24)$$

$$k = \int \{\sigma\}^T \{d\varepsilon^p\}$$

This postulate is termed work hardening.

Secondly k may be postulated to represent the total plastic deformation incurred during the loading history. The total plastic deformation is related to the effective or generalised plastic strain which is given by: [13]

$$k = \bar{\varepsilon}_p$$

$$\bar{\varepsilon}_p = \sqrt{\frac{2}{3}\{d\varepsilon^p\}^T\{d\varepsilon^p\}} \qquad (4.25)$$

For the purpose of further discussion k will be calculate cord-ing to the work hardening postulate.

The significance of parameter k is that it provides a means of monitoring the extent of plastic deformation as the yield surface progressively expands. In essence, since k is an experimentally determined function dependent on the plastic properties of the material, it directly relates the theoretical behaviour of the model to experimental observations. This concept is implemented by equating the theoretical increment of work performed during an incremental expansion of the yield surface with the incremental change in k. Since the theoretical work performed is a function of the increment of plastic strain,

$$\{d\varepsilon^p\} = d\lambda\{\frac{\partial Q}{\partial \sigma}\} ,$$

the plastic multiplier $d\lambda$ may be evaluated. This approach is implied in eqn (4.16). In this context parameter A is interpreted as a weighting factor ensuring compliance of the model with the work hardening properties of the material.

4.3 THE DRUCKER-PRAGER MATERIAL MODEL

The elasto plastic stress strain relations for a material conforming to the Drucker-Prager yield criterion were developed for both an

associated and a non associated plastic potential surface. Both models presented were based on the assumption of plane stress and have been implemented successfully in a computer code compatible with the 1981 version of the ADINA programme.

The Drucker-Prager yield criterion as stated in eqn (4.5) is repeated below

$$F(\sigma,k) = \alpha(k)J_1 + J_2^{1/2} - K(k) = 0 \qquad (4.26)$$

This is a more general form where α and K may be dependent in some way on the hardening properties of the surface. It is possible to show that if the parameter α maintains a constant value the yield surface expands isotropically[1] as illustrated in Fig 4.4a.

On the other hand if α is a function of k, then the yield surface expands in an isotropic-kinematic[2] fashion (Fig 4.4b).

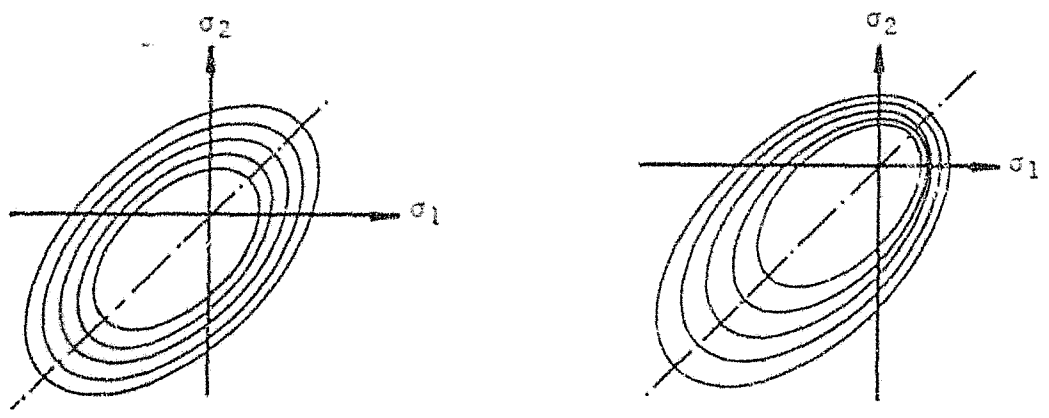

$F(\sigma) = \alpha J_1 + J_2^{1/2} - K(k) = 0$ (a) Isotropic expansion

$F(\sigma) = \alpha(k)J_1 + J_2^{1/2} - K(k) = 0$ (b) Isotropic-kinematic expansion

Figure 4.4 - Alternative Modes of Expansion of the Yield Locus in Plane Stress

---

1. By isotropic it is meant that the yield surface expands gradually and uniformly [22] in all directions as straining proceeds.
2. By kinematic it is meant that the yield surface does not expand but translates as a rigid body. In this context isotropic-kinematic behaviour implies that the yield surface translates along the mean stress axis and simultaneously expands from the initial yield surface to the failure surface [22].

The final computer code incorporates both cases. The more general case is required if the material properties obtained from experiment indicate that the initial yield surface (defined from the values of the yield limit in tension and compression) has a different cone angle to that of the final failure surface (defined by the values of the rupture stress in tension and compression). This case is illustrated in Fig 4.5 below.

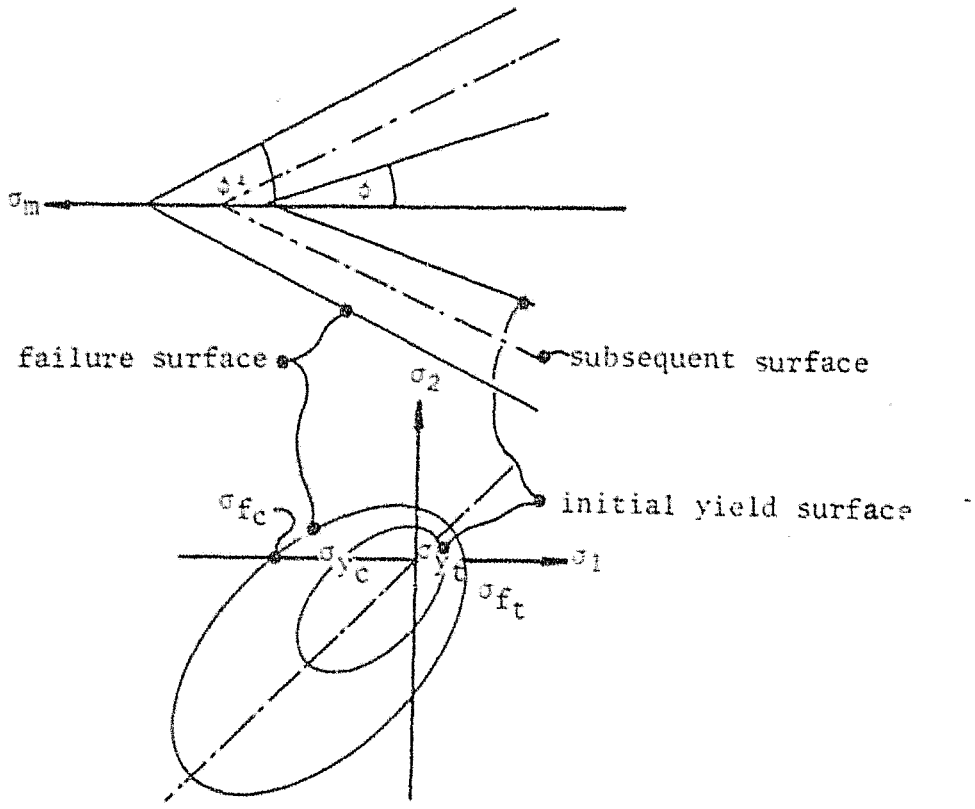

Figure 4.5

4.3.1 The Elasto plastic Matrix

The elasto plastic matrix given by eqn (4.19) defines the elasto plastic response of the material

$$[D_{ep}] = [D] - [D]\{\frac{\partial Q}{\partial \sigma}\}\{\frac{\partial F}{\partial \sigma}\}^T[D]\left[A + \{\frac{\partial F}{\partial \sigma}\}^T[D]\{\frac{\partial Q}{\partial \sigma}\}\right]^{-1}$$

where $F(\sigma,k) = \alpha(k)J_1 + J_2^{1/2} - K(k)$ (4.27)

Q - represents the plastic potential surface

A - as defined in eqn 4.17

$$[D] = \frac{E}{1-\nu^2}\begin{bmatrix} 1 & \nu & 0 \\ \nu & 1 & 0 \\ 0 & 0 & \frac{1-\nu}{2} \end{bmatrix}$$

E - represents the elastic modulus of the material

ν - represents Poisson's ratio

The explicit form of the elastoplastic matrix is obtained from an evaluation of the plastic potential and yield function gradients in the principal stress space. Since the model of the sheave, as discussed in the latter part of Chapter 3, is based on the assumption of plane stress three components of stress and four components of strain are considered. An explicit form of the elastoplastic matrix, for both a non associated (von Mises) and associated plastic potential surface, is presented in Appendix 2.1.

4.3.2 Parameter A

Parameter A has been introduced previously where it was stated that its function is to ensure compliance of the theoretical model with the work hardening properties of the material. The formulation of parameter A is presented in Appendix 2.4 where it is shown that its evaluation depends on the determination of the tangent modulus E_T for each subsequent yield surface.

In order to evaluate the tangent modulus and hence parameter A, which varies continuously as straining proceeds, the stress state was related to a single parameter; The ratio R [1], which defines the current yield surface as illustrated in Fig 4.6. The initial yield surface is defined by $R = 0$, whilst the final surface at fracture

---

1. The derivation of this ratio is presented in Appendix A2.5.

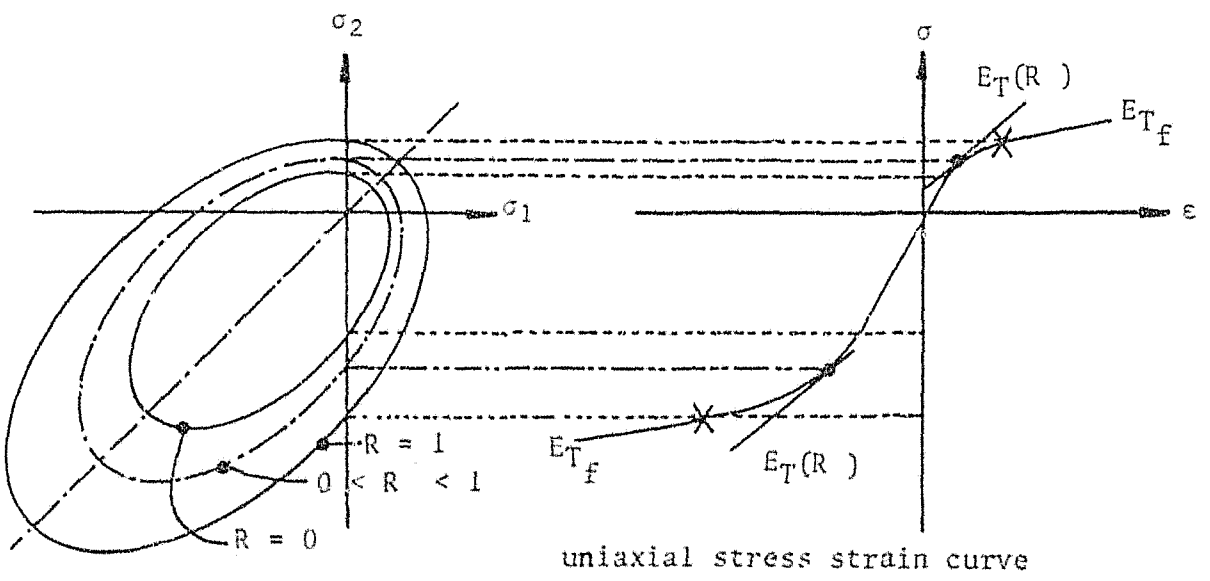

Figure 4.6 - The Dimensionless Ratio R

attains a value of $R = 1$. In the interval $0 < R < 1$ the uniaxial stress is defined by

$$\sigma = f(R) .$$

This made it possible to fit the tangent modulus (determined from uniaxial tension and compression experiments) at any post yield stress state to a single function, $E_T = f(R)$.

To implement the technique outlined above a certain amount of manipulation was required. Essentially the tension part of the curve must be geometrically similar to the compression part as illustrated in Fig 4.6.

4.4 IMPLEMENTATION OF THE DRUCKER-PRAGER CONSTITUTIVE RELATIONS

The ADINA finite element package has the facility to incorporate a user supplied material model applicable to two-dimensional solid elements. This facility enables the user to model the nonlinear properties of materials which cannot be adequately represented by

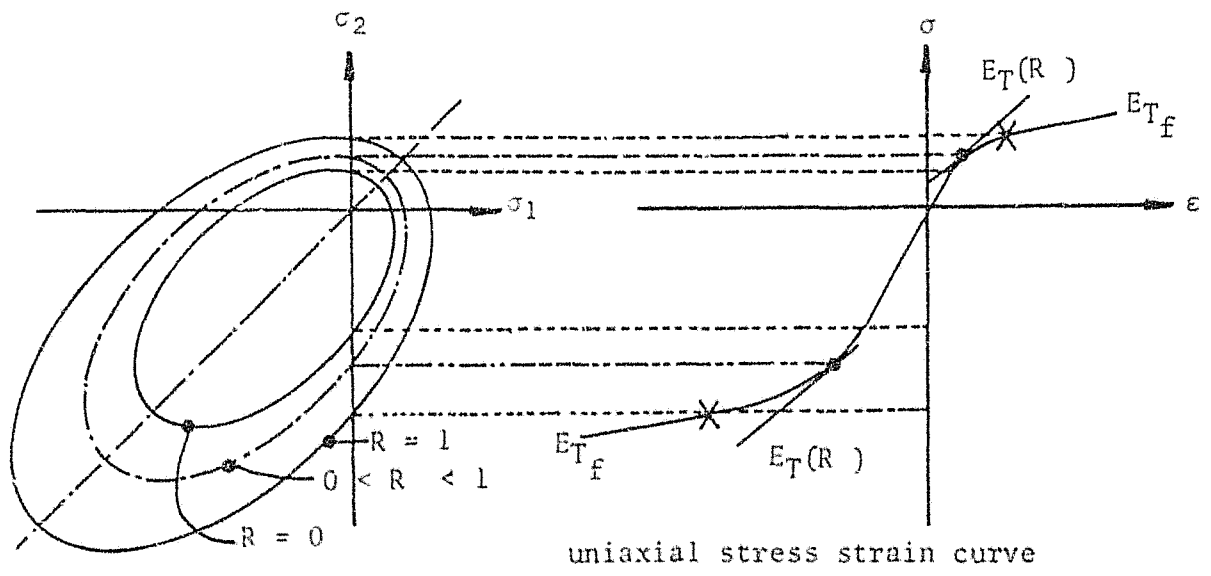

Figure 4.6 - The Dimensionless Ratio R

attains a value of $R = 1$. In the interval $0 < R < 1$ the uniaxial stress is defined by

$$\sigma = f(R) .$$

This made it possible to fit the tangent modulus (determined from uniaxial tension and compression experiments) at any post yield stress state to a single function, $E_T = f(R)$.

To implement the technique outlined above a certain amount of manipulation was required. Essentially the tension part of the curve must be geometrically similar to the compression part as illustrated in Fig 4.6.

4.4 IMPLEMENTATION OF THE DRUCKER-PRAGER CONSTITUTIVE RELATIONS

The ADINA finite element package has the facility to incorporate a user supplied material model applicable to two-dimensional solid elements. This facility enables the user to model the nonlinear properties of materials which cannot be adequately represented by

the standard models available in the ADINA two-dimensional solid element library.

An insight into the function of the material model may be obtained by reviewing the options available in the package for the solution of elastoplastic problems. Three techniques are employed which are briefly outlined in the following section.

4.4.1 Procedures Employed in the Solution of Elastoplastic Problems

The finite element method applied to elasticity problems results in a set of linear simultaneous equations of the form

$$[K]\{a\} + \{f\} = 0 \qquad (4.28)$$

In the linear region these equations can be solved directly to obtain an approximation to the unknown nodal displacements $\{a\}$. In the post yield region however the stress strain relationship is non linear and hence the stiffness of the material varies continuously as the applied loads increase. This results in the stiffness matrix being dependent in some way on the displacements $\{a\}$, and their derivatives. The governing equations become nonlinear and are generally of the form

$$\psi(a) = [K(a)]\{a\} + \{f\} \qquad (4.29)$$

where $\psi(a)$ represents the residual load vector.

The equations are theoretically satisfied once the residual load vector $\psi(a) = 0$. Owing to the method of formulating the stiffness matrix it is not possible to determine explicitly the dependence of the stiffness coefficient matrix on the nodal displacements, ie $[K(a)]$ and hence an iterative procedure is employed. In essence these procedures linearise and solve the governing equations (eqn 4.29) repetitively by maintaining a constant stiffness

coefficient matrix[1] over each iterative interval, until the residual load vector $\psi(a)$ is within an acceptable tolerance.

In order to evaluate the residual load vector for the purpose of tracking solution convergence a technique termed 'stress transfer' [1] is applied. This technique transforms eqn (4.29) into a form whereby $\psi(a)$ may be determined explicitly during the iterative procedure, ie

$$\psi_n(a) = \{P(a^n)\} + \{f\} \tag{4.30}$$

where $\{P(a^n)\}$ represents the equivalent nodal loads required to balance the actual stresses generated within the element by the nodal displacements $\{a\}^n$, calculated up to iteration n.

$\psi_n(a)$ represents the discrepancy between the external load vector $\{f\}$, and the load vector $\{P(a^n)\}$ which would in practice generate the actual stresses within the element.

In this context eqn (4.30) represents the requirement of equilibrium between the external load vector $\{f\}$ and the internal stress state which is only satisfied when $\psi_n(a) = 0$. By treating the total stress induced in the element during iteration n in an analagous manner to distributed loads $\{P(a^n)\}$ may be evaluated, ie

$$\{P(a^n)\} = \int_V [B]^T \{\sigma^n\} dV \tag{4.31}$$

whilst the total stress incurred up to iteration n, $\{\sigma^n\}$ may be calculated by integrating the constitutive stress strain relations in an accumulative fashion for each iterative interval, ie

$$\{d\sigma\} = [D_{ep}]\{d\varepsilon\}$$

Thus the total stress at the end of iteration n is given by

---

1. The evaluation of the constant coefficient matrix employed during the iterative process is dependent on the particular technique applied as discussed in Section 4.4.2 - 4.4.4.

$$\{\sigma_1^n\} = \left[\int_{\{\varepsilon^{n-1}\}}^{\{\varepsilon^n\}} [D_{ep}]\{d\varepsilon\} \right] + \{\sigma^{n-1}\} \qquad (4.32)$$

This concept is illustrated diagramatically in Fig 4.7 .

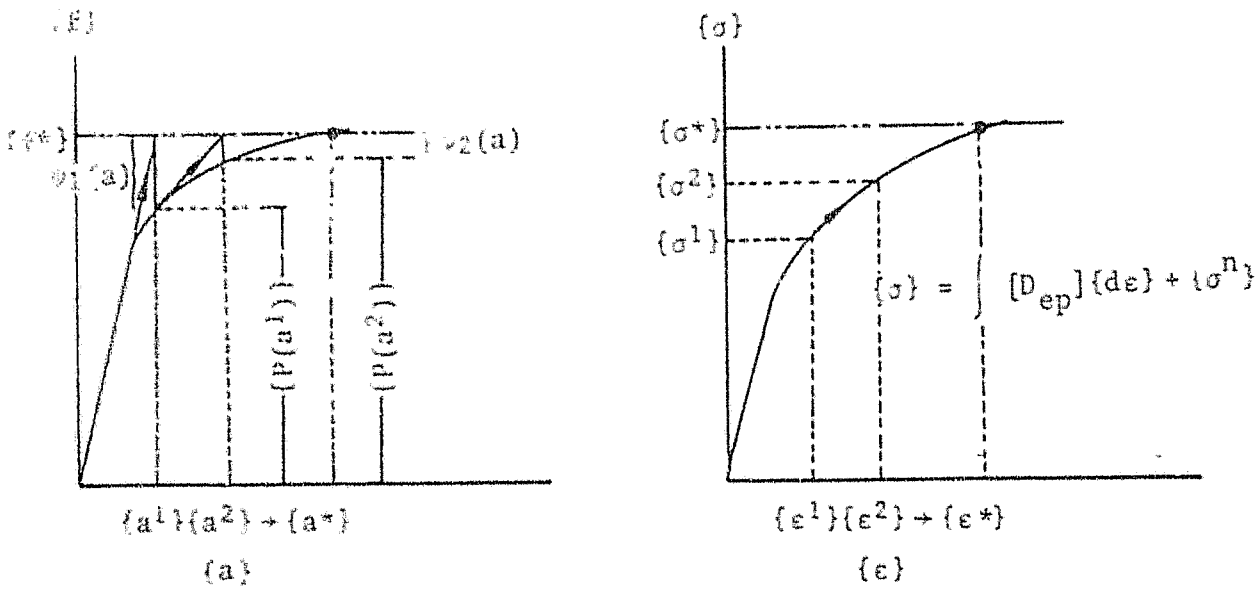

$\{f^*\}$ represents the external load vector

$\{a^*\}$, $\{\varepsilon^*\}$, $\{\sigma^*\}$ represents the converged solution

Figure 4.7 - A Graphical Representation of an Iterative Scheme Employed in the Solution of Non-Linear Problems

A flow chart illustrating the overall solution procedure is presented in Fig 4.9 at the end of this section.

4.4.2 The Newton Raphson Method

If an approximate solution to eqn (4.29) is available, $\{a\} = \{a\}^n$, for which $\psi(a^n) \neq 0$, then an improved estimate $\{a\}^{n+1}$ can be found by means of a curtailed Taylor series expansion about $\psi(a^{n+1})$

$$\psi(a^{n+1}) = \psi(a^n) + \left(\frac{d\psi}{da}\right)_n \Delta a^n = 0 \qquad (4.33)$$

where the superscript n, n+1 refers to the nth or $(n+1)^{th}$ iteration.

The improved estimate is given by

$$\{a\}^{n+1} = \{a\}^n + \{\Delta a\}^n$$

where

$$\{\Delta a\}^n = -\left(\frac{d\psi}{da}\right)_n^{-1} \psi(a^n) \qquad (4.34)$$

and

$$\left(\frac{d\psi}{da}\right)_n = [K]_T^n \qquad (4.35)$$

$[K]_T^n$ represents the tangent stiffness matrix for the nth iteration. It is shown in [1], that the tangent stiffness may be calculated at any step in the solution by substituting the current value of $[D_{ep}]$ for $[D]$ when evaluating the stiffness coefficients.

Thus

$$[K] = \int_V [B]^T [D][B] dV \qquad (4.36)$$

$$[K]_T^n = \int_V [B]^T [D_{ep}][B] dV \ .$$

4.4.3 The Modified Newton Raphson Method

In the previous method the tangent stiffness matrix is reformulated at each stage of iteration and consequently a complete factorisation of the stiffness matrix is necessary for each iteration. In order to reduce the computational effort involved in this approach, the

linear elastic stiffness matrix is substituted for the tangent stiffness matrix in eqn (4.35). Thus

$$\{\Delta a\}^n = -([K]_T^0)^{-1} \psi(a^n) \qquad (4.37)$$

The Newton Raphson, Modified Newton Raphson techniques applied to plasticity problems are termed the tangent and initial stiffness methods respectively. Although the tangent stiffness matrix results in a more rapid convergence, the initial stiffness method may provide an overall economy of solution. [1]

It is important to note that the modified Newton Raphson technique is the only method capable of attaining a solution to non associated plasticity problems [1].

4.4.4 The BFGS Matrix Update Method, [3]

The BFGS technique belongs to a class of methods known as matrix update or quasi-newton methods. These methods seek to refine the existing stiffness coefficient matrix (without having to formulate the tangential stiffness matrix explicitly) to provide a secant approximation from iteration n to n+1 . The technique operates on the increments of displacement as well as the increment of the residual load vector during iteration n to n+1 , in order to refine the stiffness coefficient matrix by means of a matrix multiplication. This technique is well documented in the literature [3]. The three methods presented are illustrated in Fig 4.8 on the next page.

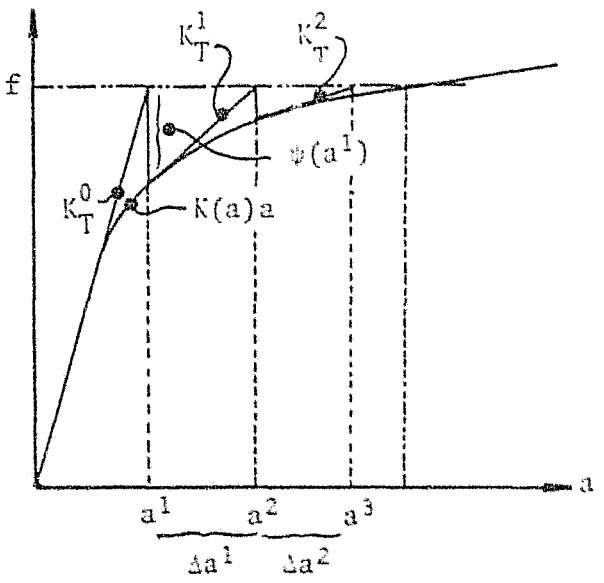

Tangent Stiffness Method

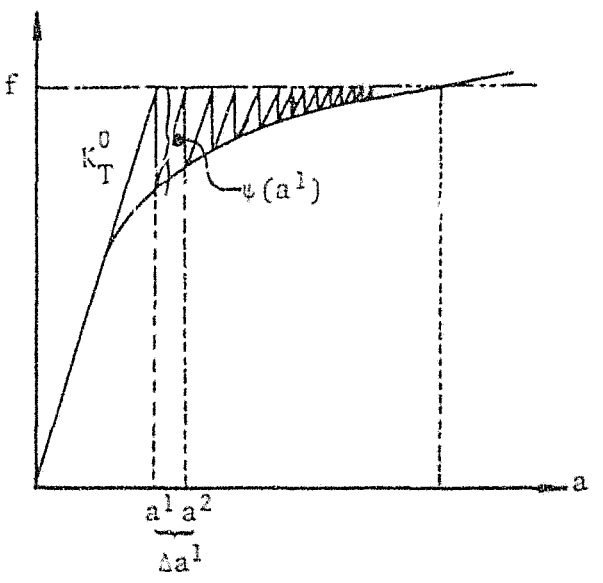

Initial Stiffness Method

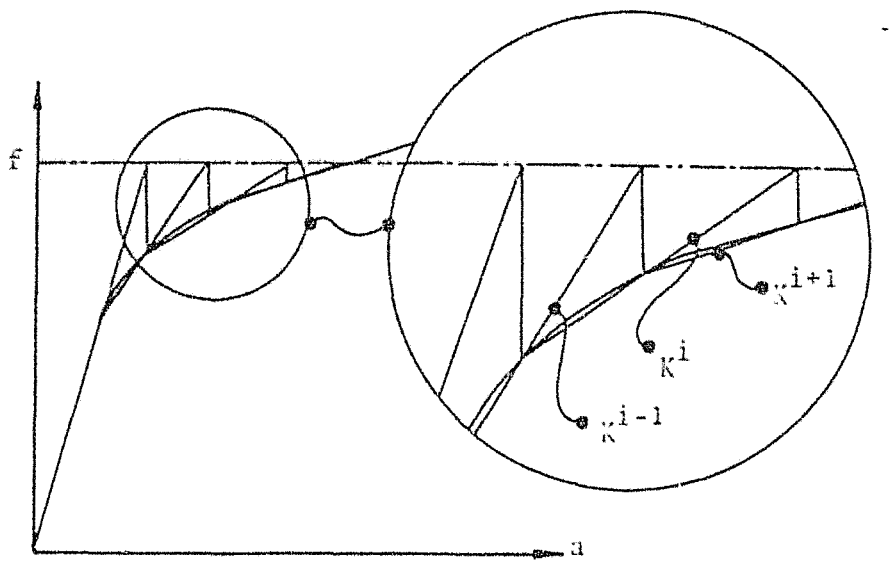

The BFGS Method

Figure 4.8 - Iterative Schemes Available in the ADINA Library

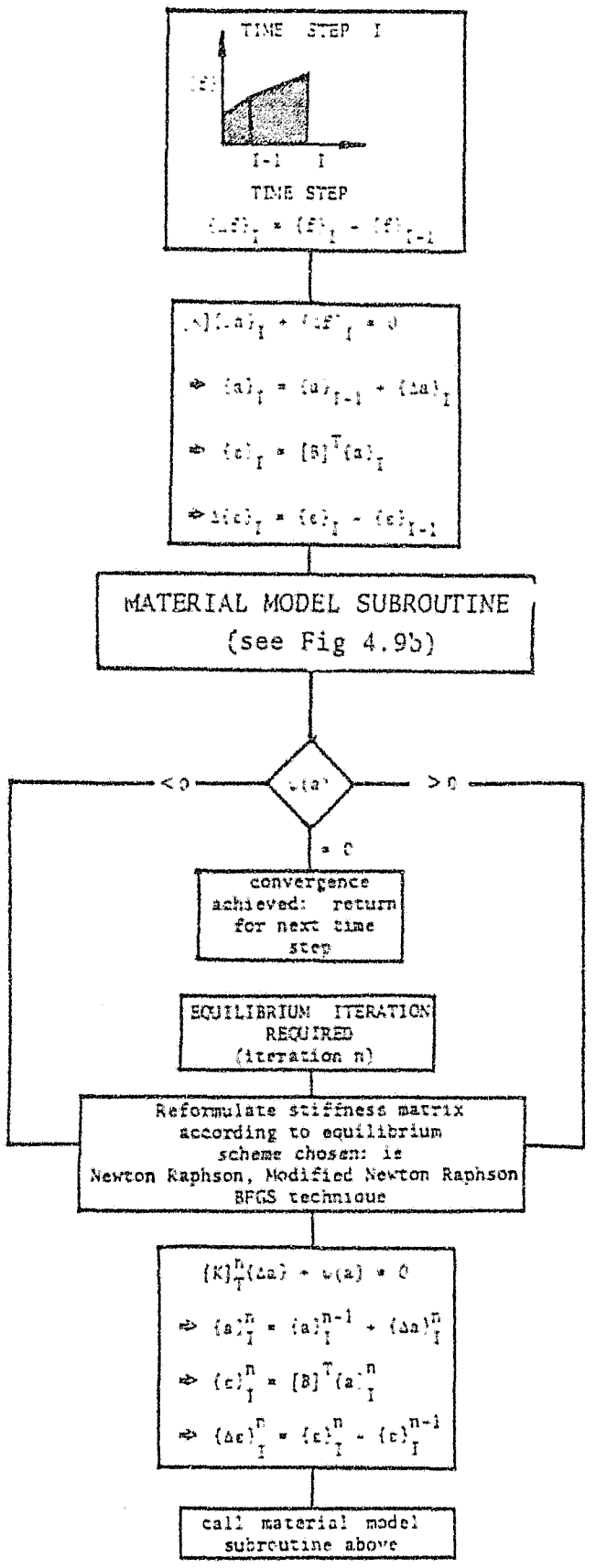

Figure 4.9 - Flow Chart of Elasto Plastic Solution Prodecures

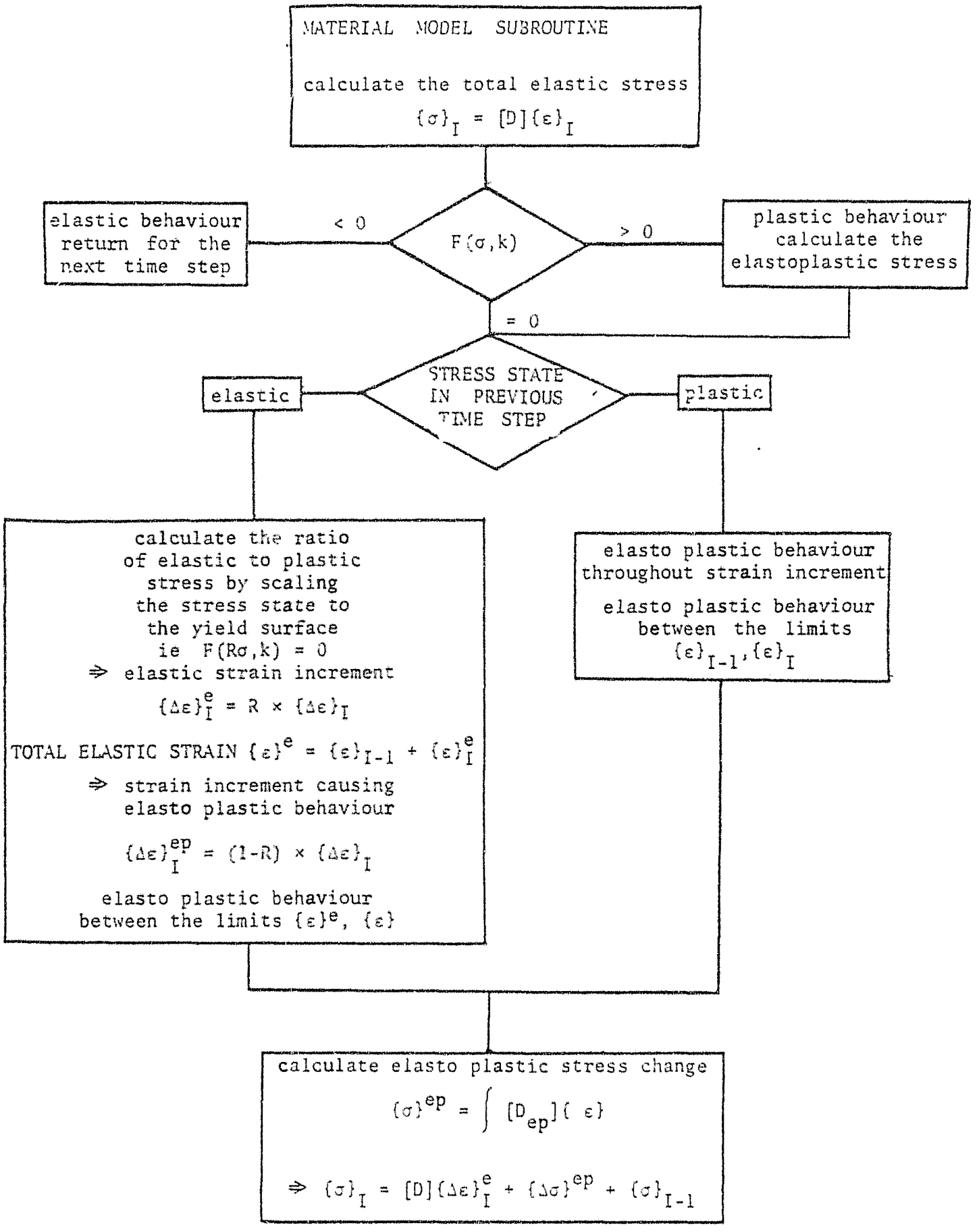

Figure 4.9b - Material Model Subroutine

4.5 FINITE ELEMENT SIMULATION OF THE UNIAXIAL BEHAVIOUR OF CAST IRON

A uniaxial tension/compression test was simulated by loading the surface of a single plane stress two-dimensional element with a compressive/tensile pressure load. This verified that the subroutine was operating correctly and provided a means of comparing the material model behaviour with experimentally observed results.

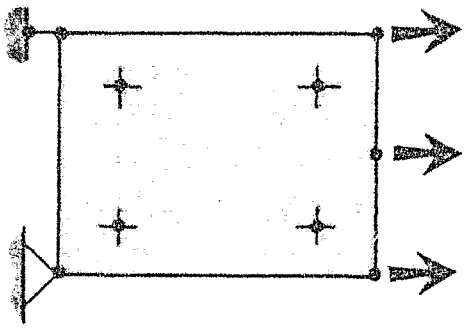

Figure 4.10 - Five Noded 2-D Plane Stress Element 2 x 2 Gaussian Integration

Before executing this simulation the material properties of the cast iron, as determined from the experimental tests, were manipulated so as to evaluate the parameters[1] required by the material model. It was decided to select these parameters on the basis of the results obtained from tensile test 3 and compression test 2 since these specimens were machined from the sheave in question.

The procedure for selecting these parameters relies on manipulating the yield surface and failure surface parameters so as to obtain a single function describing the tangent modulus at any uniaxial tensile/compression stress state. This procedure is summarised in point form below:

- select the yield limit in tension; (R = 0)

---

1. The material parameters required by the model are presented with a detailed flow chart of the subroutine in Appendix 3.

- select the yield limit in compression; (R = 0)
- evaluate Young's modulus between these limits
- select the failure stress in tension; (R = 1)
- calculate the tangent modulus at the tensile failure stress defined above
- select the failure stress in compression on the basis that the tangent modulus should correspond to that defined at the tensile failure stress
- evaluate the parameters, α_y, K_y, α_f, K_f, which define yield and failure surfaces
- employ these parameters to map the tangent moduli obtained from the tension/compression tests on a graph of E_T versus R. (The method of calculating R is presented in Appendix 2.)
- if it is possible to fit a single curve $E_T = f(R)$ through the data, then satisfactory parameters have been selected.

The material parameters selected are listed below; these were employed in all subsequent analyses.

- tensile yield stress 60 MPa
- ultimate tensile stress 222 MPa
- compressive yield stress -120 MPa
- compressive failure stress -340 MPa
- Young's modulus 95 GPa
- yield surface parameters

  $\alpha_y = 0,192\ 45$

  $K_y = 46,188$
- failure surface parameters

  $\alpha_f = 0,121\ 223$

  $K_f = 155,083$
- the function selected for the purpose of describing the tangent modulus is illustrated in Plot 4.1.

- select the yield limit in compression; (R = 0)
- evaluate Young's modulus between these limits
- select the failure stress in tension; (R = 1)
- calculate the tangent modulus at the tensile failure stress defined above
- select the failure stress in compression on the basis that the tangent modulus should correspond to that defined at the tensile failure stress
- evaluate the parameters, α_y, K_y, α_f, K_f, which define yield and failure surfaces
- employ these parameters to map the tangent moduli obtained from the tension/compression tests on a graph of E_T versus R. (The method of calculating R is presented in Appendix 2.)
- if it is possible to fit a single curve $E_T = f(R)$ through the data, then satisfactory parameters have been selected.

The material parameters selected are listed below; these were employed in all subsequent analyses.

- tensile yield stress 60 MPa
- ultimate tensile stress 222 MPa
- compressive yield stress -120 MPa
- compressive failure stress -340 MPa
- Young's modulus 95 GPa
- yield surface parameters

  $\alpha_y = 0,192\ 45$

  $K_y = 46,188$
- failure surface parameters

  $\alpha_f = 0,121\ 223$

  $K_f = 155,083$
- the function selected for the purpose of describing the tangent modulus is illustrated in Plot 4.1.

The simulated uniaxial tension/compression behaviour of the material conforming to both an associated and non associated material law is illustrated in Plots 4.2 and 4.3.

The results of this analysis indicate that the uniaxial behaviour of the cast iron is adequately modelled. The essential difference between the associated and non associated formulation is apparent in Plots 4.4 and 4.5 where volumetric strain effects are considered.

The associated material law characterises the cast iron material better, but not accurately (the volumetric strain is under evaluated in tension and over evaluated in compression). In view of the relationship between the volumetric strain component and the inclination of the plastic strain rate vector to the potential surface, it is likely that a parabaloid potential surface would characterise the volumetric behaviour of the material more accurately.

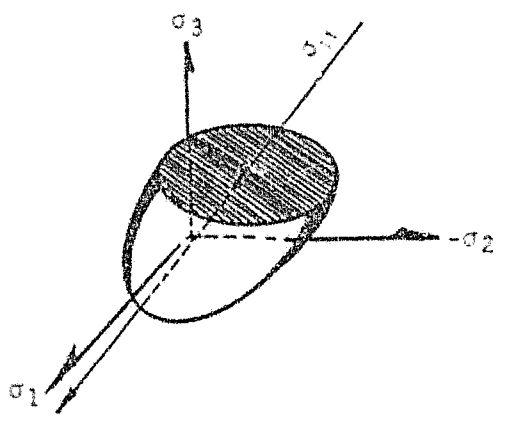

Figure 4.11 - Parabaloid Plastic Potential Surface

It was decided that a redevelopment of the constitutive laws based on a parabaloid plastic potential surface would be beyond the purpose of this dissertation. However an attempt was made to define a non associated Drucker Prager plastic potential surface requiring minor modifications to the subroutine. This was unsuccessful but for the sake of completeness the concept is presented in Appendix 2.7.

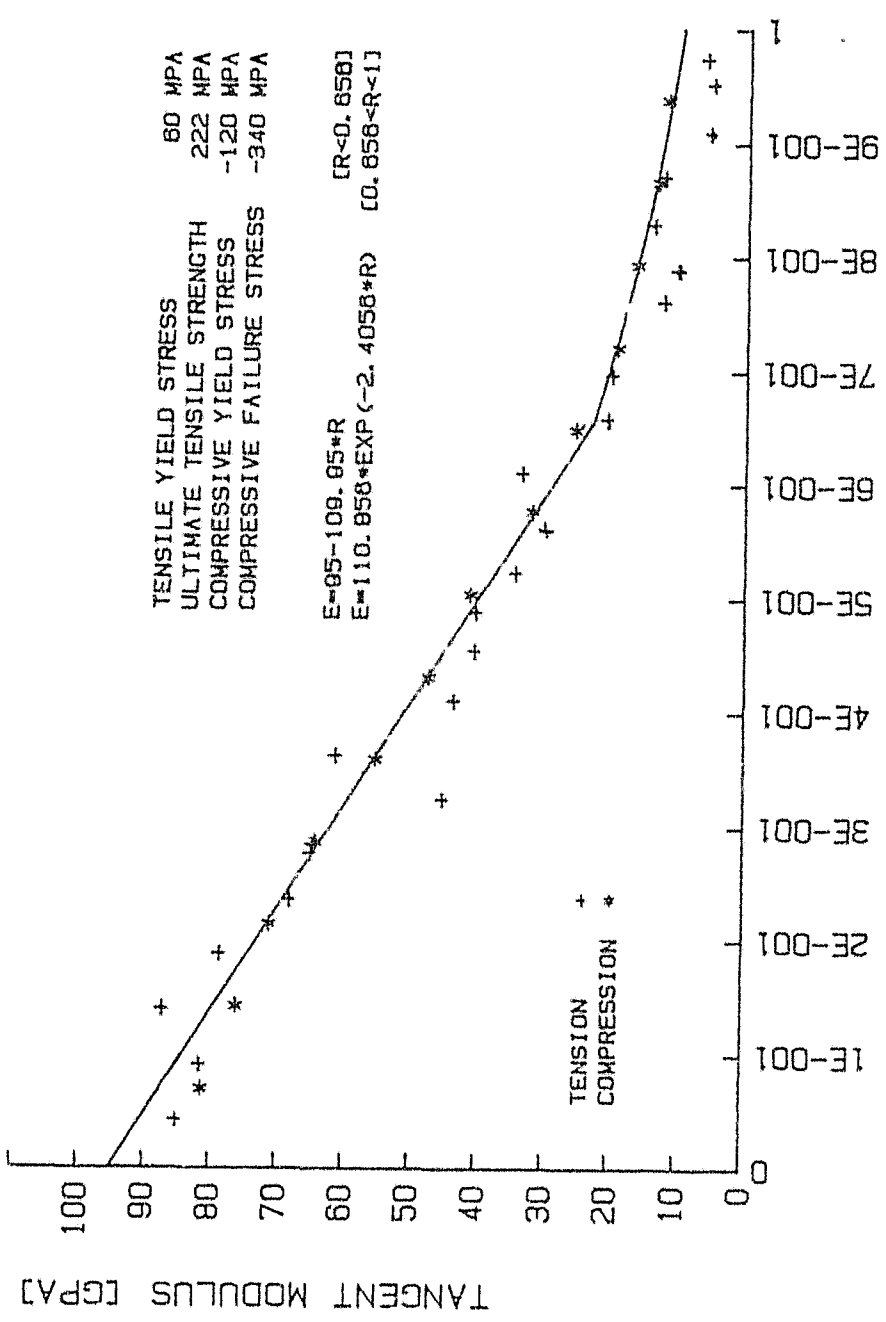

PLOT 4.1 - Specification of the Tangent Modulus as a Function of the Stress Ratio R

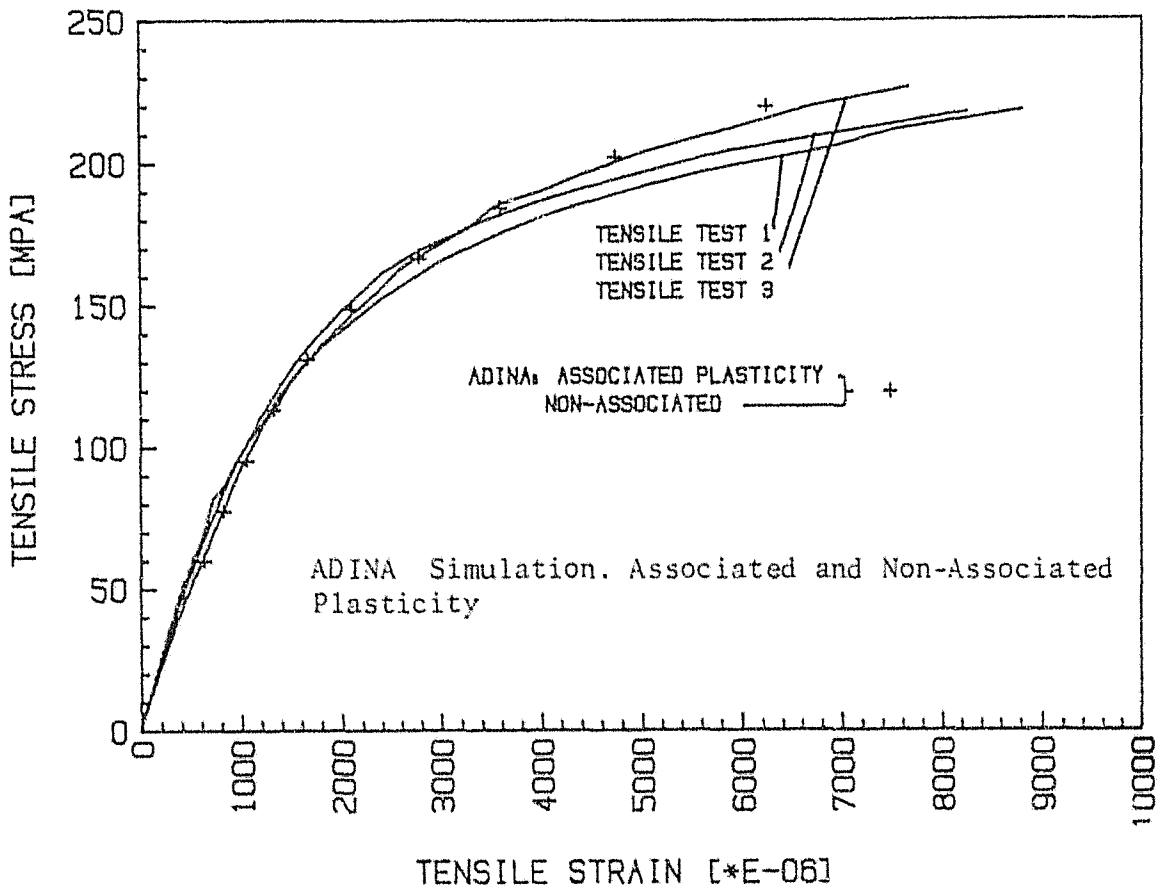

Plot 4.2 - Uniaxial Tension

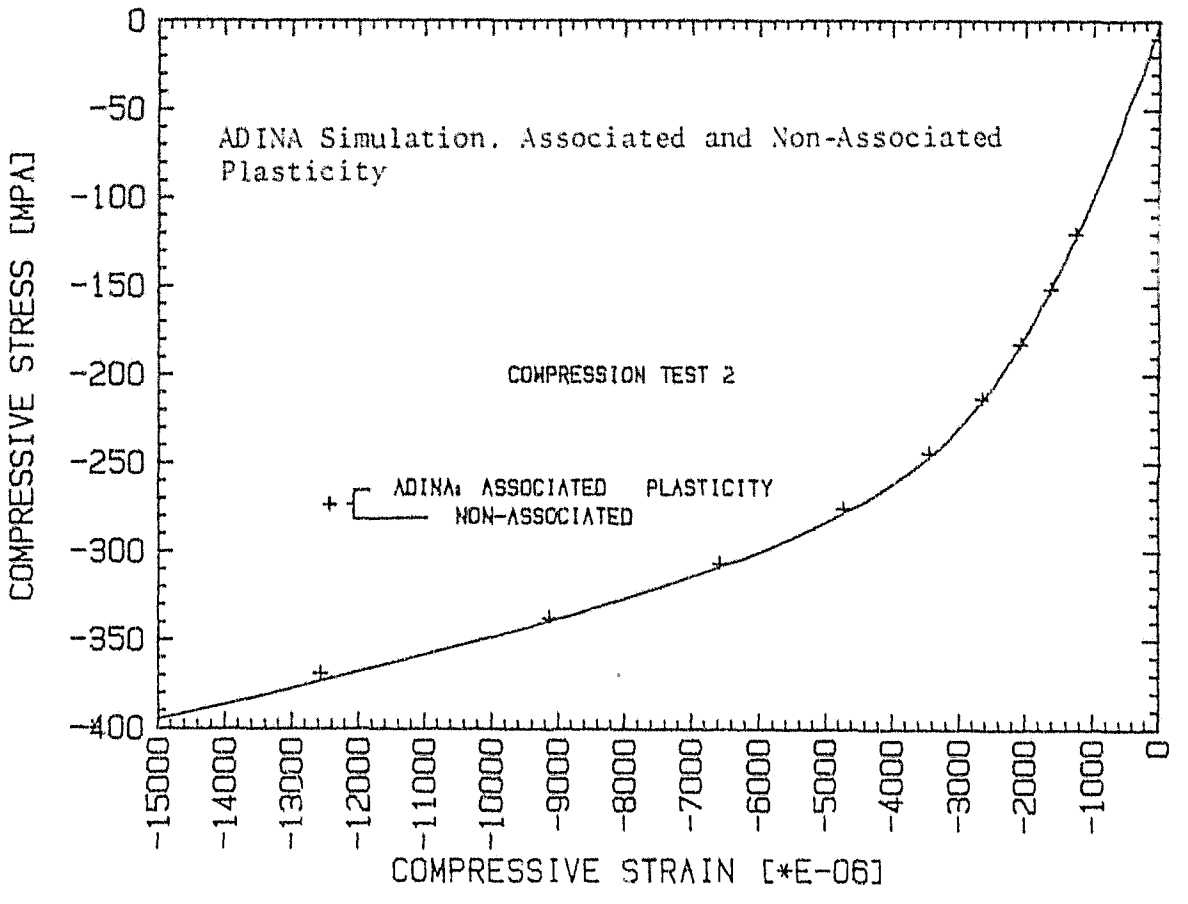

Plot 4.3 - Uniaxial Compression

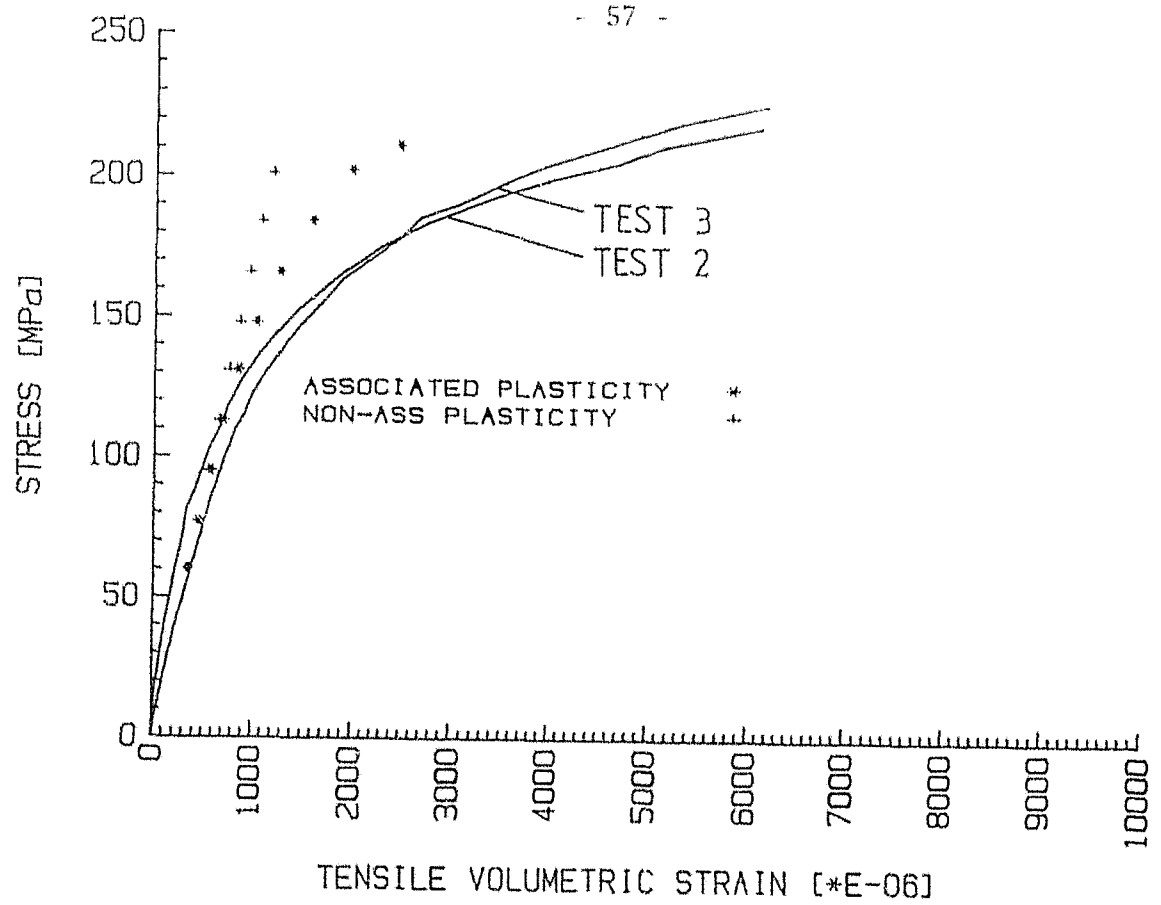

Plot 4.4 - Tensile Volumetric Strain

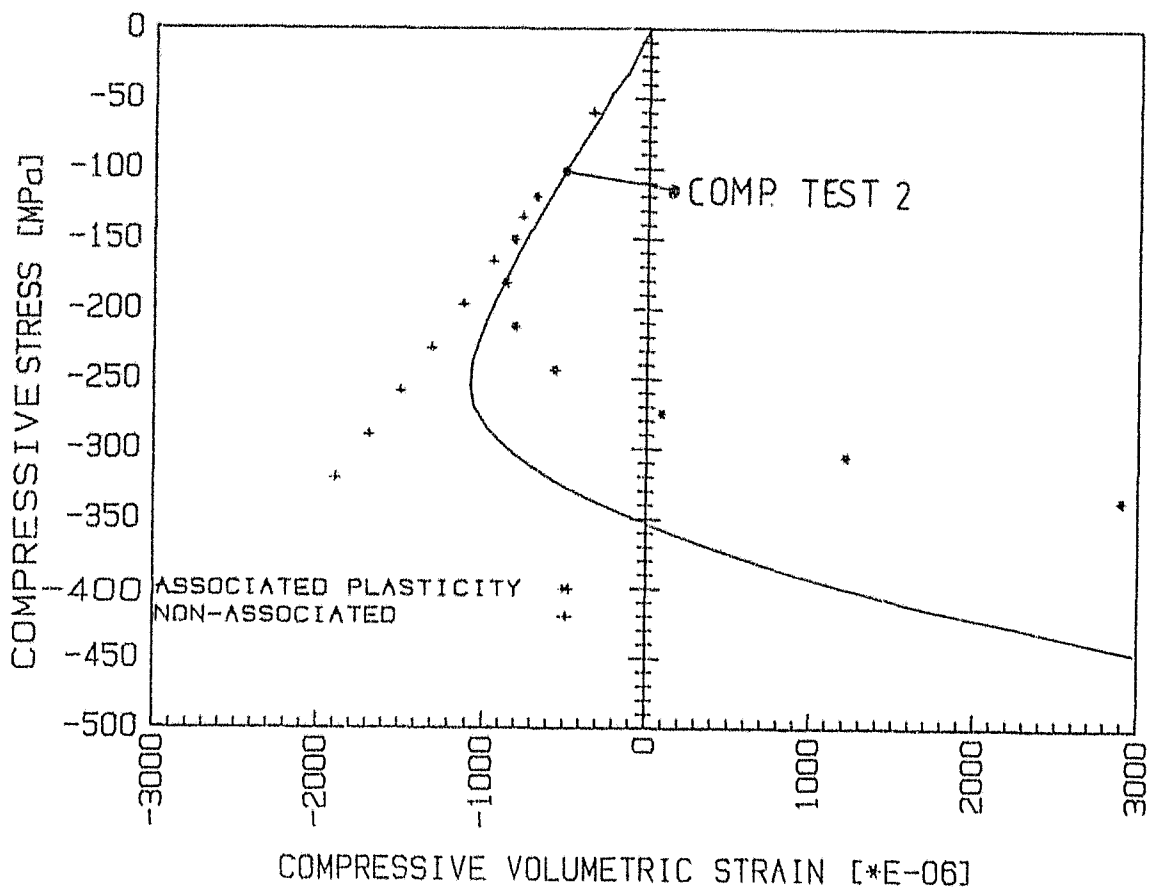

Plot 4.5 - Compressive Volumetric Strain

4.6 CONCLUDING REMARKS

4.6.1 Material Modeling

Bilinear or trilinear variations in the tangent modulus are commonly employed to model the uniaxial stress strain characteristics of a material as depicted in Fig 4.6. The ratio R was employed to model this variation more accurately, although this was achieved for the uniaxial stress strain behaviour (see Plot 4.2, 4.3) new difficulties became apparent when comparing dilatency in tension and compression, which limits the accuracy of the model

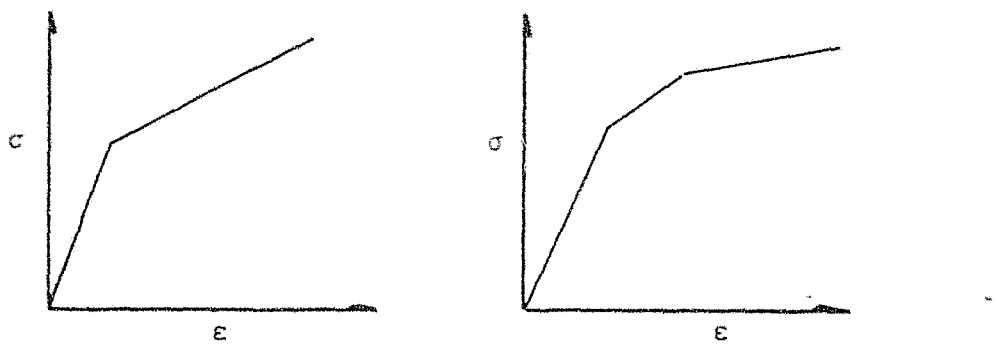

Figure 4.12 - Techniques of modelling the tangent modulus

4.6.2 Subroutine

Although the user supplied material model is a listed option available in the ADINA package, difficulties were experienced when attempting to utilise the option.

- The source program contained statements preventing the user from erroneously defining such an option. This difficulty was overcome by deleting these statements and recompiling the source program.
- Information regarding the operation of such a model in the context of the ADINA program, is scarce. This necessitated a study of similar material models in the ADINA source, ie material model 7

(elastoplastic, Drucker-Prager yield criterion with a hardening cap and tension cut-off); Material Model 8 (elastoplastic, von Mises yield criterion, isotropic hardening), in order to define arrays and variables common to the source program, which facilitate data transfer during solution. More information regarding these requirements and the structure of the subroutine would reduce the effort and the time required to utilise this option.

This exercise provided an introduction to the basic concepts of plasticity as well as finite element techniques employed in the solution to elastoplastic problems. In addition an overall view of the structure of the ADINA source was obtained through the implementation of the elastoplastic relations derived.

CHAPTER 5

TWO-DIMENSIONAL SOLID ELEMENT ANALYSIS OF THE SHEAVE

5.1 INTRODUCTION

The preliminary study of the sheave initiated in Chapter 3 was extended by applying the nonlinear constitutive stress/strain relationship, developed in the previous chapter, so that a more comprehensive analysis of the sheave could be executed.

An experimental study of the sheave behaviour when loaded to failure was undertaken for the purpose of comparison with the finite element simulation. In the experiment electrical resistance strain gauges were mounted at significant positions on the sheave, monitoring the strain incurred when the sheave was loaded to failure. These readings enabled the overall effectiveness of the finite element simulation to be evaluated.

5.2 EXPERIMENTAL PROCEDURE

The sheave had been machined in accordance to the dimensions specified in Chapter 3. The dimensions are illustrated in Appendix 4.3. The sheave was mounted on a shaft and then placed on a pedestal. In order to apply a rope load a special loading rig (see Fig 3.1) was inserted between the upper and lower platens of an Amsler compression testing machine. The upper platen and hence the loading rig was raised and the assembly of the sheave and pedestal inserted. Before testing commenced the loading rig was lowered and the alignment of the loading rig with the sheave was checked. This arrangement is illustrated in Plates 5.1 and 5.2.

Twenty four electrical resistance strain gauges were mounted at positions on the sheave as illustrated in Fig 5.1. From this figure it can be seen that pairs of gauges were placed on either side of the outer rim. The reason for this was to ascertain whether asymmetrical loading occurred during the test. The gauges were connected to Wheatstone bridges excited by a constant voltage source. Dummy gauges were included in the bridges to compensate for changes in temperature. The output voltage from each bridge was monitored by Esterline[1] Angus data loggers.

On a headgear and under steady running conditions the rope is fully tensioned on contact with the sheave and little friction or creep is present. Since the test performed in the experiment was concerned with the static response of the sheave, pre-tension does not exist in the rope and considerable friction may develop between the rope and the tread of the sheave as the load is increased. This was obviated by ringing a series of brass strips along the length of the rope and using grease liberally prior to testing.

The purpose of the analysis undertaken in Chapter 3 was to select the dimensions of the rim section of the sheave. The sheave was remachined in accordance to these specifications and failure was expected to occur in the 400 KN range. Hence a range from 0 - 500 KN was selected on the Amsler testing machine. However at the maximum load of 500 KN, failure had not occurred. Subsequently the sheave was unloaded; on reloading, in the 0 - 1 000 KN range, failure occurred at 680 KN (see Plate 5.3). This corresponds to a rope tension of 402,26 KN.

---

1. Since each data logger provides a twenty channel facility, two instruments were employed.

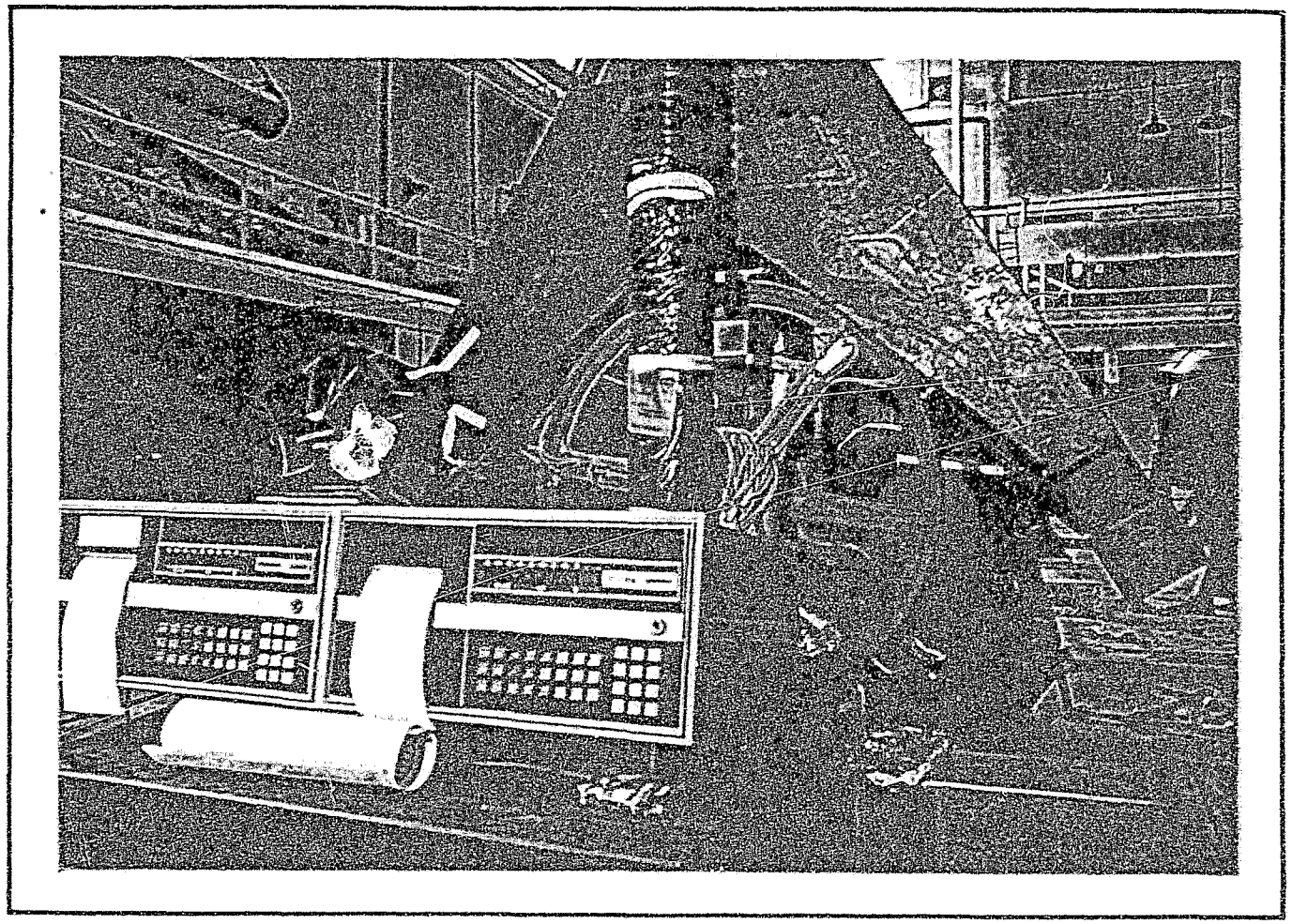

Plate 5.1 - The sheave mounted in the loading rig (Esterline Angus data loggers in lower left corner)

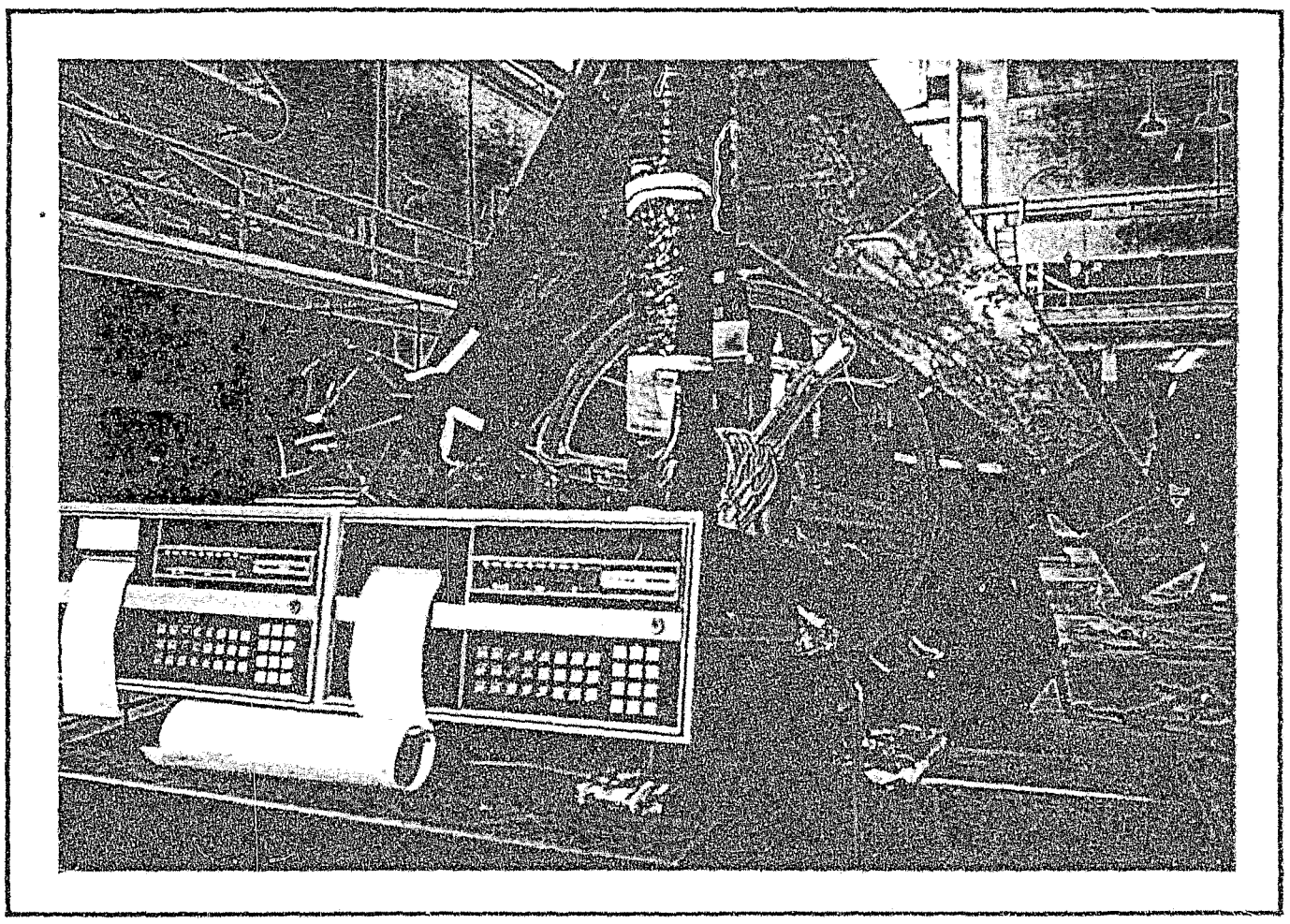

Plate 5.1 The sheave mounted in the loading rig (Esterline Angus data loggers in lower left corner)

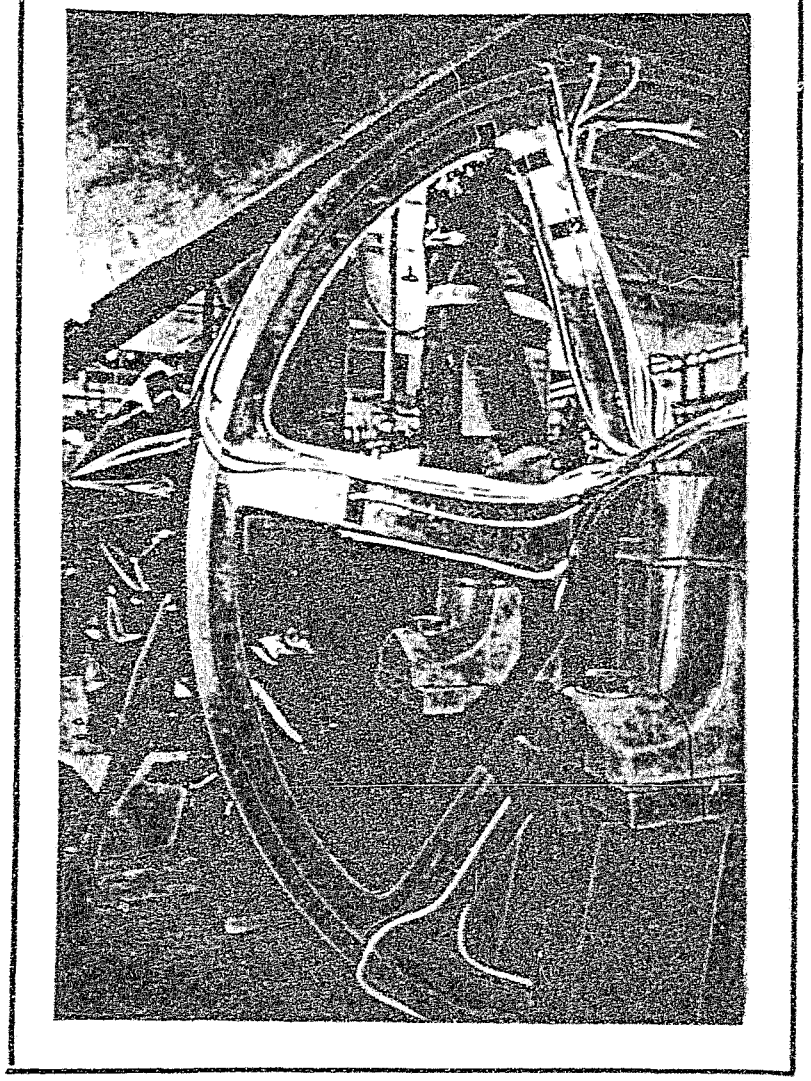

Plate 5.2 - The sheave mounted on the pedistal

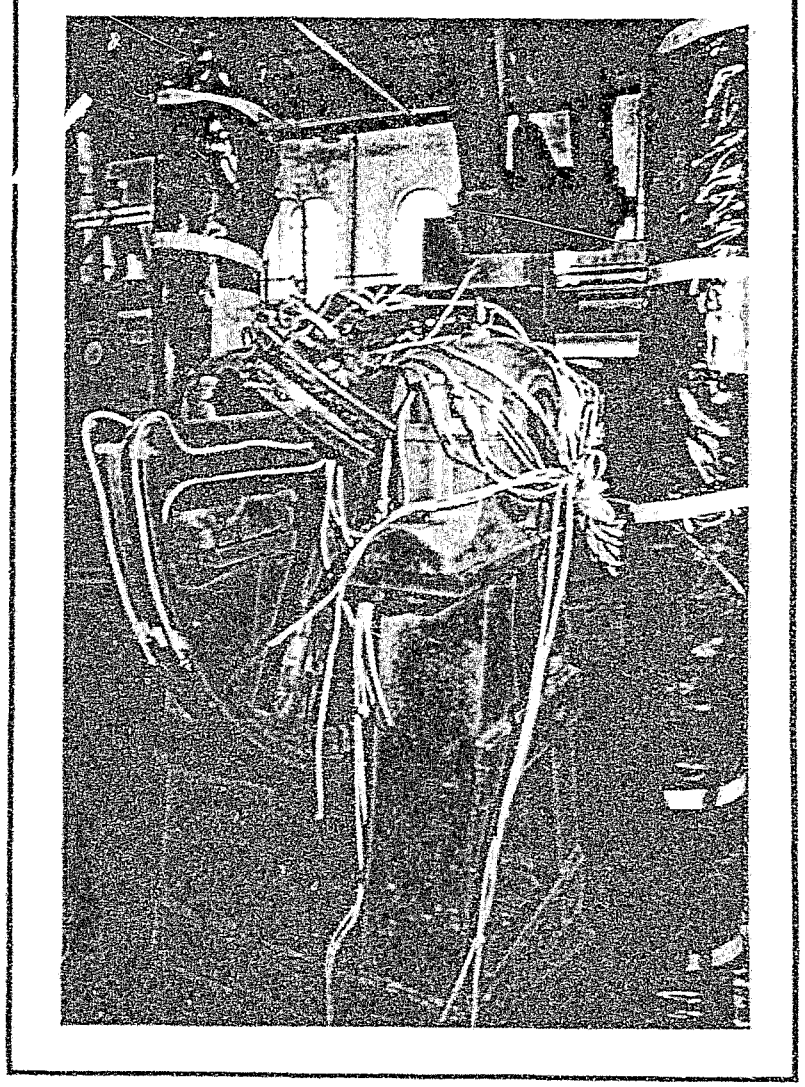

Plate 5.3 - The sheave after the destructive test

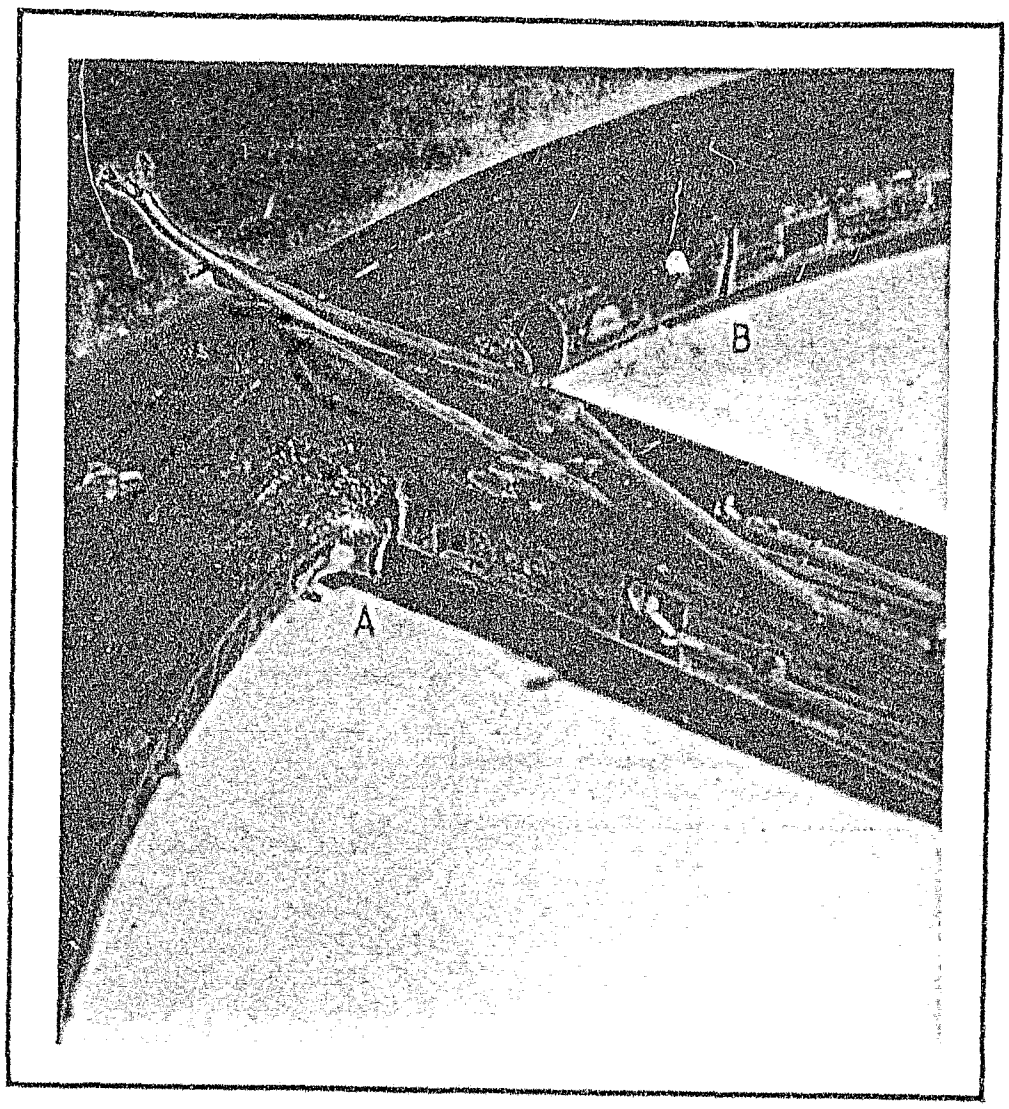

PLATE 5.4 - Primary and Secondary Failure of the Rim Section

A - primary failure B - secondary failure

Author Constancon C P
Name of thesis A study of the finite element method, with reference to the Adina finite element package 1983

PUBLISHER:
University of the Witwatersrand, Johannesburg
©2013

LEGAL NOTICES:

Copyright Notice: All materials on the University of the Witwatersrand, Johannesburg Library website are protected by South African copyright law and may not be distributed, transmitted, displayed, or otherwise published in any format, without the prior written permission of the copyright owner.

Disclaimer and Terms of Use: Provided that you maintain all copyright and other notices contained therein, you may download material (one machine readable copy and one print copy per page) for your personal and/or educational non-commercial use only.

The University of the Witwatersrand, Johannesburg, is not responsible for any errors or omissions and excludes any and all liability for any errors in or omissions from the information on the Library website.

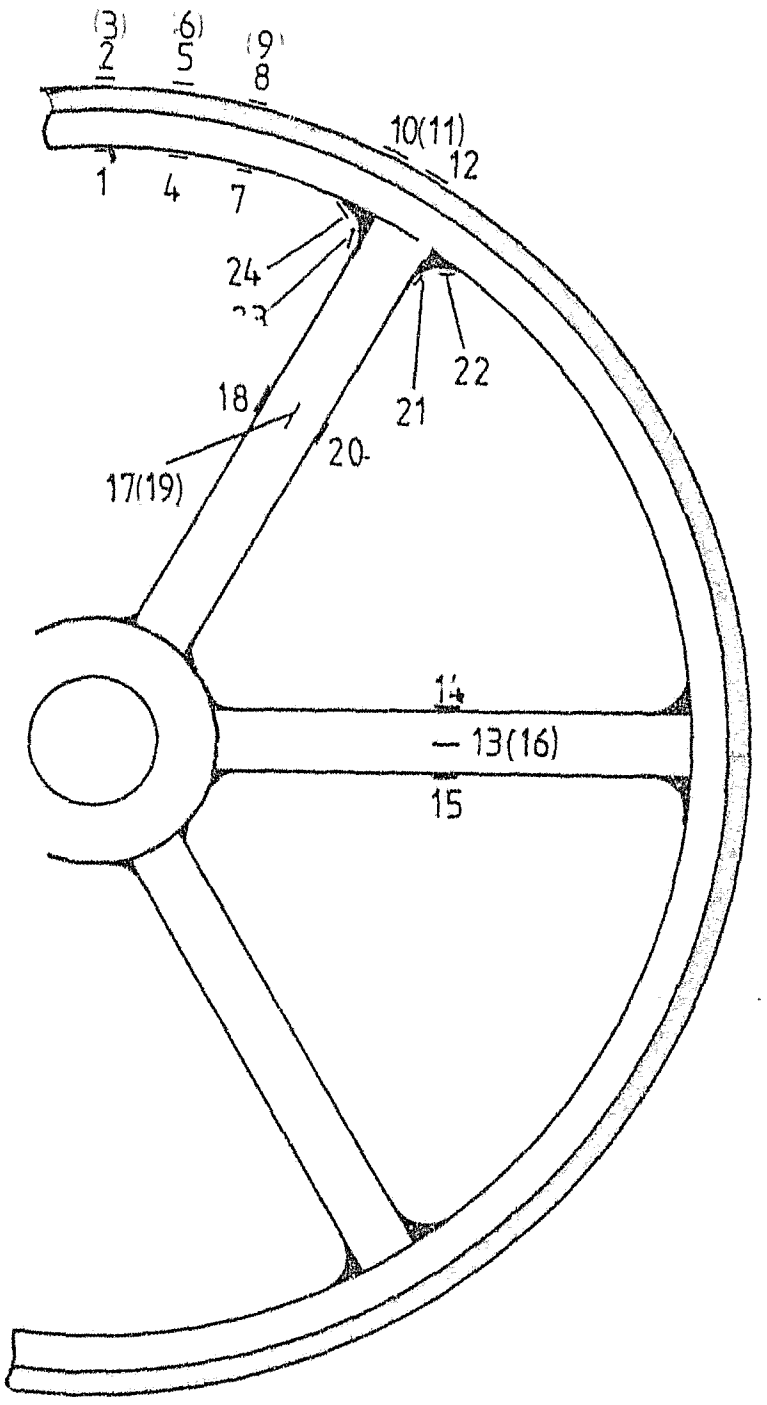

Figure 5.1 - Strain Gauge Locations

The positions of the gauges on the sheave are shown on Fig A4.6, in Appendix 4.

NB: Where a single number is shown, the gauge is in the central plane of symmetry of the sheave. Where two numbers are shown, two gauges lie in positions symmetrical about that central plane, the number in brackets denoting the gauge at the back.

5.2.1 Experimental Results

Two sets of readings were taken: the first set corresponded to those taken in the 0 - 500 KN range and the second corresponded to those taken in the 0 - 1 000 KN range.

In the first set only the first nine gauges were monitored owing to an electrical fault in the remaining bridges.

After correcting the fault and resetting the range (0 - 1 000 KN) the entire set of gauges were monitored up to rim failure.

The mode of fracture was brittle fracture which appeared simultaneously at the centre of arc and at the junction of the rim to the spoke. After further examination it was evident that other fractures were caused by secondary effects. Fig 5.2 illustrates areas where the rim and spokes fractured.

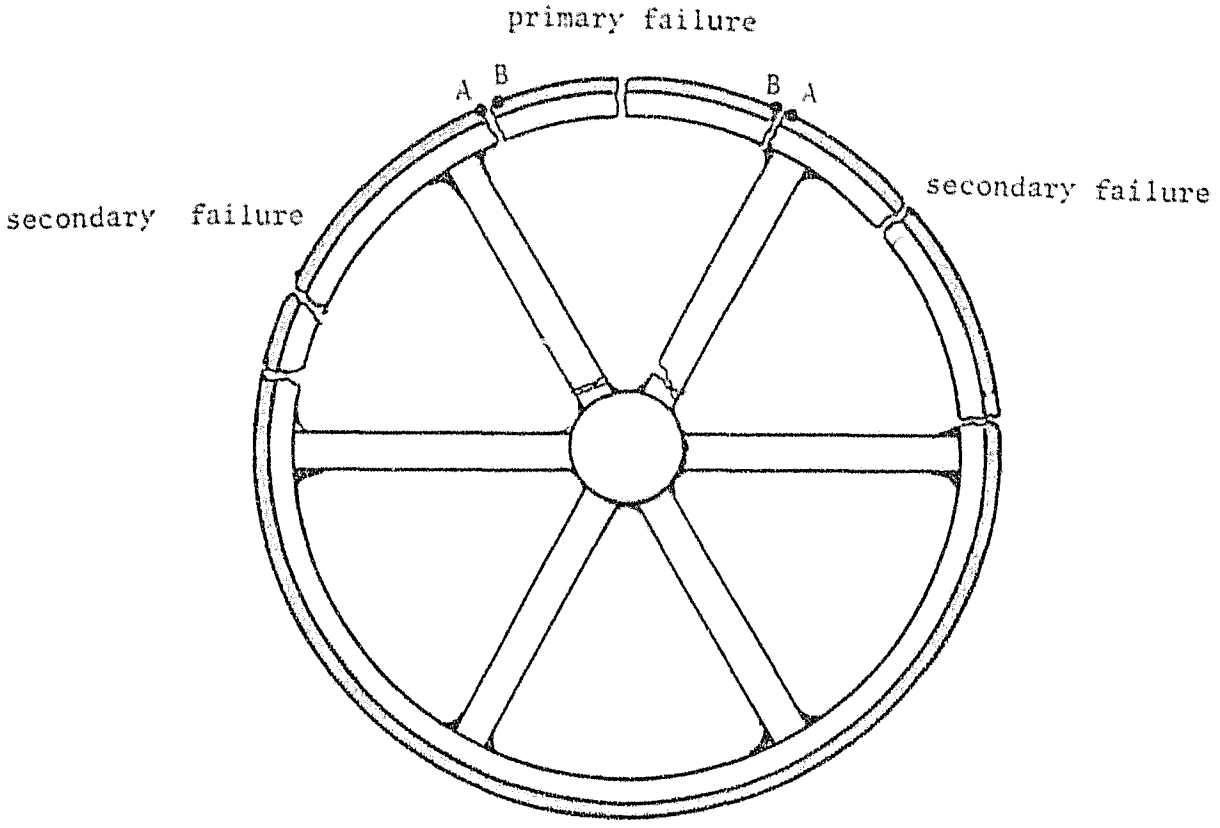

Figure 5.2 - Primary and Secondary Areas of Fracture of the Sheave

Experimental verification of the second mode of failure was based on circumstantial evidence. The tread at position A on the lower failure surface was striated by the rope, however, the tread on the upper surface was unmarked (position B). This leads to the conclusion that the sector BB of the rim failed before other fractures occurred. These secondary fractures were caused by the impact of the rope and loading frame immediately after the primary failure. The failed sheave is illustrated in Plate 5.3 whilst the failure at the junction of the spoke to the rim and the secondary failure, are illustrated in Plate 5.4.

The experimental results from the two sets of loadings are tabulated in Tables 5.1 and 5.2.

5.3 FINITE ELEMENT SIMULATION

It was decided to simulate a realistic situation by introducing self imposed limitations of time and money. Accordingly the sheave was simplified by treating it as a two-dimensional body. To further conserve on computational costs the sheave was modelled by two sets of elements. Two-dimensional plane[1] stress elements of varying thickness were utilised in areas where plastic behaviour was expected. The constitutive stress/strain relation derived in the previous chapter was applied to these elements. In the remaining areas, where linear behaviour was expected, beam elements were utilised.

Two simulations were executed. The first accounted for the assumption of a non associated plastic potential gradient thus implying plastic incompressibility. Further investigation revealed that the material dilates plastically under applied stresses (see Appendix 1) and

---

1. The plane stress option was selected since the stress through the thickness of the rim is likely to be negligible with respect to the in-plane stresses.

Experimental verification of the second mode of failure was based on circumstantial evidence. The tread at position A on the lower failure surface was striated by the rope, however, the tread on the upper surface was unmarked (position B). This leads to the conclusion that the sector BB of the rim failed before other fractures occurred. These secondary fractures were caused by the impact of the rope and loading frame immediately after the primary failure. The failed sheave is illustrated in Plate 5.3 whilst the failure at the junction of the spoke to the rim and the secondary failure, are illustrated in Plate 5.4.

The experimental results from the two sets of loadings are tabulated in Tables 5.1 and 5.2.

5.3 FINITE ELEMENT SIMULATION

It was decided to simulate a realistic situation by introducing self imposed limitations of time and money. Accordingly the sheave was simplified by treating it as a two-dimensional body. To further conserve on computational costs the sheave was modelled by two sets of elements. Two-dimensional plane[1] stress elements of varying thickness were utilised in areas where plastic behaviour was expected. The constitutive stress/strain relation derived in the previous chapter was applied to these elements. In the remaining areas, where linear behaviour was expected, beam elements were utilised.

Two simulations were executed. The first accounted for the assumption of a non associated plastic potential gradient thus implying plastic incompressibility. Further investigation revealed that the material dilates plastically under applied stresses (see Appendix 1) and

---

1. The plane stress option was selected since the stress through the thickness of the rim is likely to be negligible with respect to the in-plane stresses.

subsequently an associated plastic potential gradient was applied in the second simulation.

In both analyses the load was applied in seven equal steps with equilibrium iteration allowed in each. The magnitude of each step coincided with that of a 100 KN machine load which corresponds to nearly 62 KN of rope tension. In the simulation which applied the non associated f rmulation the initial stress method (the modified Newton-Raphson technique) was used to achieve a solution, whilst for the associated formulation, a BFGS matrix update technique was selected.

In both analyses a gaussian integration order of 3 × 3 was specified. Although it is common practise to underintegrate the stiffness coefficients in problems pertaining to linear elasticity to achieve an artificial convergence, the higher integration order is more acceptable since it enables a more accurate tracking of the plastic growth, [2].

5.3.1 The finite element mesh

The sheave was treated as a plane body loaded in its plane by a uniform compressive radial load over a 108° arc of contact. A symmetrical half was modelled as shown in Fig 5.3.

Plastic behaviour was expected under the arc of contact and the two-dimensional elements were employed in this region. Beam elements were employed to model the sheave rim and spokes in the remaining portions of the sheave.

In areas where two-dimensional elements were utilised, the rim section was simulated by elements of differing thickness as

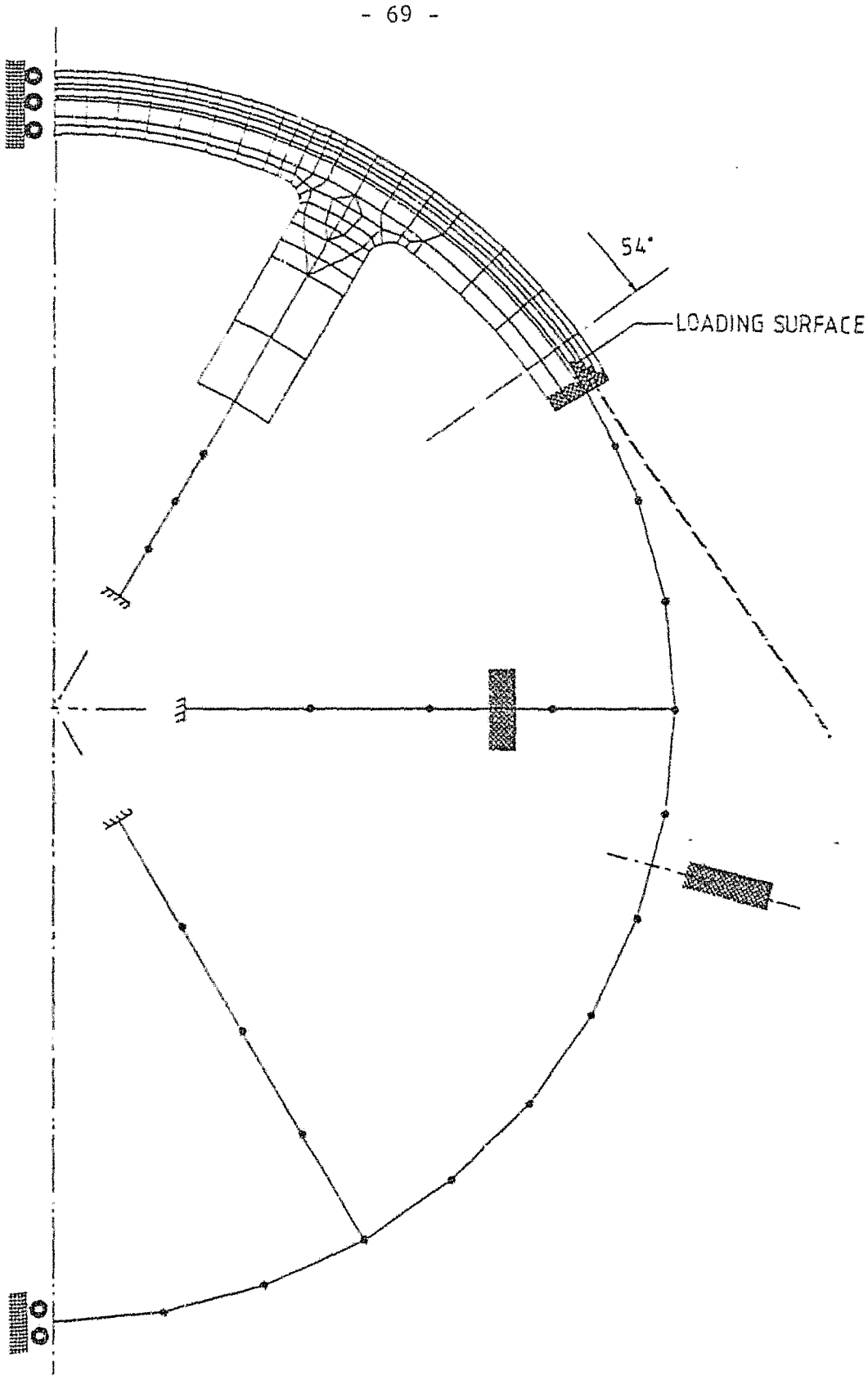

Fig 5.3 - Finite element mesh

illustrated in Fig 5.4. Originally six elements were used to model the varying thickness of the rim. Poor results were obtained and eight elements were used in the final mesh. The dimension of the eight elements are presented in Appendix 4.4

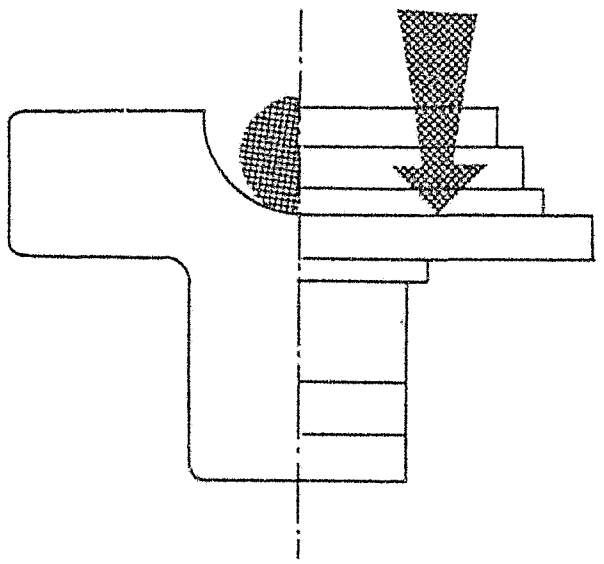

Figure 5.4 - FEM Idealisation of the Rim Profile

In areas where beam elements were utilised they were specified as having a rectangular section which accounted for the depth and second moment of area of the actual section modelled. The spokes could be accurately modelled owing to their naturally rectangular properties. In the case of the rim section, the depth and second moment of area were considered of primary importance since significant stresses generated are likely to be caused by bending effects.

Compatibility was achieved at the transition between the two sets of elements by defining displacement constraint equations.

At the boundaries of the sheave the spokes were fixed rigidly to the hub, whilst the nodes lying on the plane of symmetry were allowed one degree of freedom in the vertical direction.

5.4 FINITE ELEMENT RESULTS

The finite element results extracted from the two analyses pertain to those positions corresponding to the area modelled by the two-dimensional elements. The output results from the two-dimensional elements was obtained in terms of both stress and strain at the integration points. For the purpose of comparison with experimental values, the results for the two-dimensional elements were considered more significant than those obtained from the beam elements.

Since the strain results output are in terms of global coordinate axes, ie ε_y , ε_z , these were converted to radial and tangential coordinates applicable to the particular guage location for the purpose of direct comparison. The technique employed in this conversion is documented in Appendix 4.6.

The growth of the plastic zone for the non associated simulation is illustrated in Fig 5.5. Regions exhibited plastic behaviour at a low load where high bending stresses were expected: At the centre of the loaded arc of the rim and at the fillet junction to the spoke. The growth of the plastic zone in the spoke implies inaccuracy in the model since the beam element beyond section X has a linear behaviour. Nevertheless the maximum stress at X at the rope tension of 371 KN is less than 200 MPa compressive, and the tangent modulus has not decreased substantially below that of the elastic modulus. Hence this is not viewed as a major fault.

Region Y in this figure is a region of contraflexure where the shear force is sufficiently high to cause plastic flow at the neutral axis. A close examination of the output results indicate a state of almost pure shear in this area.

The displacements corresponding to a rope tension of 124 KN are illustrated in Fig 5.6 and conform to the expected pattern. No significant change was noticeable in the pattern of the deformations at high loads.

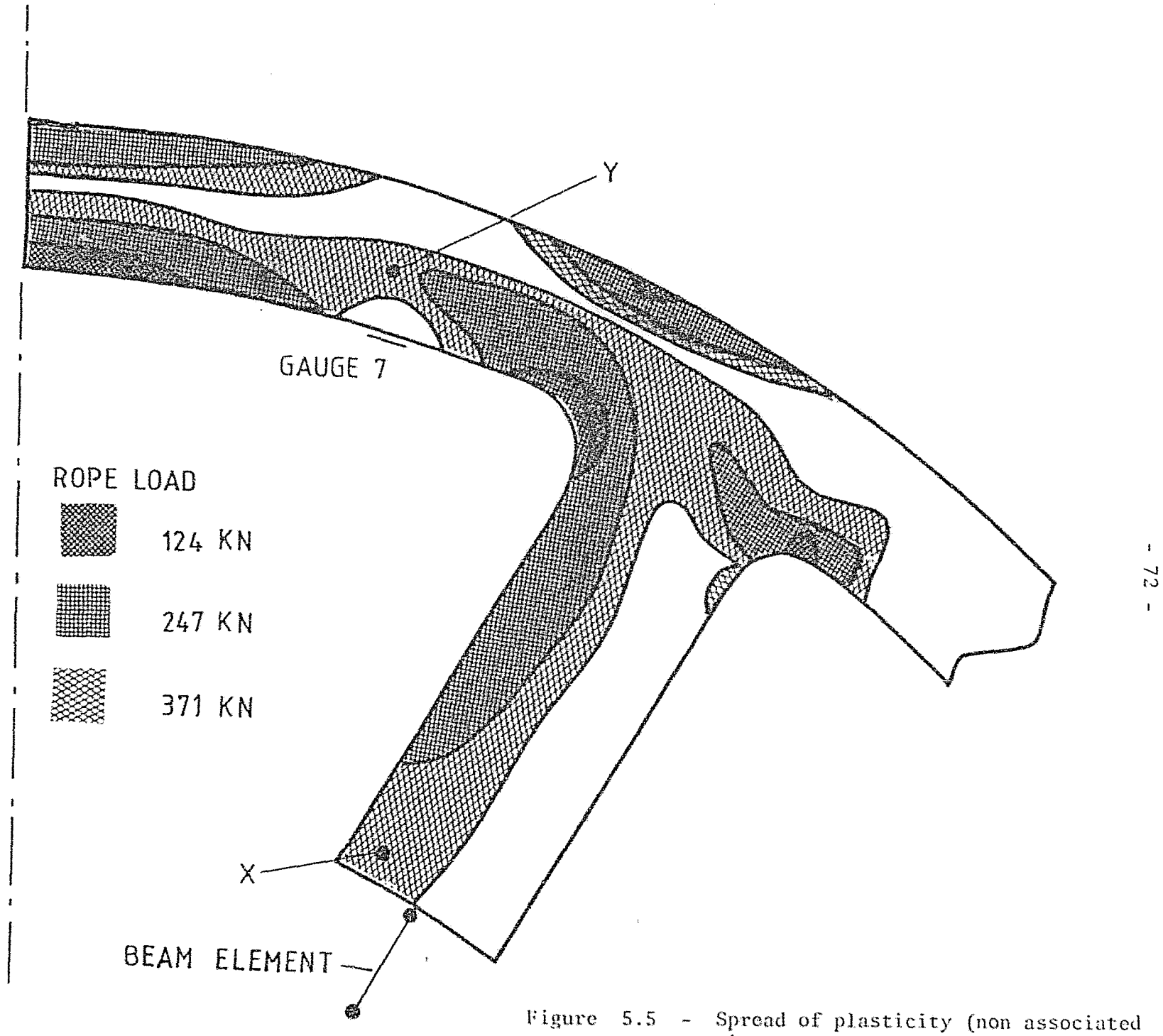

Figure 5.5 - Spread of plasticity (non associated simulation)

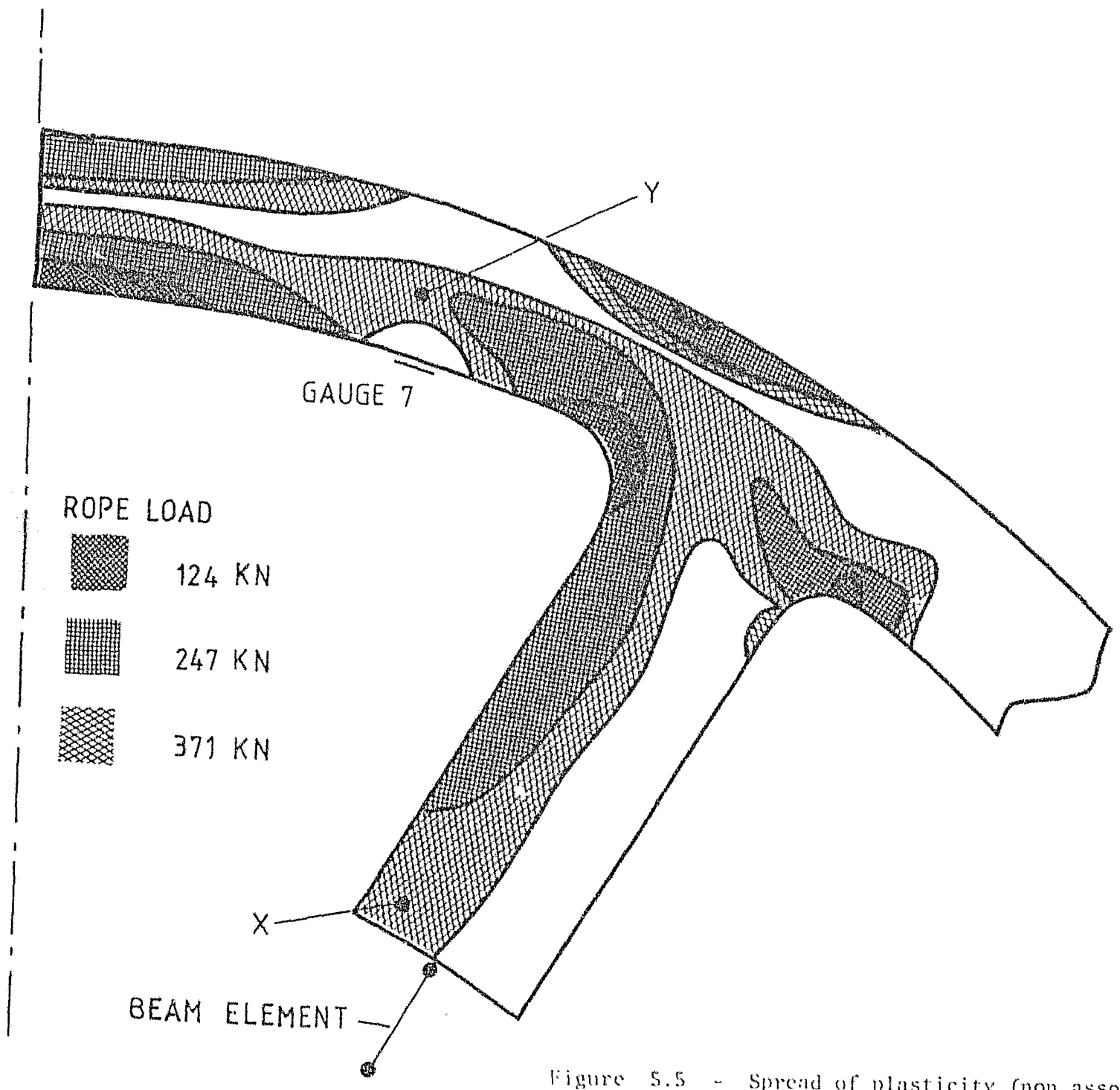

Figure 5.5 - Spread of plasticity (non associated simulation)

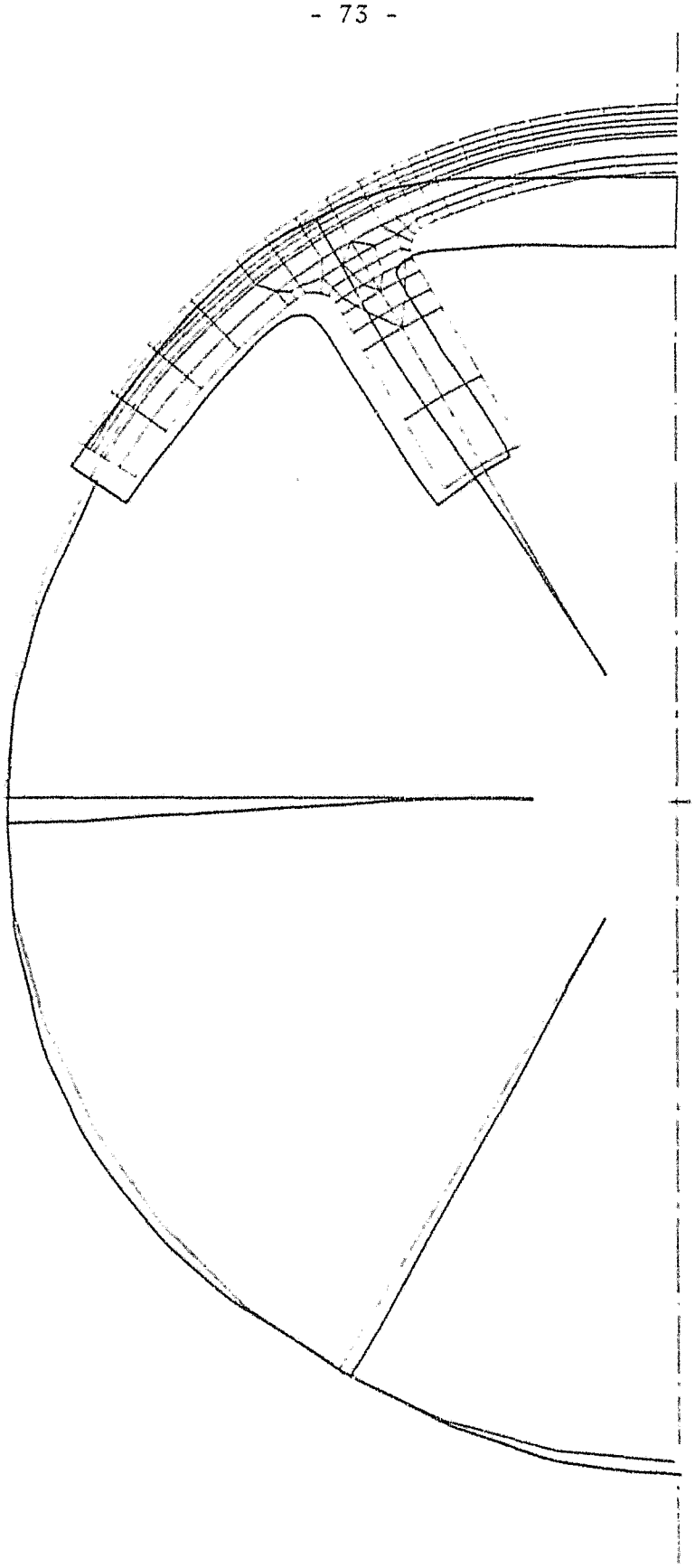

Figure 5.6 - Deformation of Sheave: Rope tension = 124 KN
(non associated plasticity)

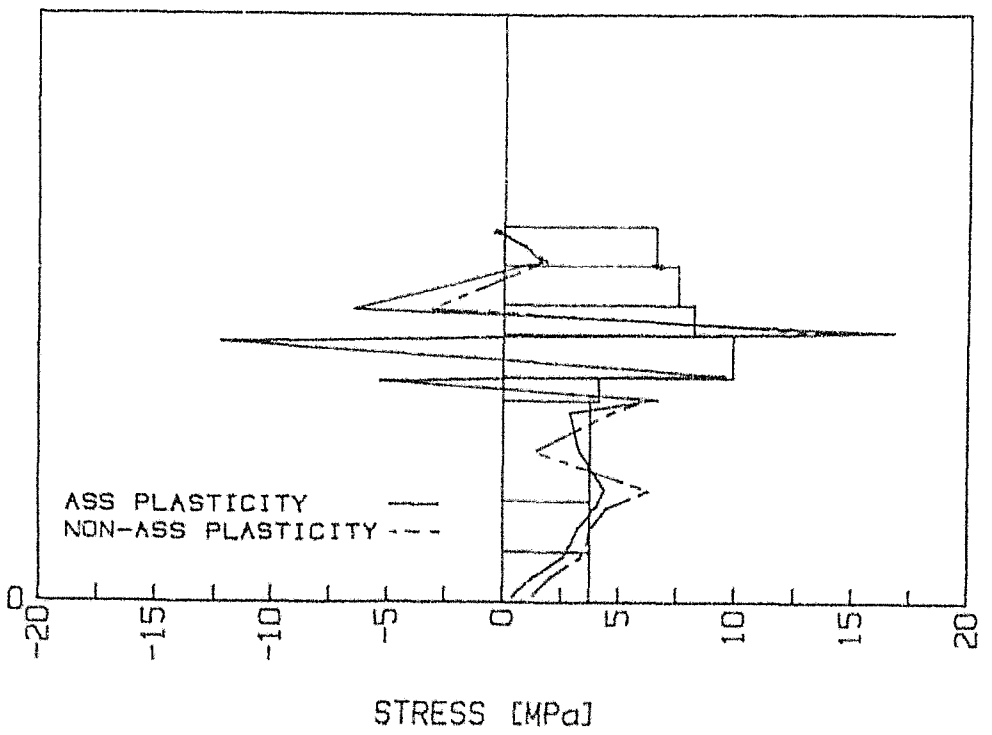

Figure 5.7a - Radial Stress Distribution
(Rope tension = 309 KN)

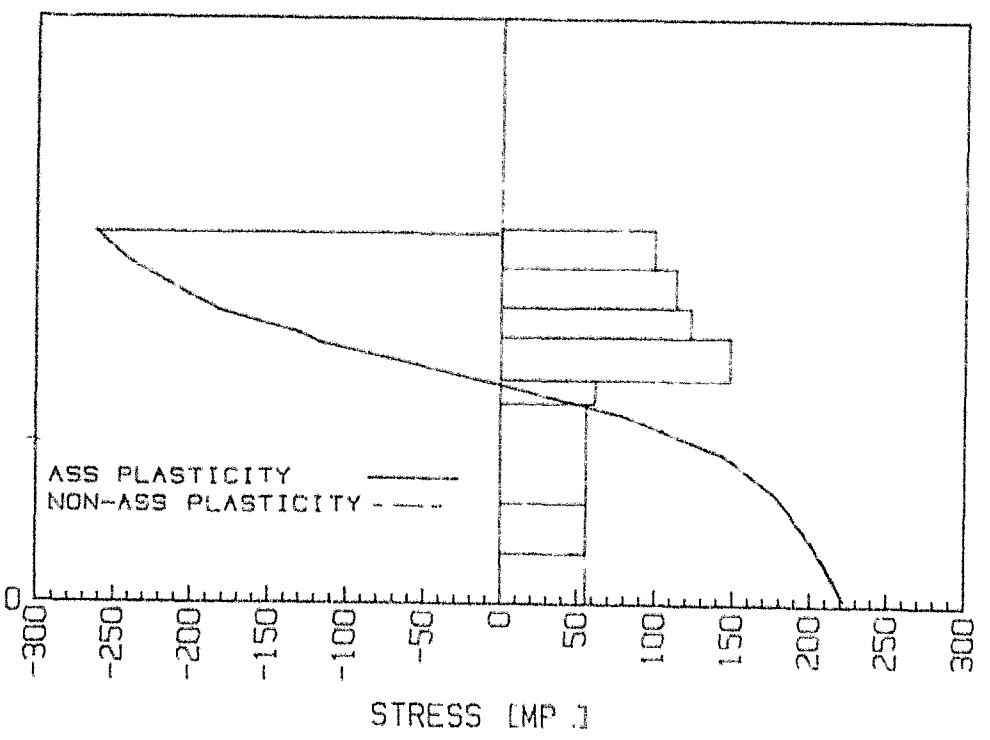

Figure 5.7b - Circumferential stress distribution
(Rope tension = 309 KN)



Figure 5.8 - Vector plot of principal stresses:
Rope Load = 370,8 KN (associated plasticity)

ORIGINAL — COPIE D.I.

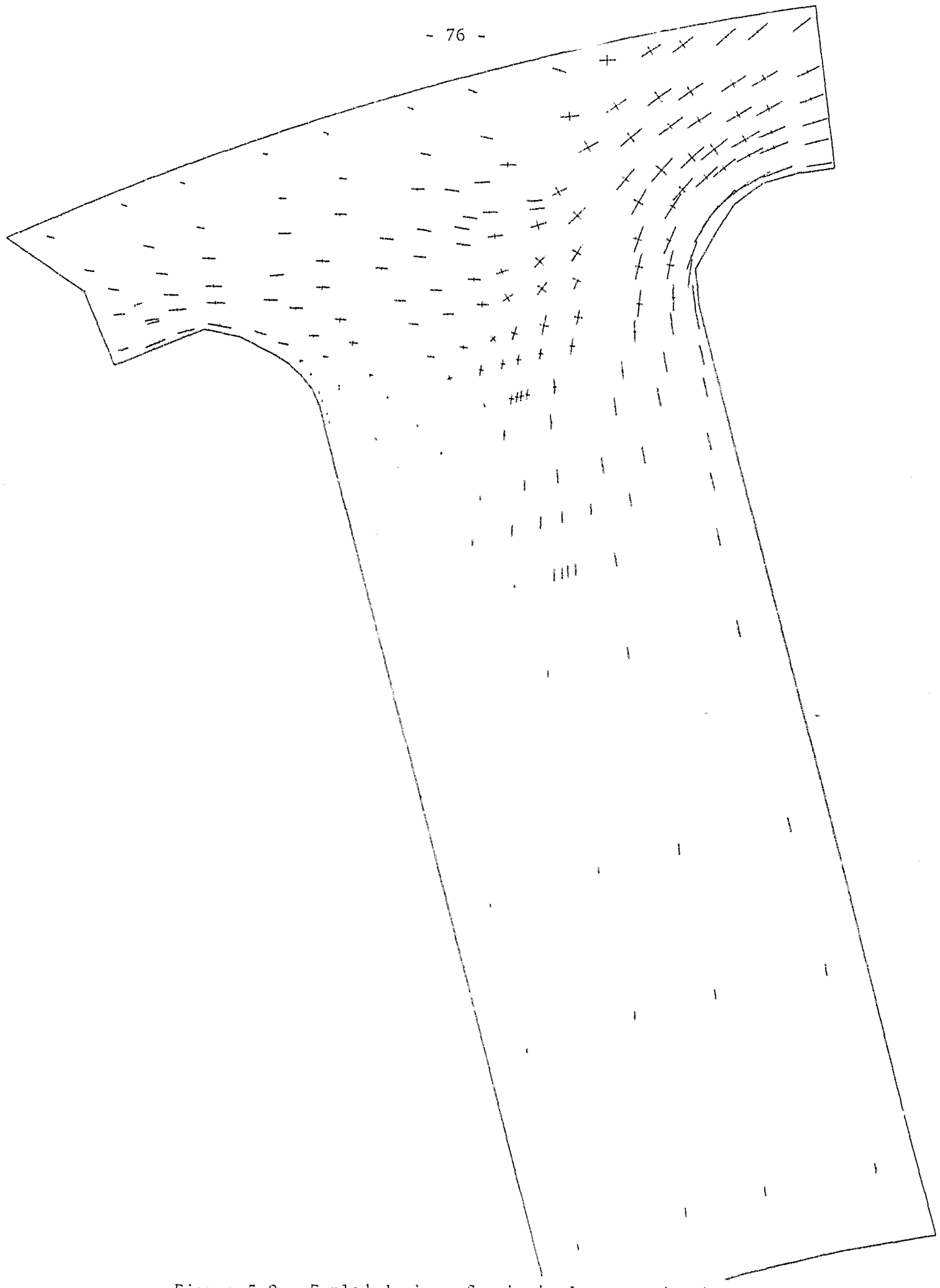

Figure 5.9: Exploded view of principal stress in the spoke:
Rope Load = 370,8 KN (associated plasticity)

The nonlinear radial and circumferential stress distribution through the depth of the rim section lying on the plane of symmetry is illustrated in Fig 5.7. Discontinuities in the radial stress are due essentially to discontinuities of the plane two-dimensional elements. A further discontinuity arises at the boundary where the load is applied. Although this may suggest the need for further mesh refinement in this region it is pertinent to note that the maximum radial stress is less than 5% of the maximum circumferential stress.

A vector plot of the principal stresses (presented in Figs 5.8, 5.9) in the two-dimensional element domain, confirms that the maximum stress occurs at the fillet junction between rim and spoke and at the centre of arc on the line of symmetry. These plots were obtained from the associated material simulation. The state of pure shear on the neutral axis in the midspan region, ie between the centre of arc and the spoke, is clearly depicted. (Region Y in Fig 5.5.)

The results are tabulated in Tables 5.3 and 5.4 for the non associated and associated simulations respectively.

5.5 COMPARISON OF RESULTS

A comparison of the experimental results, cited in Tables 5.1 and 5.2 with the corresponding finite element results presented in Tables 5.3 and 5.4, is illustrated in Plots 5.1 to 5.9.

In the test the change in machine range required to achieve failure necessitated unloading at 490 KN with subsequent reloading as stated in Section 5.2. This is reflected in the plots of the first nine gauges and not in the plots for gauges 10 - 24.

The nonlinear radial and circumferential stress distribution through the depth of the rim section lying on the plane of symmetry is illustrated in Fig 5.7. Discontinuities in the radial stress are due essentially to discontinuities of the plane two-dimensional elements. A further discontinuity arises at the boundary where the load is applied. Although this may suggest the need for further mesh refinement in this region it is pertinent to note that the maximum radial stress is less than 5% of the maximum circumferential stress.

A vector plot of the principal stresses (presented in Figs 5.8, 5.9) in the two-dimensional element domain, confirms that the maximum stress occurs at the fillet junction between rim and spoke and at the centre of arc on the line of symmetry. These plots were obtained from the associated material simulation. The state of pure shear on the neutral axis in the midspan region, ie between the centre of arc and the spoke, is clearly depicted. (Region Y in Fig 5.5.)

The results are tabulated in Tables 5.3 and 5.4 for the non associated and associated simulations respectively.

5.5 COMPARISON OF RESULTS

A comparison of the experimental results, cited in Tables 5.1 and 5.2 with the corresponding finite element results presented in Tables 5.3 and 5.4, is illustrated in Plots 5.1 to 5.9.

In the test the change in machine range required to achieve failure necessitated unloading at 490 KN with subsequent reloading as stated in Section 5.2. This is reflected in the plots of the first nine gauges and not in the plots for gauges 10 - 24.

TABLE 5.1 - Experimental Results: First Loading

ROPE LOAD [KN]	STRAIN GAUGE LOCATION								
	1 [x10^{-6}]	2 [x10^{-6}]	3 [x10^{-6}]	4 [x10^{-6}]	5 [x10^{-6}]	6 [x10^{-6}]	7 [x10^{-6}]	8 [x10^{-6}]	9 [x10^{-6}]
21,63	179,85	- 139	- 129	145	- 111	- 106	17	- 35	- 27
33,99	298	- 234	214	242	- 189	- 180	26	- 61	- 46
46,35	421	- 331	- 303	345	- 272	- 254	36	- 87	- 65
58,71	544	- 428	- 391	450	- 357	- 331	45	-112	- 82
71,38	683	- 537	- 490	565	- 450	- 415	54	-140	-104
80,34	786	- 615	- 563	650	- 518	- 477	61	-160	-117
89,61	897	- 700	- 644	743	- 593	- 546	68	-182	-133
99,50	1 014	- 790	- 728	840	- 670	- 617	73	-205	-150
109,39	1 134	- 880	- 814	939	- 750	- 689	80	-227	-167
117,43	1 234	- 954	- 884	1 019	- 812	- 747	85	-244	-180
126,70	1 355	-1 041	- 969	1 119	- 886	- 817	91	-265	-192
135,97	1 485	-1 133	-1 060	1 227	- 962	- 890	96	-287	-209
145,24	1 614	-1 225	-1 145	1 328	-1 039	- 961	102	-307	-222
153,27	1 725	-1 298	-1 218	1 414	-1 102	-1 019	106	-324	-235
160,69	1 835	-1 374	-1 293	1 501	-1 167	-1 079	109	-340	-249
168,41	1 962	-1 458	-1 374	1 599	-1 235	-1 144	113	-359	-262
176,14	2 090	-1 539	-1 454	1 697	-1 304	-1 207	118	-376	-275
182,94	2 204	-1 609	-1 526	1 784	-1 364	-1 263	120	-391	-285
190,35	2 330	-1 685	-1 605	1 877	-1 431	-1 324	124	-408	-298
197,77	2 469	-1 774	-1 689	1 981	-1 500	-1 388	128	-426	-311
203,95	2 582	-1 843	-1 758	2 062	-1 555	-1 439	130	-439	-321
210,13	2 693	-1 911	-1 825	2 143	-1 606	-1 491	132	-453	-332
216,31	2 823	-1 989	-1 902	2 236	-1 669	-1 547	136	-468	-343
222,49	2 947	-2 060	-1 974	2 324	-1 725	-1 706	139	-481	-353
228,67	3 081	-2 130	-2 048	2 417	-1 785	-1 656	142	-496	-363
235,47	3 236	-2 230	-2 137	2 523	-1 855	-1 720	144	-515	-376
241,65	3 371	-2 307	-2 215	2 615	-1 913	-1 775	146	-527	-387
247,21	3 507	-2 382	-2 292	2 706	-1 970	-1 828	148	-540	-399
253,39	3 667	-2 472	-2 382	2 812	-2 034	-1 890	151	-555	-409
259,57	3 822	-2 557	-2 468	2 916	-2 098	-1 949	154	-569	-421
265,75	3 992	-2 649	-2 562	3 028	-2 165	-2 012	157	-585	-432
271,93	4 163	-2 742	-2 657	3 138	-2 232	-2 075	159	-599	-445
278,12	4 328	-2 832	-2 746	3 245	-2 296	-2 136	161	-612	-456
284,30	4 533	-2 944	-2 857	3 376	-2 374	-2 208	164	-630	-469
290,40	4 716	-3 042	-2 958	3 492	-2 442	-2 272	170	-645	-482
296,66	4 898	-3 140	-3 056	3 602	-2 508	-2 335	167	-660	-495
302,84	5 100	-3 247	-3 166	3 733	-2 578	-2 404	170	-676	-508
309,00	5 291	-3 349	-3 270	3 851	-2 646	-2 467	171	-690	-520
0	1 326	- 731	-789,6	837	- 493	- 441	41	-103	-263

TABLE 5.2a - Experimental Results: Second Loading

ROPE LOAD [KN]	STRAIN GAUGE LOCATION													
	1 [x10^{-6}]	2 [x10^{-6}]	3 [x10^{-6}]	4 [x10^{-6}]	5 [x10^{-6}]	6 [x10^{-6}]	7 [x10^{-6}]	8 [x10^{-6}]	9 [x10^{-6}]	10 [x10^{-6}]	11 [x10^{-6}]	12 [x10^{-6}]	13 [x10^{-6}]	14 [x10^{-6}]
25,95	223	- 166	- 151	175	- 130	- 125	18	- 45	- 34	130	154	108	17	15
49,44	479	- 356	- 324	389	- 291	- 269	35	- 95	- 68	270	331	227	37	27
67,98	699	- 516	- 468	572	- 426	- 392	48	-136	- 94	387	482	331	56	41
92,71	983	- 720	- 657	808	- 600	- 550	61	-187	-130	548	680	466	77	52
120,52	1 319	- 952	- 876	1 083	- 804	- 734	73	-245	-166	734	915	621	105	66
148,33	1 652	-1 181	-1 094	1 358	- 998	- 915	83	-299	-204	920	1 148	772	132	83
173,05	1 973	-1 396	-1 290	1 620	-1 178	-1 079	92	-348	-238	1 099	1 371	925	155	97
197,77	2 298	-1 609	-1 493	1 885	-1 [illegible]7	-1 244	100	-393	-271	1 279	1 597	1 068	182	111
222,49	2 638	-1 826	-1 700	2 158	-1 539	-1 412	107	-440	-304	1 462	1 836	1 223	207	126
247,21	2 995	-2 048	-1 911	2 441	-1 721	-1 578	115	-488	-337	1 655	2 083	1 377	230	138
259,57	3 174	-2 161	-2 019	2 583	-1 810	-1 663	118	-511	-353	1 753	2 209	1 455	246	147
271,93	3 371	-2 279	-2 131	2 736	-1 906	-1 750	121	-535	-370	1 856	2 347	1 542	262	154
284,30	3 566	-2 394	-2 244	2 884	-2 002	-1 836	124	-558	-386	1 959	2 483	1 623	275	158
293,57	3 721	-2 487	-2 332	3 000	-2 075	-1 903	127	-576	-400	2 041	2 586	1 687	284	165
301,60	3 853	-2 564	-2 [illegible]	3 097	-2 135	-1 957	131	-592	-410	2 109	2 681	1 737	295	169
307,78	3 986	-2 641	-2 478	3 191	-2 192	-2 010	132	-606	-420	2 177	2 774	1 787	302	173
315,20	4 164	-2 740	-2 573	3 312	-2 263	-2 074	134	-622	-433	2 270	2 902	1 851	312	174
321,38	4 348	-2 840	-2 669	3 431	-2 323	-2 135	136	-637	-445	2 364	3 032	1 913	320	179
327,56	4 559	-2 953	-2 778	3 563	-2 403	-2 203	139	-652	-456	2 478	3 177	1 974	329	186
333,74	4 769	-3 064	-2 888	3 692	-2 473	-2 267	139	-665	-467	2 591	3 325	2 037	339	189
339,92	5 017	-3 195	-3 015	3 841	-2 556	-2 340	143	-682	-480	2 721	3 502	2 110	349	194
346,10	5 263	-3 324	-3 142	3 988	-2 633	-2 414	145	-698	-493	2 863	3 694	2 184	362	200
352,28	5 516	-3 455	-3 272	4 141	-2 715	-2 487	145	-715	-506	2 987	3 854	2 249	373	208
359,70	5 843	-3 624	-3 441	4 352	-2 816	-2 582	148	-734	-520	3 172	4 098	2 346	387	212
364,64	6 066	-3 739	-3 555	4 503	-2 884	-2 645	150	-749	-531	3 286	4 252	2 402	395	214
370,82	6 342	-3 883	-3 698	4 692	-2 965	-2 722	152	-765	-544	3 434	4 454	2 481	407	219
377,00	6 619	-4 027	-3 841	4 893	-3 051	-2 800	155	-783	-550	3 582	4 649	2 556	421	223
383,18	6 908	-4 179	-3 992	4 999	-3 137	-2 877	158	-801	-568	3 742	4 863	2 637	454	232
389,36	7 180	-4 330	-4 142	5 200	-3 222	-2 955	160	-817	-581	3 899	5 082	2 722	441	234
395.54	7 384	-4 482	-4 291	5 320	-3 310	-3 032	161	-835	-594	4 059	5 297	2 804	461	241
401,72	7 581	-4 649	-4 456	5 415	-3 400	-3 114	164	-853	-608	4 231	5 529	2 892	472	245
407,9	-1 524	-4 810	-4 613	5 561	-3 485	-3 194	164	-871	-621	4 391	5 756	2 974	486	249
414,08	-1 524	-4 994	-4 788	5 702	-3 491	-3 266	163	-878	-631	4 570	6 006	3 071	502	253
420,26	-1 524	-7 367	-7 932	6 212	-2 706	-2 508	-964	-275	-81	7 323	9 487	3 265	587	340

TABLE 5.2b - Experimental Results: Second Loading

ROPE LOAD [KN]	STRAIN GAUGE LOCATION									
	15 [x10^{-6}]	16 [x10^{-6}]	17 [x10^{-6}]	18 [x10^{-6}]	19 [x10^{-6}]	20 [x10^{-6}]	21 [x10^{-6}]	22 [x10^{-6}]	23 [x10^{-6}]	24 [x10^{-6}]
25,95	28	0,7	- 142	- 252	- 151	8	,0	- 236	- 455	- 615
49,44	57	6	- 198	- 359	- 218	10	10	- 500	- 960	- 1 307
67,98	78	8	- 281	- 507	- 308	11	17	- 723	- 1 389	- 1 906
92,71	109	13	- 369	- 666	- 404	13	21	-1 013	- 1 935	- 2 703
120,52	145	22	- 455	- 834	- 503	16	26	-1 344	- 2 538	- 3 632
148,30	176	24	- 536	- 982	- 595	14	27	-1 667	- 3 134	- 4 516
173,65	208	28	- 623	-1 129	- 883	15	26	-1 974	- 3 699	- 5 314
197,77	246	30	- 706	-1 278	- 772	10	20	-2 280	- 4 271	- 6 117
222,49	278	31	- 790	-1 426	- 860	7	13	-2 597	- 4 865	- 6 958
247,21	312	37	- 833	-1 494	- 906	7	5	-2 922	- 5 482	- 7 846
259,57	331	35	- 881	-1 575	- 951	6	6	-3 078	- 5 792	- 8 299
271,93	352	38	- 922	-1 645	- 995	3	3	-3 250	- 6 128	- 8 799
284,30	368	46	- 956	-1 701	-1 028	- 1	1	-3 419	- 6 463	- 9 307
293,60	385	38	- 980	-1 744	-1 055	- 2	3	-3 547	- 6 729	- 9 712
301,60	393	42	-1 003	-1 783	-1 081	- 3	4	-3 654	- 6 957	-10 065
307,78	405	42	-1 031	-1 830	-1 107	- 5	9	-3 753	- 7 184	-10 428
315,20	417	46	-1 057	-1 864	-1 131	- 6	17	-3 879	- 7 483	-10 921
321,38	429	47	-1 081	-1 906	-1 152	- 7	30	-3 993	- 7 775	-11 457
327,56	439	49	-1 103	-1 941	-1 173	-13	39	-4 115	- 8 103	-12 028
333,74	449	51	-1 131	-1 978	-1 200	-17	56	-4 228	- 8 424	-12 622
339,92	463	53	-1 158	-2 018	-1 223	-18	70	-4 358	- 8 795	-13 319
346,10	477	56	-1 181	-2 052	-1 244	-20	85	-4 503	- 9 196	-14 068
352,28	491	56	-1 215	-2 104	-1 275	-25	97	-4 630	- 9 538	-14 708
359,70	513	60	-1 237	-2 132	-1 293	-24	117	-4 867	-10 036	-15 655
364,64	523	64	-1 264	-2 169	-1 320	-31	135	-4 923	-10 357	-16 247
370,82	533	69	-1 291	-2 208	-1 340	-31	148	-5 070	-10 762	-17 016
377,00	551	67	-1 315	-2 247	-1 361	-35	165	-5 213	-11 159	-17 764
383,18	567	69	-1 346	-2 281	-1 383	-43	176	-5 368	-11 588	-18 575
389,36	581	73	-1 377	-2 321	-1 405	-48	194	-5 521	-12 012	-19 384
395,54	596	73	-1 402	-2 358	-1 427	-53	205	-5 680	-12 438	-20 202
401,72	610	75	-1 431	-2 394	-1 449	-56	219	-5 848	-12 882	-21 877
407,90	627	78	-1 462	-2 430	-1 471	-59	233	-6 011	-13 304	-22 771
414,08	648	73	-1 424	-2 592	-1 431	-65	250	-6 182	-13 758	- 3 583
420,26	626	271	- 347	-2 878	- 153	-70	1 190	-6 039	-15 838	- 3 583

TABLE 5.3 - Finite Element Results - Associated Plasticity

	GAUGE NUMBER (ASS-PLASTICITY)										
ROPE TENSION (KN)	1	2,3	4	5,6	7	8,9	10,11	12	20	17,19	18
61.803	718.69	-578.1	551.18	-483.31	48.261	-148.18	479.5	321.38	-23.983	-225.52	-378.39
123.81	1515	-1178.9	1161.1	-932.38	93.393	-291.89	988.24	646.93	-47.372	-450.2	-755.8
185.41	2571	-1873.6	1776.4	-1429.1	129.68	-438.05	1634.4	988.53	-68.07	-671.59	-1127.3
247.21	4119.1	-2800.2	2569.5	-1993.6	152.99	-594.12	2553.3	1359	-79.929	-891.62	-1490.3
309.02	6399.4	-4137.3	3649.8	-2704.7	155.07	-769.14	3928.9	1769.5	-71.348	-1123.8	-1870
370.82	9750.8	-6135	4991.9	-3610.5	126.03	-963.65	5974.8	2230.7	-42.797	-1378.4	-2307.8
432.62	13093	-8735.3	6796.2	-4817.2	72.155	-1188.3	8351.3	2724.1	-3.5024	-1863	-2704.6

TABLE 5.4 - Finite Element Results - Non Associated Plasticity

	GAUGE NUMBER (NON ASS-PLASTICITY)										
ROPE TENSION (KN)	1	2,3	4	5,6	7	8,9	10,11	12	20	17,19	18
61.803	718.64	-578.1	551.18	-483.31	48.264	-148.18	479.52	321.38	-23.983	-225.52	-378.39
123.81	1512.5	-1178.3	1117.8	-932.17	93.391	-291.63	988.98	648.78	-47.377	-450.23	-755.65
185.41	2546.5	-1867.1	1778.2	-1427.8	131.59	-438.83	1619.7	988.08	-68.6	-671.89	-1127.3
247.21	4048.9	-2785.8	2598.7	-1995.6	153.05	-592.07	2493.6	1366.4	-79.142	-893.8	-1492.6
309.02	6306.9	-4131.3	3697	-2707.9	159.54	-765.49	3795.9	1783.7	-78.747	-1127.7	-1874
370.82	9518.3	-6089.9	5111.5	-3815.9	136.52	-951.2	5552.9	2252.3	-43.802	-1393.5	-2281.7
432.62	13683	-8757.2	6872.2	-4789.6	83.8	-1156.9	7810.6	2773.4	-3.9433	-1672	-2709.6

The electrical fault necessitated careful selection of the readings for comparison with the FEM results. It is known [16], that the material properties of cast iron are non-linear even at low loads and that any previous plastic deformation will modify the stress/strain response of the material. Owing to this, at locations where plastic deformation occurred in the first loading, a modified response resulted in the second loading (see Plots 5.1, 5.2 etc). This modified response is linear up to the point where the previous loading was discontinued. Therefore, readings taken from this response, without regard to the previous loading can lead to error. Where, however, the plastic strain originally induced was small, the error will be small.

The effect discussed above is illustrated in Plot 5.6 of the readings for gauges 11 and 12, ie a pronounced linear region followed by a knee in the curve and consequently the experimental readings are less than those of the FEM results. For this reason the comparison presented in Plot 5.6 is not considered valid. However the strains measured by gauges 17 to 20 are within the linear region and it is likely that the plastic deformation induced in the first load application was negligible.

Four gauges (21-24) were mounted on the fillets at the junction of the spoke to the rim as it was expected that high stresses would occur in these regions. Owing to imperfections caused by the manufacturing process, the small radius of curvature of the fillet was variable and could not be modelled accurately. Consequently, in view of the high stress gradients at these fillets a comparison of rsults was considered invalid. However it is noted that the readings obtained from these gauges are of the same order of magnitude as predicted by the finite element results.

The locations of gauges where beam elements modelled the horizontal spoke were not considered valid for comparison (gauges 13-16). The mesh used in that region was coarse in order to reduce the number of degrees of freedom involved in the analysis. These extra readings were monitored to provide experimental data for the purpose of

qualitative comparison with the FEM results. In fact, if the apparently erratic readings of gauge 16 are disregarded, the other three gauges confirm the deflections of the spoke as predicted by the FEM analysis, as illustrated in Fig 5.10.

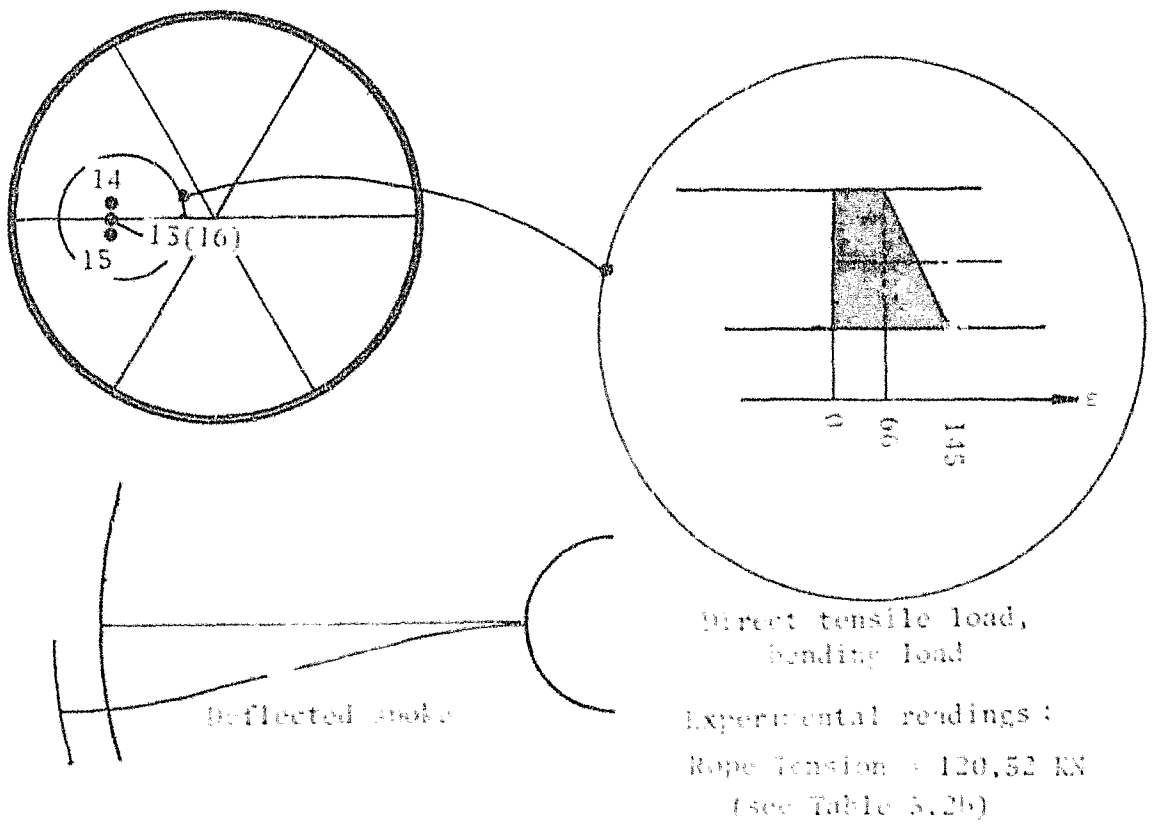

Figure 5.10

The results of the associated and non associated simulations are illustrated in the plots appearing at the end of this section, where * denotes associated plasticity and + denotes non associated plasticity. Overall no distinct difference between the associated and non associated results is apparent.

The experimental and FEM results compare well at low loads (up to approximately 1 000 με) where plastic deformation is small. At higher loads where plastic deformation becomes promenent the experimental and FEM results deviate. For gauges 1, 2, 3 the deviation is approximately 20% at failure. Higher accuracy was obtained for

gauges 4 - 9 and 17 - 20. The FEM results for gauge 7 indicates stress relaxation which is due to stress redistribution following pronounced plastic deformation in adjacent areas (see Fig 5.5).

The deflection of the upper rim surface of the centre of arc on the line of symmetry is tabulated for both analyses in Table 5.5. It is apparent that the two sets of deflections are not significantly different. Since they are less than 1,5 percent of the radius, they are not large enough to warrant a non linear geometric analysis.

TABLE 5.5 - Central Deflection of the Sheave (FEM Results)

		DEFLECTION (mm)	
TIME STEP	ROPE TENSION (KN)	ASSOCIATED	NON ASSOCIATED
1	61,80	0,540 376	0,540 376
2	123,60	1,098 50	1,098 00
3	185,41	1,728 06	1,723 27
4	247,21	2,501 13	2,492 77
5	309,01	3,524 02	3,513 48
6	370,82	4,900 34	4,865 17
7	432,62	6,634 51	6,615 62

5.6 CONCLUSIONS

The main purpose of this excercise was to achieve an understanding of, and familiarisation with, the capabilities of the ADINA programme in a non-linear application and to assess, thereby, the programme's performance.

Originally it was envisaged that the performance of ADINA would be evaluated on its ability to simulate the sheave behaviour accurately. In retrospect it is evident that the two dimensional simplification of the sheave, and the approximation of the material model, introduce inaccuracies. During the course of the excercise the options available

for the analysis of nonlinear material problems (initial stress method, modified newton raphson and BFGS method) were utilised and found to work without interruption.

The comparison of the finite element simulation with the experimental values obtained proved to be useful and led to reappraisal, improved understanding and some necessary corrections to the mesh design and the material model.

Although the comparison of the theoretical and experimental work was satisfactory it does not necessarily support the notion that cast iron behaves in accordance with the constitutive stress/strain relations relating to the Drucker Prager yield criterion. This is based on the observation that the stress distribution in most of the zones where plasticity developed is almost uniaxial.

Allowing for the difficulties in measuring the section of the sheave rim, the approximations involved in representing the nonlinear behaviour of the cast iron and the discontinuity of the loading, the comparison of the finite element simulations with the experimental results is satisfactory.

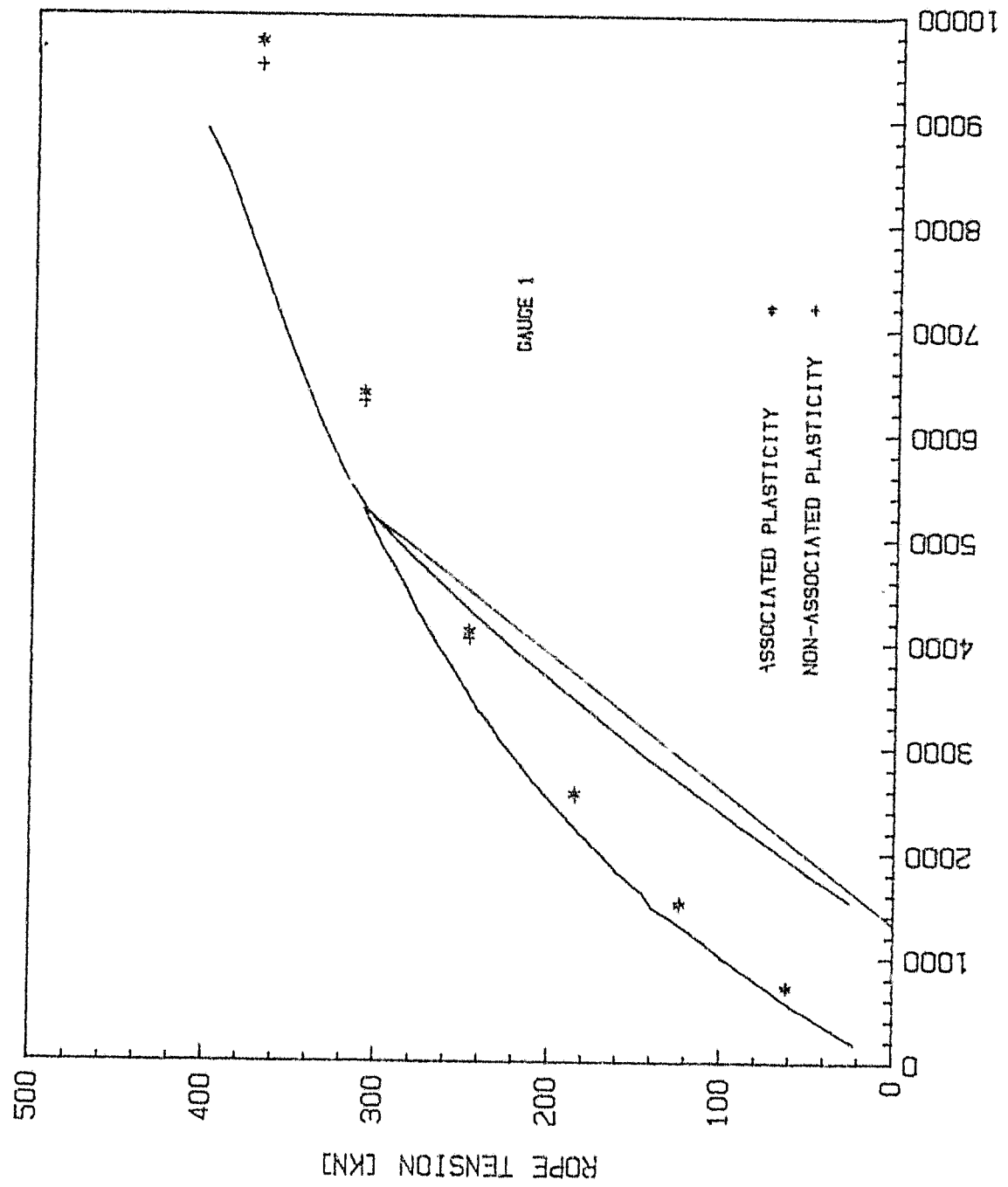

PLOT 5.1 - (Gauge 1

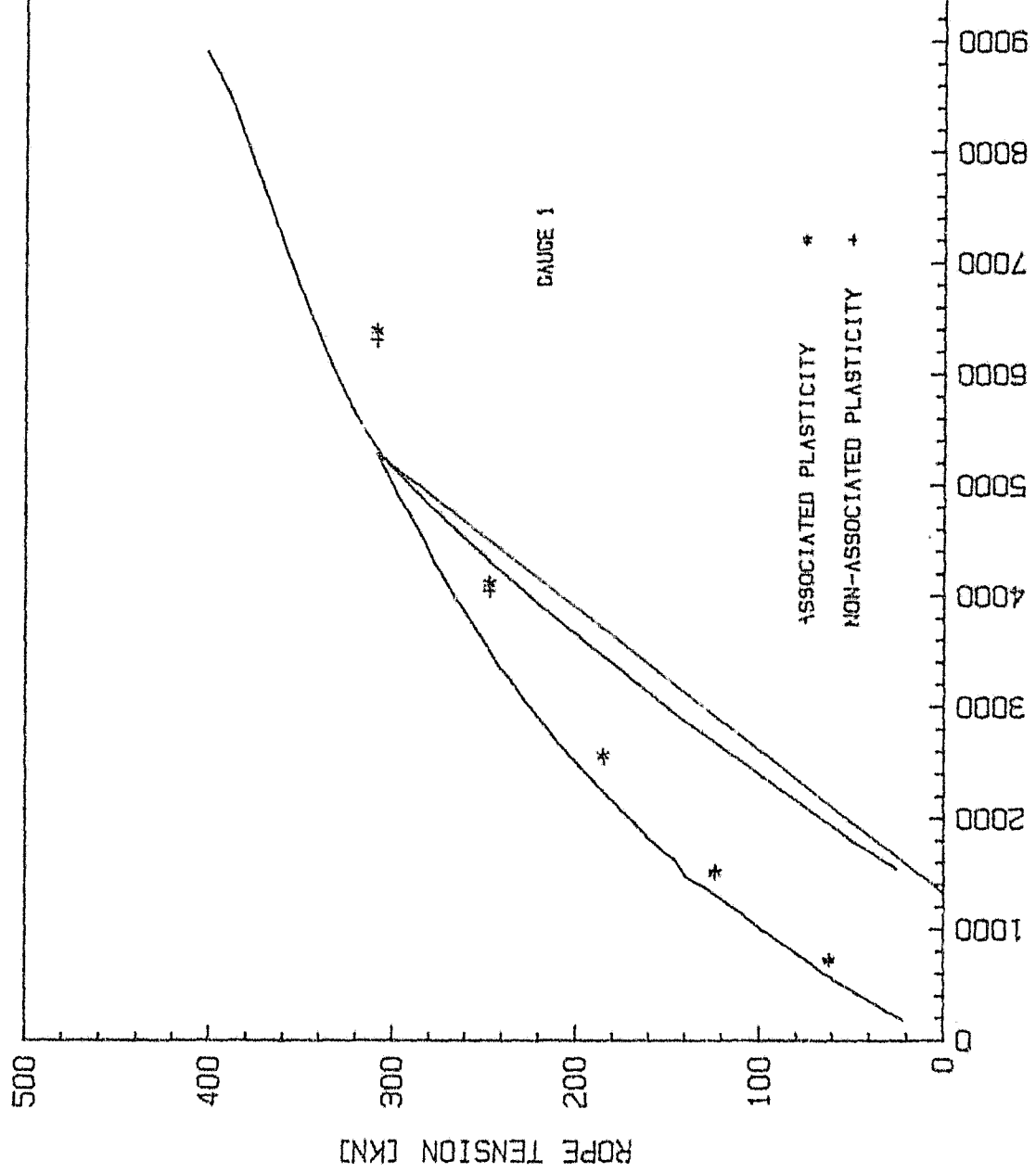

PLOT 5.1 - Gauge 1

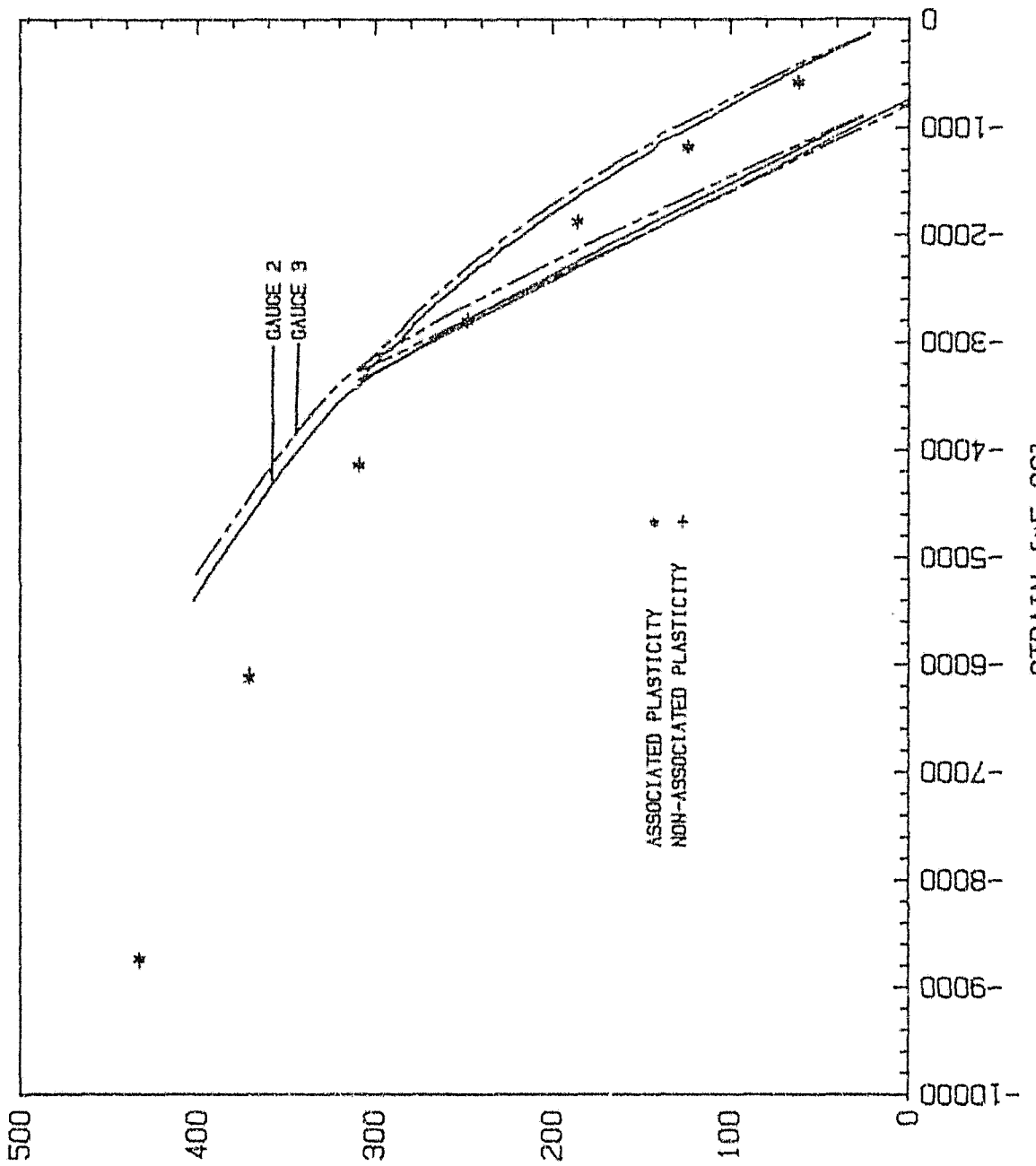

PLOT 5.2 - Gauges 2(3)

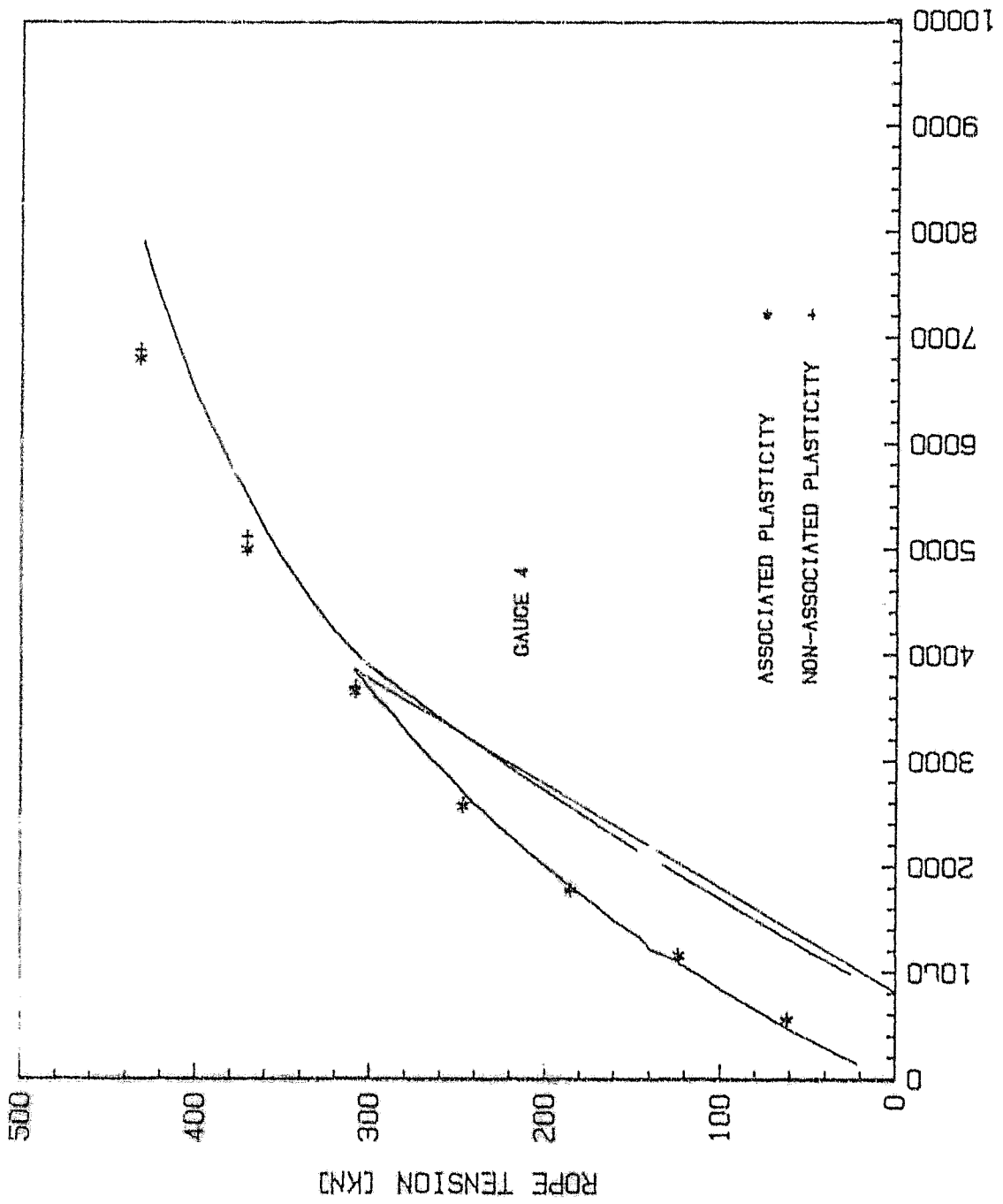

PLOT 5.3 - Gauge 4

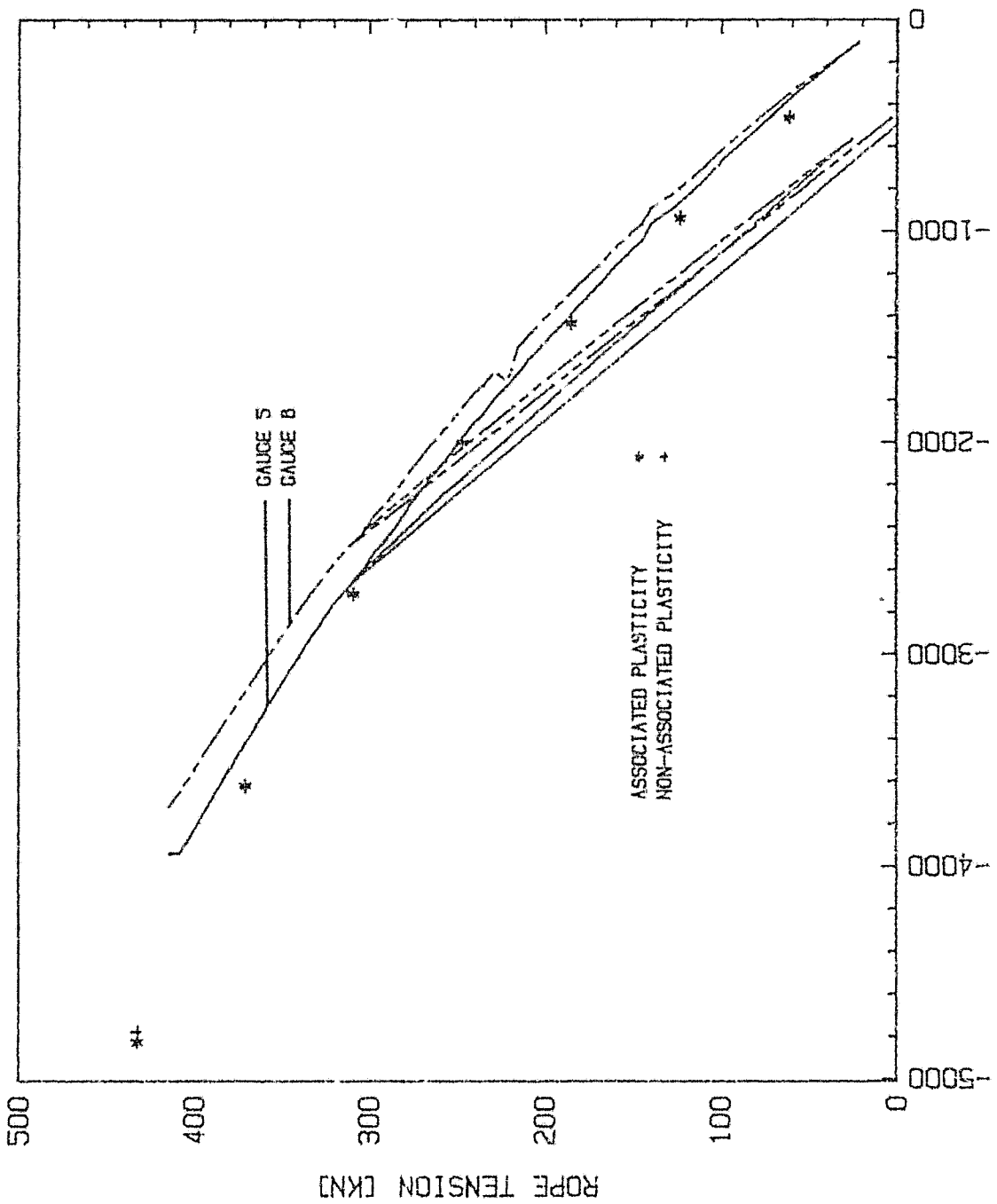

PLOT 5.4 - Gauges 5, 6

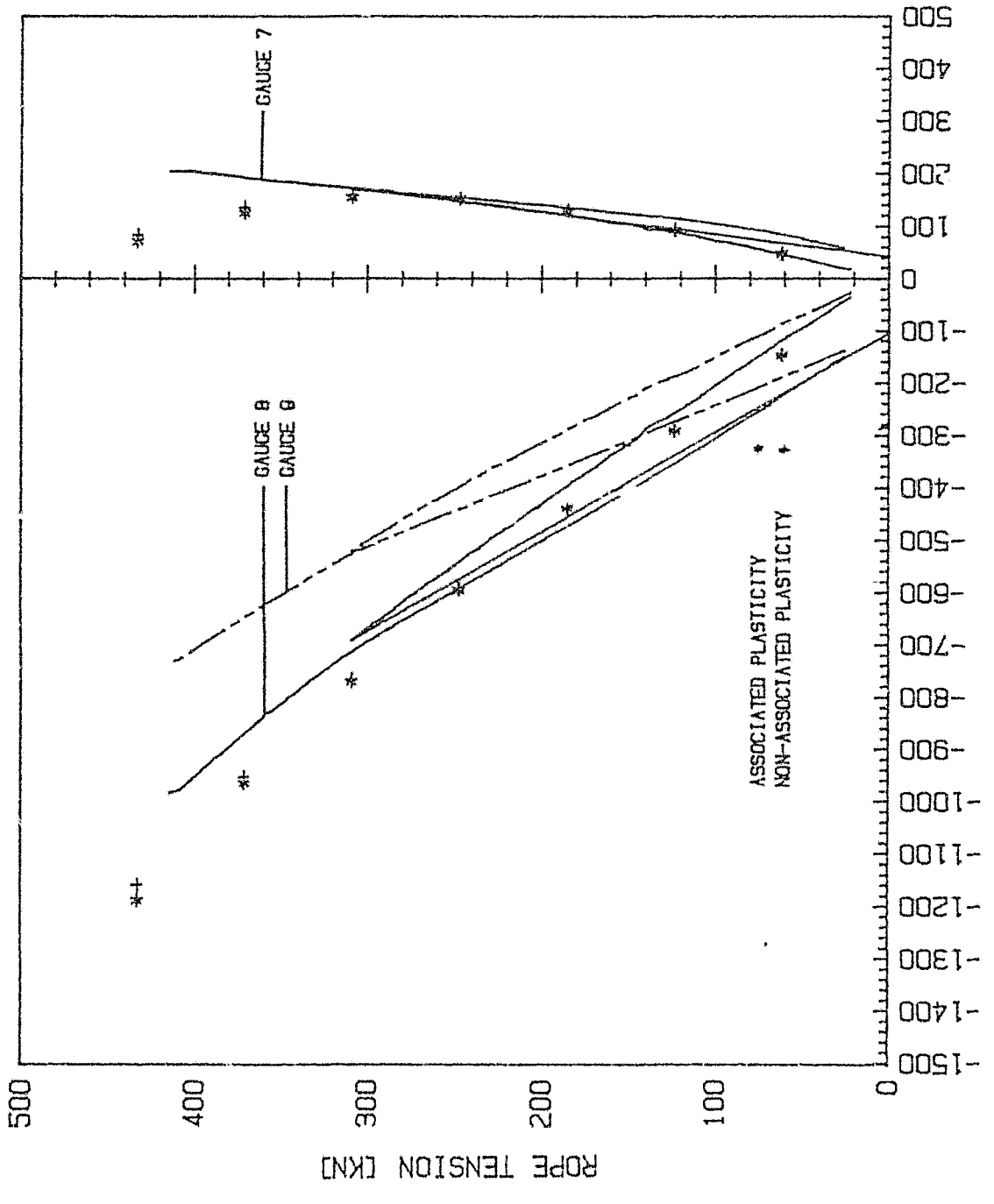

PLOT 5.5 - Gauges 7, 8, 9

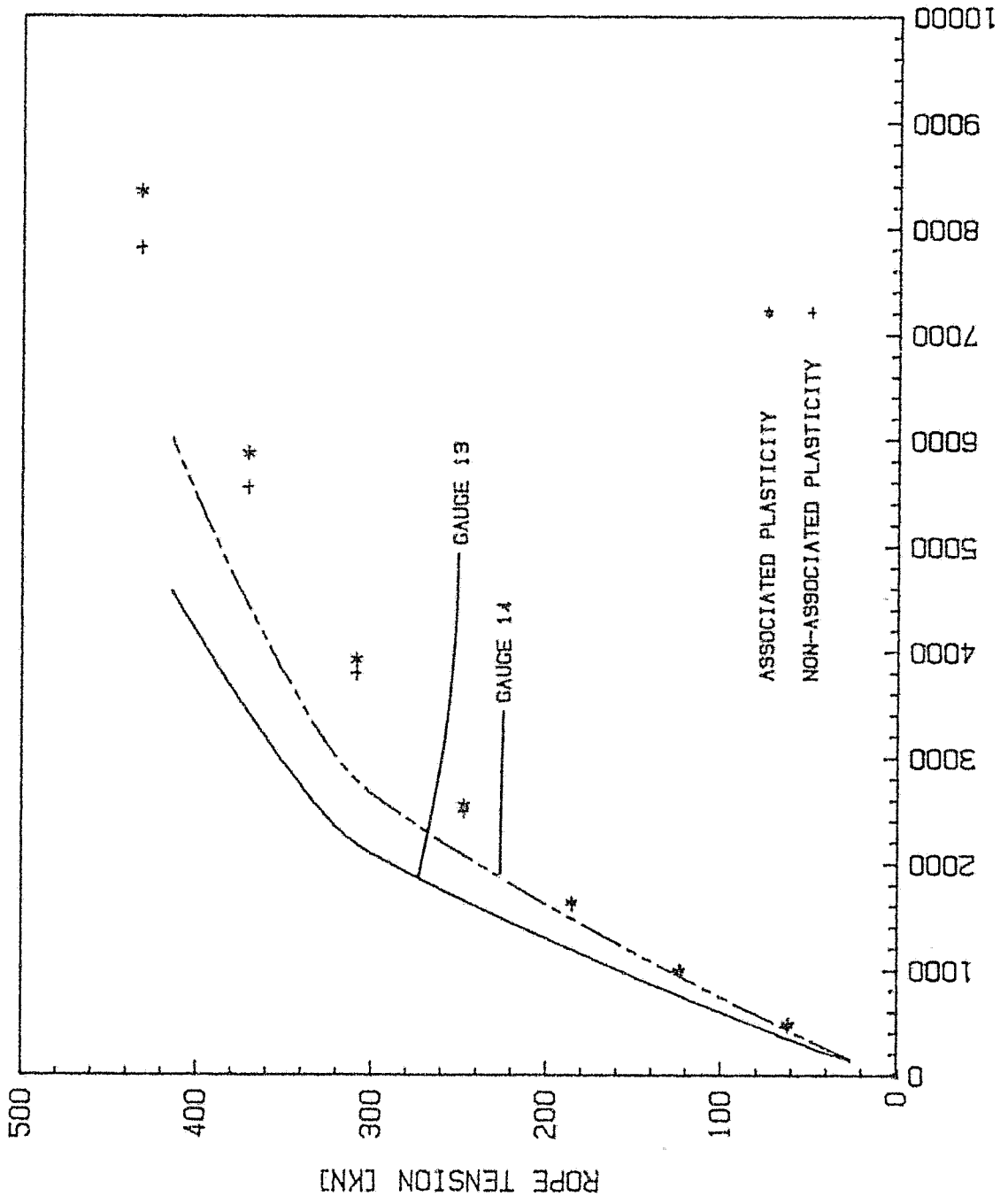

Plot 5.6 - Gauges 10 and 11

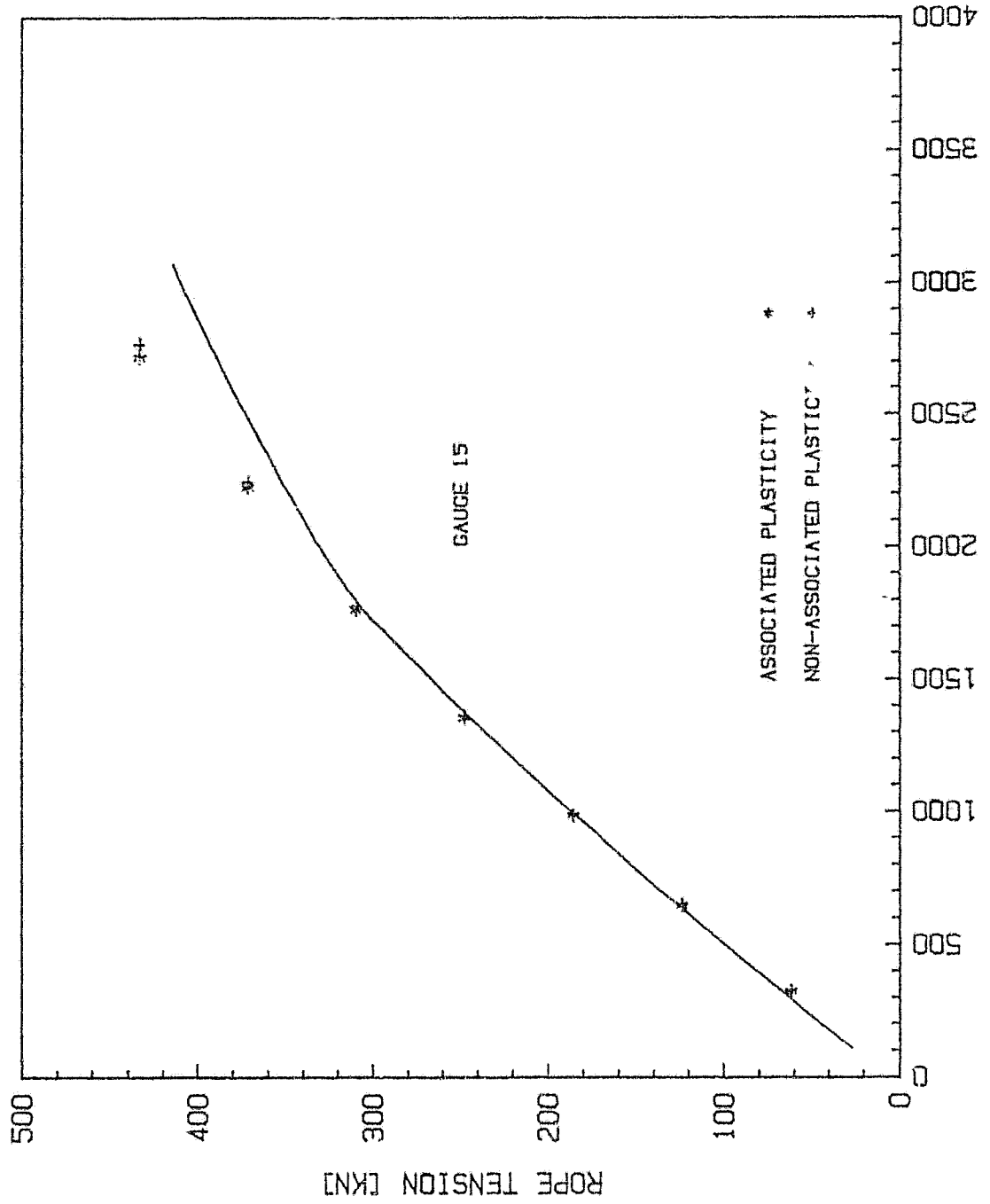

Plot 5.7 - Gauge 12

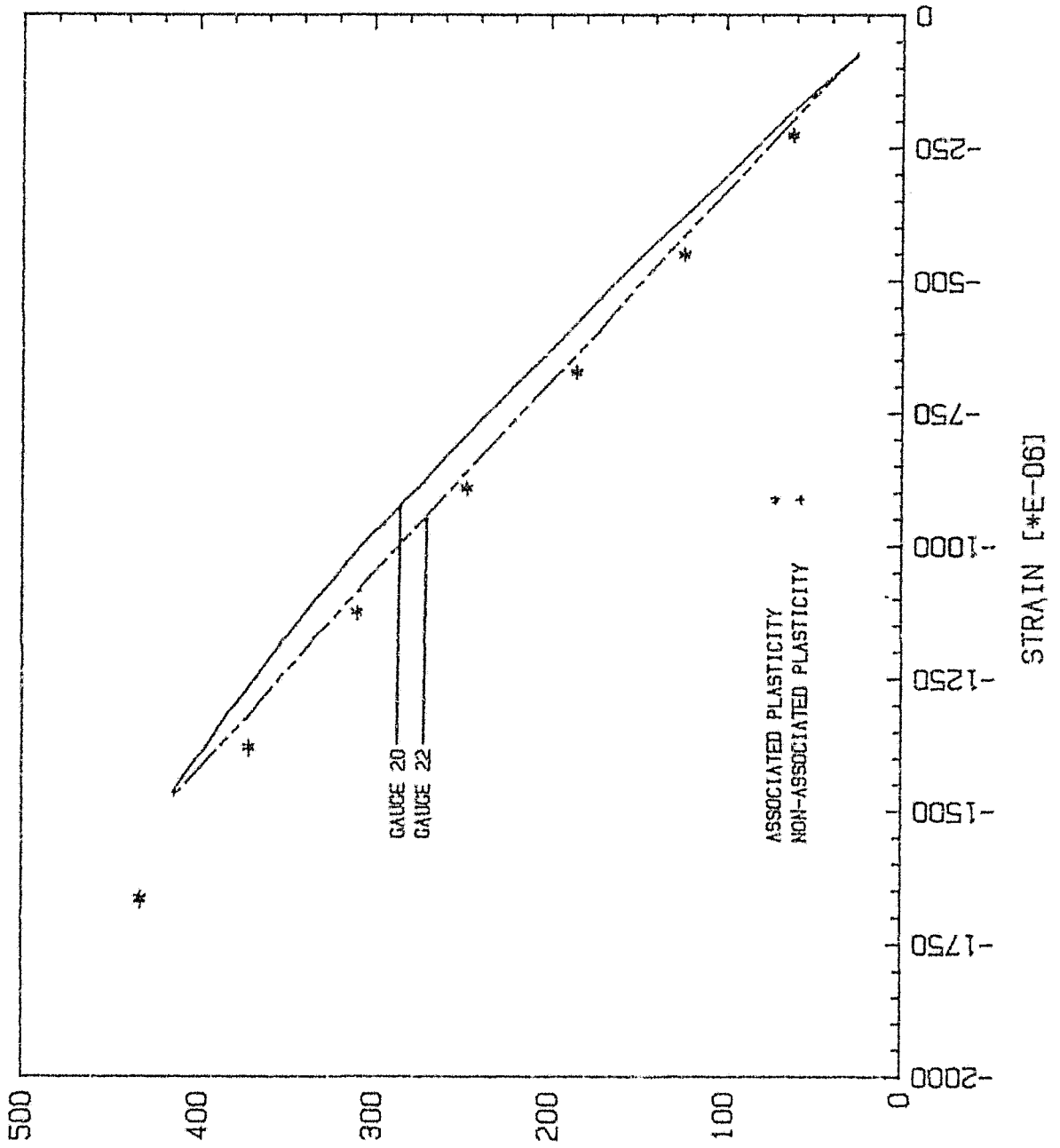

Plot 5.8 - Gauges 17 and 19

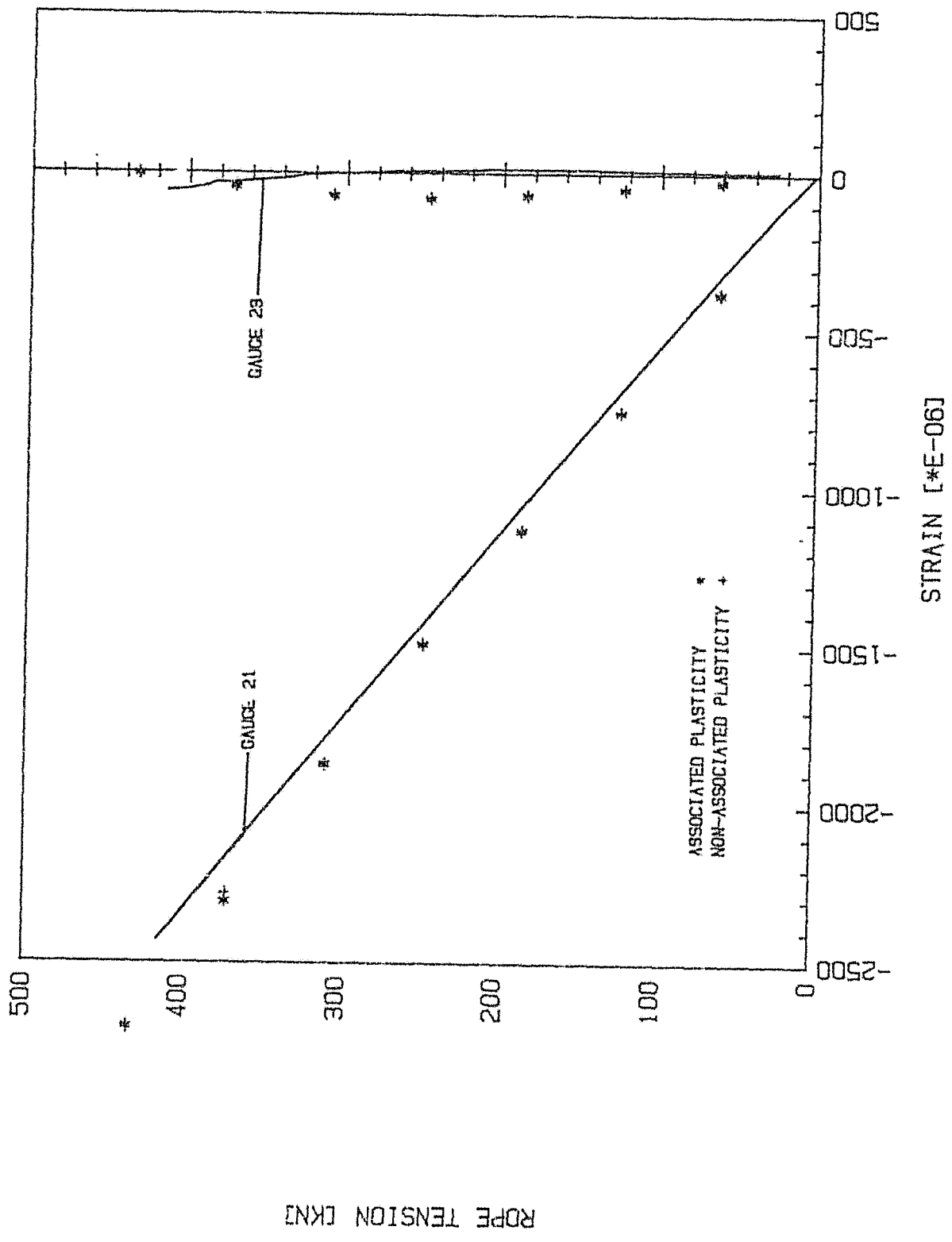

Plot 5.9 - Gauges 18 and 20

CHAPTER 6

MECHANICAL VIBRATIONS

6.1 THE ANALYSIS OF MECHANICAL VIBRATIONS

A powerful technique for analysing mechanical vibrations and other time-dependent phenomena can be obtained by extending the finite element concept to incorporate the time dimension.[1] The most common approach adopted is to formulate a matrix differential equation in which the spatial domain is discretised by finite elements, whilst a numerical time-stepping technique is employed to integrate the equations in the temporal domain.

6.2 DIRECT FORMULATION OF TIME DEPENDENT PROBLEMS WITH SPATIAL FINITE ELEMENT DISCRETISATION: *THE DYNAMIC BEHAVIOUR OF ELASTIC STRUCTURES WITH LINEAR DAMPING* [1]

The static equilibrium equations derived for a finite element in the spatial domain can be modified to include damping and inertia effects. The resulting matrix equation is a second order differential equation in displacements with respect to time.

The static equilibrium equation for an isolated element e, as

---

1 The nodal point interpolation functions can be generalised to include the time dimension

$$\{U\} = \sum_{i=1}^{n} N_i(x,y,z)\bar{N}_i(t)\{a\}_i$$

This approach has been used to formulate recurrence relations for integrating the resulting equations of motion. These are generally different to finite difference techniques. [1]

derived in Chapter 2, is repeated below for convenience.

$$[K]^e\{a\}^e + \{f\}^e = \{q\}^e \tag{6.1}$$

where

$$\{f\}^e = \{f_p\}^e + \{f_{\varepsilon 0}\}^e + \{f_b\}^e + \{f_{\sigma 0}\}^e \tag{6.2}$$

When an element is subjected to forces which vary rapidly with time, inertia and damping effects must be considered In such instances the resulting displacements are time dependent and consequently the behaviour is termed dynamic. It is possible to convert the dynamic effects mentioned into equivalent static loads by applying d'Alembert's principle. These loads are distributed uniformly through the volume of the element and are thus included as additional body forces in the equilibrium equation which now becomes a statement of equilibrium required at any point in time.

The total body force component $\{\bar{P}_e\}$ acting per unit volume on an element e, at any given time is

$$\{\bar{P}_e\} = \{P_e\} - \rho\frac{\partial^2}{\partial t^2}\{u\}^e - \dot{\varsigma}\frac{\partial}{\partial t}\{u\}^e \tag{6.3}$$

where $\{P_e\}$ represents the static body force component acting per unit volume on element e

and $\rho, \dot{\varsigma}$ represents the density and damping factor of element e respectively.

The body force $\{\bar{P}_e\}$ can be converted into an equivalent nodal load $\{\bar{f}_p\}^e$, hence $\{f\}^e$ in the element equilibrium equation (6.1) becomes

$$\{f\}^e = \{\bar{f}_p\}^e + \{f_{\varepsilon 0}\}^e + \{f_b\}^e$$

where

$$\{\bar{f}_p\}^e = -\int_{V_e} [N_e]^T \{\bar{P}_e\} dV_e$$

$$= -\underbrace{\int_{V_e} [N_e]^T \{P\} dV_e} + \int_{V_e} \left[[N_e]^T [\rho \frac{\partial^2}{\partial t^2} \{u_e\}^e + \zeta \frac{\partial}{\partial t} \{u\}^e \right] dV_e$$

$$= \{f_p\}^e + \left[\int_{V_e} [N_e]^T \rho [N_e] dV_e \right] \{\ddot{a}\}^e + \left[\int_{V_e} [N_e]^T \zeta [N_e] dV_e \right] \{\dot{a}\}^e \qquad (6.4)$$

where

$$\{u\}^e = [N_e] \, a^e$$

$$\frac{\partial^2}{\partial t^2} \{u\}^e = [N_e] \frac{\partial^2}{\partial t^2} \{a\}^e = [N_e] \{\ddot{a}\}^e$$

Equation (6.4) can be written in a simplified form

$$\{\bar{f}_p\}^e = \{f_p\}^e + [M]^e \{\ddot{a}\}^e + [\zeta]^e \{\dot{a}\}^e \qquad (6.5)$$

Thus

$$\{f\}^e = \{f_p\}^e + \{f_{\varepsilon 0}\}^e + \{f_b\}^e + [M]^e \{\ddot{a}\}^e + [\zeta]^e \{\dot{a}\}^e \qquad (6.6)$$

The element equilibrium eqn(6.1) transforms to

$$[M]^e \{\ddot{a}\}^e + [\zeta]^e \{\dot{a}\}^e + [K]^e \{a\}^e + \{f_p\}^e + \{f_{\varepsilon 0}\}^e + \{f_b\}^e = \{q\}^e \qquad (6.7)$$

assembling all elements, this reduces to

$$[M]\{\ddot{a}\} + [\zeta]\{\dot{a}\} + [K]\{a\} = \{R'\} \qquad (6.8)$$

where

$$\{R'\} = \{R\} - \{f_p\} - \{f_{\varepsilon 0}\} - \{f_b\}$$

and

$$[M] = \sum_e \underbrace{\int_{V_e} [N_e]^T \rho_e [N_e] dV_e}_{[M]^e} \tag{6.9}$$

$$[\dot{\varphi}] = \sum_e \underbrace{\int_{V_e} [N_e]^T \dot{\varphi}_e [N_e] dV_e}_{[\dot{\varphi}]^e}$$

Matrix [M] represents the mass matrix of the structure. When it is derived as in the above manner, it is termed the consistent mass matrix since it is consistent with the virtual work formulation. This matrix is symetric, containing both diagonal and off-diagonal terms. It is possible to reduce the computation cost involved in evaluating the consistent mass matrix by distributing the mass of the element equally between its nodes. A mass matrix derived in this manner is termed the lumped mass matrix, which is always diagonal.

Although the consistent mass matrix should theoretically give superior results, this increased solution accuracy may not warrant the increase in cost, thus the lumped diagonal mass matrix is often used.

Matrix [$\dot{\varphi}$] represents the consistent damping matrix which is related to the damping characteristics of the material. Usually significant damping effects in a structure are caused by concentrated dampers. For this reason a diagonal lumped damping matrix is employed where the diagonal coefficients represent concentrated nodal damping effects.

6.2.1 Free Vibration Analysis

The natural frequencies and mode shapes of an undamped[1] structure can be calculated from eqn(6.8) by substituting

$$[\dot{C}] = 0$$

$$\{R'\} = 0$$

Hence eqn(6.8) reduces to

$$[M]\{\ddot{a}\} + [K]\{a\} = 0 \tag{6.11}$$

This can be transformed into an eigenvalue problem by assuming that the response is periodic with an amplitude $\{a_0\}$

$$\{a\} = \{a_0\}\cos\omega t \tag{6.12}$$

This results in a set of homogeneous linear equations

$$\left[[K] - \omega^2[M]\right]\{a_0\} = 0 \tag{6.13}$$

This matrix equation may be solved by a transformation to the special eigenvalue problem

$$[H]\{x\} = \lambda\{x\} \tag{6.14}$$

Such a transformation is presented in ref [1]. Once the solution to the special eigenvalue problem has been obtained an inverse transformation provides an evaluation of the natural frequencies and mode shapes of the structure.

---

1 It is possible to account for damping in the free vibration problem, however this requires a more complicated solution technique since the resulting mode shapes are complex quantities. A method of solving such problems is presented in [14]

6.2.2 Forced Vibration Analysis

By solving the equations of motion it is possible to study the response of a structure when a forced periodic or transient excitation is applied. Two methods are available to obtain a solution. Either a direct time integration technique or a modal analysis may be employed.

The direct time integration technique relies on a numerical approach to integrate the equations of motion, eqn (6.8). Since these methods are based on time-stepping, care must be taken to ensure that the time step selected is sufficiently small to ensure solution stability.[1] In addition, the time step selected should be less than the smallest period likely to occur in the response, thus ensuring solution convergence.[2]

The method of modal analysis transforms the coupled simultaneous equations of motion into a set of decoupled ordinary differential equations. This technique is referred to as the normalised mode procedure in Ref [1], where it is shown that by making a coordinate transformation the equations of motion can be decoupled, ie

$$\{a\} = [\Delta_0]\{Z\} \qquad (6.15)$$

where

$$[\Delta_0] = [\{a_0\}_1, \{a_0\}_2 \ldots \{a_0\}_n]$$

$\{a_0\}_i$ represents the ith normalised[3] mode obtained from the eigenvalue analysis.

---

1. This is dependent on the numerical algorithm employed. By stability it is implied that errors made at one stage of the calculations do not increase as the calculations proceed but rather damp out.

2. By convergence it is meant that the results of the solution would approach the analytical values if they were available, [16].

3. Normalisation implies that the mode vectors $\{\delta_0\}_i$ are scaled such that $\{\delta_0\}_i^T[M]\{\delta_0\}_j = \begin{matrix} 1 & i = j \\ 0 & i \neq j \end{matrix}$

substituting eqn (6.15) into the equation of motion, eqn (6.8) is transformed to

$$[\Delta_0]^T[M][\Delta_0]\{\ddot{Z}\} + [\Delta_0]^T[\Phi][\Delta_0]\{\dot{Z}\} + [\Delta_0]^T[K][\Delta_0]\{Z\} = [\Delta_0]^T\{R\}$$

Since the mass and stiffness matrices are orthogonal to the eigenvector column matrix $[\Delta_0]$,

$$[\Delta_0]^T[M][\Delta_0] = \Lambda_M$$

$$[\Delta_0]^T[K][\Delta_0] = \Lambda_K$$

where Λ indicates that these matrices are diagonal.

If the damping matrix exhibits the above orthogonal properties when operated on by $[\Delta_0]$, then the equations are decoupled and can be solved independently. In general, orthogonality of the damping matrix with the eigenvector column matrix does not occur for viscous damping unless the natural frequencies and mode shapes are evaluated for the damped system in question. Since this requires a more complicated algorithm capable of handling complex numbers, it is common practice to assume the damping matrix is such that

$$\{a_0\}_i[\Phi]\{a_0\}_j = \begin{cases} 2\omega_i C_i & i = j \\ 0 & i \neq j \end{cases} \qquad (6.16)$$

where C_i represents the ith modal damping coefficient corresponding to the ith mode of vibration. This assumption is tantamount to imposing proportional damping, where the overall damping effect is some linear combination of the mass and stiffness matrices, ie

$$[\Phi] = \alpha[M] + B[K]$$

In such cases the damping matrix can be proved to be orthogonal to the mode shape vectors obtained from an undamped free vibration

analysis. This indicates that the assumption introduced in eqn (6.16) is valid, however it is difficult to ascertain the modal damping factors required to model a structure which in practice, is damped in specific areas only. (This is not a limitation with the direct time integration technique since the diagonal coefficients of the damping matrix represent concentrated nodal damping effects.)

An important aspect of a modal analysis is that the entire structure must be discretised even if symmetry in loading and geometry exists. This is necessary since non symmetric mode shapes are possible. Ultimately a modal analysis is only effective if the structure behaves linearly. That is where the stiffness matrix remains unchanged throughout the solution.

6.3 ADINA PROGRAM CAPABILITIES

It is possible to simulate a variety of mechanical vibration problems with the ADINA package. The options available to analyse such problems are summarised in Fig 6.1 and Fig 6.2.

6.3.1 Free Vibration Analysis

In a free vibration analysis the natural frequencies and mode shapes are computed. Either a lumped or consistent mass matrix can be selected. Additional concentrated nodal masses can be specified if required. An important feature of the program is its ability to apply a rigid body mode shift to eliminate zero frequencies during the eigenvalue solution. These frequencies may occur if a structure is inadequately constrained. A damped free vibration analysis is not possible with the current [7] version of ADINA.

6.3.2 Forced Vibration Analysis

For both linear and nonlinear analyses a periodic or transient forcing function may be modelled by prescribing nodal displacements or concentrated and distributed loads, as a function of time. Proportional loading may be superimposed to include effects where the entire structure undergoes a simultaneous acceleration. This may be of considerable importance when analysing the response of a structure to ground vibrations. If this option is selected, a lumped mass matrix must be specified.

6.3.3 Linear Forced Vibration Analysis

This applies to structures which respond linearly to a transient or forced excitation. The resulting equations of motion may be solved by applying a modal or a direct time integration technique (implicit or explicit).

In a modal analysis, modal damping factors are defined prior to the solution. Alternatively concentrated nodal dampers may be specified for translational and rotational degrees of freedom if a direct time integration technique is employed.

The user has the option of selecting either a lumped or a consistent mass matrix. In addition, concentrated nodal masses may be specified.

If an explicit time integration technique is selected then a lumped mass matrix must be used. This is applicable in both linear and nonlinear dynamic analyses, the latter analysis will be discussed in the next section.

6.3.4 Nonlinear Forced Vibration Analysis

In a nonlinear dynamic analysis, nonlinear behaviour of the structure

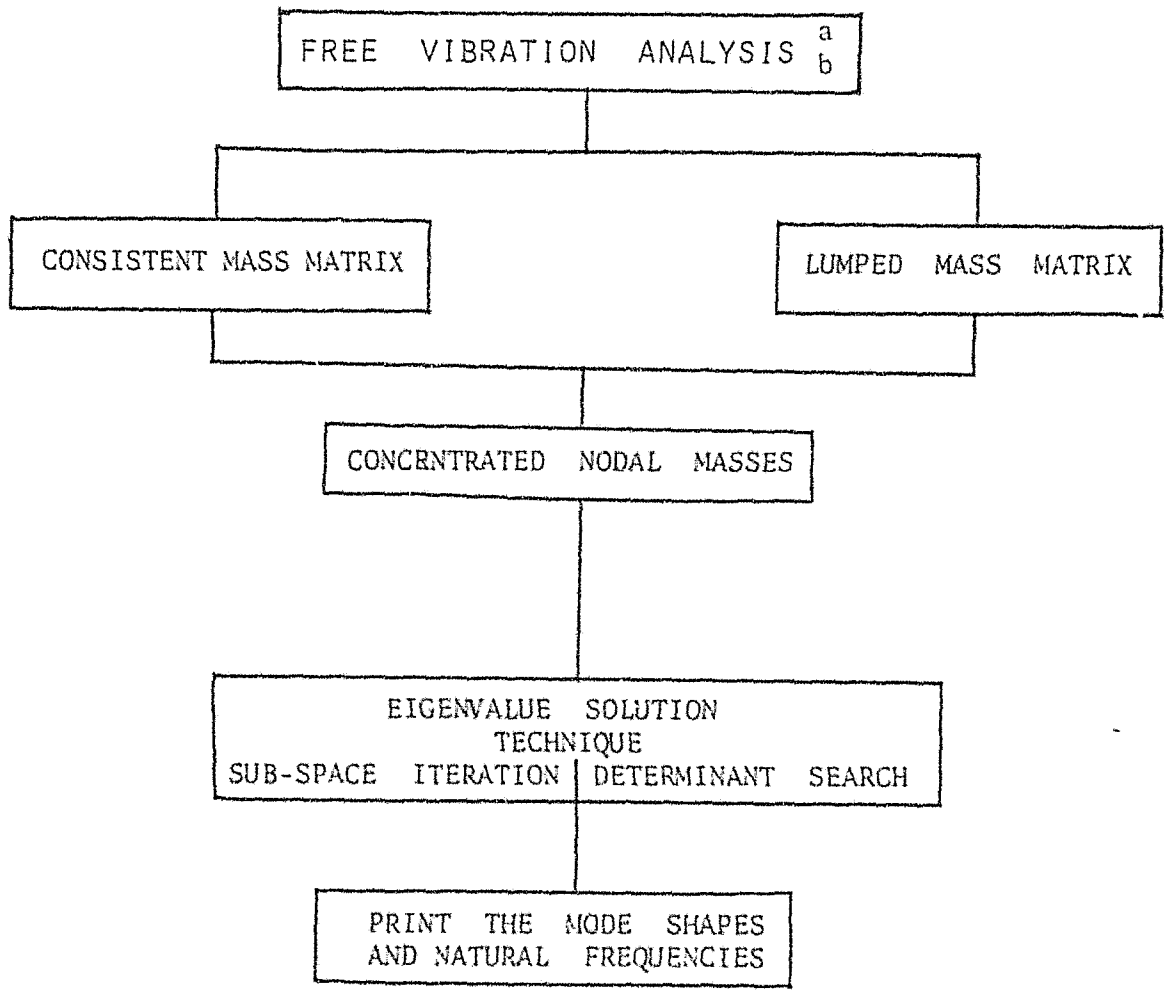

a. No damping is assumed

b. Zero frequencies can be eliminated, avoiding numerical difficulties

Figure 6.1 - Flow Chart Illustration of Options Available when Executing a Free Vibration Analysis with ADINA

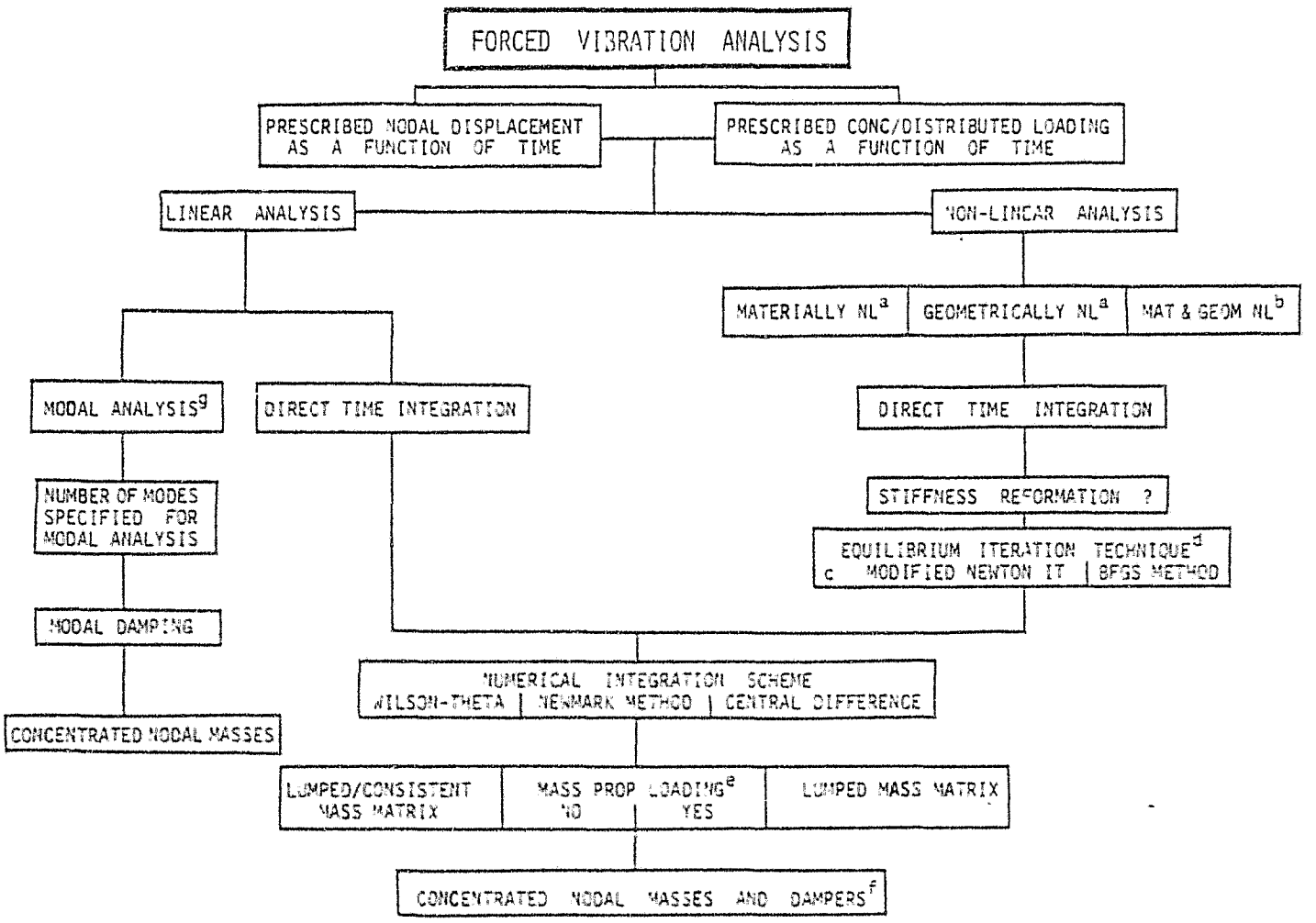

a. Total Lagrangian
b. Updated Lagrangian
} Lumped Mass Matrix should be used

c. Aitken Acceleration Scheme optional with Modified Newton Iteration

d. Maximum number of Iterations permitted = 15

e. If Mass Proportional Loading is specified, a Lumped Mass Matrix must be used

f. For Large Displacement Nonlinear Analysis, Concentrated Masses should not be specified for Rotational Degrees of Freedom [7]. Modal Analysis may be used for slightly Nonlinear problems [3]

Figure 6.2 - Flow Chart Illustration of the Options Available when Executing a Forced Vibration Analysis with ADINA (1981 version)

may be induced by material, geometric, or both material and geometric effects. Stiffness reformation as well as equilibrium iteration may be performed during the solution at selected time intervals.

Direct time integration is employed to integrate the equations of motion; an explicit (central differences) or implicit (Wilson-θ, Newmark Method) technique may be selected.

The damping matrix is formed by defining concentrated dampers. This always results in a diagonal damping matrix. A lumped or consistent mass matrix may be selected with the option of defining additional concentrated masses.

6.4 APPLICATION OF THE METHOD: *FREE VIBRATION ANALYSIS OF SIMPLE BEAM STRUCTURES*

6.4.1 Introduction

Two physical models were built to investigate the correlation between a finite element simulation of a simple structure and experimentally observed results. The experiment involved measuring and observing the natural frequencies and associated mode shapes induced by exciting the models with an electromagnetic vibrator. Dimensions of the models are shown in Fig 6.3.

To increase the number of experimental parameters concentrated masses were attached to the model as illustrated in Fig 6.4. The mass of the electromagnetic vibrator was accounted for in all three configurations.

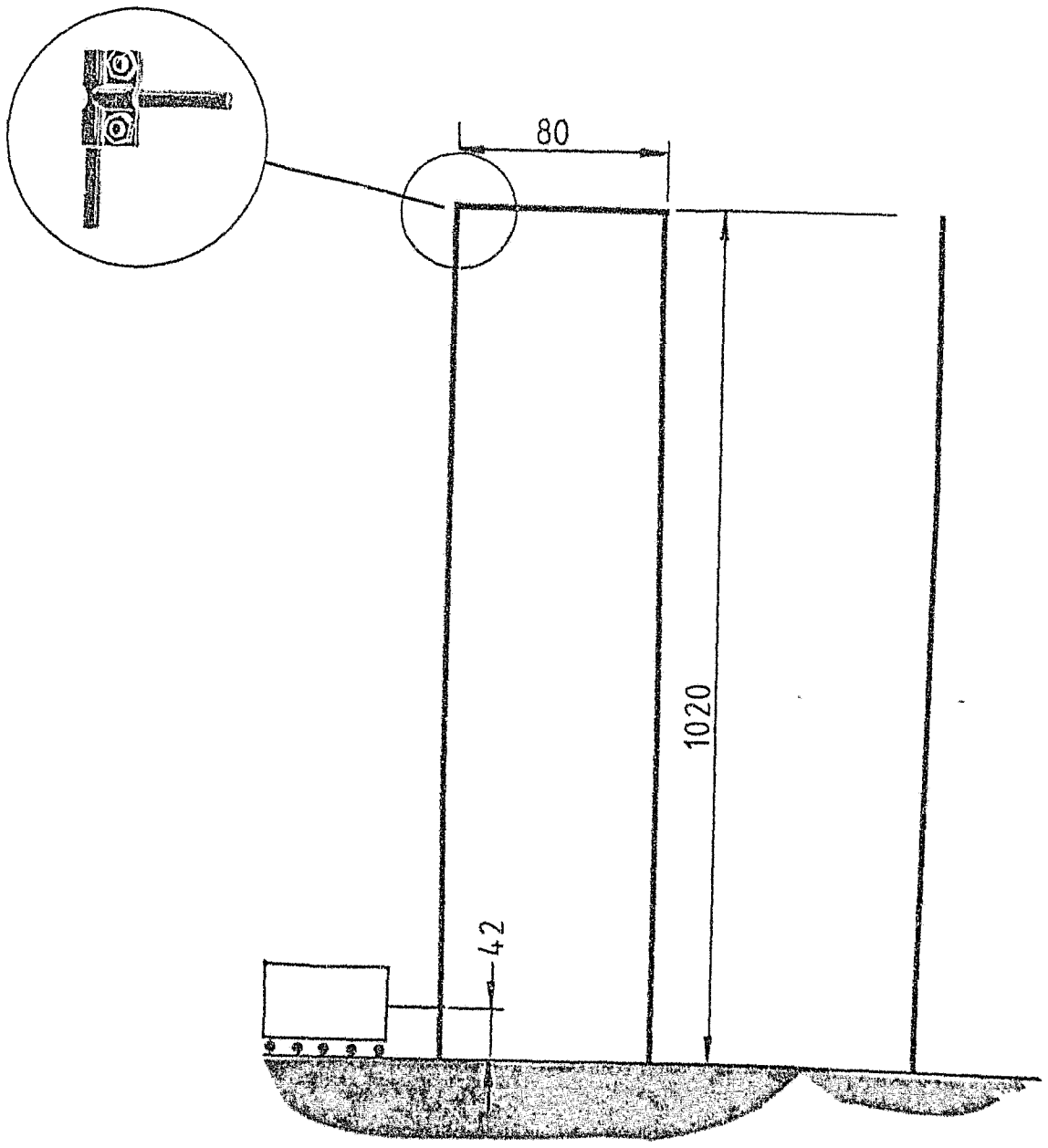

M - ELECTROMAGNETIC VIBRATOR
vibrator mass = 1,25 kg

Figure 6.3 - Portal Frame and Cantilever Beam Models

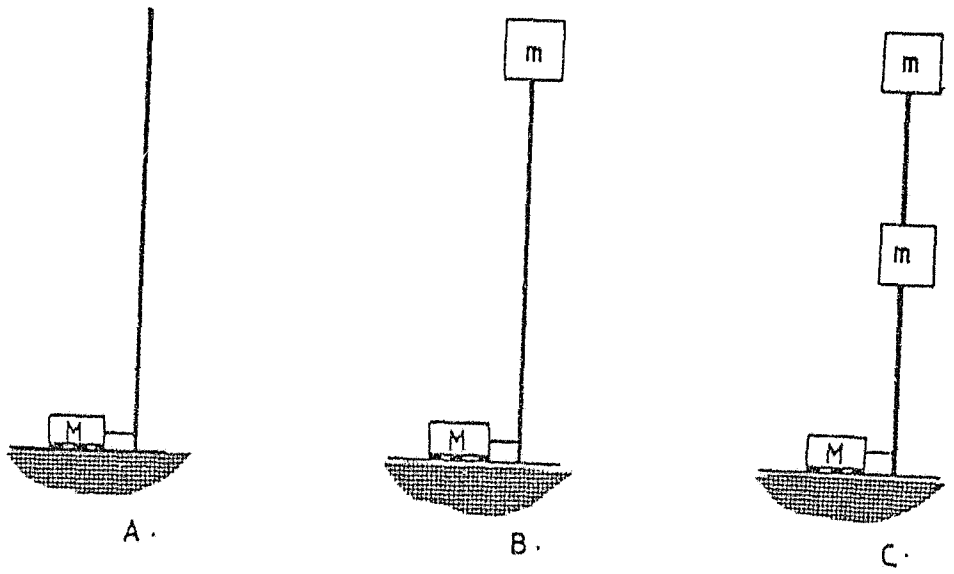

Model 1 - Cantilever beam

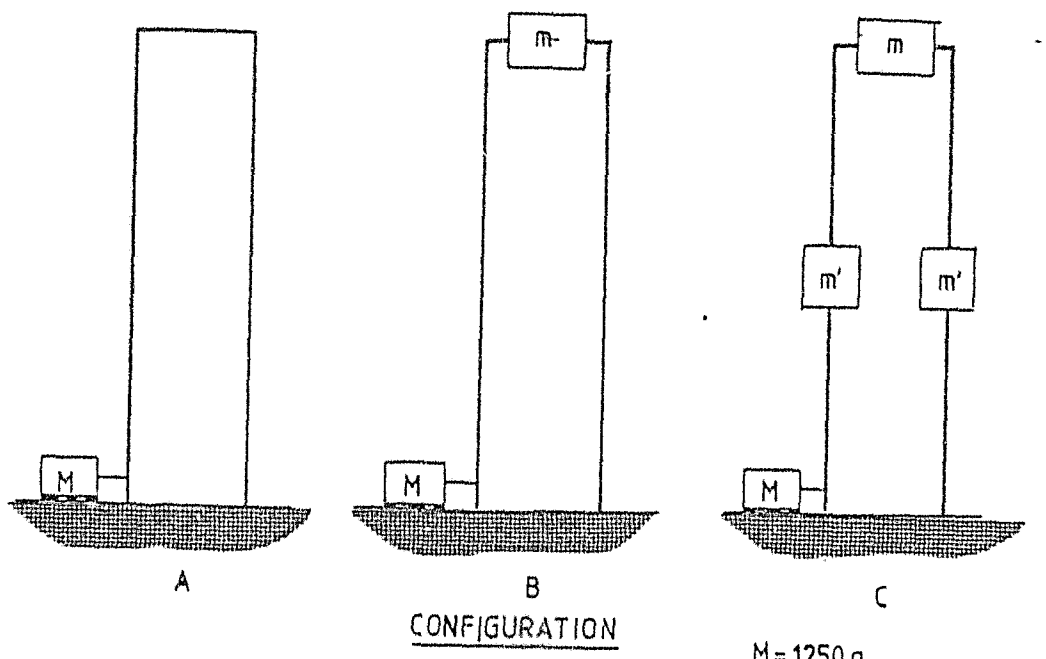

Model 2 - Portal Frame

Figure 6.4 - Mass Configurations

6.4 2 Experimental Apparatus

ELECTRO-MAGNETIC VIBRATOR	:	Ling Dynamic Systems: Model 100
		Max Shaking Force : 9 N
		Max Displacement : 2,5 mm PK-PK
POWER AMPLIFIER - WAVE GENERATOR	:	Ling Dynamic Systems: Model TPO 25
		Frequency : 0,5 Hz - 20 kHz

The models were constructed with 4 mm diameter steel rods screwed into a heavy base plate. Connectors from a FAG universal construction system were used to secure the crossbar of the portal frame. This facilitates easy modification for future experiments.

An electromagnetic vibrator applied an oscillatory excitation to near the base of the model. The frequency of excitation was controlled by means of a wave generator. This served as a measuring device for ascertaining the resonant frequencies of the model. The resonant frequency was ascertained through direct observation and was taken to be the frequency at which the model experienced the maximum displacements.

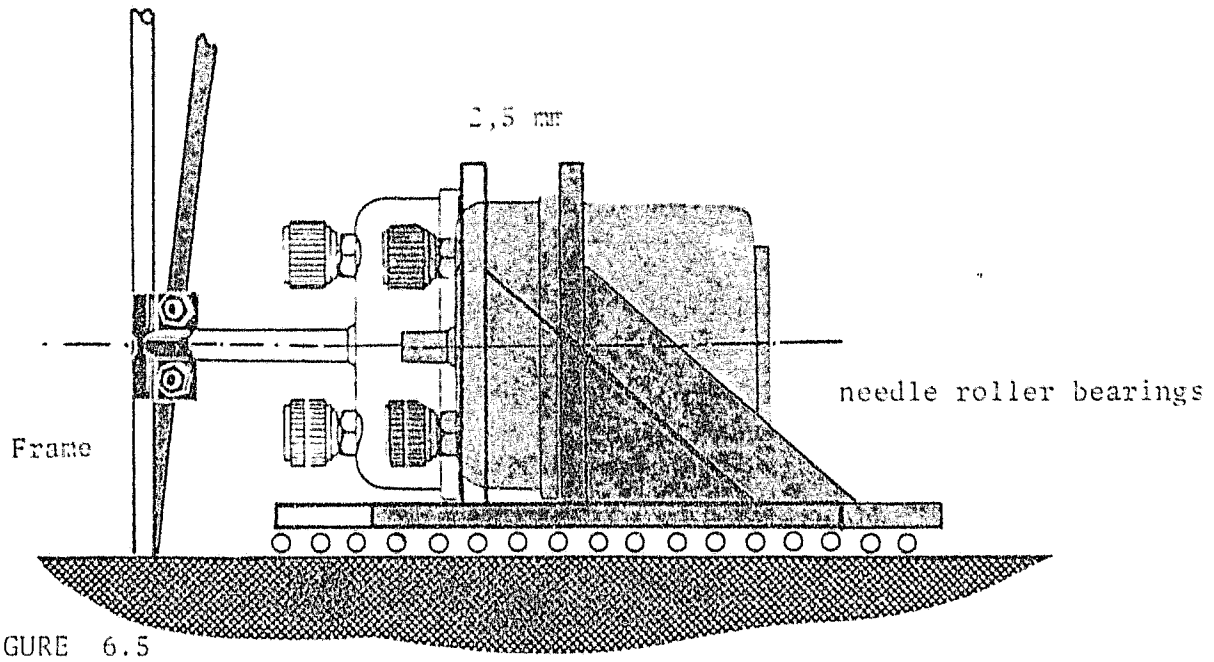

FIGURE 6.5

Figure 6.5 - Electromagnetic Vibrator Attachment

6.4.3 Experimental Procedure

According to the configuration to be tested, masses were attached to the model and the frequency of the electromagnetic vibrator was slowly increased. When resonance occurred the frequency was noted and the associated mode shape was observed by using stroboscopic effects. Ascertaining both the resonant frequency and the mode shape, proved to be difficult for the higher modes of vibration where the displacements were small and resonance less obvious.

In cases where the resonant frequency occurred below the graduated range of the wave generator (1 hz), the frequency of vibration was determined by recording the time taken for the model to complete 10 cycles. In such cases the procedure was repeated at least three times to obtain an average reading.

6.4.4 Limitations of the Measuring Technique

Owing to the mechanism employed to attach the vibrator to the frame of the model the particular excitation force produced is proportional to the frequency of oscillation (Fig 6.5). At low frequencies (< 4 hz) it is difficult to detect precisely when resonance occurs since:

- insufficient energy is applied to the model and hence the displacements are relatively small
- once the model begins to vibrate the vibrator frequency can be changed substantially before the oscillation dies out. Thus the band width over which resonance occurs is about 10 percent.

It was possible to determine resonance accurately for the intermediate modes of vibration (4 hz < f < 50 hz). Whereas in this range resonance was observable, the displacements became substantially reduced once this range was exceeded (f > 50 hz). Here resonance was audible, however careful observation was required

to determine the particular mode shape.

The graduated scale on the wave generator was accurate to one significant figure. This further impaired the accuracy of measurement at low frequencies.

6.4.5 Mechanical Properties of the Steel Rod

Material properties of the steel rod are required as input when executing a finite element simulation. The properties required are Poisson's Ratio ν, and Young's Modulus E.

Owing to the dimensions of the rod it was not possible to mount the required number of electrical resistance strain gauges needed to obtain an accurate determination of Poisson's Ratio. Since the rod appeared to be a mild steel, a value of 0,3 was assumed.

It was possible however, to determine the value of Young's modulus experimentally. A rod was mounted in an Instron Testing Machine. An Amsler mechanical extensometer with a 200 mm gauge length monitored the increase in gauge length with increase in load.

The experimental results are tabulated in Table 6.1. A least squares fit to the data gives a value of 195,8 GPa for Young's Modulus. Error analysis indicates that the maximum error expected in the above calculation is of the order of 2,5%. In view of this, the commonly accepted value for steel, namely 200 GPa was assumed in subsequent work. Plot 6.1 illustrates the experimental results graphically.

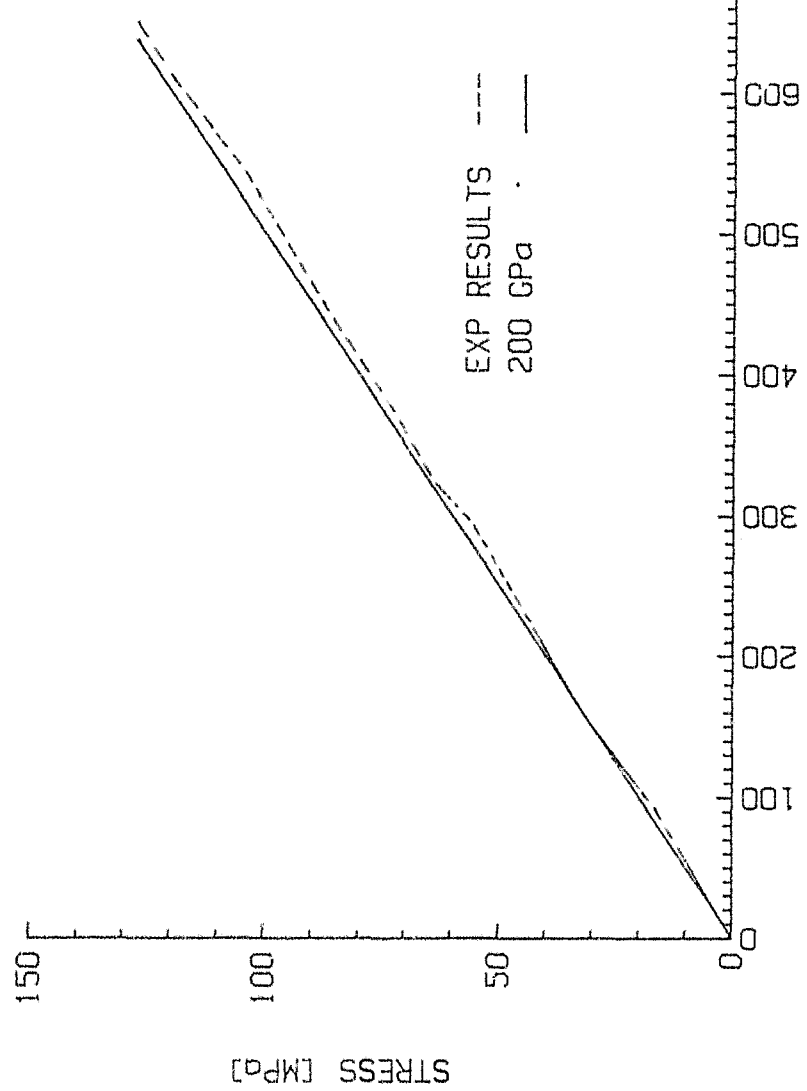

Plot 6.1 - Stress/Strain Curve for the Steel Rod

TABLE 6.1 - MECHANICAL PROPERTIES OF THE STEEL ROD: EXPERIMENTAL RESULTS

LOAD [N]	δ [$x10^{-2}$ mm]	STRESS [MPa]	STRAIN [$x10^{-6}$]
0	0		0
200	1,8	15,9	19
300	2,5	23,9	125
400	3,2	31,8	160
500	4,1	39,8	205
600	5,0	47,7	250
700	5,9	55,7	295
800	6,5	63,7	325
900	7,4	71,6	370
1 000	8,2	79,6	410
1 100	9,0	87,5	450
1 200	9,9	95,5	495
1 300	10,8	103,5	540
1 400	11,5	111,4	575
1 500	12,2	119,4	610
1 600	13,0	127,3	650

6.5 FINITE ELEMENT ANALYSIS

The initial stage of any finite element analysis involves modelling the structure by discretising it into a mesh of elements. The model should be idealised so as to simplify the analysis by eliminating unnecessary complexities. It is for this reason that the portal frame and cantilever beam were idealised as planar bodies. This simplification was employed once it had been ascertained that no out of plane motion occurred during the experiment.

Since the vibrator was attached to the lower part of the portal frame/cantilever beam, its mass was accounted for in the idealised

model. It was assumed that the vibrator contributed a translational mass equivalent to its static mass, at its point of contact with the structure.

6.5.1 Finite Element Mesh

Two[1] dimensional beam elements were used to idealise the physical models. These are two noded elements with three degrees of freedom

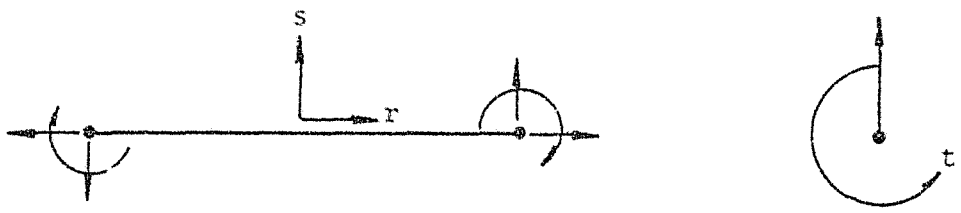

rs local coordinate axes
[for a circular section, t represents a tangential coordinate]

FIGURE 6.6 - 2-Noded Beam Element

The reader is referred to the ADINA users manual [7] for further information regarding these elements.

Three meshes were defined for the first model whilst two were defined for the second. These are illustrated in Sections 6.5.2

---

1 When a beam element is used in two-dimensional action an option is available to increase the computational efficiency of the element [7]. This option is only applicable if a nonlinear analysis is specified. Advantage was taken of the option by specifying a nonlinear material analysis with a linear material model.

and 6.5.3.

In all the analyses a consistent mass matrix was selected with additional concentrated masses defined where applicable. For the purpose of numerical integration to evaluate the stiffness matrix, the default option was adopted. That is, five point integration for the r direction, one point for the s direction and three point for the t direction.

6.5.2 Free Vibration Analysis of a Cantilever Beam

The first phase of the experiment involved determining the natural frequencies and mode shapes of the cantilever beam illustrated in Fig 6.3 (model 1). Concentrated masses were added to the beam as illustrated in Fig 6.4. Three meshes were defined (Fig 6.7). In the analysis the vibrator's mass was modelled by specifying a concentrated translational mass at node 2.

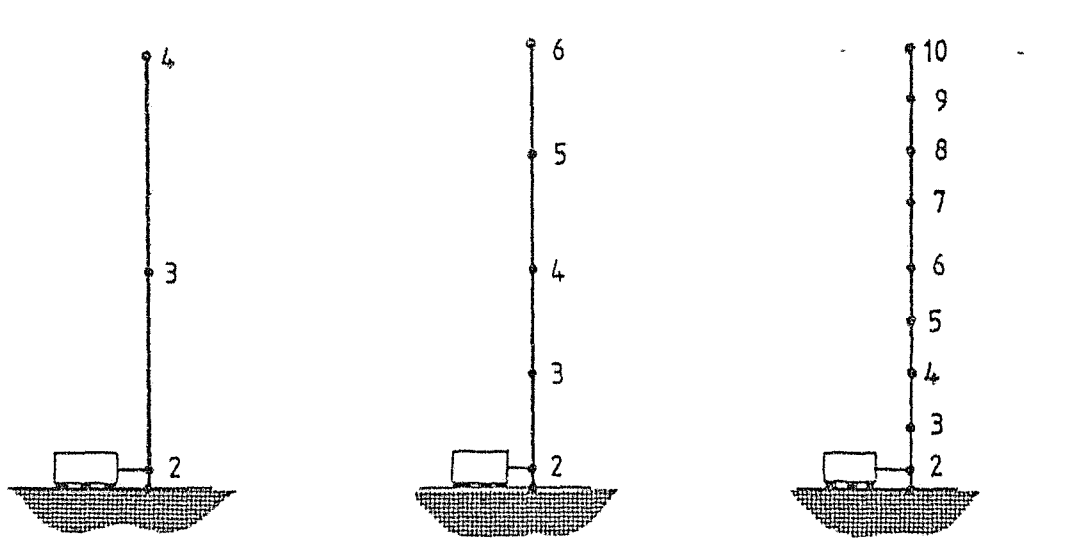

MESH 1
3 elements 4 nodes

MESH 2
5 elements 6 nodes

MESH 3
9 elements 10 nodes

(2 dimensional beam elements)

FIGURE 6.7 - Mesh Topology for Model 1

The first three resonant frequencies determined experimentally are tabulated in Table 6.2, together with the finite element results. In the finite element analysis, the first four natural frequencies were extracted.

TABLE 6.2 - FREE VIBRATION ANALYSIS OF A CONTILEVER BEAM

			ADINA FINITE ELEMENT ANALYSIS		
CONFIG:	MODE No.	f (hz) EXPER:	f MESH 1	f MESH 2	f MESH 3
A 	1	2,1	2,381	2,380	2,380
	2	14,0	14,910	14,830	14,810
	3	40,0	40,510	38,070	37,930
	4		60,330	54,170	53,890
B 	1	0,76	0,898	0,898	0,898
	2	11,0	10,890	10,805	10,800
	3	32,5	35,740	32,630	32,501
	4		52,625	50,000	49,800
C 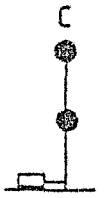	1	0,680	0,861	0,861	0,861
	2	5,6	5,510	5,508	5,508
	3	30,0	35,140	31,690	31,560
	4		47,680	44,330	44,210

Although the fourth frequency was not determined experimentally, the fourth frequency from the finite element analysis served to evaluate the accuracy which could be expected with the mesh. That is, if convergence is achieved for the fourth mode, it is expected that the first three modes will be accurately modelled. The first four mode shapes for Configuration A are illustrated in Fig 6.8.

The experimental and finite element results correlate satisfactorily for the second and third frequencies. The first natural frequency is inaccurately predicted for all three configurations (see Table 6.4.1). This discrepancy is due to the experimental technique of determining resonance as discussed in Section 6.4.4.

In order to ascertain whether the discrepancies cited in Table 6.4.1 for the second and third mode are due to a poor mesh design, or

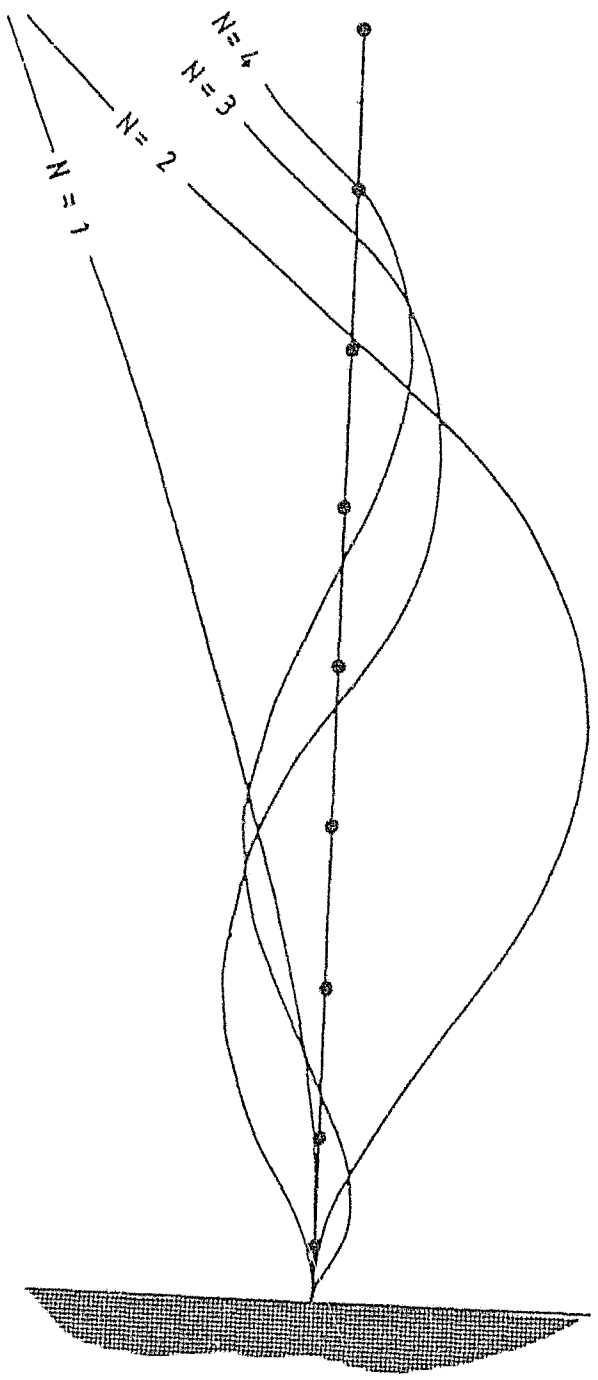

FIGURE 6.8 - Mode Shapes of the Cantilever beam

TABLE 6.3 - DISCREPANCY BETWEEN EXPERIMENTAL MEASUREMENTS AND FINITE ELEMENT RESULTS FOR MESH 3

	% ERROR = 100 $(\frac{f_{exp}-f_3}{f_{exp}})$		
	CONFIGURATION		
MODE NO	A	B	C
1	-13,30%	-18,16%	-26,62%
2	- 5,79%	1,82%	1,64%
3	5,25%	- 0,003 1%	- 5,00%

the assumption that the vibrator contribues its full mass, a further analysis was executed. The object of this analysis was to compare the finite element results obtained from mesh 3, when the vibrator mass is neglected, with a theoretical solution cited in the literature [14]. The comparison is presented in Table 6.4.

TABLE 6.4 - NATURAL FREQUENCIES OF A CANTILEVER BEAM

MODE NO	f(Hz) REF [14]	f(Hz) FEM
1	2,38	2,38
2	14,92	14,92
3	41,79	41,79
4	81,87	82,05

It is apparent from this analysis that Mesh 3 is sufficiently well refined to achieve a high degree of accuracy up to the fourth resonant frequency. This indicates that the discrepancies cited in Table 6.3 are chiefly due to the assumption that the vibrator acts as a concentrated mass attached to Node 2. In fact its motion is larger and more complex because of internal flexibility at this point of application.

6.5.3 Free Vibration Analysis of a Portal Frame

The second phase of the experiment involved a similar analysis of the portal frame illustrated in Fig 6.3. Concentrated masses were defined as illustrated in Fig 6.4. Two meshes were selected as in Fig 6.9.

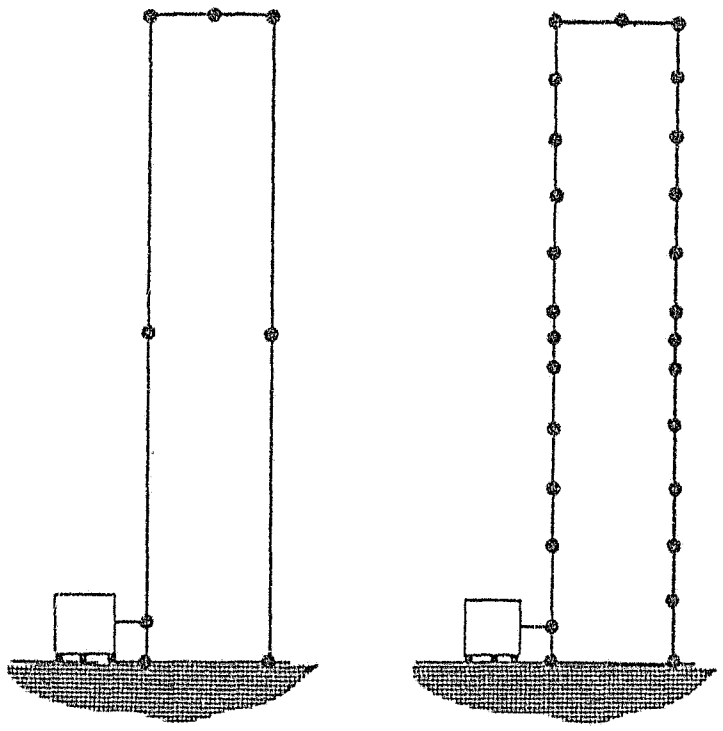

MESH 1
7 elements 8 nodes

MESH 2
26 elements 27 nodes

(2 dimensional beam elements)

FIGURE 6.9 - Mesh Topology for Model 2

The first eight resonant frequencies are tabulated in Table 6.5 together with the finite element results.

The analysis yields similar trends to those observed in the previous study. The percentile discrepancy between the experimental results and those obtained from the analysis (employing Mesh 2) are tabulated in Table 6.6.

TABLE 6.5 - VIBRATION ANALYSIS OF A PORTAL FRAME

			FINITE ELEMENT ANALYSIS	
CONFIGURATION	MODE No	f (hz) EXPERIMENT	f MESH 1	f MESH 2
A 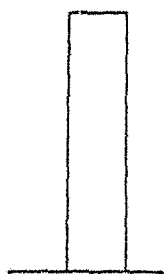	1	3,4	3,441	3,462
	2	13,2	11,04	13,760
	3	18,0	15,86	18,87
	4	37,5	22,42	37,19
	5	44	51,72	44,55
	6	62	66,76	56,36
	7	75	142,4	79,27
	8	85	252,5	92,56
B 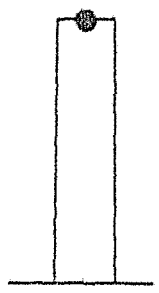	1	1,5	1,65	1,65
	2	12,9	10,72	13,72
	3	14,5	14,68	15,27
	4	37	19,71	36,45
	5	40	47,94	40,05
	6	49	59,34	53,94
	7	75	78,28	69,05
	8	81	203,41	83,08
C 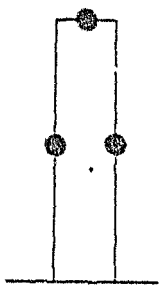	1	1,45	1,511	1,513
	2	6,5	6,275	6,411
	3	7,75	7,512	7,66
	4	36	14,69	36,27
	5	40	46,62	39,80
	6	47,5	51,75	49,33
	7	60	77,62	59,80
	8	65	181,9	70,75

TABLE 6.5 - VIBRATION ANALYSIS OF A PORTAL FRAME

CONFIGURATION	MODE No	f (hz) EXPERIMENT	FINITE ELEMENT ANALYSIS f MESH 1	FINITE ELEMENT ANALYSIS f MESH 2
A 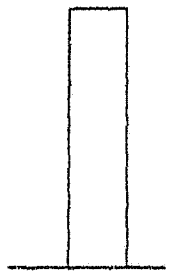	1	3,4	3,441	3,462
	2	13,2	11,04	13,760
	3	18,0	15,86	18,87
	4	37,5	22,42	37,19
	5	44	51,72	44,55
	6	62	66,76	56,36
	7	75	142,4	79,27
	8	85	252,5	92,56
B 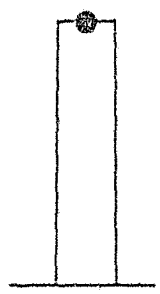	1	1,5	1,65	1,65
	2	12,9	10,72	13,72
	3	14,5	14,68	15,27
	4	37	19,71	36,45
	5	40	47,94	40,05
	6	49	59,34	53,94
	7	75	78,28	69,05
	8	81	203,41	83,08
C 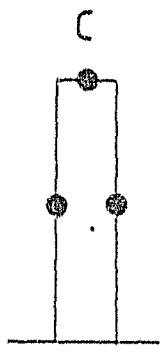	1	1,45	1,511	1,513
	2	6,5	6,275	6,411
	3	7,75	7,512	7,66
	4	36	14,69	36,27
	5	40	46,62	39,80
	6	47,5	51,75	49,33
	7	60	77,62	59,80
	8	65	181,9	70,75

Author Constancon C P
Name of thesis A study of the finite element method, with reference to the Adina finite element package 1983

PUBLISHER:
University of the Witwatersrand, Johannesburg
©2013

LEGAL NOTICES:

Copyright Notice: All materials on the University of the Witwatersrand, Johannesburg Library website are protected by South African copyright law and may not be distributed, transmitted, displayed, or otherwise published in any format, without the prior written permission of the copyright owner.

Disclaimer and Terms of Use: Provided that you maintain all copyright and other notices contained therein, you may download material (one machine readable copy and one print copy per page) for your personal and/or educational non-commercial use only.

The University of the Witwatersrand, Johannesburg, is not responsible for any errors or omissions and excludes any and all liability for any errors in or omissions from the information on the Library website.

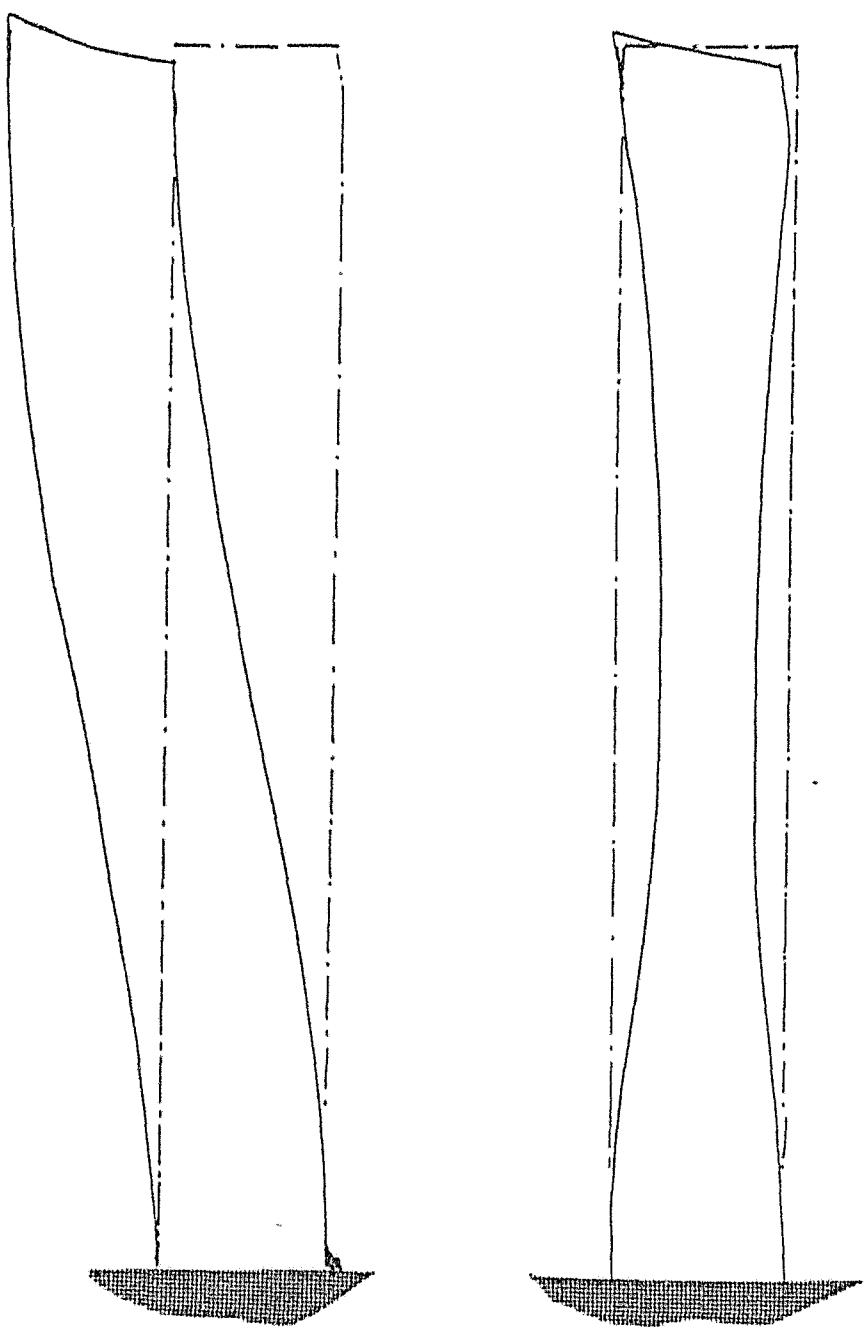

FIGURE 6.10

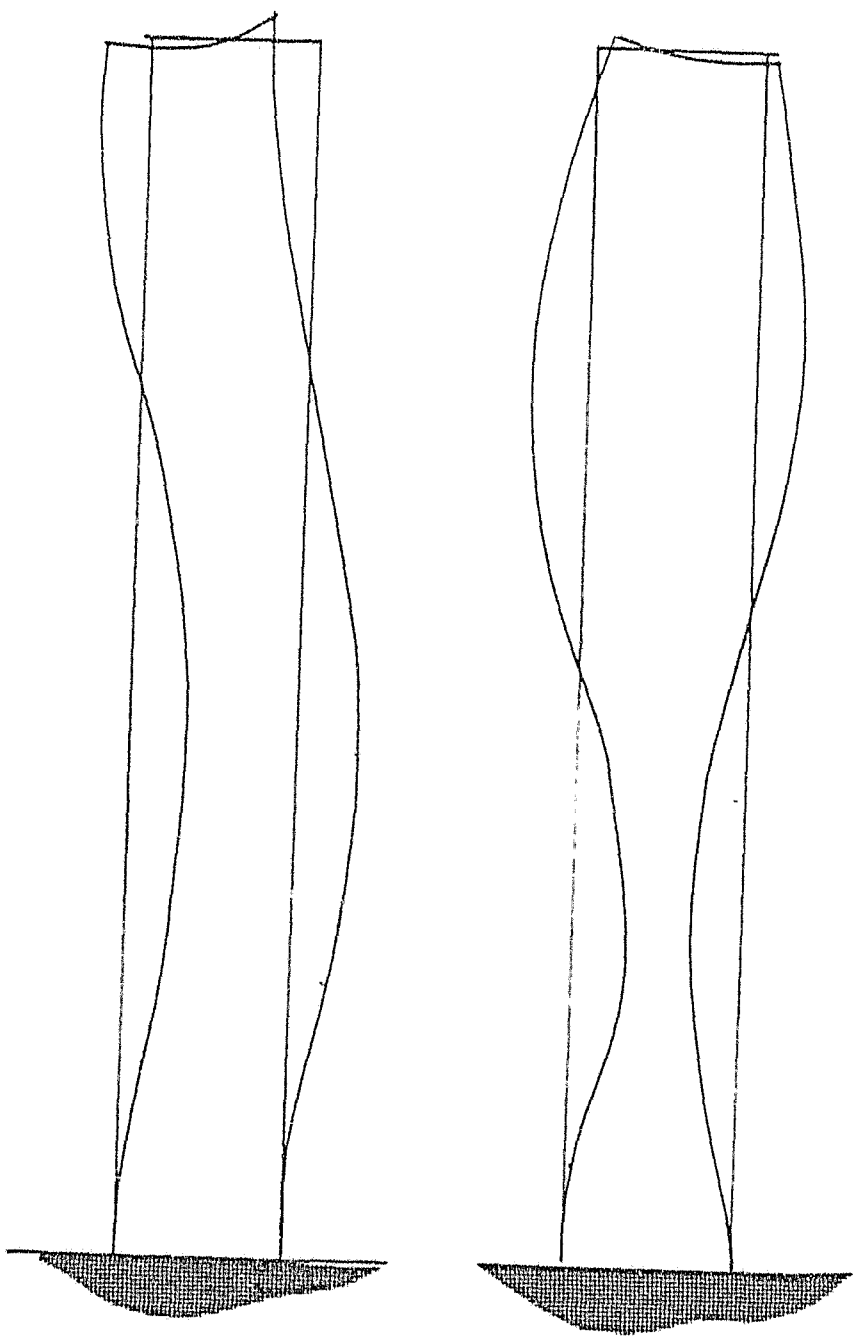

FIGURE 6.11

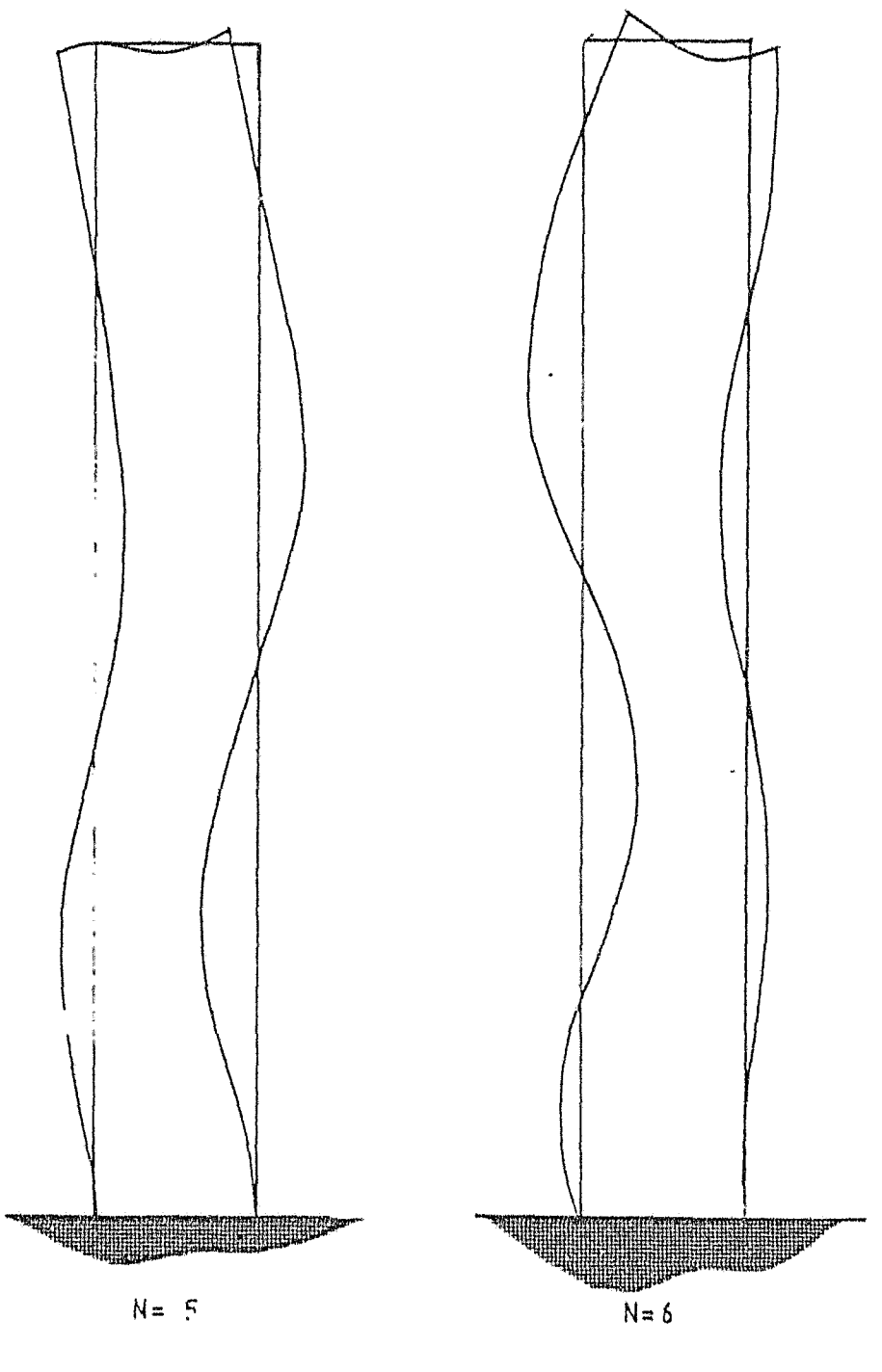

FIGURE 6.12

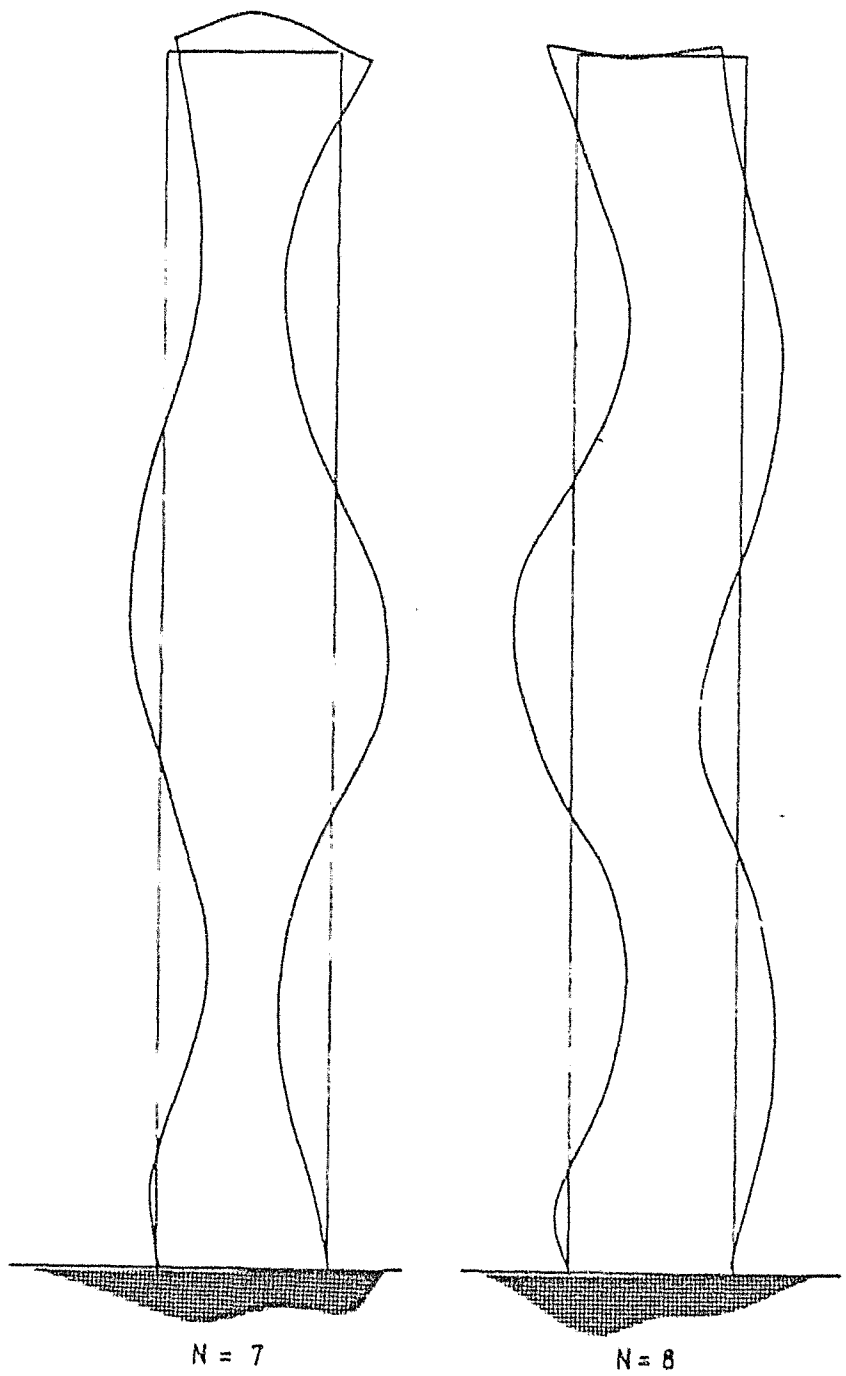

FIGURE 6.13

ABLE 6.6 - DISCREPANCY BETWEEN EXPERIMENTAL MEASUREMENTS AND FINITE ELEMENT RESULTS (MESH 2)

	$E = (\frac{f_{ex}-f_z}{f_{ex}}) \times 100$		
	CONFIGURATION		
MODE	A	B	C
1	1,82%	10,0%	4,3%
2	4,20%	6,3%	1,3%
3	4,80%	5,3%	1,1%
4	0,80%	1,4%	0,7%
5	1,20%	0,1%	0,5%
6	9,10%	10,0%	3,8%
7	5,30%	7,9%	0,3%
8	8,20%	2,4%	8,8%

For configuration B, C there is a large discrepancy for the first mode since the resonant frequencies fall below 3 hz. The results appear satisfactory up to mode 5 for configuration A,B, and up to mode 7 for configuration C. This may be a result of the vibrator mass becoming a less predominant feature as the total mass of the frame increases. Further scrutiny of the mode shapes indicates that the vibrator mass undergoes its largest relative displacement for modes 6, 7 and 8 (see Figs 6.14 and 6.15) and thus its effect should be predominant in these modes. This is supported by the results cited in Table 6.6.1. The eight mode shapes are plotted for configuration A in Figs 6.12 to 6.15.

6.6 CONCLUSIONS

This study confirms that the finite element technique is a powerful tool for estimating the natural frequencies of complex structures.

It is evident when comparing the finite element results obtained from the different meshes that the first resonant frequency is well estimated even by the coarsest mesh. (In both applications presented, the first resonant frequencies evaluated were within 2% of one another). Further examination reveals that as the mesh is refined, the magnitude of the resonant frequencies predicted decreases. (A coarse mesh overestimates [3] the stiffness matrix and consequently the predicted resonant frequencies are high.) As the mesh is refined, the stiffness matrix is more accurately evaluated hence convergence to the true solution will be achieved.

The degree of refinement required to obtain accurate results depends on the number of mode shapes requested. It is common practice to define the minimum number of degrees of freedom as five times the number of mode shapes requested. The validity of this rule is supported by Table 6.7, where a subjective comparison of mesh accuracy versus degrees of freedom is presented (the mesh is considered adequate if the resonant frequencies predicted are within 5% of the true (datum) values).

In the case of the cantilever beam, it has been shown that the finite element results obtainable with Mesh 3, compare favourably with analytic results (see Table 6.5). For the purpose of comparison, Mesh 3 - configuration A, denotes the datum (see Table 6.4).

For the case of the portal frame, Mesh 2 - configuration C was selected as the datum, where it is assumed that if the exact solution was available, the results would be within 5%, up to and including Mode 7.

TABLE 6.7

	MESH NO	DEGREES OF FREEDOM	WITHIN 5% UP TO MODE:
CANTILEVER BEAM	1 2 3	9 15 27	2 4 4-5
PORTAL FRAME	1 2	18 75	3 ~7

Ultimately, when comparing the experimental with the finite element results in Tables 6.2 and 6.6, it must be emphasised that the following effects have been neglected in the finite element idealisation.

- The vibrator has been treated as a concentrated mass equivalent to its static mass. In reality the vibrator is separated from the model by an elastic component.

- Frictional damping effects have been neglected. These may occur at the following places:
  - the connection of the crossbar to the columns of the portal frame
  - at the fixture of the columns to the base
  - between the needle roller bearings on which the vibrator oscilates

Experimentally the following extraneous effects occur:

- Inaccuracies are inherent when measuring low resonant frequencies (<4hz)

- The graduated scale on the wave generator limits the accuracy of frequency measurement to one significant figure

- The material was assumed to be isotropic and geometrically perfect. For example the rod diameter was modelled as 4 mm throughout. Young's modulus and Poisson's Ratio were based on experimental assumptions.

The author has found the ADINA program easy to use for simulating dynamic problems. Various options regarding the numerical techniques employed in the analysis are available. Default options are available to guide the user if there is uncertainty as to which technique to select.

Output data from the program is explicit and well formatted. With the ADINA PLOT plottir facility, plots of the mode shapes

calculated by the analysis can be easily obtained thus reducing the amount of output data required. Informative messages regarding the error bounds on the eigenvalues are printed if requested.

The author has subsequently been involved with more advanced dynamic analyses where both the modal analysis method and an implicit direct-time integration technique were employed on different occasions [24]. The package performed well and the results obtained were sufficiently accurate to enable design decisions to be made.

CHAPTER 7

ADINAT

7.1 INTRODUCTION

At the time of this study, finite element users at WITS University had not made use of the ADINAT finite element program. This necessitated an installation check to verify that the program as well as its back-up routines, were operating correctly. Firstly, the sample analyses supplied with the ADINAT source were executed. This was followed by a simple linear steady state problem which was analysed in order to become familiar with the package.

7.2 ADINAT PROGRAM CAPABILITIES

The package is capable of modelling linear and non-linear steady state or transient heat conduction problems only. This does not include the case of conduction convection, which is described by:

$$\frac{\partial}{\partial x}(K_x\frac{\partial \phi}{\partial x}) + \frac{\partial}{\partial y}(K_y\frac{\partial \phi}{\partial y}) + u\frac{\partial \phi}{\partial x} + v\frac{\partial \phi}{\partial y} + Q = 0$$

where u, v represent fluid velocities [1].

The program utilises one-dimensional (2 noded), two-dimensional (4-8 noded) and three-dimensional (8-21 noded) isoparametric or subparametric heat conduction elements. Boundary conditions encountered in real situations, can be accurately modelled. A typical situation is illustrated in Figure 1 where convection as well as radiation occurs on an external surface.

The finite element analysis of the kiln could involve either a steady state solution or a more sophisticated study of its transient response during warm-up.

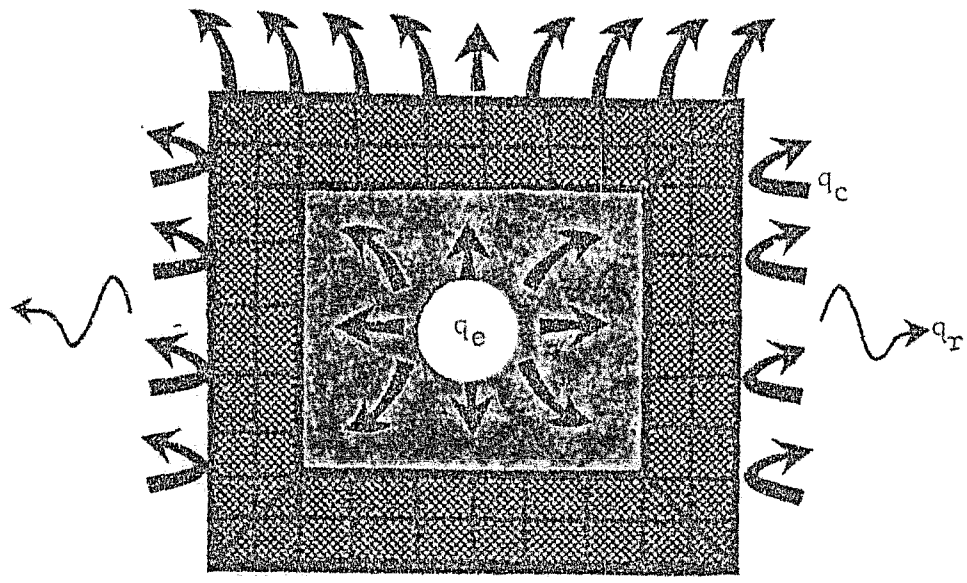

q_e - heat flux due to electrical heating

q_r - radiative heat loss

q_c - convective heat loss

Figure 7.1 - Finite Element Simulation of a High Temperature Kiln

An additional feature of the program is its ability to model material phase changes. This is accomplished by balancing the amount of heat liberated or absorbed during the transition with the volumetric rate of phase conversion. An overall heat balance is simultaneously maintained in the region.

Although ADINAT is primarily a thermal finite element program designed for use with ADINA to facilitate the study of thermal stress distributions, it may also be utilised to solve analogous field problems. A typical analogy occurs in electrostatic field

problems. This feature extends the capabilities of the ADINAT package beyond thermal analysis.

7.3 THE GOVERNING FIELD EQUATIONS

An understanding of the method of transforming the governing field equations into a form suitable for modelling by the finite element method is advantageous if the program is to be used effectively. The basic equations are derived in the ADINAT users manual. However a more complete derivation exposes the ease with which natural boundary conditions can be defined. This aspect of the finite element formulation constitutes a significant advantage over similar finite difference techniques.

7.3.1 Variational Formulation

In problems where the differential operator is linear, self-adjoint and positive-definite, the Galerkin and variational formulations are synonymous [6]. The variational approach to casting the governing equations in a finite element form is preferred, since it ensures that a best approximation to the exact solution can be found and furthermore, it is unique [6].

It is possible to transform the differential equations describing the temperature field in a continuum into an integral form. This integral is termed the fundamental integral or functional of the problem, which when minimised satisfies the governing equations exactly at all points within the body. If minimisation of the functional implicitly satisfies the natural boundary conditions, a natural variational principle arises [1,3,6]

The equation describing steady state heat conduction in a continuum is given by:

$$A(\phi) = \nabla^{T}\underline{K}\nabla\phi + Q = 0 \quad \text{in the domain} \quad \Omega \tag{7.1}$$

where

$$\underline{K} = \begin{bmatrix} K_x & 0 & 0 \\ 0 & K_y & 0 \\ 0 & 0 & K_z \end{bmatrix}$$

Equation (7.1) can be rewritten as

$$A(\phi) = L\phi + Q = 0 \tag{7.2}$$

where ϕ - temperature

Q - the rate of heat generated per unit volume

$\underline{K}$ - thermal conductivity matrix

L - $\nabla^T \underline{K} \nabla$ (linear differential operator)

∇^T - Laplaceian Operator $(\frac{\partial}{\partial x}, \frac{\partial}{\partial y}, \frac{\partial}{\partial z})$

7.3.2 Establishment of a Natural variational Principle

The aim in this section is to establish that a natural variational principle exists for the heat conduction equation. A variational formulation to the problem can be found if the differential operator L forms an inner product space. This requires that the operator is selfadjoint positive definite [1,4,5]. In the case of the heat conduction equation the operator L fulfills this requirement and the variational principle can be written directly as: [1]

$$\pi = \int_{\Omega} [\frac{1}{2}\phi L\phi + \phi Q] d\Omega + bt \tag{7.3}$$

(where bt represents boundary terms).

This represents the functional of the heat conduction equation in the domain Ω. The functional is expanded to account for boundary conditions

$$q = \bar{q} = n^T \underline{K} \nabla\phi \qquad \text{on} \quad \Gamma_q \tag{7.3a}$$

$$\phi = \bar{\phi} \qquad \text{on} \quad \Gamma_\phi \tag{7.3b}$$

where $n^T = (n_x, n_y, n_z)$

Γ_q - represents the surface of the body subject to heat flow, $\bar{q}$

Γ_ϕ - represents the surface of the body with prescribed temperatures, $\bar{\phi}$

Thus the functional (3) becomes:

$$\pi = \int_\Omega [\tfrac{1}{2}\phi L\phi + \phi Q]d\Omega + \int_{\Gamma_q} \phi\bar{q}d\Gamma + \int_{\Gamma_\phi} \phi\bar{\phi}d\Gamma \qquad (7.4)$$

hence

$$\delta\pi = -\int_\Omega \delta\phi[\nabla^T \underline{K}\nabla\phi + Q]d\Omega + \int_{\Gamma_q} \delta\phi[n^T \cdot \underline{K}\nabla\phi - \bar{q}]d\Gamma \qquad (7.5)$$

Since $\delta\phi \equiv 0$ on Γ_ϕ, the last integral in eqn (7.4) is eliminated when π is minimised in eqn (7.5). A necessary condition for the functional to be stationary is

$$\delta\pi = 0$$

If this condition is satisfied, then

$$\nabla^T \underline{K}\nabla\phi + Q = 0 \qquad \text{on} \quad \Omega \qquad (7.6a)$$

and

$$n^T \underline{K}\nabla\phi - \bar{q} \equiv 0 \qquad \text{on} \quad \Gamma_q \qquad (7.6b)$$

This indicates that the conduction equation as well as the natural boundary conditions are satisfied as a consequence of minimising the functional.

Although eqn (7.5) can be used for implementing the finite element method, it requires second order continuity for the nodal point temperature interpolation functions ϕ, whereas only first order continuity is required for the test functions $\delta\phi$. The weak form of eqn (7.5) rectifies this situation [1]. It is derived by applying

Green's Theorem and noting that

$$\delta\left(\frac{\partial\phi}{\partial x}\right) = \frac{\partial}{\partial x}(\delta\phi)$$

hence

$$\delta\pi = \int_{\Omega}\left[\delta\left(\frac{\partial\phi}{\partial x}\right)K_x\left(\frac{\partial\phi}{\partial x}\right) + \delta\left(\frac{\partial\phi}{\partial y}\right)K_y\left(\frac{\partial\phi}{\partial y}\right) + \delta\left(\frac{\partial\phi}{\partial z}\right)K_z\left(\frac{\partial\phi}{\partial z}\right)d\Omega\right.$$

$$\left. - \oint_{\Gamma=\Gamma_q+\Gamma_\phi} \delta\phi\left[K_x\frac{\partial\phi}{\partial x}\cdot n_x + K_y\frac{\partial\phi}{\partial y}\cdot n_y + K_z\frac{\partial\phi}{\partial z}\cdot n_z\right]d\Gamma\right.$$

$$\left. - \int_{\Omega}\delta\phi Q d\Omega + \int_{\Gamma_q}\delta\phi(n\cdot\underline{K}\nabla\phi - \bar{q})d\Gamma\right. \qquad (7.7)$$

Since $\delta\phi = 0$ on Γ_ϕ, the second term in eqn (7.7) can be eliminated and the final form of the minimised functional is

$$\delta\pi = \int_{\Omega}\delta(\phi')^T\underline{K}\phi' d\Omega - \int_{\Omega}\delta\phi Q d\Omega - \int_{\Gamma_q}\delta\phi\bar{q}d\Gamma \qquad (7.8)$$

since $\delta\pi \equiv 0$

$$\int_{\Omega}\delta(\phi')^T\underline{K}\phi' d\Omega = \int_{\Omega}\delta\phi Q d\Omega + \int_{\Gamma_q}\delta\phi\bar{q}d\Gamma \qquad (7.9)$$

where $\phi'^T = \left(\frac{\partial\phi}{\partial x}, \frac{\partial\phi}{\partial y}, \frac{\partial\phi}{\partial z}\right)$ and $\phi = \Sigma N_i\phi_i$

$$\delta(\phi')^T = \left(\frac{\partial N}{\partial x}, \frac{\partial N}{\partial y}, \frac{\partial N}{\partial z}\right)$$

$$\underline{K} = \begin{bmatrix} K_x & 0 & 0 \\ 0 & K_y & 0 \\ 0 & 0 & K_z \end{bmatrix}$$

These are the basic equations employed in ADINAT, where the trial functions are the temperature interpolation functions whilst the undetermined coefficients are the unknown nodal point temperatures.

7.3.3 Boundary Conditions

Either forced or natural boundary conditions can be specified at points and on surfaces of the body. Specification of temperature represents a forced boundary constraint, whilst heat flow to or from the body represents a natural boundary condition. Natural boundary conditions include convection, radiation, heat flux input, as well as any combination of the latter. Thus in eqn(9) $\bar{q}$ may represent

$$\bar{q} = q_{\text{convection}} + q_{\text{radiation}} + q_{\text{heat flux input}}.$$

7.3.4 Finite Element Discretisation

The finite element discretisation follows the standard method. When isoparametric elements are employed, the interpolation functions are used to interpolate both nodal coordinates and nodal point temperatures.

$$\begin{Bmatrix} x \\ y \\ z \end{Bmatrix} = \sum_{i=1}^{n} [N_i] \begin{Bmatrix} x_i \\ y_i \\ z_i \end{Bmatrix} \qquad \phi = \sum_{i=1}^{n} [N_i]\phi_i$$

hence $$\phi'^{T} = \left(\frac{\partial N_i}{\partial x}, \frac{\partial N_i}{\partial y}, \frac{\partial N_i}{\partial z}\right)\phi_i$$

$$\delta(\phi')^{T} = \left(\frac{\partial N_i}{\partial x}, \frac{\partial N_i}{\partial y}, \frac{\partial N_i}{\partial z}\right)$$

Eqn (7.9) can be written in a standard linear form

$$[\bar{K}]\{\phi\} + \{f\} = 0 \qquad (7.10)$$

where $[\bar{K}]$ represents the 'thermal stiffness' matrix
$\{f\}$ represents the 'thermal load' vector

$$\bar{K}_{ij} = \bar{K}_{ji} = \int_{\Omega} [K_x(\frac{\partial N_i}{\partial x} \cdot \frac{\partial N_j}{\partial x}) + K_y(\frac{\partial N_i}{\partial y} \cdot \frac{\partial N_j}{\partial y}) + K_z(\frac{\partial N_i}{\partial z} \cdot \frac{\partial N_j}{\partial z})] d\Omega \qquad (11)$$

and

$$f_i = -\int_{\Omega} N_i Q d\Omega - \int_{\Gamma_q} N_i \bar{q} d\Gamma$$

For transient analyses Q is adjusted to take account of the heat stored in the material

$$\bar{Q} = Q - C\frac{d\phi}{dt}$$

where C represents the specific heat capacity of the material. Hence

$$f_i = -\int_{\Omega} QN_i d\Omega + \frac{d\phi_i}{dt}\int_{\Omega} N_i C N_i dt - \int_{\Gamma_q} N_i \bar{q} d\Gamma$$

Equation (10) becomes

$$\bar{C}\{\dot{\phi}\} + \bar{K}\{\phi\} + \{f\} = 0 \ *$$

This equation is numerically integrated during the finite element solution.

7.4 TEST PROBLEM

The test problem selected involved a linear steady state solution to the temperature distribution over a flat rectangular plate, subject to the boundary conditions indicated in Fig 7.2

---

*$\bar{C}$ represents the heat capacity matrix

where $\bar{C} = \int_{\Omega} N_i C N_i d\Omega$

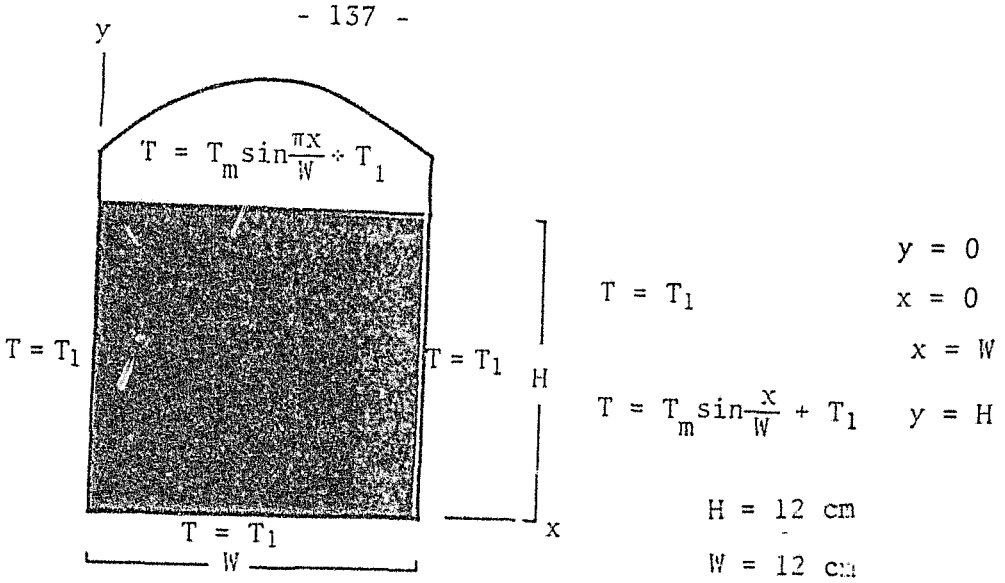

FIGURE 7.2 - Flat Plate Subjected to a Sinusoidal Temperature Distribution

$$T = \frac{T_m \sinh(\frac{\pi Y}{W})}{\sinh(\frac{\pi H}{W})} \sin\frac{\pi x}{W} + T_1 \qquad (11)$$

7.4.1 Finite Element Analysis

A symmetrical half of the plate was modelled using eight noded two-dimensional conduction elements. Two meshes were defined to study the rate of convergence of the finite element results to the exact solution, Fig 3. The linear material model 1 was specified, with values of specific heat and thermal conductivity as

K = 386 W/m °C

C = 382

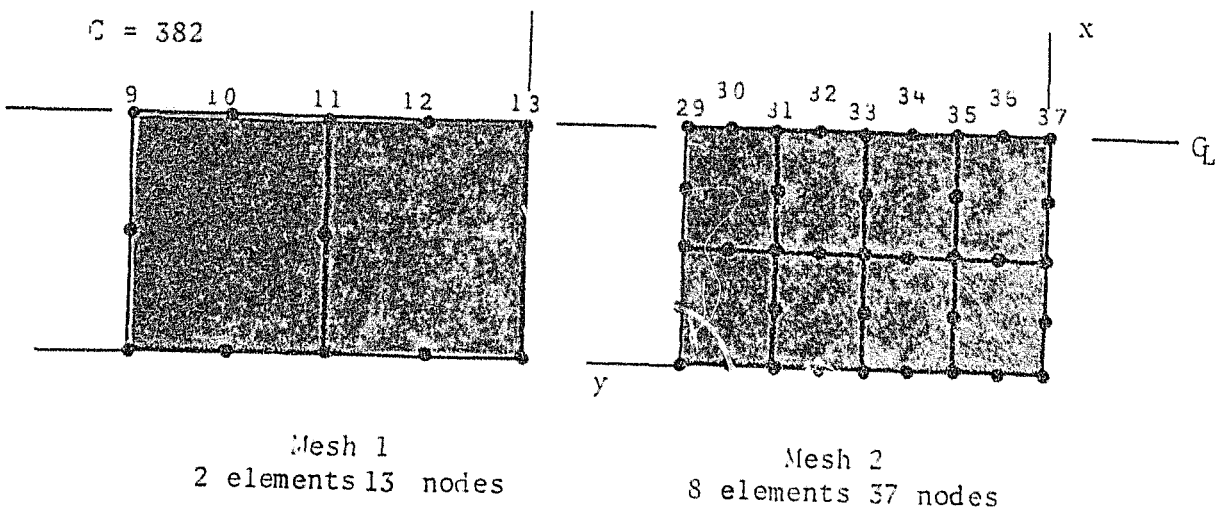

Mesh 1
2 elements 13 nodes

Mesh 2
8 elements 37 nodes

FIGURE 7.3 - Finite Element Mesh Topology

The sinusoidal temperature loading was approximated linearly between nodal points as shown in Fig 7.4.

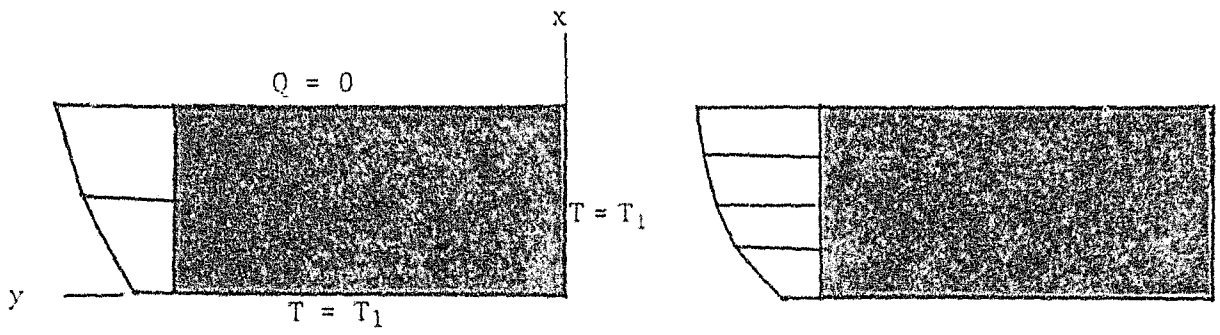

FIGURE 7.4 - Sinusoidal Temperature Loading

The more accurate modelling of the thermal loading for the refined mesh contributes to convergence of the results to the exact solution. To isolate the effect of mesh refinement, thermal Loading 1, as indicated in Fig 7.4 for Mesh 1 was used for both meshes. This is compared with the effect of the more accurate thermal Loading 2 in Table 7.1.

7.4.2 Comparison with the Exact Results

The results from the analyses are presented graphically in Plot 7.1; but the numerical values in Table 7.1 provide a clearer comparison.

TABLE 7.1 - FINITE ELEMENT AND EXACT RESULTS

MESH 1		MESH 2			EXACT
			LOADING 1	LOADING 2	
Node	Temp °C	Node	Temp °C		Temp °C
9	100	29	100,000	100,000	100,000
		30	79,316	80,288	80,423
10	65,750	31	65,192	67,299	67,161
		32	56,972	58,128	58,141
11	53,572	33	51,583	51,982	51,956
		34	47,312	47,621	47,638
12	43,565	35	44,260	44,550	44,513
		36	41,966	42,091	42,093
13	40,000	37	40,000	40,000	40,000

7.5 CONCLUSIONS - GENERAL COMMENTS

The results cited in Table 7.1 indicate convergence to the exact solution with mesh refinement. Errors appear to be due mainly to coarseness of mesh rather than to errors in modelling the load.

The style and format used in the ADINAT users manual is similar to that of the ADINA manual. This enables an ADINA user to become familiar with ADINAT very rapidly.

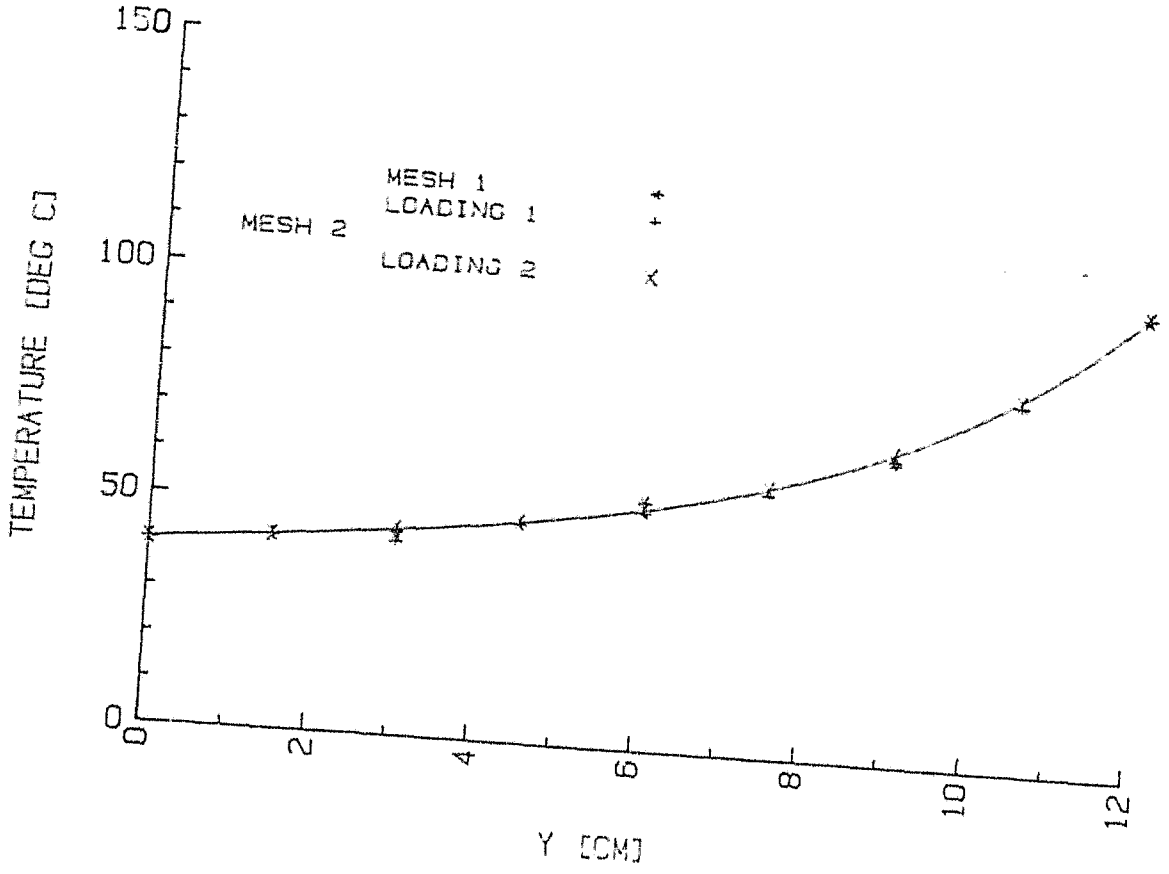

PLOT 1 - Thermal Analysis of a flat square plate: Finite Element and exact results

CHAPTER 8

CONCLUDING CHAPTER

8.1 INTRODUCTION

Through the course of this study experience has been gained in both the theory and application of the finite element method. Scope for further study in this topic is vast and increasing postgraduate research is likely to be realised in the future. It is hoped that adequate stimulus will be provided at undergraduate level for this field to be further extended at the University of the Witwatersrand.

Professor C Dimitriou of the School of Mechanical Engineering at the University of the Witwatersrand is involved in introducing the finite element method as a fourth year elective in the coming year (1984). This decision was prompted by the response of final year students to pilot projects proposed over the past year (1982 - 83); in all cases these projects stimulated discussion indicative of an increasing interest in the subject. These projects are summarised briefly in Appendix 6.

A discussion of the installation checks and problems encountered during the execution of the ADINA/ADINAT/ADINA-PLOT programmes are presented in the following sections together with an assessment[1] of each. This leads to an overall conclusion of the study undertaken.

---

1. No direct comparisons will be made with other packages since the author has limited experience with these and performance will be assessed on the basis of experience gained in using the ADINA package.

The procedure involved in the preparation of the ADINA/ADINAT/ADINA-PLOT package, prior to execution, is presented in Appendix 5.

8.2 ADINA

8.2.1 Installation

The 1977 version of the ADINA program was installed on the IBM 370 in late 1981. In March 1983 the updated 1981 version replaced the older edition. Backup routines written for the 1977 version were adapted in accordance with the updated program. These routines define the typical read write units required for execution and are briefly summarised in Appendix 5.

Installation of the ADINA (1977,1981) program was satisfactory and no difficulties were encountered during execution.

8.2.1.1 *Assessment of performance*

Over the past year the package has been successfully applied to analyse a variety of problems [23,24,25] employing different options and elements.

In these analyses the following elements of the package were employed[1]

- two dimensional solid element/linear, materially nonlinear analysis
- beam elements/linear; materially nonlinear analysis; free vibration analysis
- isoparametric beam elements/linear modal/direct time integration dynamic analysis [24].

---

1. Although these options have been employed, not all the options available for defining a material model, have been utilised.

- shell elements/linear geometrically nonlinear static analysis; linear modal/direct time integration dynamic analysis [25]
- plate shell elements/linear geometrically nonlinear static analysis; linear modal direct time integration dynamic analysis [25]

The author has had no direct or indirect information on the use of the following:

- two-dimensional fluid elements
- three-dimensional solid and fluid elements
- truss elements

In addition the nonlinear dynamic analysis option has not been employed.

In the analyses undertaken above, satisfactory execution was achieved and comprehensive results were obtained.

It was found that the program was not user friendly : Much time and effort were required in order to become familiar with the structure and layout of the user's manual. However, once this had been done, it became apparent that the program layout was concise in the hands of an experienced user thus confirming that ADINA was developed primarily as a research facility.

The ADINA finite element program employs an overlay structure corresponding to four phases of execution [7], ie

(i) finite element mesh and element data input

(ii) assembly of constant structure matrices

(iii) load vector calculations

(iv) step by step solution.

The programme is modular and consists of a series of separate subroutines. A driving programme (utilising data entered on the master control cards) assembles the various routines required during execution. This reduces the storage requirements for an execution and enables special purpose programmes to be assembled from the subroutines available. In addition updates or modifications to a routine can be implemented and compiled separately from the main programme.

Data preparation for the purpose of executing analysis follows the format outlined in the user's manual. Once the data file is created a data check can be initiated together with a plot of the mesh defined.

In a FEM analysis, it is sometimes useful to begin with a coarse mesh which is successively refined until convergence is achieved. The speed of these analyses is related to the band width of the coefficient matrix, which can be reduced by consistent nodal point numbering. The present version of ADINA (1981) does not provide a facility for automatically renumbering the nodes of an existing mesh when it is refined. Thus mesh refinement involves renumbering the nodes in order to minimise the size of the band width. It is suggested that a facility be introduced for eliminating this time consuming task.

Efficient analysis implies also efficient interpretation and manipulation of results. This can be achieved in either a tabular or a graphical form. Presently it is not possible to select limited element output in tabular form and to simultaneously retain information pertaining to other areas in the structure, which could be viewed in graphical form at a later stage. For example, it was not possible to obtain a vector plot of the principal stress field in the two-dimensional solid element mesh defined for the sheave wheel without extracting information pertaining to all elements. An improvement in selective extraction and retention of output in a future edition of the ADINA/ ADINA-PLOT program would be welcome.

The format of the listing file created for output data may be structured to some extent by the user. For example, detailed listing of the input

data may be included for future reference or deleted as required. The layout of the information obtained was easily interpreted and explicit diagnostic messages were issued in circumstances where an input error was apparent or as general comments pertaining to the solution. Although diagnostic messages detailed solution time for the different phases of the solution, there was no indication whether these messages referred to real time or CPU time.

In essence ADINA requires prior experience in order for its full potential to be realised. But once the initial difficulties of becoming familiar with the program have been overcome, ADINA is found to be a powerful and comprehensive analytical tool.

8.3 ADINAT

The brief study of the ADINAT program undertaken in Chapter 7, indicated that the program had been satisfactorily installed on the IBM 370. The test analyses [8] supplied with the source were executed and in subsequent applications no difficulties were encountered.

8.3.1 Assessment of Performance

The user's manual accompanying the program was concise and followed a similar layout to that stipulated in the ADINA manual. Thus the experience gained in working with the ADINA package facilitated easy adaptation to the formatting of data input and program execution for ADINAT.

Plotting facilities are not presently available for obtaining graphical verification of mesh definitions or for the presentation of results. This however does not detract from the program's ability to analyse complex thermal systems, except that pre- and post-processing can be laborious.

Although the ADINAT facility warrants a more comprehensive study of its own, experience gained in this limited analysis indicates that

the package is applicable to a broad spectrum of thermal system analyses which are commonly encountered in practice.

8.4 ADINA-PLOT

The ADINA-PLOT program was installed on the IBM 370 in March 1983. A description of the program is presented in Appendix 7, together with the installation difficulties encountered.

8.4.1 Assessment of the ADINA-PLOT Program

The purpose of this program is to reduce the amount of output data associated with a finite element simulation by selectively extracting significant results for graphical display. The program contains options which enable the user to design the layout of a plot for direct presentation in a report.

Experience gained in practical applications confirmed the program's ability to do this. In addition it was found that the control langauage was flexible enabling intricate plots to be obtained with relatively little effort. For example, the vector plots and mesh deflections presented in Chapter 5, and also REM plots presented in reference [24].

Apart from the difficulties documented in Appendix 7, no further problems were encountered and the program performed efficiently in all subsequent analyses.

8.5 CONCLUSIONS

This study, as outlined in Chapter 1, was primarily concerned with generating experience with the ADINA finite element package at the University of the Witwatersrand, thus providing the basis for further research at postgraduate level.

In order to evaluate the ADINA package and acquire experience in FEM analysis, the package was used to solve three problems. These were: A static analysis of a sheave wheel; a dynamic analysis of a simple beam structure and a thermal analysis of a square plate subjected to a sinusoidal temperature load. In the first two problems the results were compared with experimental observations. In this way experience was gained with experimental measurement techniques as well as finite element modelling and the execution of a FEM analysis with the ADINA package.

8.5.1 The Sheave Wheel Experiment

The analysis undertaken in this study was aimed at extending previous research to include the use of the finite element method which is capable of accounting for the nonlinear behaviour of the material used to cast the sheave.

Owing to self imposed limitations on computer resources the sheave analysis was simplified by introducing three important approximations, ie

- The sheave behaviour was simulated by a two dimensional model
- Beam elements were used to model certain areas of the sheave
- The Drucker Prager material model does not describe the nonlinear behaviour of the cast iron material accurately.

The wisdom of inducing these approximations in the analysis is questionable since it impairs the basis for assessing the accuracy of the package. Nevertheless, the finite element results obtained for the linear elastic region compare favourably with those obtained in the experiment. This confirms that the elastic behaviour of the sheave wheel can be adequately treated as a two dimensional phenomenon.

It is pertinent to note that when the associated and non-associated material routines were used to simulate the sheave behaviour, the FEM results did not differ greatly. This indicates that the FEM results are not sensitive to the dilatancy of the material and implies that a more accurate material model (which could model the dilatancy of the cast iron more accurately) would have a small effect on the outcome of the FEM results.

The FEM results in the nonlinear region do in some cases deviate substantially (20 percent) from the experimental values but do follow the general behaviour indicated by the experimental trends. In view of the discussion presented in the previous paragraph it is likely that the two dimensional approximation of the sheave behaviour may not be applicable in the nonlinear domain.

Taking into account the approximations introduced in sheave simulation, the correlation between the FEM and experimental results, is viewed as satisfactory.

8.3.2 Vibration Analysis

Being familiar with the dynamic capabilities of the package a [illegible] structure (as outlined in Chapter 6) was analysed in order to [illegible] its natural frequencies. Although it was a simple application it effectively illustrated the importance of mesh design. The [illegible] indicated that by employing a coarse mesh the lowest natural [illegible] of the structure could be accurately determined, whilst a [illegible] required to achieve convergence at higher fre-

[illegible] ADINA.

[illegible] is a subsidiary program supplied with the ADINA [illegible] study of thermal systems, as well as thermal [illegible]. Although the ADINAT program was not utilised [illegible], a brief study was undertaken to assess its [illegible] of application. In this context a simple [illegible] experimental counterpart. The experience [illegible] with the main package.

[illegible] program is not user friendly and is [illegible] environment. Although experience is [illegible] effectively, in the context of the [illegible] requirement in fact promotes a better

appreciation of both ADINA and the finite element method. The package has been developed at an academic institution (M I T) and functions in both the commercial and academic worlds. The developers view the package as becoming a comprehensive teaching facility and intend supplying further test analyses and manuals pertaining to the solution techniques employed in the package, thus transforming it into an independent teaching facility[1].

It is felt that the experience gained during the course of the study qualifies the conclusion that the ADINA package is comprehensive and efficient and provides a good introduction to the finite element method for students.

---

1. BATHE K J, FEMSA 1984

REFERENCES

1. ZIENKIEWICZ, O C: 'The Finite Element Method', 3rd Ed, McGraw-Hill, 1977.
2. BATHE, K J: 'Numerical Methods in Finite Element Analysis', Prentice-Hall, 1977.
3. BATHE, K J: 'Finite Element Procedures in Engineering Analysis', Prentice-Hall, 1982.
4. MARTIN, H C: 'Introduction to Finite Element Analysis', McGraw-Hill, 1973.
5. PRENTER, H C: 'Splines and Variational Methods', Wiley, 1975.
6. CHEUNG, Y K and YEO, M F: 'A Practical Introduction to Finite Element Analysis', Pitman International Text, 1979.
7. ADINA USERS MANUAL 1981.
8. ADINAT USERS MANUAL 1981.
9. ADINA-PLOT USERS MANUAL 1981.
10. DRUCKER, D C: 'A more fundamental approach to plastic stress strain relations', Proceedings of the first US National Congress of Applied Mechanics, pg 487.
11. MENDELSON, A: 'Plasticity: Theory and Application', MacMillan, 1968.
12. GADALA, M S, MULLINS, M L, DOKAINISH, M A: 'A Modified Plasticity Theory for Porous Metals', *IJNME*, Vol]5, 649-660 (1980).
13. OWEN, D R J: Numerical Techniques and Implementation for Finte Elements in Plasticity', FEMSA/82 Pre-Conference Seminars on Plasticity, ISE, University of Stellenbosch, Feb 1982.
14. TSE, MORSE, HINK: 'Mechanical Vibrations', 2nd Ed, Allyn and Bacon, 1978.
15. KREYSIG: 'Advanced Engineering Mathematics', 4th Ed, Wiley, 1979.
16. CURTIS, GERALD: 'Applied Numerical Analysis', 2nd Ed, Addison Wesley, 1978.

17. DONOHUE, J P: 'Stresses in Headsheaves', BSc research report, School of Mechanical Engineering, University of the Witwatersrand, Johannesburg, Nov 1976.

18. GRAHAM, L N: 'Research on Headsheaves', BSc research report, School of Mechanical Engineering, University of the Witwatersrand, Johannesburg, Nov 1981.

19. DIMITRIOU, C: 'Strength of Large Spoked Sheaves', Report CD/7410, 1974.

20. BIEZENO, C B, GRAMMEL, R: 'Engineering Dynamics', Volume II, Blackie & Son Limited, 1956.

21. CONSTANCON, C, DIMITRIOU, C: 'The Rim Strength of a Cast Iron Sheave', FEMSA/83, University of Cape Town, Feb 1983.

22. CHEN, W: 'Limit Analysis and Soil Plasticity', Elsevier, 1975.

23. LANE, N, HACK, G: 'Replacing the Human Knee', BSc design report, School of Mechanical Engineering, University of the Witwatersrand, Johannesburg 1982.

24. VALENTIM, L M: Thesis for the degree of MSc to be submitted to the University of the Witwatersrand in 1983. In preparation.

25. BIZOS, A: 'Shell/Plate-Shell Elements', BSc Mini-Lab report, School of Mechanical Engineering, University of the Witwatersrand, Johannesburg, June 1983.

26. NAUDE, B: Kentron. Personal contact and discussion.

27. ANGUS, H T: 'Cast Iron', 2nd Ed, Butterworths, 1976.

28. GILBERT, G N J: 'The components of Strain due to Deformation of the Matrix and due to Volume Changes in Flake Graphite Cast Iron and the Uniaxial Strength', *BIRCA Journal*, 1963, 11, No 4, pp 512-524.

APPENDIX 1

THE MECHANICAL PROPERTIES OF CAST IRON

A1.1 INTRODUCTION

The purpose of this study was to determine the mechanical properties of the material used in casting the sheave. The particular properties required were the tangent modulus and Poisson ratio which were necessary parameters required to execute a finite element simulation.

A1.2 STANDARD TESTING PROCEDURES (BS 1452.1961)

Standard testing procedures for obtaining representative values of the quality and strength of cast iron specify that the specimen should be machined from independently cast bars. Since the strength of cast iron is dependent on the cooling rate after casting and hence the section size of the component the diameter of the 'cast bar' from which the specimen is machined affects the ultimate tensile strength attained in the physical test [27]. Conversion tables are available for inter-relating the tensile strength of five standard diameters of cast test bars. The metal quality is measured on a scale of seven grades (grade 14 - grade 21) which denote the tensile strenth (ton/inch^2) required to fail a test specimen machined from a 30 mm diameter bar.

Since independently cast bars were not available specimens were initially machined from portions of a similar sheave (of the same pour) which had previously been lightly loaded (tension test 1, 2; compression test 1). At a later stage an additional tension and

compression specimen was extracted from the current sheave after the destruct test had been completed (tension test 3, compression test 2, this served to verify that the material properties of the two sheaves were similar.

In all instances the specimens were machined from material which had been lightly stressed. This ensured that the results would be representative of the virgin material behaviour.

A1.3 MATERIAL SPECIMENS

Hounsfield specimens were used in the tensile test whilst the larger specimens with button ends and generous fillets were used for compression testing.

The dimensions of the two types of specimens are shown in Fig A1.1 below.

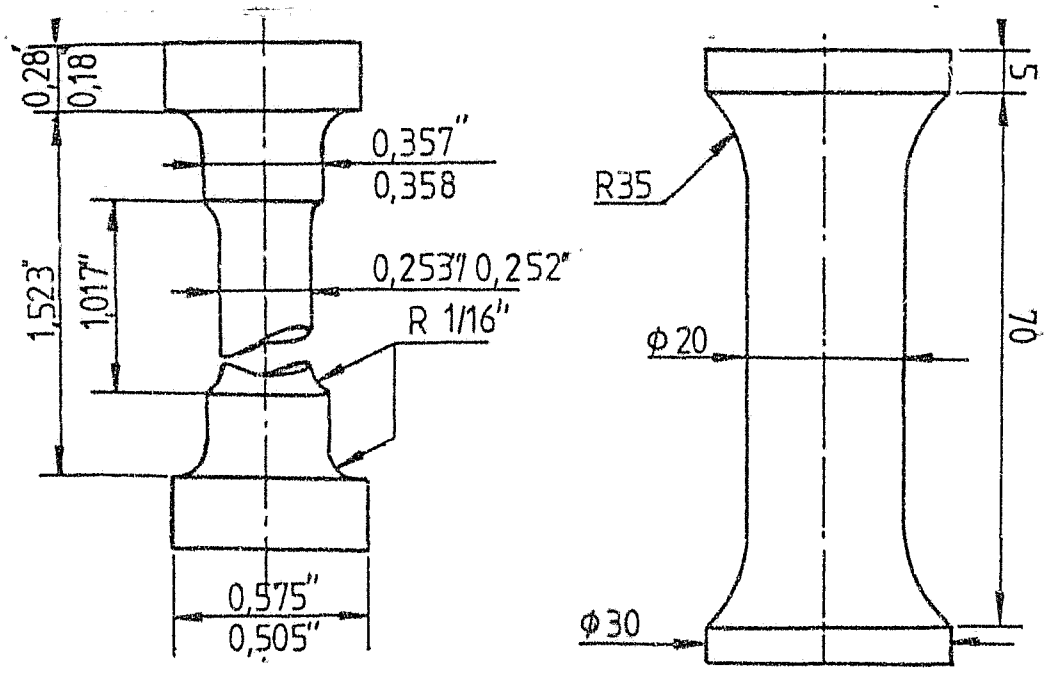

Tensile Specimen

Compression Specimen

Figure A1.1 - Tensile/Compression Test Specimens

A1.4 STRAIN MEASUREMENT TECHNIQUE

Electrical resistance strain gauges were mounted 120° apart around the circumference of the specimens.[1] These were connected to Wheatstone bridges excited by a constant voltage power supply; the output voltage across the bridge was monitored by an Esterline Angus[2] data logger. Final strains were obtained by converting the output bridge voltage to strain. ie,

$$\varepsilon = 4V_0/kV_i \qquad \text{(A1)}$$

ε = strain

V_0 = output voltage from the bridge

V_i = input voltage to the bridge

k = gauge factor

A1.5 EXPERIMENTAL PROCEDURE

The main source of error during the experiment was due to bending of the specimen. This was caused by 'high spots' on the specimen bearing surfaces. In order to minimise this effect the specimen was rotated, inverted, etc, until at a low load the strain readings were within 5%-10% of one another. Once satisfactory readings were obtained the loading was applied in steps in the elastic region and continuously in the plastic region.

---

1. In tension and compression test 1 only, three gauges were mounted longitudinally. In all subsequent tests three extra gauges were mounted to measure the circumferential strain.
2. This facility was not available at the time of performing the first compression test. A Huggenberger Tepic indicator IT1 portable strain indicator was employed in this instance.

A1.6 THE CALCULATION OF THE TANGENT MODULUS AND POISSON'S RATIO

Since cast iron is a nonlinear material even at very low loads the modulus of elasticity and proportional limit are ficticious quantities. Consequently the tangent modulus was calculated at various stress levels. In order to evaluate the tangent modulus from the experimental results obtained, a difference technique was employed. ie,

$$E_T = \frac{\sigma^i - \sigma^{i-1}}{\varepsilon^i - \varepsilon^{i-1}} \qquad \text{at} \qquad \sigma = \frac{\sigma^i + \sigma^{i-1}}{2}$$

This technique is sensitive to experimental pertubations thus an adequate stress/strain increment should be selected to smooth out these effects.

The maximum error introduced by experimental pertubations is given by

$$\frac{\Delta E_T}{E_T} \times 100 = 100\frac{B}{A}\sqrt{\left(\frac{\Delta A}{B}\right)^2 + \left(\frac{\Delta B \cdot A}{B^2}\right)^2}$$

where $A = \sigma^i - \sigma^{i-1}$

$B = \varepsilon^i - \varepsilon^{i-1}$

ΔA - represents the experimental error involved in evaluating the stress

ΔB - represents the experimental strain measurement error

The estimated values of ΔA, ΔB are

$\Delta A \simeq \pm 0{,}05$ MPa

$\Delta B \simeq \pm 2 \times 10^{-6}$

In order to reduce this error to within ±3,5% the step size of A, B should be selected as

$A \geq 10$ MPa

$B \geq 60 \times 10^{-6}$

The error introduced by selecting a small step size is illustrated in Fig A1.2 below

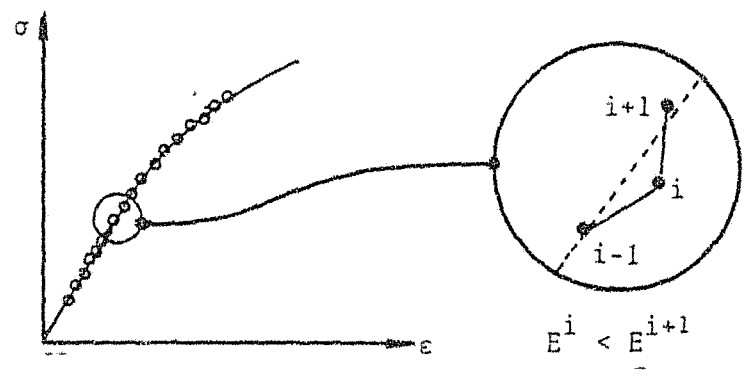

Figure A1.2 - Step Size Sensitivity of the Tangent Modulus

Poisson's ratio was evaluated at the same stress levels selected for the evaluation of the Tangent Modulus. Similarly a difference technique was employed

$$\nu = \frac{\Delta\varepsilon_c}{\Delta\varepsilon_L}$$

where

$\Delta\varepsilon_c = \varepsilon_c^i - \varepsilon_c^{i-1}$ - represents the increment of circumferencial strain

$\Delta\varepsilon_L = \varepsilon_L^i - \varepsilon_L^{i-1}$ - represents the increment of longitudinal strain.

TABLE A1.1: TENSION TEST 1

STRESS [MPa]	STRAIN 1 [x10^{-6}]	STRAIN 2 [x10^{-6}]	STRAIN 3 [x10^{-6}]	AVERAGE STRAIN [x10^{-6}]
11,00	73	80	122	91,66
15,71	109	117	169	132
21,69	161	154	235	183
27,97	217	215	296	243
33,16	264	256	345	288
37,64	304	294	391	330
46,6	397	374	485	419
55,72	492	456	582	510
66,01	610	554	703	622
75,29	722	644	820	728
83,46	820	723	927	823
98,87	1 029	883	1 164	1 025
110,81	1 218	1 024	1 385	1 209
122,13	1 418	1 169	1 625	1 404
131,88	1 612	1 312	1 860	1 594
142,09	1 871	1 499	2 173	1 848
150,27	2 094	1 666	2 441	2 067
161,59	2 451	1 939	2 857	2 416
169,45	2 842	2 245	3 300	2 796
180,13	3 514	2 821	4 027	3 454
186,42	4 023	3 303	4 553	3 959
194,91	4 878	4 094	5 454	4 808
204,03	5 919	5 021	6 570	5 836
210,63	7 656	6 033	7 790	6 960
217,86	8 378	7 204	9 216	8 266
221,63	9 411	8 037	10 317	9 255

TABLE A1.2 - Tension Test 2

	LONGITUDINAL STRAIN				TANGENTIAL STRAIN				
STRESS [MPa]	STRAIN 1 [x10^{-6}]	STRAIN 2 [x10^{-6}]	STRAIN 3 [x10^{-6}]	AVERAGE [x10^{-6}]	STRAIN 4 [x10^{-6}]	STRAIN 5 [x10^{-6}]	STRAN 6 [x10^{-6}]	AVERAGE [x10^{-6}]	AVERAGE VOLUMETRIC STRAIN [x10^{-6}]
2,98	20	20	22	20	- 8	- 8	- 10	- 9	2
5,98	37	47	41	41	- 21	- 22	- 23	- 22	- 3
9,17	56	78	62	65	- 27	- 32	- 30	- 30	5
12,20	77	106	83	89	- 33	- 40	- 35	- 36	16
15,54	99	138	105	114	- 39	- 48	- 42	- 43	27
18,65	120	167	125	137	- 45	- 56	- 48	- 50	36
21,60	137	204	143	161	- 49	- 66	- 54	- 56	48
25,18	162	240	169	190	- 57	- 76	- 61	- 65	60
27,67	182	267	187	212	- 62	- 84	- 66	- 71	70
31,86	210	308	216	245	- 70	- 94	- 74	- 79	85
37,30	253	368	256	292	- 80	- 110	- 85	- 92	108
42,28	295	423	295	338	- 91	- 124	- 96	- 104	130
48,19	348	491	341	393	- 103	- 142	- 108	- 118	157
52,38	388	541	376	435	- 113	- 154	- 117	- 128	178
56,74	431	592	413	479	- 123	- 166	- 127	- 139	200
61,40	479	649	453	527	- 133	- 180	- 137	- 150	226
65,84	540	719	504	588	- 146	- 196	- 151	- 164	258
71,19	597	778	549	641	- 158	- 210	- 161	- 176	288
81,77	686	872	618	725	- 176	- 230	- 179	- 195	334
86,27	796	983	701	827	- 196	- 254	- 199	- 216	393
94,20	930	1 113	797	947	- 220	- 280	- 219	- 240	467
102,60	1 085	1 257	906	1 083	- 246	- 307	- 243	- 266	550
110,01	1 276	1 429	1 039	1 240	- 277	- 339	- 270	- 295	651
118,92	1 455	1 585	1 160	1 400	- 304	- 367	- 293	- 321	757
128,56	1 722	1 809	1 337	1 623	- 342	- 405	- 325	- 358	906
136,64	1 997	2 035	1 519	1 850	- 380	- 442	- 357	- 393	1 063
145,35	2 353	2 319	1 747	2 140	- 424	- 488	- 394	- 435	1 268
153,12	2 710	2 602	1 973	2 428	- 469	- 533	- 431	- 478	1 472
166,34	3 486	3 204	2 456	3 049	- 562	- 627	- 506	- 565	1 918
175,97	4 212	3 768	2 908	3 629	- 648	- 715	- 573	- 645	2 339
183,44	4 932	4 321	3 347	4 200	- 735	- 804	- 638	- 725	2 748
191,99	5 977	5 130	3 981	5 029	- 859	- 932	- 731	- 841	3 347
198,97	7 073	5 951	4 616	5 880	- 987	-1 067	- 824	- 960	3 960
205,20	8 351	6 911	5 342	6 868	-1 133	-1 288	- 931	-1 097	4 672
211,42	9 186	7 531	5 800	7 505	-1 223	-1 335	- 998	-1 185	5 134
218,41	10 930	8 871	6 648	8 816	-1 395	-1 564	-1 121	-1 360	6 095

TABLE A1.3 - Tension Test 3

	LONGITUDINAL STRAIN				TANGENTIAL STRAIN				
STRESS [MPa]	STRAIN 1 [x10^{-6}]	STRAIN 2 [x10^{-6}]	STRAIN 3 [x10^{-6}]	AVERAGE [x10^{-6}]	STRAIN 4 [x10^{-6}]	STRAIN 5 [x10^{-6}]	STRAIN 6 [x10^{-6}]	AVERAGE [x10^{-6}]	AVERAGE VOLUMETRIC STRAIN [x10^{-6}]
7,8	71	73	74	72	- 17	- 18	NO	- 18	36
11,7	106	104	111	107	- 25	- 25	READINGS	- 25	56
15,7	143	138	151	144	- 35	- 32	RECORDED	- 33	77
23,5	227	195	246	223	- 54	- 47		- 51	120
31,4	329	266	317	304	- 75	- 57		- 66	171
39,2	429	335	384	383	- 96	- 66		- 81	220
47,1	522	417	475	471	-114	- 79		- 96	278
55,0	612	497	570	560	-131	- 92		-111	336
62,8	706	580	671	652	-149	-106		-127	397
70,7	798	663	772	744	-166	-118		-142	459
78,5	893	751	879	841	-184	-132		-158	524
86,4	981	835	977	931	-199	-144		-171	587
94,3	1 079	930	1 083	1 031	-216	-158		-187	656
102,1	1 195	1 043	1 200	1 146	-236	-172		-204	738
110,0	1 321	1 161	1 320	1 267	-255	-186		-221	825
114,7	1 430	1 261	1 424	1 372	-269	-196		-233	908
122,6	1 565	1 382	1 553	1 500	-288	-212		-250	999
130,4	1 743	1 573	1 724	1 680	-310	-230		-270	1 139
136,7	1 914	1 697	1 892	1 835	-330	-243		-286	1 261
141,4	2 034	1 807	2 012	1 951	-343	-255		-299	1 352
147,7	2 222	1 977	2 199	2 133	-363	-271		-317	1 497
154,0	2 437	2 171	2 414	2 341	-384	-289		-337	1 666
163,4	2 728	2 430	2 701	2 620	-413	-310		-361	1 896
169,7	3 041	2 712	3 010	2 923	-441	-334		-387	2 148
176,0	3 383	3 000	3 326	3 236	-469	-359		-414	2 408
185,4	3 735	3 301	3 652	3 563	-497	-385		-441	2 680
190,1	4 217	3 707	4 091	4 005	-536	-420		-478	3 048
198,0	4 837	4 216	4 640	4 564	-583	-463		-523	3 518
204,0	5 367	4 643	5 101	5 037	-622	-498		-560	3 917
210,6	6 181	5 272	5 778	5 744	-679	-548		-614	4 515
215,3	6 742	5 685	6 224	6 217	-717	-581		-649	4 917
220,0	7 312	6 101	6 669	6 694	-756	-611		-683	5 326
226,3	8 521	6 920	7 530	7 657	-827	-676		-752	6 152

TABLE A1.4: COMPRESSION TEST 1

STRESS [MPa]	STRAIN 1 [x10^{-6}]	STRAIN 2 [x10^{-6}]	STRAIN 3 [x10^{-6}]	AVERAGE [x10^{-6}]
- 16,2	- 145	- 174	- 130	- 150
- 32,1	- 528	- 329	- 274	- 310
- 63,6	- 689	- 690	- 612	- 664
- 94,8	-1 067	-1 070	- 967	-1 015
-127,3	-1 476	-1 371	-1 341	-1 396
-159,15	-1 930	-1 765	-1 744	-1 813
-190,90	-2 440	-2 230	-2 243	-2 304
-	-2 615 *[202]	-2 610 [213]	-2 795 [224]	
	-3 250 [230]	-3 140 [236]	-3 318 [243]	
	-4 025 [254]	-3 880 [260]	-4 075 [265]	
	-4 910 [275]	-4 785 [280]	-5 025 [285]	
	-6 060 [294]	-5 991 [300]	-6 330 [305]	
-190,98	-5 685	-5 195	-5 205	-5 361
-222,81	-5 755	-5 435	-5 460	-5 550
- 0	-4 435	-3 945	-3 955	-4 111

* Continuous loading applied in the plastic region

[ ] Stress value at which strain reading was recorded.

TABLE A1.5 - Compression Test 2

	LONGITUDINAL STRAIN				TANGENTIAL STRAIN				
STRESS (MPa)	STRAIN 1 [x10⁻]	STRAIN 2 [x10⁻]	STRAIN 3 [x10⁻]	AVERAGE [x10⁻]	STRAIN 4 [x10⁻]	STRAIN 5 [x10⁻]	STRAIN 6 [x10⁻]	AVERAGE [x10⁻]	AVERAGE VOLUMETRIC STRAIN [x10⁻]
- 14,5	- 128	- 127	- 115	- 123	33	33	30	32	- 58
- 31,8	- 273	- 313	- 250	- 279	71	82	64	72	- 133
- 46,1	- 442	- 520	- 405	- 456	111	129	99	113	- 229
- 63,6	- 596	- 671	- 551	- 606	151	167	137	151	- 302
- 79,6	- 776	- 851	- 721	- 783	196	214	179	196	- 389
- 95,5	- 952	- 1 041	- 883	- 959	241	265	222	243	- 472
-111,4	- 1 131	- 1 230	- 1 049	- 1 136	290	320	267	292	- 551
-127,3	- 1 320	- 1 438	- 1 226	- 1 328	343	383	317	348	- 632
-143,2	- 1 514	- 1 651	- 1 407	- 1 524	400	451	370	407	- 709
-159,2	- 1 721	- 1 879	- 1 601	- 1 734	465	528	431	474	- 784
-175,1	- 1 943	- 2 121	- 1 810	- 1 958	539	614	500	551	- 854
-191,0	- 2 190	- 2 384	- 2 044	- 2 206	626	717	583	642	- 921
-206,9	- 2 477	- 2 685	- 2 321	- 2 494	735	841	688	754	- 984
-222,8	- 2 812	- 3 052	- 2 646	- 2 830	875	995	821	897	- 1 036
-238,8	- 3 199	- 3 428	- 3 025	- 3 217	1 046	1 182	988	1 072	- 1 072
-254,7	- 3 699	- 3 932	- 3 513	- 3 715	1 287	4 377	1 222	1 315	- 1 083
-270,6	- 4 324	- 4 557	- 4 131	- 4 337	1 605	1 771	1 539	1 639	- 1 059
-286,5	- 5 158	- 5 389	- 4 953	- 5 167	2 059	2 238	1 989	2 096	- 957
-302,4	- 6 124	- 6 365	- 5 911	- 6 134	2 606	2 803	2 538	2 649	- 835
-318,4	- 7 305	- 7 571	- 7 085	- 7 320	3 290	3 517	3 226	3 344	- 631
-334,3	- 8 604	- 8 018	- 8 381	- 8 634	4 052	4 324	4 002	4 126	- 381
-350,2	-10 122	-10 517	- 9 890	-10 176	4 946	5 294	4 923	5 054	- 66
-366,1	-11 720	-12 228	-11 491	-11 813	5 891	6 343	5 915	6 050	287
-382,0	-13 357	-13 965	-13 143	-13 488	6 868	7 431	6 953	7 084	680
-398,2	-15 209	-15 879	-15 015	-15 368	7 979	8 660	8 142	8 260	1 153
-413,9	-17 147	-17 837	-16 988	-17 324	9 147	9 953	9 410	9 504	1 683
-429,8	-19 414	-20 081	-19 405	-19 633	10 518	11 470	10 991	10 993	2 353
-445,7	-21 298	-21 989	-21 471	-21 586	11 670	12 805	12 358	12 277	2 969

TABLE A1.6 - The Tangent Modulus and Poisson's Ratio in tension

T E S T 1		T E S T 2			T E S T 3		
STRESS [MPa]	YOUNGS MODULUS [GPa]	STRESS [MPa]	YOUNGS MODULUS [GPa]	POISON RATIO	STRESS [MPa]	YOUNGS MODULUS [GPa]	POISON RATIO
7.9	119,0	13,9	131,8	0,278	9,8	114,0	0,221
21,8	110,4	23,1	120,6	0,280	15,8	105,9	0,212
32,8	111,1	32,4	119,7	0,261	19,6	100,0	0,223
46,6	100,4	42,7	107,9	0,258	27,5	97,0	0,188
60,7	91,9	52,4	100,2	0,246	35,4	99,8	0,189
70,6	87,5	61,2	83,4	0,229	45,2	88,8	0,175
79,4	86,0	76,0	85,4	0,224	51,1	89,1	0,170
91,2	76,3	90,2	66,0	0,207	58,9	84,9	0,173
104,8	65,0	98,4	61,8	0,195	66,8	85,3	0,160
116,5	58,1	110,8	51,4	0,174	74,7	81,5	0,166
127,0	51,2	123,7	43,3	0,166	82,5	87,2	0,149
136,9	40,3	132,6	35,5	0,154	90,4	78,6	0,155
146,2	37,3	141,0	30,1	0,145	98,2	68,1	0,146
156,0	32,4	149,2	26,9	0,149	106,1	64,8	0,139
165,5	20,7	159,7	21,3	0,140	112,4	45,2	0,118
174,8	16,2	171,2	16,6	0,138	118,7	61,3	0,133
183,3	12,5	179,7	13,1	0,14	126,5	43,6	0,112
190,7	10,0	187,7	10,3	0,140	133,6	40,6	0,104
194,5	8,9	195,5	8,2	0,139	139,1	40,4	0,110
207,3	5,9	202,1	6,3	0,138	144,6	34,6	0,101
214,2	5,5	211,8	6,8	0,134	150,9	30,3	0,093
219,7	3.3				158,8	33,7	0,088
					166,6	20,7	0,085
					172,9	20,0	0,086
					180,8	28,9	0,082
					187,8	10,6	0,084
					194,1	14,0	0,080
					201,0	12,6	0,078
					207,3	9,3	0,077
					212,9	9,9	0,075
					217,7	9,8	0,072
					223,2	6,5	0,071

TABLE A1.7: THE TANGENT MODULUS AND POISSON'S RATIO IN COMPRESSION

COMPRESSION TEST 1		COMPRESSION TEST 2		
STRESS [MPa]	YOUNGS MODULUS [GPa]	STRESS [MPa]	YOUNGS MODULUS [GPa]	POISON RATIO
8,1	108	23,1	112	0,257
24,9	99	39,0	80	0,229
47,9	88	54,9	116	0,256
79,2	88	71,6	90	0,253
111,0	85	87,0	90	0,264
143,2	76	103,5	89	0,278
175,0	64	119,4	83	0,288
195,5	54	135,3	81	0,302
216,0	44	151,2	76	0,322
242,0	31	167,2	71	0,342
264,5	23	183,1	64	0,366
284,5	16	199,0	55	0,389
		214,9	47	0,423
		230,8	41	0,452
		246,8	32	0,488
		262,7	25	0,519
		278,6	19	0,551
		294,5	16	0,572
		310,4	13	0,586
		326,4	12	0,594
		342,3	10	0,602
		358,2	9	0,608
		374,1	9	0,617
		390,0	8	0,625
		405,9	8	0,635
		421,8	6	0,645
		437,8	8	0,657

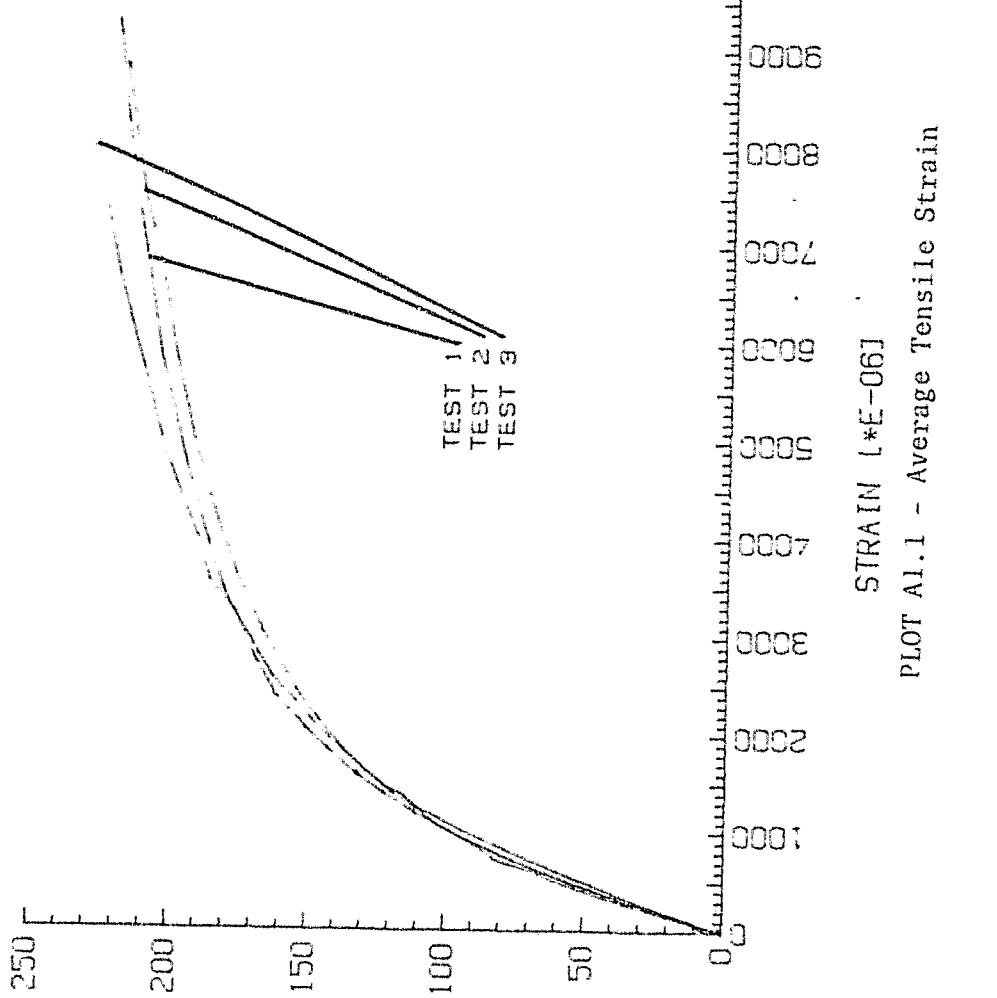

PLOT A1.1 - Average Tensile Strain

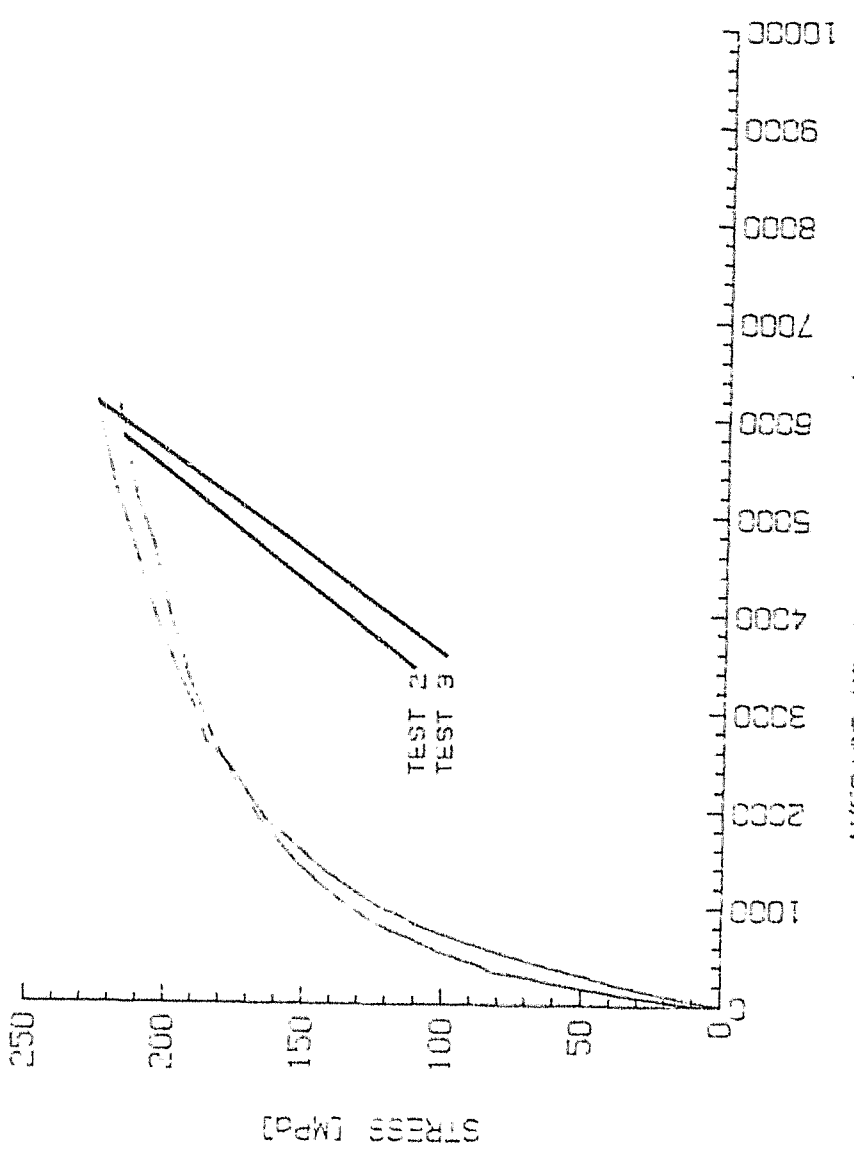

PLOT A1.2 - Average Volumetric Strain vs Stress
Compression Test (Tests 2-3)

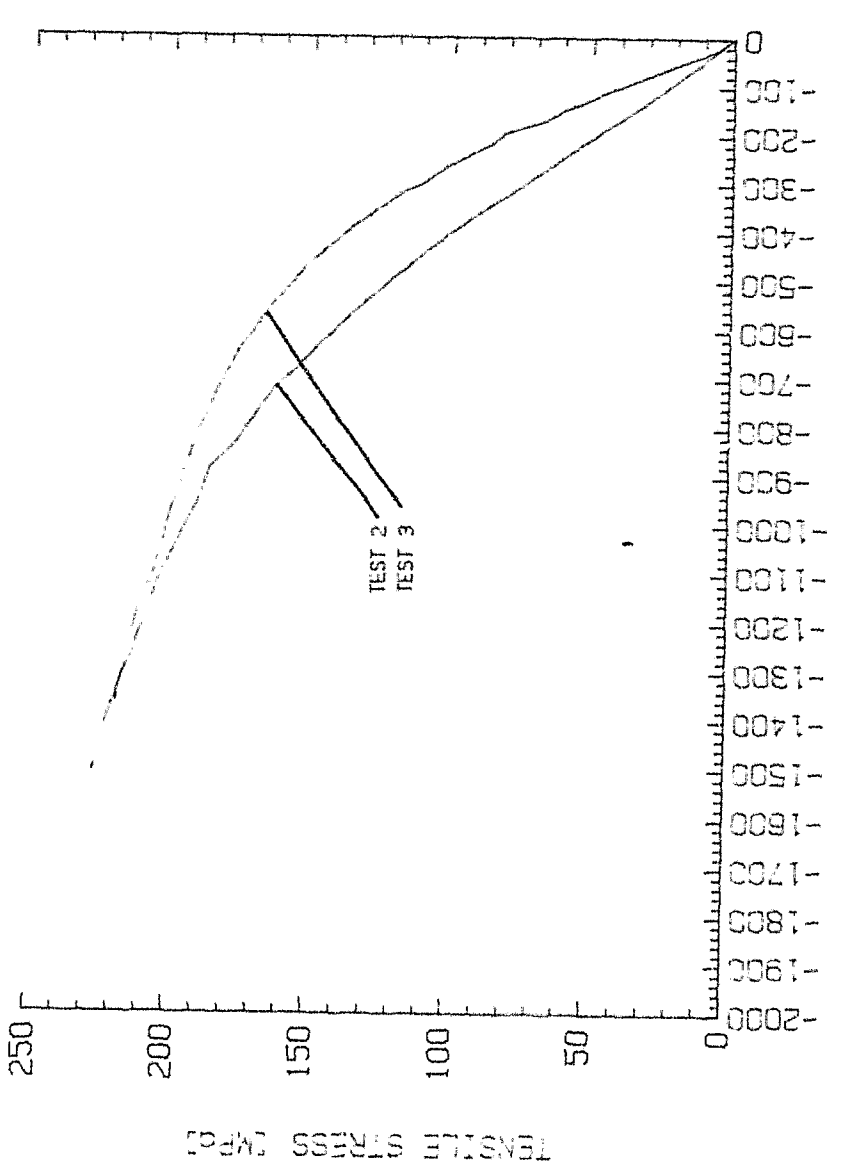

PLOT A1.3 - Average Circumferential Strain vs Stress
(Tests 2-3)

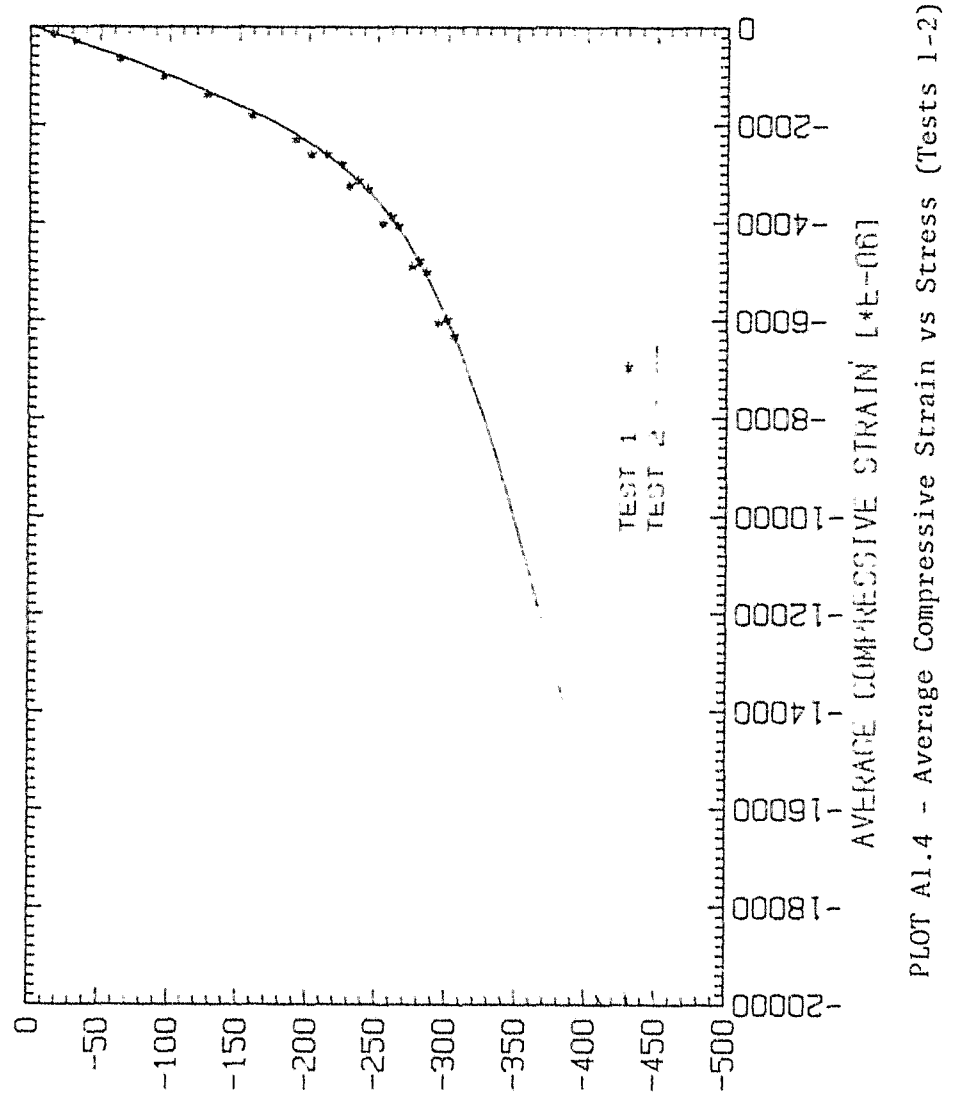

PLOT A1.4 - Average Compressive Strain vs Stress (Tests 1-2)

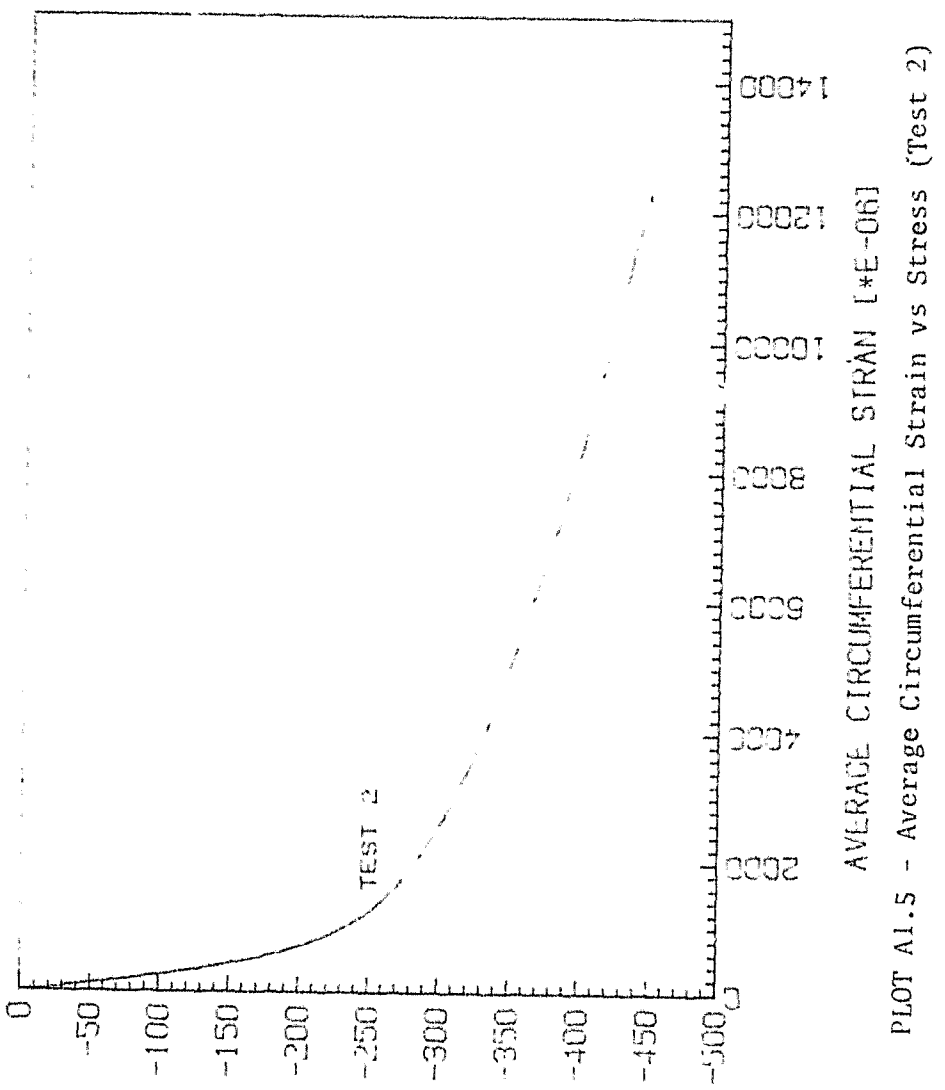

PLOT A1.5 - Average Circumferential Strain vs Stress (Test 2)

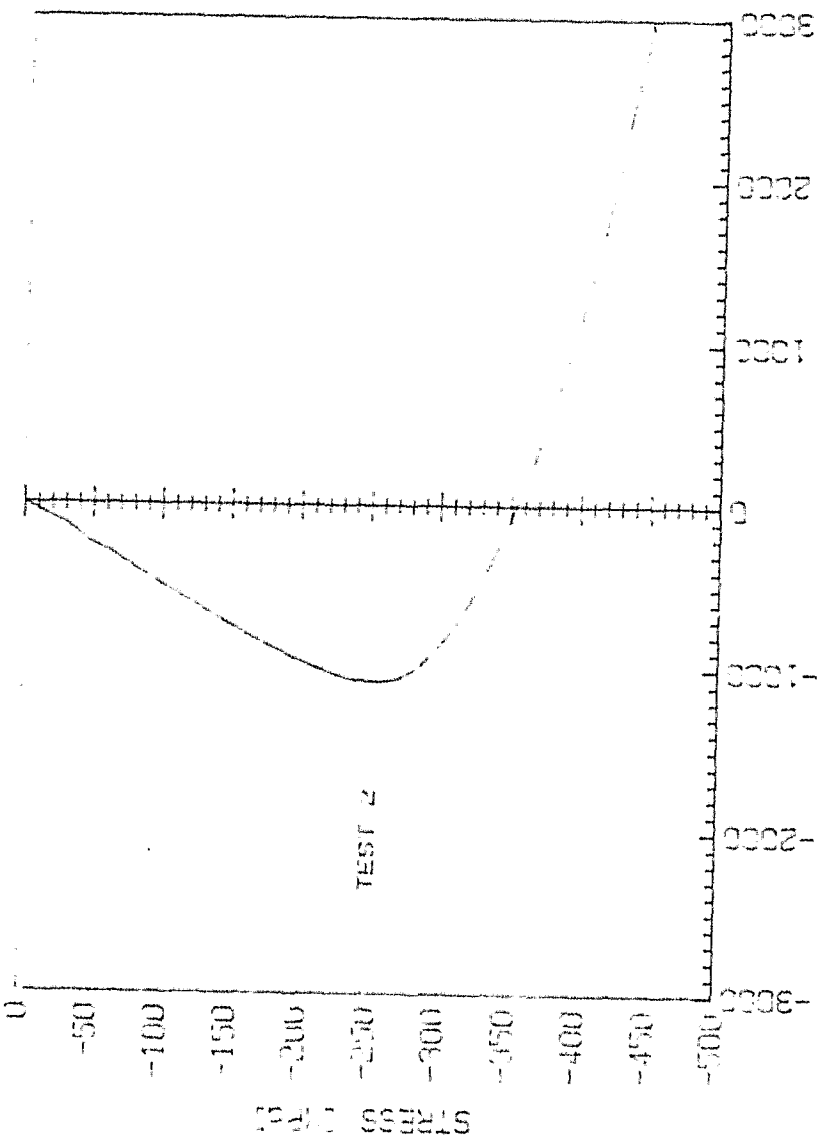

PLOT A1.6 - Average Volumetric Strain vs Stress (Test 2)

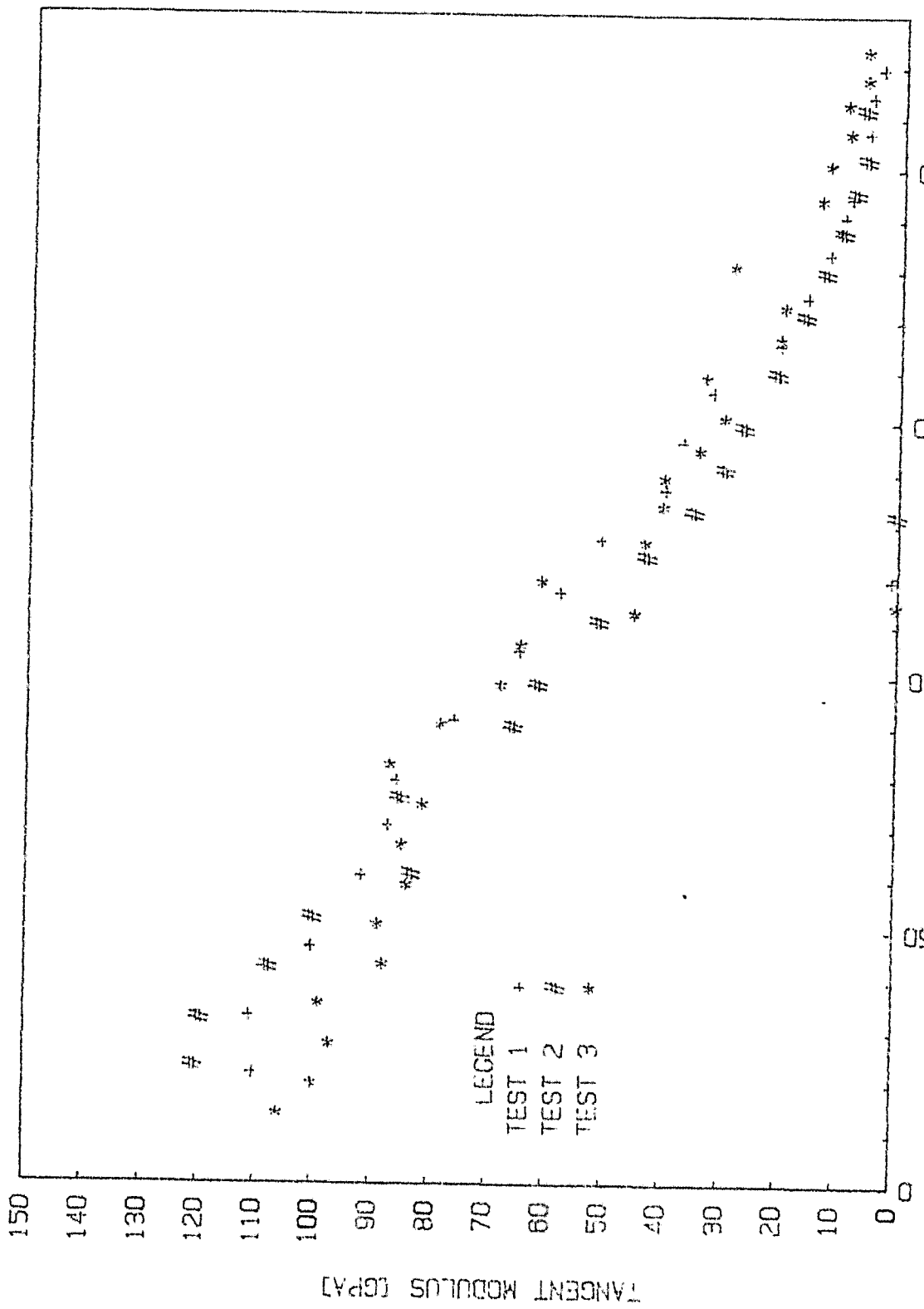

PLOT A1.7 - Tangent Modulus vs Tensile Stress (Tests 1-2-3)

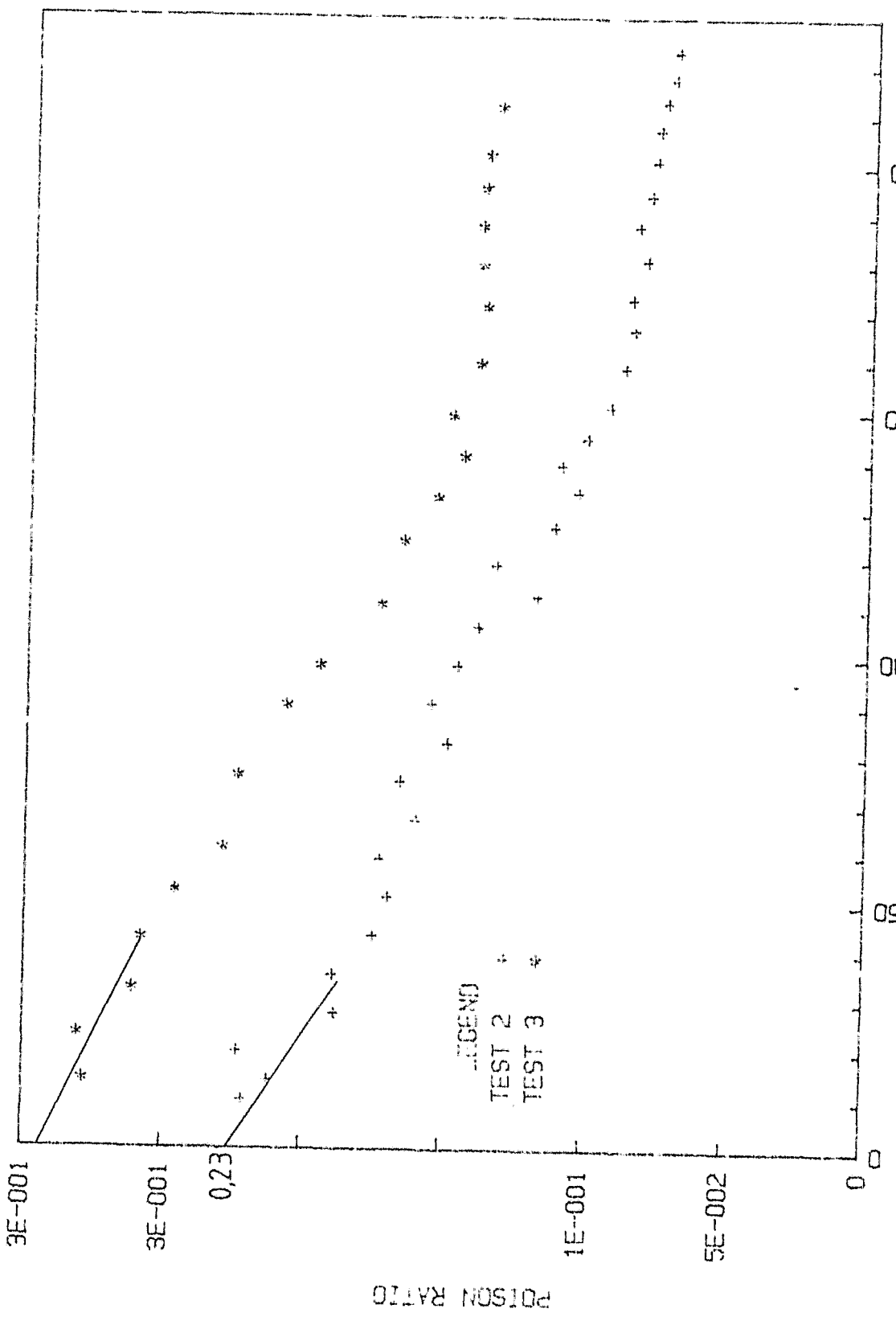

PLOT A1.8 - Poisson's Ratio vs Tensile Stress (Tests 2-3)

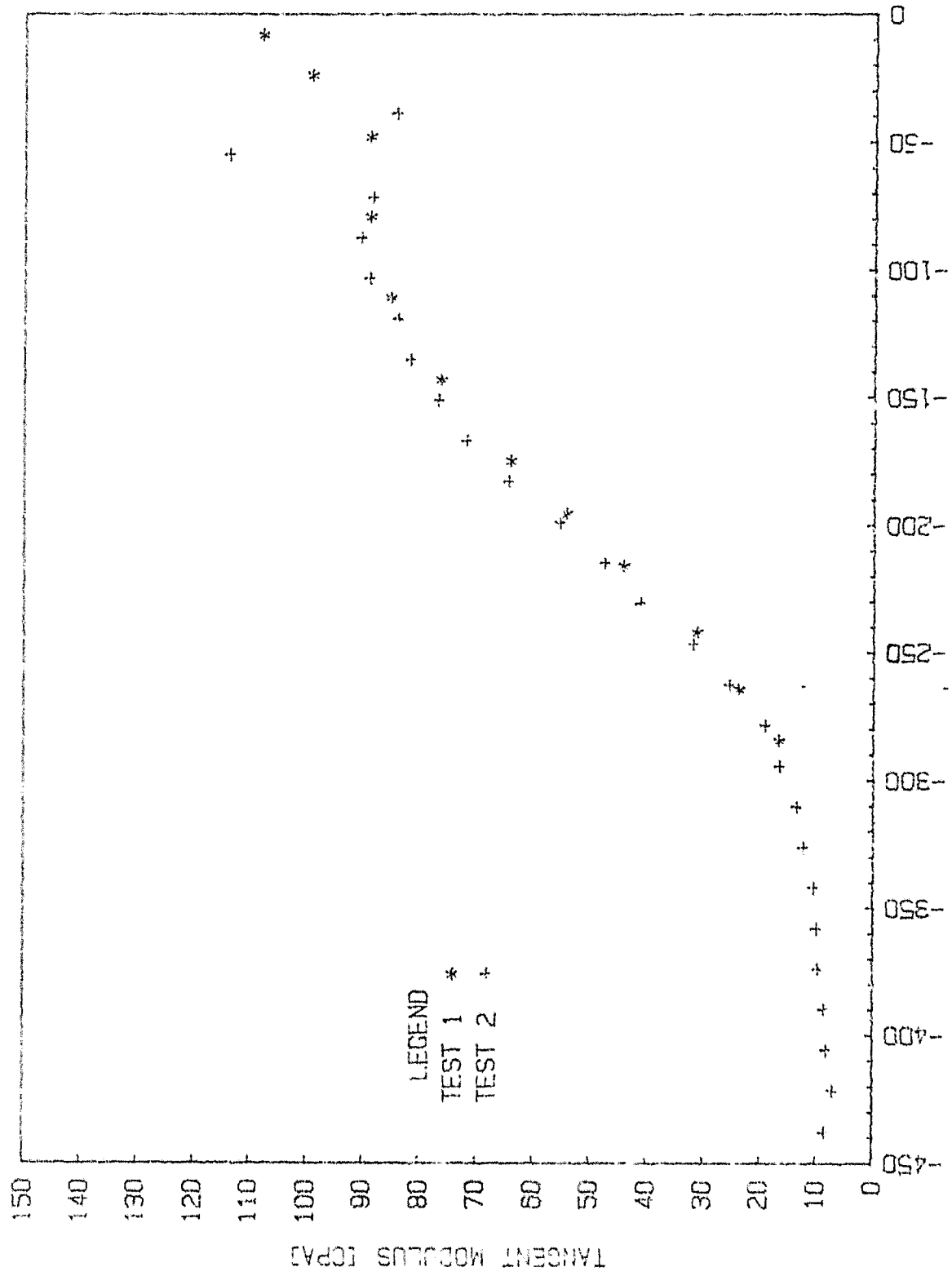

PLOT A1.9 - Tangent Modulus vs Compressive Stress (Tests 1-2)

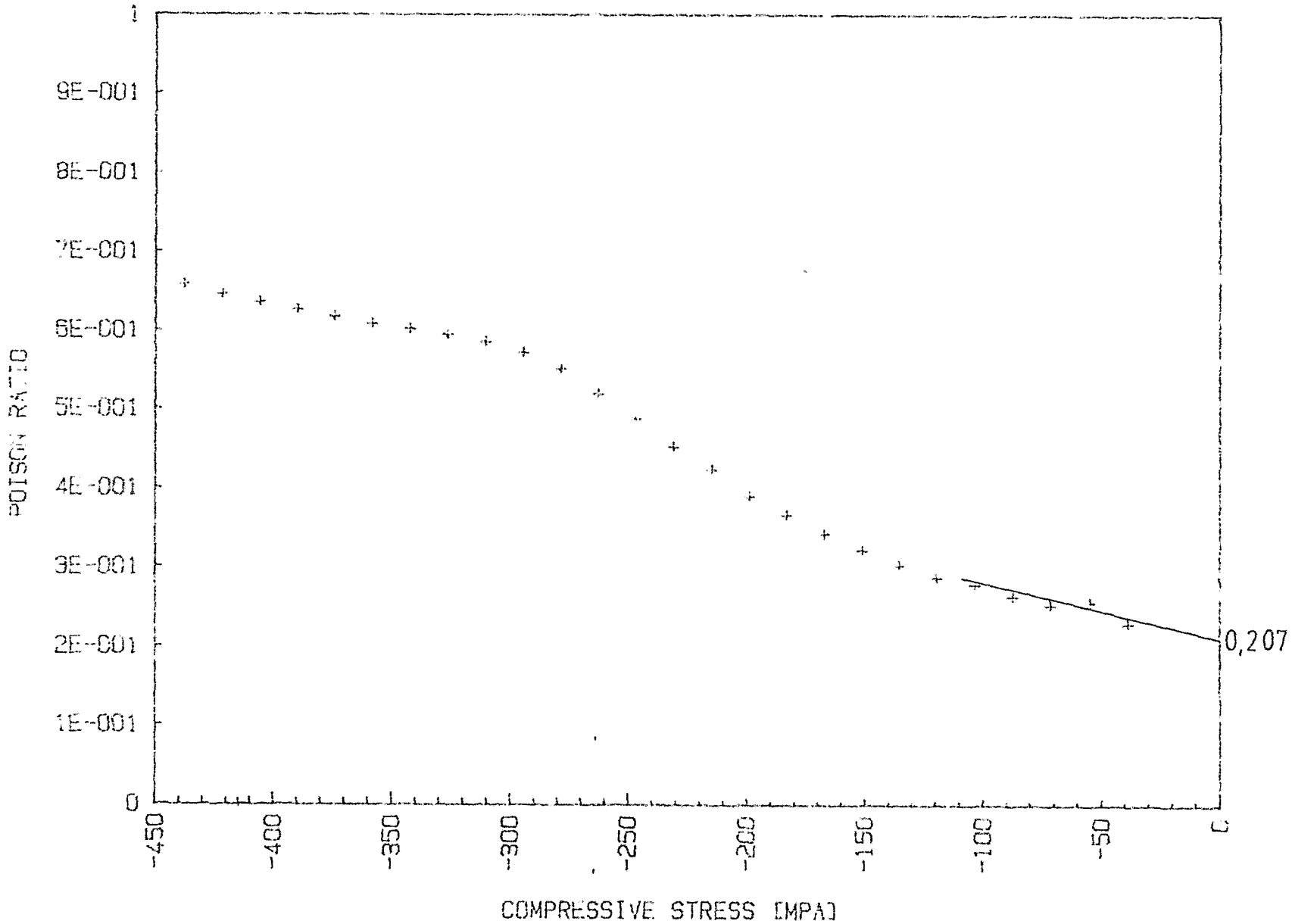

PLOT A1.10 - Poisson's Ratio vs Compressive Stress (Test 2)

A1.7 ASSESSMENT OF THE BEHAVIOUR OF CAST IRON

The variation of the 'elastic contants' of cast iron in tension and compression has been investigated by Gilbert [28], and the total strain response is shown to comprise of four components

(i) purely elastic deformation of the material matrix

(ii) plastic deformation of the matrix in regions of high stress

(iii) recoverable strain due to the opening up of graphite cavities

(iv) permanent strain associated with the opening up of cavities.

This behaviour is induced by the presence of graphite flakes which act as discontinuites modifying the stress strain response of the material. The behaviour is characterised by no definite proportional limit and hence the tangent modulus varies continuously with increasing stress.

The effect of the graphite flake causes the material to undergo a volumetric expansion when subject to stress as illustrated simply in Fig A1.3 below

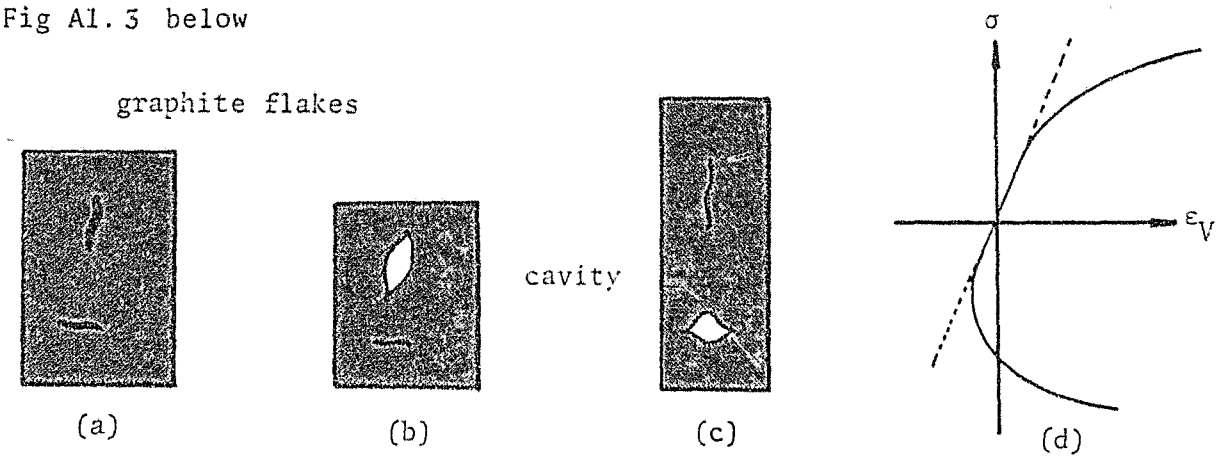

(a) Unloaded specimen. (b) Specimen subject to a compressive stress.
(c) Specimen subject to a tensile stress.
(d) Stress volumetric strain response.

Figure A1. 3 - The Stress Strain Behaviour of Cast Iron

The results obtained in these tests confirm those presented by Gilbert [28], which are essentially characterised by

(i) a positive volumetric change with increasing stress

(ii) an increasing Poisson's ratio with increasing stress

(iii) no distinct proportional limit and consequently a continuous variation of the tangent modulus.

A1.8 THE ELASTIC CONSTANTS OF CAST IRON

'Young's modulus' was evaluated from the results by selecting a proportional limit of 60 MPa in tension and -120 MPa in compression. On the basis of these values Young's modulus was selected as E = 95 GPa. These three figures appear to be rather arbitrary but they represent a compromise achieved by trial and error, in an attempt to satisfy as far as possible, all the criteria for the material model listed in Section 4.5. Plots A1.7 and A1.9 indicate that a higher value of E and lower values of the proportional limits would be more appropriate but these alternative values would have resulted in a far greater discrepancy in the volumetric strain than that obtained with the selected values.

Poisson's ratio was evaluated by taking the average reading obtained in tension and compression extrapolated to zero load as shown on Plots A1.8 and A1.10, ie

$\nu = (0,20 + 0,29 + 0.23)/3 = 0,24$

$\nu = 0,23$ was selected, since it coincides with the value commonly quoted in the literature.

A1.9 CONCLUSIONS

The manufacturers of the sheave specified that the material conformed to a grade 17 cast iron. Although the tensile tests indicate that a grade 14 is probably more accurate, a direct comparison is invalid

since it was not possible to conform to standard testing techniques.

The results futher confirm similarity in the material properties of the two sheaves. Furthermore, since the specimens were machined from different portions of the sheave (see Fig A1.4), the results suggest that the material is relatively homogeneous throughout.

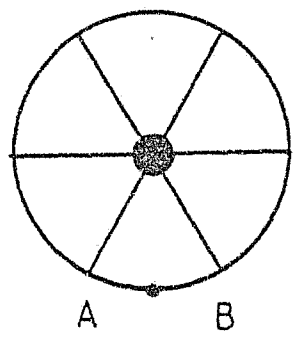

Previous sheave (1981)
Tensile specimens 1, 2
Compression specimen 1
Machined from Section AB

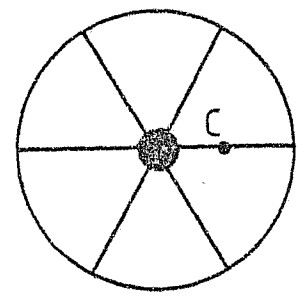

Current sheave
Tensile specimen 3
Compression specimen 2
Machined from spoke C

Figure A1. 4 - Material Origin of the Test Specimens

APPENDIX 2

PLASTICITY

A2.1 EXPLICIT FORMULATION OF THE ELASTOPLASTIC MATRIX

$$[D_{ep}] = [D] - \frac{[D]\{\frac{\partial Q}{\partial \sigma}\}\{\frac{\partial F}{\partial \sigma}\}^T [D]}{A + \{\frac{\partial F}{\partial \sigma}\}^T [D]\{\frac{\partial Q}{\partial \sigma}\}} \qquad (A2.1)$$

The elastoplastic matrix was formulated for a plane stress element with coordinates as indicated in Fig A2.1

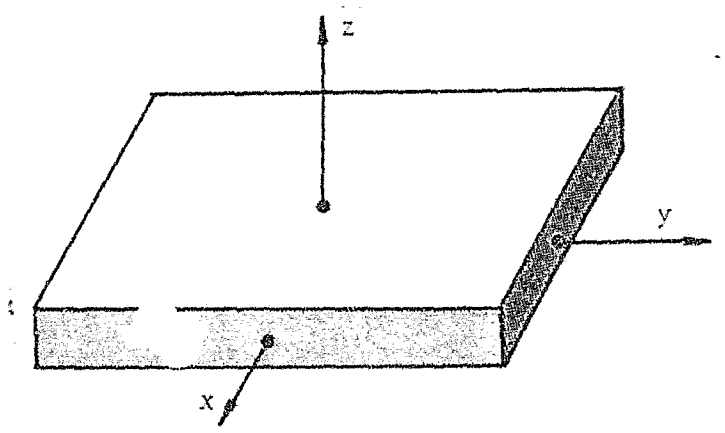

Figure A2.1 - Plane Stress Element

The components of stress/strain which are considered are:

$$\{\sigma\}^T = (\sigma_x, \sigma_y, \tau_{xy}) \quad , \quad \text{with} \quad \sigma_z, \tau_{yz}, \tau_{zx} \equiv 0$$

$$\{\epsilon\}^T = (\epsilon_x, \epsilon_y, \epsilon_z, \gamma_{xy}) \quad , \quad \text{with} \quad \gamma_{xz}, \gamma_{yz} \equiv 0$$

The elastic constitutive matrix [D] for plane stress is given by

$$[D] = \frac{E}{1-\nu^2}\begin{bmatrix} 1 & \nu & 0 \\ \nu & 1 & 0 \\ 0 & 0 & \frac{1-\nu}{2} \end{bmatrix}$$

and relates the stress σ_x, σ_y, τ_{xy} to the elastic strain components ε_x, ε_y, γ_{xy} ; whilst ε_z^e is given by

$$\varepsilon_z^e = -\frac{\nu}{E}(\sigma_x + \sigma_y)$$

For convenience in representing the plastic potential and yield function gradients the elements of $\{\frac{\partial F}{\partial \sigma}\}$, $\{\frac{\partial Q}{\partial \sigma}\}$ will be referred to by lower case letters, a to g, ie

$$\{\frac{\partial F}{\partial \sigma}\}^T = (a,\ b,\ c)$$

$$\{\frac{\partial Q}{\partial \sigma}\}^T = (d,\ e,\ f)$$

and

$$\frac{\partial Q}{\partial \sigma_z} = g$$

Substituting these values into eqn A2.1

$$[D]\{\frac{\partial Q}{\partial \sigma}\}\{\frac{\partial F}{\partial \sigma}\}^T[D] = (\frac{E}{1-\nu^2})^2\begin{bmatrix} (a+\nu b)(d+\nu e) & (\nu a+b)(d+\nu e) & c(\frac{1-\nu}{2})(d+\nu e) \\ (a+\nu b)(\nu d+e) & (\nu a+b)(\nu d+e) & c(\frac{1-\nu}{2})(\nu d+e) \\ f(\frac{1-\nu}{2})(a+\nu b) & f(\frac{1-\nu}{2})(\nu a+b) & (\frac{1-\nu}{2})^2 cf \end{bmatrix}$$

and

$$\{\frac{\partial F}{\partial \sigma}\}^T[D]\{\frac{\partial Q}{\partial \sigma}\} = (\frac{E}{1-\nu^2})[(a+\nu b)d + e(\nu a+b) + (\frac{1-\nu}{2})fc]$$

$$[D] = \frac{E}{1-\nu^2}\begin{bmatrix} 1 & \nu & 0 \\ \nu & 1 & 0 \\ 0 & 0 & \frac{1-\nu}{2} \end{bmatrix}$$

and relates the stress σ_x, σ_y, τ_{xy} to the elastic strain components ε_x, ε_y, γ_{xy} ; whilst ε_z^e is given by

$$\varepsilon_z^e = -\frac{\nu}{E}(\sigma_x + \sigma_y)$$

For convenience in representing the plastic potential and yield function gradients the elements of $\{\frac{\partial F}{\partial \sigma}\}$, $\{\frac{\partial Q}{\partial \sigma}\}$ will be referred to by lower case letters, a to g, ie

$$\{\frac{\partial F}{\partial \sigma}\}^T = (a,\ b,\ c)$$

$$\{\frac{\partial Q}{\partial \sigma}\}^T = (d,\ e,\ f)$$

and

$$\frac{\partial Q}{\partial \sigma_z} = g$$

Substituting these values into eqn A2.1

$$[D]\{\frac{\partial Q}{\partial \sigma}\}\{\frac{\partial F}{\partial \sigma}\}^T[D] = (\frac{E}{1-\nu^2})^2\begin{bmatrix} (a+\nu b)(d+\nu e) & (\nu a+b)(d+\nu e) & c(\frac{1-\nu}{2})(d+\nu e) \\ (a+\nu b)(\nu d+e) & (\nu a+b)(\nu d+e) & c(\frac{1-\nu}{2})(\nu d+e) \\ f(\frac{1-\nu}{2})(a+\nu b) & f(\frac{1-\nu}{2})(\nu a+b) & (\frac{1-\nu}{2})^2 cf \end{bmatrix}$$

and

$$\{\frac{\partial F}{\partial \sigma}\}^T[D]\{\frac{\partial Q}{\partial \sigma}\} = (\frac{E}{1-\nu^2})[(a+\nu b)d + e(\nu a+b) + (\frac{1-\nu}{2})fc]$$

$$[D_{ep}] = \frac{E}{1-\nu^2}\begin{bmatrix} 1 & \nu & 0 \\ \nu & 1 & 0 \\ 0 & 0 & \frac{1-\nu}{2} \end{bmatrix}$$

$$- \left[\frac{1}{A + (\frac{E}{1-\nu^2})[(a+\nu b)d + (\nu a+b) + (\frac{1-\nu}{2})fc]}\right]\left[[D]\{\frac{\partial Q}{\partial \sigma}\}\{\frac{\partial F}{\partial \sigma}\}^T[D]\right]$$

(A2.2)

This relates the increments of σ_x, σ_y, τ_{xy} to the increments of total strain ε_x, ε_y, γ_{xy} respectively. To evaluate the strain through the thickness of the element ε_z the following approach was used

$$d\varepsilon_z = d\varepsilon_z^e + d\varepsilon_z^p$$

where

$$d\varepsilon_z^e = -\frac{\nu}{E}[d\sigma_x + d\sigma_y]$$

Associated plasticity

$$d\varepsilon_z^p = d\lambda \cdot \frac{\partial Q}{\partial \sigma_z} \equiv d\lambda \cdot g$$

where [1]

$$d\lambda = \frac{\{\frac{\partial F}{\partial \sigma}\}^T [D]\{d\varepsilon\}}{\{\frac{\partial F}{\partial \sigma}\}^T [D]\{\frac{\partial Q}{\partial \sigma}\} + A}$$

Non associated plasticity (von Mises plastic potential)

$$d\varepsilon_z^p = -(d\varepsilon_x^p + d\varepsilon_y^p)$$

A2.2 ASSOCIATED PLASTICITY

Yield function and plastic potential gradients

$$Q \equiv F \equiv \alpha J_1 + J_2^{1/2} - K$$

$$\{\frac{\partial F}{\partial \sigma}\}^T \equiv \{\frac{\partial Q}{\partial \sigma}\}^T = (\alpha + \frac{s_x}{2J_2^{1/2}}, \alpha + \frac{s_y}{2J_2^{1/2}}, \frac{\tau_{xy}}{2J_2^{1/2}})$$

To formulate the elastoplastic matrix the terms a to g must be substituted into eqn A2.2 where

$$a = d = \alpha + \frac{s_x}{2J_2^{1/2}}$$

$$b = e = \alpha + \frac{s_y}{2J_2^{1/2}}$$

$$c = f = \frac{\tau_{xy}}{J_2^{1/2}}$$

$$g = \alpha + \frac{s_z}{2J_2^{1/2}}$$

where

$$s_x = \sigma_x - \sigma_m$$

$$s_y = \sigma_y - \sigma_m$$

$$s_z = \sigma_z - \sigma_m$$

$$\sigma_m = \frac{J_1}{3} = \frac{\sigma_x + \sigma_y + \sigma_z}{3}$$

It is apparent that for the associated model volumetric plastic strain effects occur, ie

$$d\varepsilon_v^p = d\varepsilon_x^p + d\varepsilon_y^p + d\varepsilon_z^p$$

$$= d\lambda\left[\frac{\partial Q}{\partial \sigma_x} + \frac{\partial Q}{\partial \sigma_y} + \frac{\partial Q}{\partial \sigma_z}\right]$$

$$= d\lambda[3\alpha]$$

Since $d\lambda$ is always a positive constant the volumetric plastic strain is always positive.

A2.3 NON ASSOCIATED PLASTICITY

Yield function and plastic potential gradients.

$$F = \alpha J_1 + J_2^{1/2} - K$$

$$Q = J_2^{1/2}$$

In this case the direction of the plastic strain increment is defined by a von Mises plastic potential surface. This results in plastic incompressibility commonly observed in metal plasticity.

$$\{\frac{\partial F}{\partial \sigma}\} = (\alpha + \frac{s_x}{2J_2^{1/2}}, \alpha + \frac{s_y}{2J_2^{1/2}}, \frac{\tau_{xy}}{J_2^{1/2}})$$

$$\{\frac{\partial Q}{\partial \sigma}\}^T = (\frac{s_x}{2J_2^{1/2}}, \frac{s_y}{2J_2^{1/2}}, \frac{\tau_{xy}}{J_2^{1/2}})$$

ie

$$a = \alpha + \frac{s_x}{2J_2^{1/2}} \qquad d = \frac{s_x}{2J_2^{1/2}}$$

$$b = \alpha + \frac{s_y}{2J_2^{1/2}} \qquad e = \frac{s_y}{2J_2^{1/2}}$$

$$c = \frac{\tau_{xy}}{J_2^{1/2}} \qquad f = \frac{\tau_{xy}}{J_2^{1/2}}$$

Similarly the volumetric plastic component may be evaluated by considering

$$d\varepsilon_v^p = d\varepsilon_x^p + d\varepsilon_y^p + d\varepsilon_z^p$$

$$= d\lambda\left[\frac{\partial Q}{\partial \sigma_x} + \frac{\partial Q}{\partial \sigma_y} + \frac{\partial Q}{\partial \sigma_z}\right]$$

$$= d\lambda\left[\frac{s_x + s_y + s_z}{2J_2^{1/2}}\right]$$

$$\equiv 0$$

since $s_x + s_y + s_z \equiv 0$

A2.4 PARAMETER A

$$A = -\frac{\partial F}{\partial k} dk \frac{1}{d\lambda} \qquad \text{(A2.3)}$$

If the work hardening hypothesis is considered

$$k = \int \{\sigma\}^T \{d\varepsilon^p\}$$

$$dk = \{\sigma\}^T \{d\varepsilon^p\} \qquad \text{(A2.4)}$$

since

$$\{d\varepsilon^p\} = d\lambda \{\frac{\partial Q}{\partial \sigma}\}$$

$$dk = d\lambda\{\sigma\}^T\{\frac{\partial Q}{\partial \sigma}\} \tag{A2.5}$$

substituting eqn (A2.5) into eqn (A2.3), $d\lambda$ is eliminated, ie

$$A = -\frac{\partial F}{\partial k}\{\sigma\}^T\{\frac{\partial Q}{\partial \sigma}\} \tag{A2.6}$$

since

$$\{\frac{\partial F}{\partial \sigma}\}^T\{d\sigma\} - \frac{\partial F}{\partial k}dk = 0$$

for the stresses to remain on the expanding yield surface

$$-\frac{\partial F}{\partial k} = \frac{\{\frac{\partial F}{\partial \sigma}\}^T\{d\sigma\}}{dk}$$

Hence eqn (A2.6) becomes

$$A = \frac{\{\frac{\partial F}{\partial \sigma}\}^T\{d\sigma\}\{\sigma\}^T\{\frac{\partial Q}{\partial \sigma}\}}{dk} \tag{A2.7}$$

All terms in the numerator of this expression can be evaluated directly, however, the quotient dk is obtained by considering the experimental results of the uniaxial tension compression test where only uniaxial plastic deformation is considered; consequently eqn (A2.4) reduces to

$$dk = \sigma d\varepsilon^p$$

where σ, $d\varepsilon^p$ represent the uniaxial stress and plastic strain increment respectively.

The increment of work performed dk can be expressed in terms of an effective stress/strain expression which reduces to the actual stress/strain for the case of uniaxial loading, ie

$$dk = \bar{\sigma}\frac{d\bar{\varepsilon}_p}{d\bar{\sigma}}d\bar{\sigma} \tag{A2.8}$$

where $\bar{\sigma}$ represents the effective stress which is taken to be equivalent to $\sqrt{3}J_2^{1/2}$

$\frac{d\bar{\varepsilon}_p}{d\bar{\sigma}}$ represents the slope of the effective stress/strain curve for the uniaxial test in tension and compression at the effective stress level $\bar{\sigma}$.

since

$$\bar{\sigma} = \sqrt{3}J_2^{1/2}$$

$$d\bar{\sigma} = \{\frac{d\bar{\sigma}}{d\sigma}\}^T \{d\sigma\}$$

$$\therefore\ d\bar{\sigma} = \frac{\sqrt{3}}{2J_2^{1/2}}[s_x d\sigma_x + s_y d\sigma_y + 2\tau_{xy} d\tau_{xy}]$$

In terms of principal stresses this reduces to

$$d\bar{\sigma} = \frac{\sqrt{3}}{2J_2^{1/2}}[s_1 d\sigma_1 + s_2 d\sigma_2] \qquad \text{(A2.9)}$$

On substituting eqn (A2.9) into eqn (A2.8)

$$dk = \frac{3}{2}[s_1 d\sigma_1 + s_2 d\sigma_2]\frac{d\bar{\varepsilon}p}{d\bar{\sigma}}$$

Hence eqn (A2.7) becomes

$$A = \frac{2}{3}\frac{d\bar{\sigma}}{d\bar{\varepsilon}p}\frac{\{\frac{\partial F}{\partial \sigma}\}^T \{d\sigma\} \cdot \{\sigma\}^T \{\frac{\partial Q}{\partial \sigma}\}}{[s_1 d\sigma_1 + s_2 d\sigma_2]} \qquad \text{(A2.10)}$$

The value of $d\bar{\sigma}/d\bar{\varepsilon}p$ may be obtained directly from the uniaxial tension/compression test. Thus using E_T to represent the tangent modulus of the stress total strain curve:

The total strain increment: $d\varepsilon = \frac{1}{E_T} d\sigma$

The elastic strain increment: $d\varepsilon^e = \frac{1}{E} d\sigma$

The plastic strain increment: $d\varepsilon^p = d\varepsilon - d\varepsilon^e$

$$= \left(\frac{1}{E_T} - \frac{1}{E}\right) d\sigma$$

Hence

$$\frac{d\varepsilon^p}{d\sigma} = \frac{E - E_T}{E E_T}$$

or more generally

$$\frac{d\bar{\sigma}}{d\bar{\varepsilon}_p} = \frac{E E_T}{E - E_T}$$

This value and the corresponding value of A as per eqn (A2.10) vary continuously as straining proceeds. The evaluation is simplified by reference to a single parameter; the ratio R. As discussed in Chapter 4, the initial yield surface is defined by $R = 0$, whilst the final yield surface at fracture, by $R = 1$. Thus it is possible to define the tangent modulus by a single function $E_T = f(R)$, and hence parameter A for all plastic stress states.

By substituting the relevant par .eters into eqn (A2.10), the parameter A may be evaluated for both the associated and non associated plastic potential; ie

Associated plasticity:

$$A = \frac{2}{3} \frac{d\bar{\sigma}}{d\bar{\varepsilon}^p} \left[\frac{\left[\left(\alpha + \frac{s_1}{2J_2^{1/2}}\right) d\sigma_1 + \left(\alpha + \frac{s_2}{2J_2^{1/2}}\right) d\sigma_2\right]\left[\left(\alpha + \frac{s_1}{2J_2^{1/2}}\right)\sigma_1 + \left(\alpha + \frac{s_2}{2J_2^{1/2}}\right)\sigma_2\right]}{s_1 d\sigma_1 + s_2 d\sigma_2} \right]$$

Non associated plasticity - von Mises plastic potential

$$A = \frac{2}{3} J_2^{1/2} \frac{d\bar{\sigma}}{d\bar{\varepsilon}_p} \left[\frac{(\alpha + \frac{s_1}{2J_2^{1/2}})d\sigma_1 + (\alpha + \frac{s_2}{2J_2^{1/2}})d\sigma_2}{s_1 d\sigma_1 + s_2 d\sigma_2} \right]$$

The approach presented above is now considered to be inconsistent with the techniques employed in the literature [12]. This only became apparent at an advanced stage of the research when time limitations prevented further investigation. The alternative derivation is included in Section A2.6 for the purpose of comparison.

A2.5 THE DIMENSIONLESS STRESS RATIO R

This ratio performs two functions

- The tangent modulus determined from uniaxial tension/compression tests may be formulated as $E_T = f(R)$
- The parameters $\alpha(k)$, $K(k)$, for each subsequent yield surface may be determined from the value of R thus controling the expansion of the initial yield surface into the final failure surface in a very specific manner.

Consider the case where the initial yield and failure cones are defined by different cone angles as illustrated in Fig A2.2

These surfaces are presented on the shear stress, mean stress, axes in Fig A2.3. It is clear that the ratio R = A/B couples the movement of the apex of the cone along the σ_m axis to the radius of the cone in the π plane. This is an arbitrary assumption which has been selected for convenience in subsequent calculations.

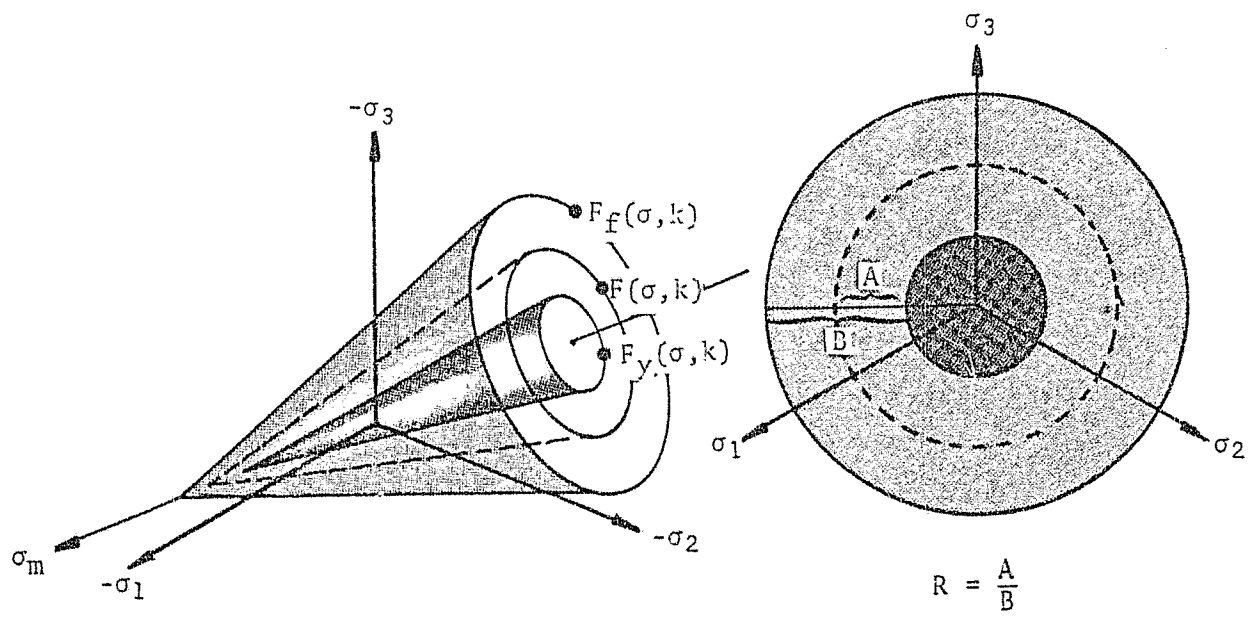

Principal Stress Space

π Plane ($\sigma_m = 0$)

$$F(\sigma,k) = \alpha(k)J_1 + J_2^{1/2} - K(k) = 0$$

where $$\alpha(k) = \frac{2\sin\phi(k)}{\sqrt{3}(3 - \sin\phi(k))}$$

$$K(k) = \frac{6\,c\,(k)\cos\phi(R)}{\sqrt{3}(3 - \sin\phi(k))}$$

$F_y(\sigma,k)$ represents the yield surface

$F(\sigma,k)$ represents any subsequent yield surface

$F_f(\sigma,k)$ represents the failure surface

Figure A2.2 - Drucker Prager Surface in the Principal Stress Space at Different Stages of Expansion

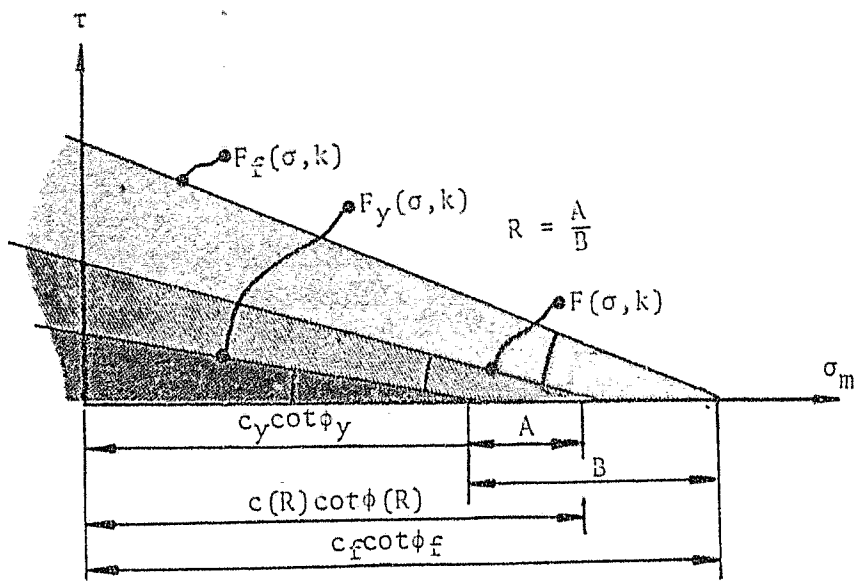

Figure A2.3 - Drucker Prager Surface in the Shear/Mean Stress Space at Different Stages of Expansion

As illustrated in Figs A2.2 and A2.3, the ratio is taken to be

$R = A/B$

In the π plane this is equivalent to

$$R = \frac{K(k) - K_y}{K_f - K_y} \qquad \text{(A2.11)}$$

whilst on the mean stress axis R represents the relative position of the apex of any subsequent yield surface with respect to the initial yield and failure surfaces. ie

$$R = \frac{c(k)\cot\phi(k) - c_y\cot\phi_y}{c_f\cot\phi_f - c_y\cot\phi_y} \qquad \text{(A2.12)}$$

From eqn (A2.11)

$$K(k) = K_y + R(K_f - K_y) \qquad \text{(A2.13)}$$

also

$$K(k) = \frac{6c(k)\cos\phi(k)}{\sqrt{3}(3-\sin\phi(k))}$$

let $K_f - K_y = X$

Then eqn (A2.13) becomes

$$K(k) = K_y + RX = \frac{6c(k)\cos\phi(k)}{\sqrt{3}(3-\sin\phi(k))} \qquad \text{(A2.14)}$$

From eqn (A2.12)

$$c(k)\cot\phi(k) = c_y\cot\phi_y + R(c_f\cot\phi_f - c_y\cot\phi_y) \qquad \text{(A2.15)}$$

let $Y = c_f\cot\phi_f - c_y\cot\phi_y$

and $\bar{c}_y = c_y \cot\phi_y$

Then eqn (A2.15) becomes

$$c(k)\cot\phi(k) = \bar{c}_y + RY \qquad \text{(A2.16)}$$

or

$$c(k)\cos\phi(k) = \sin\phi(k)(\bar{c}_y + RY) \qquad \text{(A2.17)}$$

Substituting eqn (A2.17) into eqn (A2.14)

$$\frac{6\sin\phi(k)}{\sqrt{3}(3-\sin\phi(k))} = \frac{K_y + RX}{\bar{c}_y + RY} \qquad \text{(A2.18)}$$

When yielding occurs $F(\sigma,k) = 0$, thus

$$\alpha(k)J_1 + J_2^{1/2} - K(k) \equiv 0 \qquad \text{(A2.19)}$$

Substituting the values for $\alpha(k)$, $K(k)$ into eqn (A2.19)

$$\frac{6\sin\phi(k)}{\sqrt{3}(3-\sin\phi(k))}\left[\frac{J_1}{3} - c(k)\cot\phi(k)\right] + J_2^{1/2} = 0 \qquad \text{(A2.20)}$$

Substituting eqn (A2.16) into eqn (A2.20)

$$\frac{6\sin\phi(k)}{\sqrt{3}(3-\sin\phi(k))}\left[\frac{J_1}{3} - (\bar{c}_y + RY)\right] + J_2^{1/2} = 0$$

hence

$$\frac{6\sin\phi(k)}{\sqrt{3}(3-\sin\phi(k))} = \frac{J_2^{1/2}}{\left[\bar{c}_y + RY - \frac{J_1}{3}\right]} \qquad \text{(A2.21)}$$

Equating eqn (A2.21) to eqn (A2.18)

$$\frac{K_y + RX}{\bar{c}_y + R_y} = \frac{J_2^{1/2}}{[\bar{c}_y + RY - \frac{J_1}{3}]} \qquad (A2.22)$$

Simplifying eqn (A2.22) results in

$$R^2[xy] + R[Y(K_y - J_2^{1/2}) + X(\bar{c}_y - \frac{J_1}{3})] + [K_y(\bar{c}_y - \frac{J_1}{3}) - \bar{c}_y J_2^{1/2}] = 0 \qquad (A2.23)$$

The positive root of the quadratic eqn (A2.23) determines the value of ratio R .

By rewriting eqns (A2.14), (A2.18), the values of $\alpha(k)$ and $K(k)$ defining the present yield surface may be evaluated. ie

$$K = K_y + RX$$

$$\alpha = \frac{1}{3}[\frac{K_y + RX}{\bar{c}_y + RY}]$$

The values of ϕ, c may similarly be calculated by

$$\phi = \sin^{-1}[\frac{3\sqrt{3}E}{6 + \sqrt{3}E}]$$

where

$$E = \frac{K_y + RX}{\bar{c}_y + RY}$$

$$c = \tan\phi[\bar{c}_y + RY]$$

2.6 AN ALTERNATIVE FORMULATION OF PARAMETER A

An alternative formulation of parameter A, which is consistent with the approach adopted in the literature [12], may be obtained by careful choice of the term selected to represent the effective stress.

ie

$$\bar{\sigma} = \alpha J_1 + J_2^{1/2} \quad (=K) \qquad \text{(A2.24)}$$

$$= \{\sigma\}^T \{\frac{\partial F}{\partial \sigma}\}$$

This form of the effective stress yields an invariant quantity describing any stress state lying on each subsequent yield surface. Due to this property the total effective plastic strain $\bar{\varepsilon}_p$ evaluated from the uniaxial tension/compression tests may be directly related to each subsequent yield surface, as a function of the effective stress, $\bar{\varepsilon}^p = f(\bar{\sigma})$.

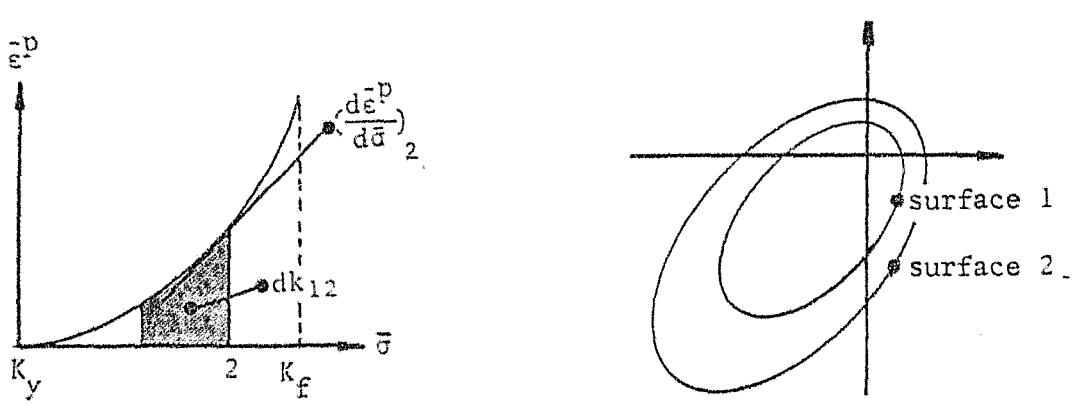

Figure A2.4 - An Altermative Formulation of the Increment of Plastic Work, dK

In order to formulate $\bar{\varepsilon}^p = f(\sigma)$, a similar technique to that employed in Chapter 4 is required to select the yield/failure surface parameters so as to ensure a satisfactory curve fit to the experimental data.

The explicit formulation of parameter A , as in the previous section, is dependent on the work hardening parameter k

$$k = \int \{\sigma\}^T \{d\varepsilon^p\}$$

where for the case of uniaxial loading

$$k = \int \bar{\sigma} d\bar{\varepsilon}^p$$

hence

$$dk = \bar{\sigma}\frac{d\bar{\varepsilon}^p}{d\bar{\sigma}}d\bar{\sigma}$$

In the context of the foregoing discussion it is apparent that k no longer represents the physical energy required to deform the material plastically; however this approach ensures that the incremental change in k, dk , corresponding to an incremental expansion of yield surface is invariant with respect to the stress path followed during the plastic deformation. This is illustrated in Fig A2.4 where the incremental change in k , incurred during the expansion of the yield surface 1-2, is represented by the shaded area dk_{12} .

$$A = \frac{\{\frac{\partial F}{\partial \sigma}\}^T \{d\sigma\}\{\sigma\}^T\{\frac{\partial Q}{\partial \sigma}\}}{dk} \qquad (A2.24)$$

where

$$dk = \bar{\sigma}\frac{d\bar{\varepsilon}^p}{d\bar{\sigma}}d\bar{\sigma}$$

and

$$\bar{\sigma} = \{\sigma\}^T\{\frac{\partial F}{\partial \sigma}\}$$

$$d\bar{\sigma} = \{\frac{\partial F}{\partial \sigma}\}^T\{d\sigma\}$$

$$\Rightarrow dk = [\{\sigma\}^T\{\frac{\partial F}{\partial \sigma}\}\cdot\{\frac{\partial F}{\partial \sigma}\}^T\{d\sigma\}]\frac{d\bar{\varepsilon}^p}{d\bar{\sigma}} \qquad (A2.25)$$

Substituting eqn (A2.25) into eqn (A2.24)

$$A = \frac{d\bar{\sigma}}{d\bar{\varepsilon}^p}\left[\frac{\{\sigma\}^T\{\frac{\partial Q}{\partial \sigma}\}}{\{\sigma\}^T\{\frac{\partial F}{\partial \sigma}\}}\right]$$

When plasticity is associated; Q = F

$$A = \frac{d\bar{\sigma}}{d\bar{\varepsilon}^p}$$

Alternatively, when plasticity is non associated, with

$$Q = J_2^{1/2}$$

$$A = \frac{J_2^{1/2}}{\bar{\sigma}} \frac{d\bar{\sigma}}{d\bar{\varepsilon}^p}$$

It is pertinent to note that a technique similar to that presented in Section A2.5 is required to define subsequent yield surface parameters α, K during plastic deformation.

A2.7 AN ALTERNATIVE PLASTIC POTENTIAL SURFACE

Experimental evidence indicates that cast iron dilates during plastic deformation. Although an associated Drucker Prager constitutive relationship predicts this effect, it is not accurate (Plots 4.4 and (4.5). In an attempt to correlate both the uniaxial and volumetric behaviour of the material with experimentally determined values, a plastic potential dependent on the first stress invariant, was selected ie

$$F(\sigma,k) = \alpha(k)J_1 + J_2^{1/2} - K(k) \qquad \text{(A2.26)}$$

$$Q = \bar{\alpha}J_1 + J_2^{1/2} \qquad \text{(A2.27)}$$

$$d\varepsilon_V^p = 3\bar{\alpha}\cdot d\lambda \qquad \text{(A2.28)}$$

The volumetric plastic strain is governed by the value of $\bar{\alpha}$, and consequently the value of this parameter determine the success of the model. In order to realise a suitable function describing the variation of $\bar{\alpha}$ during plastic deformation the following approach was adopted:

- The effective plastic strain was formulated as a function of the effective stress yielding a single curve for the tensile/ compression test results.
- In a similar fashion the total volumetric plastic strain was formulated as a function of the effective stress.

This enabled $\frac{d\bar{\varepsilon}^p}{d\bar{\sigma}}$ and $\frac{d\bar{\varepsilon}_V^p}{d\bar{\sigma}}$ to be evaluated.

The plastic multiplier $d\lambda$ may be evaluated by equating the theoretical plastic work performed in expanding the yield surface with that obtained from experiment.

That is

$$dw^p = \bar{\sigma} \frac{d\bar{\varepsilon}^p}{d\bar{\sigma}} d\bar{\sigma} \qquad \text{(A2.29)}$$

$$dw^p = \{\sigma\}^T\{d\varepsilon^p\}$$

$$= d\lambda\{\sigma\}^T\{\frac{\partial Q}{\partial \sigma}\} \qquad \text{(A2.30)}$$

equating (A2.29) and (A2.30)

$$d\lambda = \frac{\bar{\sigma} \frac{d\bar{\varepsilon}^p}{d\bar{\sigma}} d\bar{\sigma}}{\{\sigma\}^T\{\frac{\partial Q}{\partial \sigma}\}} \qquad \text{(A2.31)}$$

substituting eqn (6) into eqn (3)

$$d\varepsilon_V^p = \frac{3\bar{\alpha}\bar{\sigma} \frac{d\bar{\varepsilon}^p}{d\bar{\sigma}} d\bar{\sigma}}{\{\sigma\}^T\{\frac{\partial Q}{\partial \sigma}\}}$$

$$\therefore \quad \frac{d\varepsilon_V^p}{d\bar{\sigma}} = \frac{3\bar{\alpha}\bar{\sigma}}{\{\sigma\}^T\{\frac{\partial Q}{\partial \sigma}\}} \frac{d\bar{\varepsilon}^p}{d\bar{\sigma}}$$

$$\therefore \quad \bar{a} = \left[\frac{\frac{d\varepsilon_V^P}{d\bar{\sigma}}}{\frac{d\bar{\varepsilon}^P}{d\bar{\sigma}}} \right] \frac{\{\sigma\}^T \{\frac{\partial Q}{\partial \sigma}\}}{\bar{\sigma}}$$

The author implemented the above technique. However it became apparent that convergence could not be achieved at high tensile stress and further development of this approach was discontinued.

APPENDIX 3

MATERIAL MODEL SUBROUTINE STRUCTURE

A3.1 INTRODUCTION

The subroutine structue is similar to that of existing material model subroutines in the two-dimensional solid element library. The subroutine comprises three smaller routines, EIPLA, ELPAL, MIDEP, each performing a specific function as illustrated in the flow chart of Fig A3.1.

Elaboration on the purpose of each routine and its mode of operation will be presented in Section A3.3 together with the relevant flow charts. A listing of the program is presented in Section A3.4.

A3.2 INPUT DATA FORMAT

A3.2.1 Element Group Control Card (pg X11.4 in ADINA users manual 1981)

In order to execute an analysis employing this subroutine the following variables on the element group control card must be defined as

NPAR(15) - MATERIAL MODEL NUMBER - NPAR(15) = 14

NPAR(17) - NUMBER OF MATERIAL CONSTANTS PER SET = 13

NPAR(20) - DIMENSION OF STORAGE ARRAY (WA) PER INTEGRATION POINT = 11

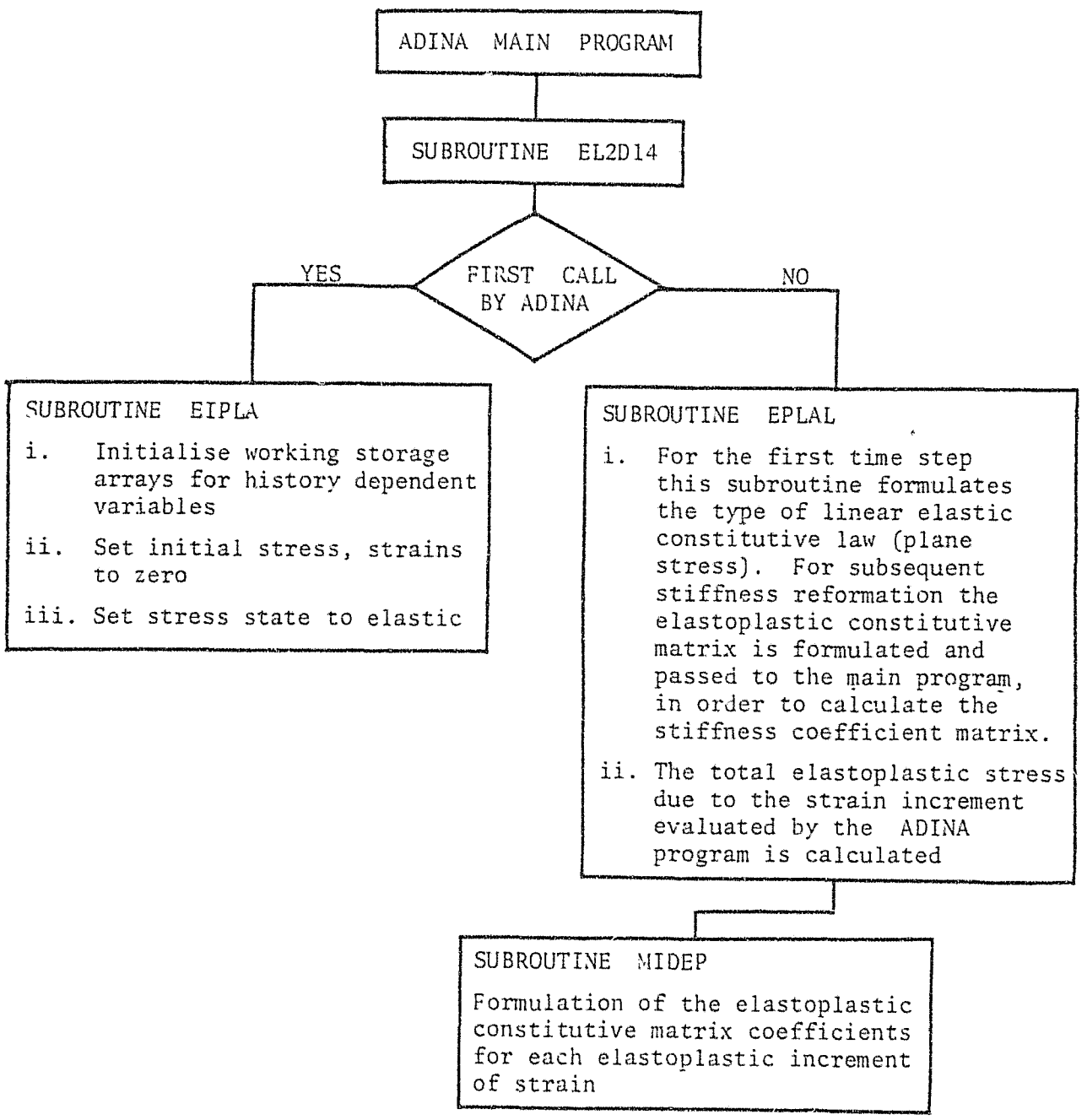

Figure A3.1 - Flow Chart of the Material Model Subroutine

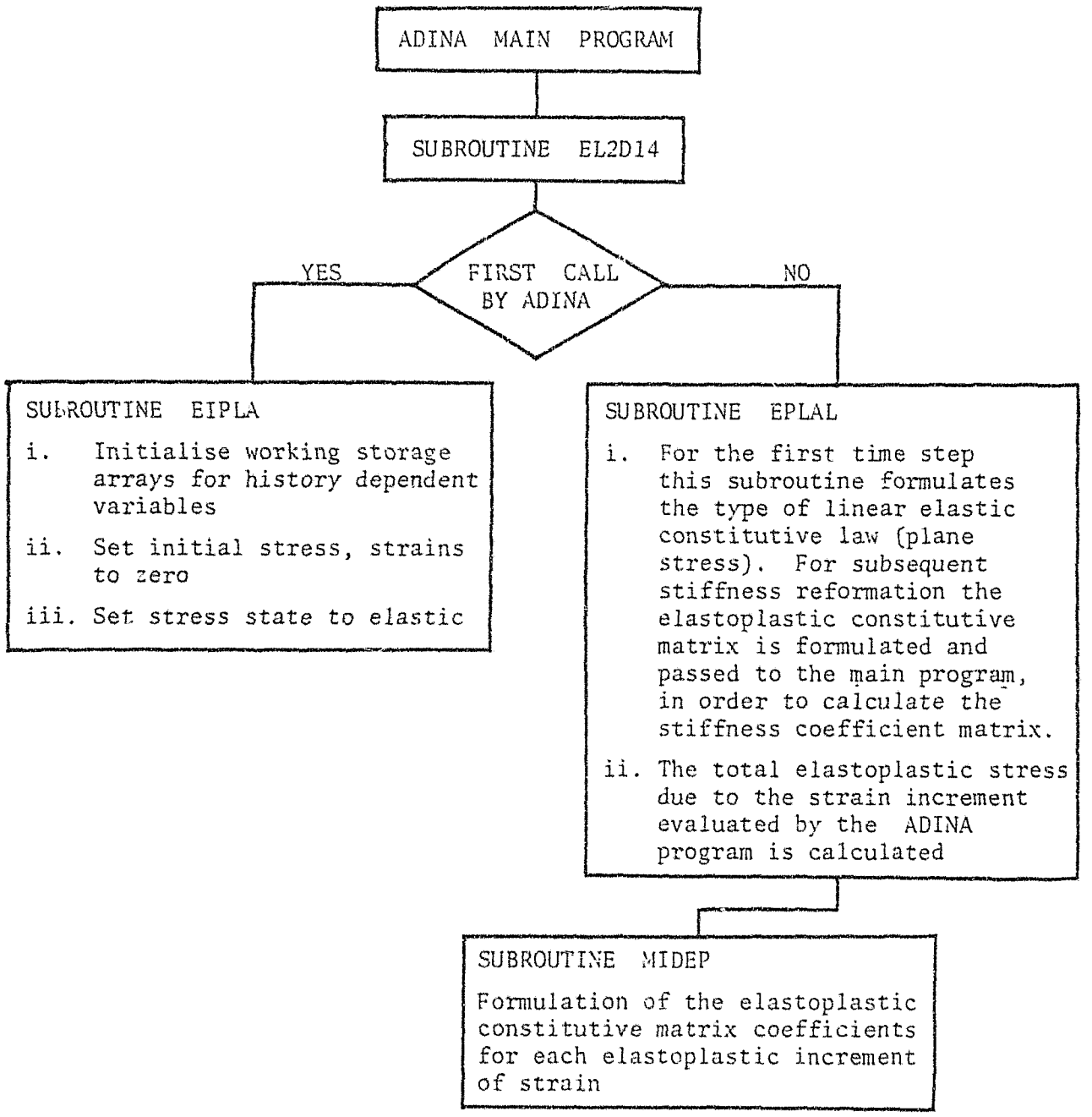

Figure A3.1 - Flow Chart of the Material Model Subroutine

A3.2.2 Material Property Data Card (pg X11.12)

a. MATERIAL NUMBER CARD: NO CHANGE

b. MATERIAL PROPERTY CARDS (2 CARDS: 8F10.0)

Sixteen material constants are defined which specify the material law initial yield/failure surfaces and the tangent modulus parameters. These values are stored in an array as PROP (1) - PROP (16), as listed below.

CARD 1

NOTE	COLUMNS	VARIABLE	ENTRY DESCRIPTION
1	1-10	PROP(1) - TMM	MODEL TYPE (VONMISES, DRUCKER PRAGER)
2	11-20	PROP(2) - PPOT	PLASTIC POTENTIAL
3	21-30	PROP(3) - SHL	HARDENING PARAMETER
	31-40	PROP(4) - RLIM	LINEAR LIMIT R
	41-50	PROP(5) - EXPA	EXPONENTIAL HARDENING CONSTANT -
	51-60	PROP(6) - EXPB	EXPONENTIAL HARDENING CONSTANT
	61-70	PROP(7) - E	YOUNG'S MODULUS
	71-80	PROP(8) - PV	POISSON'S RATIO

CARD 2

	1-10	PROP(9) - YKAP	K_y } YIELD SURFACE PARAMETERS
	11-20	PROP(10) - ALFA	α_y }
	21-30	PROP(11) - ET	FINAL TANGENT MODULUS ($R \geq 1$)
	31-40	PROP(12) - UTT	K_f } FAILURE SURFACE PARAMETERS
	41-50	PROP(13) - ALC	α_f }
	51-60	PROP(14) - YC	$\bar{c}_y = c_y \cot\phi_y$
	61-70	PROP(15) - XF	$X = K_f - K_y$
	71-80	PROP(16) - YF	$Y = \bar{c}_f - \bar{c}_y$

NOTES:

1. MODEL TYPE: TMM = 1 VON MISES CRITERION
= 2 DRUCKER PRAGER CRITERION

By setting $\alpha = 0$, the VON MISES YIELD criterion is achieved:

$$F(\sigma,k) = J_2^{1/2} - K(k) = 0$$

where

$$K(k) = \frac{\sigma_y}{\sqrt{3}}$$

2. PLASTIC POTENTIAL: PPOT = 1 ASSOCIATED PLASTIC POTENTIAL $Q \equiv F$

= 2 NON ASSOCIATED VON MEISES PLASTIC POTENTIAL $Q = J_2^{1/2}$

3. The function defining the variation of the tangent modulus is assumed to be of the form:

$$E_T(R) = E + SHL \times R \qquad 0 < R \leq RLIM$$

$$E_T(R) = EXPA \cdot e^{EXPB \cdot R} \qquad RLIM \leq R \leq 1$$

$$E_T(R) = ET \qquad R > 1$$

A3.3 SUBROUTINE EIPLA, ELPAL, MIDEP

Owing to the complexity of these routines a brief review of each is presented below. More detailed information can be obtained from the listing of the subroutine presented in Section A3.4.

A3.3.1 Subroutine EIPLA

This routine initialises a working storage array for the Gausian integration points of each element. The array facilitates storage of history dependent variables which are required to track the non-linear behaviour of the material during solution. For this particular application the history dependent variables defined by the routine, for subsequent use by subroutine ELPAL, are listed below:

SIG - the four[1] components of total stress at the time of the last update (set to zero) ie, (σ_x, σ_y, τ_{xy}, σ_z)

EPS - the four components of total strain at the time of the last update (set to zero) ie, (ε_x, ε_y, γ_{xy}, ε_z)

XK - the yield surface parameter K(k) , calculated at the time of the last update (set to YKAP; the initial yield surface parameter)

XXALFA - the yield surface parameter $\alpha(k)$, calculated at the time of the last update (set to ALFA; the initial yield surface parameter)

IPELD - STRESS STATE DEFINITION (set to 1)
= 1 elastic
= 2 plastic
= 3 failure
= 4 plasticity, followed by elastic unloading

A3.3.2 Subroutine ELPAL

This subroutine constitutes the major part of the material model subroutine. Its mode of operation is illustrated diagramatically by the flow chart presented in Fig A3.2.

A3.3.3 Subroutine MIDEP

This routine fomulates the elastoplastic constitutive matrix for the associated and non associated Drucker Prager yield criterion - the relevant flow chart is presented in Fig A3.3.

---

1. Although three components of stress (σ_x, σ_y, τ_{xy}) are required for a plane stress analysis; four components were specified in order to easily modify the routine for the case of plane strain and axisymetric analyses.

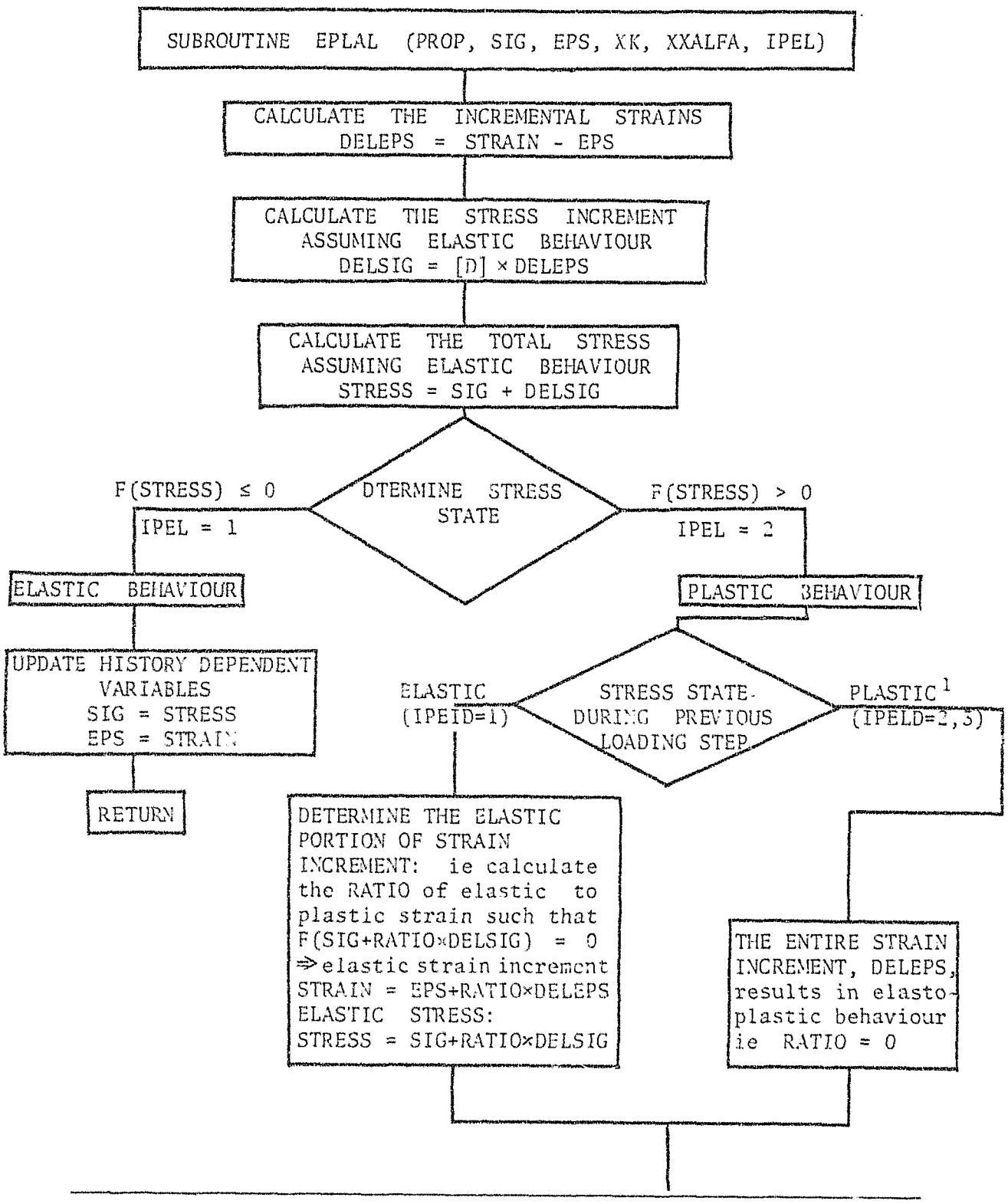

1. Additional checks are executed in the program to ascertain whether the stress state has exceeded the failure surface. These details have been deleted from the flow chart for the purpose of clarity.

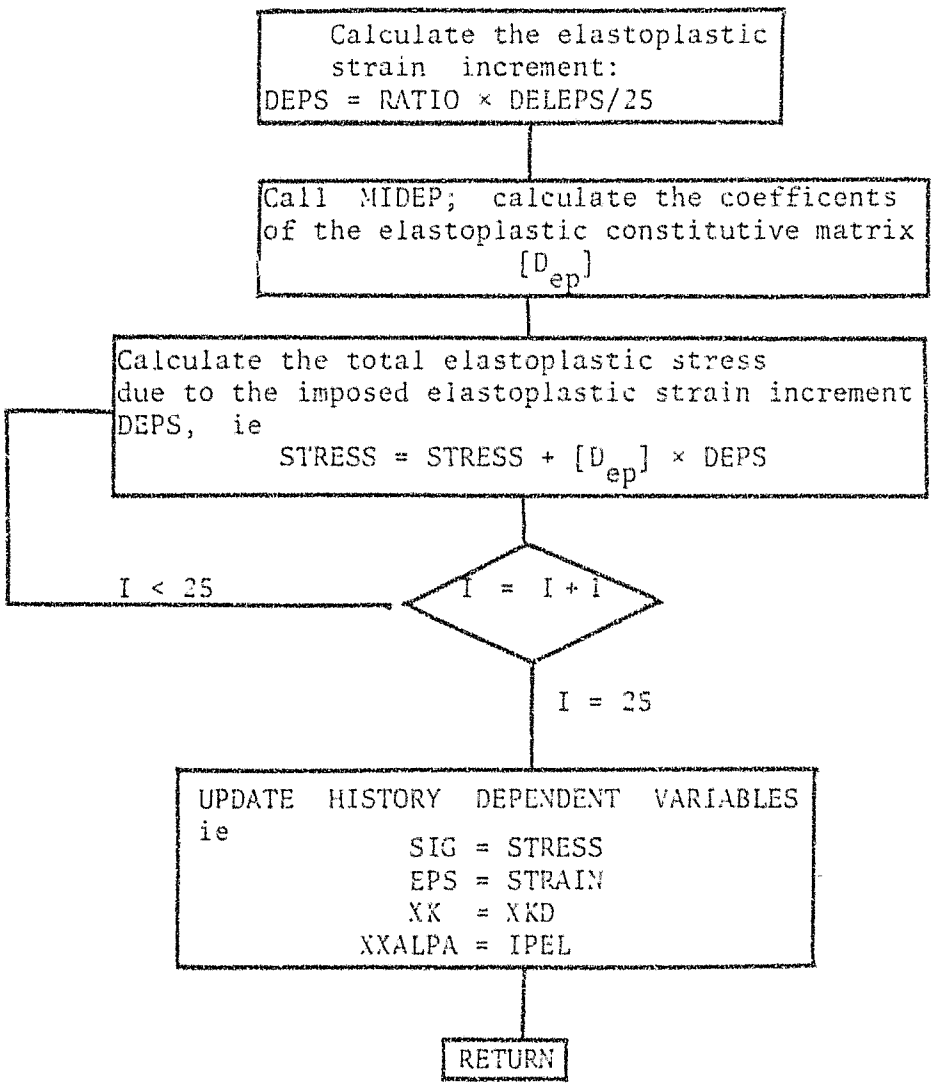

Figure A3.2 - Flow Chart of Subroutine EPLAL

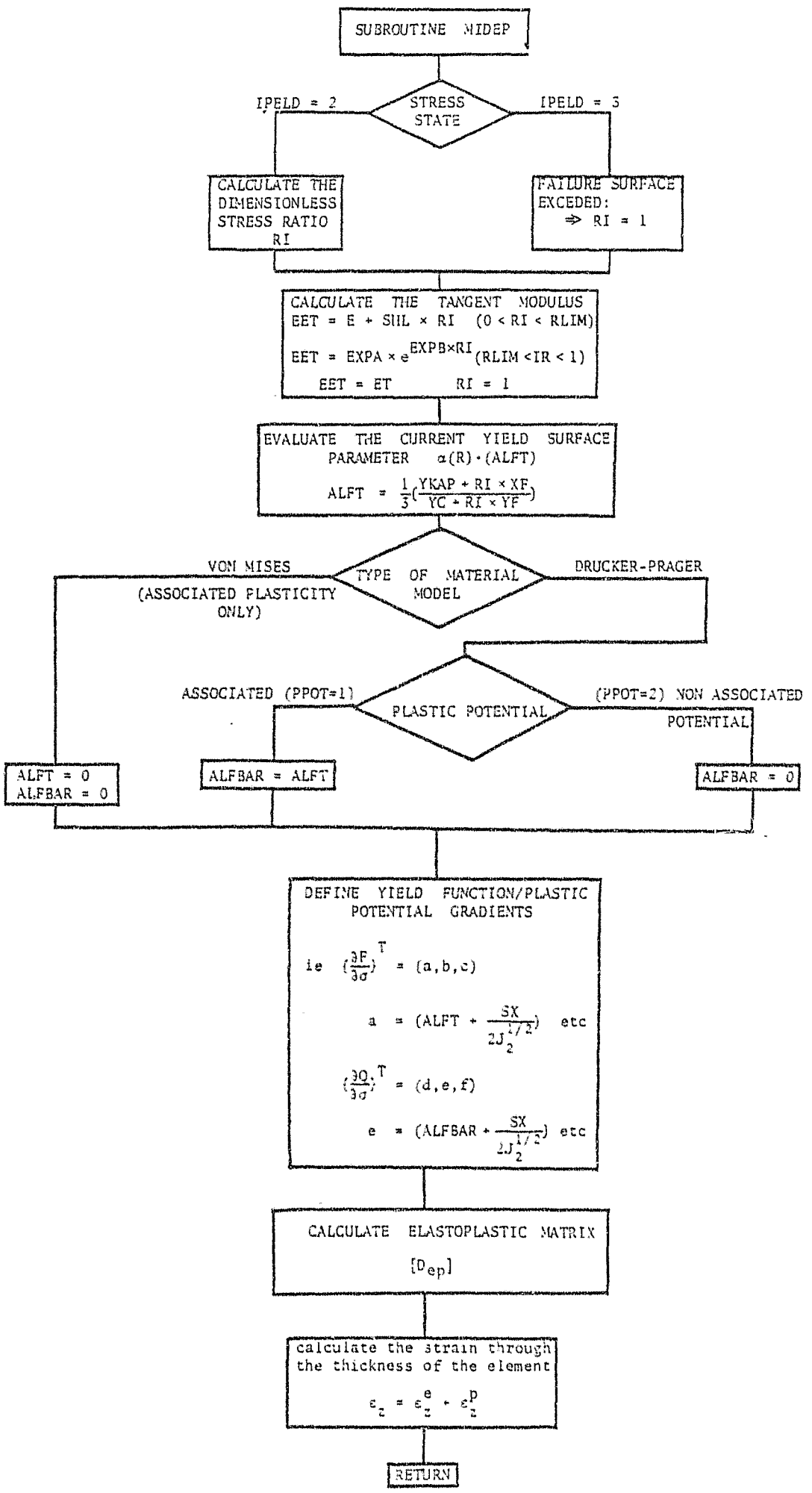

Figure A3.3 - Flow Chart of Subroutine MIPEP

Author Constancon C P
Name of thesis A study of the finite element method, with reference to the Adina finite element package 1983

PUBLISHER:
University of the Witwatersrand, Johannesburg
©2013

LEGAL NOTICES:

Copyright Notice: All materials on the University of the Witwatersrand, Johannesburg Library website are protected by South African copyright law and may not be distributed, transmitted, displayed, or otherwise published in any format, without the prior written permission of the copyright owner.

Disclaimer and Terms of Use: Provided that you maintain all copyright and other notices contained therein, you may download material (one machine readable copy and one print copy per page) for your personal and/or educational non-commercial use only.

The University of the Witwatersrand, Johannesburg, is not responsible for any errors or omissions and excludes any and all liability for any errors in or omissions from the information on the Library website.

A3.4 SUBROUTINE LISTING

```
      SUBROUTINE EL2D14                                                 YCX00010
      IMPLICIT REAL*8 (A-H,O-Z)                                         YCX00020
      COMMON /EL/ IND,ICOUNT,NPAR(20),NUMEG,NEGL,NEGNL,IMASS,IDAMP,ISTATYCX00030
     1 COMMON /DIMEL/ NDOF,KLIN,IEIG,IMASS,N,IDAMPN                     YCX00040
     1 COMMON /MATMOD/ STRESS(4),STRAIN(4),D(4,4),IPT,NEL,IPS           YCX00050
      COMMON /DPR/ ITWO                                                 YCX00060
      COMMON A(1)                                                       YCX00070
      REAL A                                                            YCX00080
      DIMENSION IA(1)                                                   YCX00090
      EQUIVALENCE (NPAR(10),NINT),(A(1),IA(1))                          YCX00100
      IDW=11*ITWO                                                       YCX00110
      NPT=NINT*NINT                                                     YCX00120
      MATP=IA(N107+NEL-1)                                               YCX00130
      NM=N109+(MATP-1)*17*ITWO                                          YCX00140
      IF (IND.NE.0) GO TO 100                                           YCX00150
C-----------------------------------------------------------------------YCX00160
C  INITIALIZE WORKING SPACE ARRAY WA                                    YCX00170
C-----------------------------------------------------------------------YCX00180
      NN=N110 +(NEL-1)*NPT*IDW                                          YCX00190
      CALL EIPLA (A(NN),A(NN),A(NN),NPT,IDW)                            YCX00200
      GO TO 599                                                         YCX00210
C-----------------------------------------------------------------------YCX00220
C  FIND STRESS STRAIN LAW AND STRESSES                                  YCX00230
C-----------------------------------------------------------------------YCX00240
  100 NN=N110+(NEL-1)*NPT*IDW+(IPT-1)*IDW                               YCX00250
      CALL EPLAL (A(NN),A(NN),A(NN+4*ITWO),A                            YCX00260
     1A(NN+10*ITWO))                                                    YCX00270
      CONTINUE                                                          YCX00280
  599 RETURN                                                            YCX00290
      END                                                               YCX00300
      SUBROUTINE EIPLA (WA,IWA,PROP,NPT,IDW)                            YCX00310
      IMPLICIT REAL*8 (A-H,O-Z)                                         YCX00320
      DIMENSION WA(11,1),IWA(IDW,1),PROP(2)                             YCX00330
      COMMON /DPR/ ITWO                                                 YCX00340
C-----------------------------------------------------------------------YCX00350
C  SET INITIAL STRESSES AND STRAINS TO ZERO                             YCX00360
C  SET INITIAL STRESS STATE TO ELASTIC.                                 YCX00370
C-----------------------------------------------------------------------YCX00380
      DO 10 J=1,NPT                                                     YCX00390
      DO 15 I=1,8                                                       YCX00400
      WA(I,J)=0.0                                                       YCX00410
      WA(9,J)=PROP(2)                                                   YCX00420
      WA(10,J)=PROP(10)                                                 YCX00430
      KJ=10*ITWO+1                                                      YCX00440
      IWA(KJ,J)=1                                                       YCX00450
   15 CONTINUE                                                          YCX00460
   10 CONTINUE                                                          YCX00470
      RETURN                                                            YCX00480
      END                                                               YCX00490
                                                                        YCX00500
                                                                        YCX00510
                                                                        YCX00520
                                                                        YCX00530
                                                                        YCX00540
                                                                        YCX00550
```

```
      SUBROUTINE EPLAL (PROP,SIG,EPS,XK,XXALPA,IPEL)                    YCX00560
C                                                                       YCX00570
CCCCC.....................................................................YCX00580
CCCCC.  THIS SUBROUTINE CALCULATES THE STRESSES AND STRESS STRAIN       .YCX00590
CCCCC.  LAW OF AN ISOTROPIC HARDENING MATERIAL ,SUBJECT TO THE          .YCX00600
CCCCC.  DRUCKER-PRAGER YEID SURFACE,IN PLANE STRESS CONDITIONS          .YCX00610
CCCCC.                                                                  .YCX00620
CCCCC.  THE FOLLOWING VARIABLES ARE USED IN THIS SUBROUTINE             .YCX00630
CCCCC.                                                                  .YCX00640
CCCCC.      IST    NUMBER OF STRESS COMPONENTS                          .YCX00650
CCCCC.      ISR    NUMBER OF STRAIN COMPONENTS                          .YCX00660
CCCCC.      SIG    STRESSES AT THE END OF THE PREVIOUS UPDATE           .YCX00670
CCCCC.      EPS     STRAINS AT THE END OF THE PREVIOUS UPDATE           .YCX00680
CCCCC.      RATIO   PART OF STRAIN INCREMENT TAKEN ELASTICALLY          .YCX00690
CCCCC.      DELEPS  INCREMENT IN STRAINS                                .YCX00700
CCCCC.      DELSIG  INCREMENT IN STRESSES                               .YCX00710
CCCCC.                                                                  .YCX00720
CCCCC.      PROP(1)   MODEL TYPE (V.MISES-D.PRAGER)                     .YCX00730
CCCCC.      PROP(2)   PLASTIC POTENTIAL (ASS.-NON ASS.)                 .YCX00740
CCCCC.      PROP(3)   LINEAR STRAIN HARDENING GRADIENT                  .YCX00750
CCCCC.      PROP(4)   LIMMIT R                                          .YCX00760
CCCCC.      PROP(5)   EXPONENTIAL CONSTANT "A"                          .YCX00770
CCCCC.      PROP(6)   EXPONENTIAL CONSTANT "B"                          .YCX00780
CCCCC.      PROP(7)   YOUNGS MODULUS                                    .YCX00790
CCCCC.      PROP(8)   POISSONS RATIO                                    .YCX00800
CCCCC.      PROP(9)   KAPPA -YIELD SURFACE PARAMETER                    .YCX00810
CCCCC.      PROP(10)   ALPA  -YIELD SURFACE PARAMETER                   .YCX00820
CCCCC.      PROP(11)   STRAIN HARDENING MODULUS                         .YCX00830
CCCCC.      PROP(12)   KCUTT-FAILURE SURFACE PARAMETER                  .YCX00850
CCCCC.      PROP(13)   ALCUTT-FAILERE SURFACE PARAMETER                 .YCX00860
CCCCC.      PROP(14)   CY  YIELD SURFACE PARAMETER C                    .YCX00870
CCCCC.      PROP(15)  DIFFERENCE BETWEEN YIELD-FAILURE PARAMETERS       .YCX00880
CCCCC.                  KAPPA                                           .YCX00890
CCCCC.      PROP(16)  DIFFERENCE BETWEEN YIELD-FAILURE PARAMETERS       .YCX00900
CCCCC.                                                                  .YCX00910
CCCCC.                                                                  .YCX00920
CCCCC.      IPEL      =1,MATERIAL ELASTIC                               .YCX00930
CCCCC.                =2,MATERIAL PLASTIC                               .YCX00940
CCCCC.                =3,FAILURE-STIFFNESS REDUCTION,PLASTIC            .YCX00950
CCCCC.                =4,FAILURE-STIFFNESS REDUCTION,PLASTIC            .YCX00960
CCCCC.                                                                  .YCX00970
CCCCC.                                                                  .YCX00980
CCCCC.                                                                  .YCX00990
CCCCC.                                                                  .YCX01000
CCCCC.....................................................................YCX01010
CCCCC                                                                   YCX01020
CCCCC.....................................................................
CCCCC.                                                                  .
CCCCC.    NOTE:CERTAIN STATEMENTS ARE REDUNDANT IN TERMS OF THE         .
CCCCC.         PROGRAMS PRESENT FORM; FURTHER MODIFICATION IS RE-        .
CCCCC.         QIRED TO INCLUDE: PLANE STRAIN                           .
CCCCC.                           AXISYMETRIC                            .
CCCCC.                           TOTAL & UPDATED LAGRANGIAN NON-        .
CCCCC.                           LINEAR FORMULATIONS                    .
```

```
      IMPLICIT REAL*8 (A-H,O-Z)                                          YCX01030
      COMMON /BL/ IND,ICOUNT,NPAR(20),IUNEG,NEGL,NEGNL,IMASS,IDAMP,ISTATYCX01040
     1           ,NDOF,KLIN,IEIG,IMASSM,IDAMPM                          YCX01050
      COMMON /VAR/ NC,NODEX,IUPDT,KSTEP,ITERMAX,IEQREF,ITE,KPRI,IREF,   YCX01060
     1     IEQUIT,IPRI,KPLOTH,KPLOTE                                    YCX01070
      COMMON /VNISES/ A1,B1,C1,D1,B2,BH,CEE,DEPS(4),TEPS(4),            YCX01080
     1           ISR,IST,ALFA,PV,ET,ST,FTB,IPELD,IPPL,RLIM,THM,PPOT     YCX01090
      COMMON /DRUCK/ UTT,YKAP,ALC,YF,XF,YC,DELP(3),YM,SHL,EXPA,EXPB,    YCX01100
     1     ALPBAR,BET                                                   YCX01110
      COMMON /METHOD/ STRESS(4),STRAIN(4),D(4,4),IPT,NEL,IPS            YCX01120
      COMMON /DISDER/ DISD(5)                                           YCX01130
      COMMON /TODIM/ BETA,THIC,DE,IEL,NNDS                              YCX01140
      DIMENSION PROP(1),SIG(1),EPS(1)                                   YCX01150
      DIMENSION DELSIG(4),DELEPS(4),STATE(5)                            YCX01160
      EQUIVALENCE (NPAR(3),INDNL),(NPAR(5),ITYP2D),(NPAR(15),NODEL)     YCX01170
      INTEGER PPOT,THM                                                  YCX01180
      DATA STATE /2H E,2H*P,2HFP,2HFE,2HFF/, NGLAST /1000/              YCX01190
      XKD=XK                                                            YCX01200
      XALFA=XXALFA                                                      YCX01210
      IPELD=IPEL                                                        YCX01220
      STRESS(4)=0.                                                      YCX01230
      DELSIG(4)=0.                                                      YCX01240
      DELEPS(4)=0.                                                      YCX01250
      THM=PROP(1)                                                       YCX01260
      PPOT=PROP(2)                                                      YCX01270
      SHL=PROP(3)                                                       YCX01280
      RLIM=PROP(4)                                                      YCX01290
      EXPA=PROP(5)                                                      YCX01300
      EXPB=PROP(6)                                                      YCX01310
      YM=PROP(7)                                                        YCX01320
      PV=PROP(8)                                                        YCX01330
      YKAP=PROP(9)                                                      YCX01340
      ALFA=PROP(10)                                                     YCX01350
      ET=PROP(11)                                                       YCX01370
      UTT=PROP(12)                                                      YCX01380
      ALC=PROP(13)                                                      YCX01390
      YC=PROP(14)                                                       YCX01400
      XF=PROP(15)                                                       YCX01410
      YF=PROP(16)                                                       YCX01420
      IF (ST.EQ.0.) ST=1.                                               YCX01430
      IF (UTT.EQ.0.) UTT=1000.*XK                                       YCX01440
      IST=3                                                             YCX01450
      ISR=3                                                             YCX01470
      CEE=1.-PV*PV                                                      YCX01500
      B2=(1.-PV)/2                                                      YCX01510
C     ..................                                                YCX01520
C     . PLANE STRESS   .                                                YCX01530
C     ..................                                                YCX01540
      A1=YM/CEE                                                         YCX01550
      B1=A1*PV                                                          YCX01560
      D1=PV/(PV-1.)
```

```
      BM=YM/(1-2.*PV)                                                   YCX01570
      C1=YM/(2.*(1.+PV))                                                YCX01580
C                                                                       YCX01610
CCC   ..........................................                        YCX01620
CCC   . CALCULATE THE INCREMENTAL STRAINS      .                        YCX01630
CCC   ..........................................                        YCX01640
C                                                                       YCX01650
      IF (INDNL.NE.3) GO TO 121                                         YCX01660
      DO 122 I=1,ISR                                                    YCX01670
122   DELEPS(I)=STRAIN(I)                                               YCX01680
      GO TO 130                                                         YCX01690
121   DO 120 I=1,ISR                                                    YCX01700
120   DELEPS(I)=STRAIN(I)-EPS(I)                                        YCX01710
C     ..........................................                        YCX01720
C     . CALCULATE THE INCREMENTAL STRESS       .                        YCX01730
C     . ASSUMING ELASTIC BEHAVIOUR             .                        YCX01740
C     ..........................................                        YCX01750
C                                                                       YCX01760
130   DELSIG(1)=A1*DELEPS(1)+B1*DELEPS(2)                               YCX01770
      DELSIG(2)=B1*DELEPS(1)+A1*DELEPS(2)                               YCX01780
      DELSIG(3)=C1*DELEPS(3)                                            YCX01790
C                                                                       YCX01800
CC    ..........................................                        YCX01810
C     .  WITH THE ASSUMPTION OF ELASTIC BEHAVIOUR,.                     YCX01820
C     .  DETERMINE WHERE THE NEW STATE OF STRESS  .                     YCX01830
C     .  FALLS IN THE STRESS SPACE                .                     YCX01840
C     ..........................................                        YCX01850
C                                                                       YCX01860
510   DM=(DELSIG(1)+DELSIG(2)+DELSIG(4))/3.                             YCX01870
      DX=DELSIG(1)-DM                                                   YCX01880
      DY=DELSIG(2)-DM                                                   YCX01890
      DZ=DELSIG(4)-DM                                                   YCX01900
C                                                                       YCX01910
      SM=(SIG(1)+SIG(2)+SIG(4))/3.                                      YCX01920
      SX=SIG(1)-SM                                                      YCX01930
      SY=SIG(2)-SM                                                      YCX01940
      SZ=SIG(4)-SM                                                      YCX01950
      SS=SIG(3)                                                         YCX01960
C                                                                       YCX01970
      RA=.5*(DX**2+DY**2+DZ**2)+DELSIG(3)**2                            YCX01980
      RB=SX*DX+SY*DY+SZ*DZ+2.*SS*DELSIG(3)                              YCX01990
      RD=.5*((SX**2)+(SY**2)+(SZ**2))+SS**2                             YCX02000
C                                                                       YCX02010
      FTA=XALFA*3.*(DM+SM)+(DSQRT(RD+RA+RB))-XKD                        YCX02020
      IF (FTA) 170,170,300                                              YCX02030
C                                                                       YCX02040
CC    ..........................................                        YCX02050
C     . STATE OF STRESS WITHIN LOADING SURFACE -ELASTIC BEHAVIOUR .     YCX02060
C     ..........................................                        YCX02070
170   IPELD=1                                                           YCX02080
      IF (IPEL.EQ.3) IPELD=4                                            YCX02090
      IF (IPEL.EQ.4) IPELD=4                                            YCX02100
      DO 176 I=1,IST                                                    YCX02130
176   STRESS(I)=SIG(I)+DELSIG(I)                                        YCX02140
      STRAIN(4)=EPS(4)+D1*(DELEPS(1)+DELEPS(2))                         YCX02150
```

```
      GO TO 622                                                                 YCX02160
C                                                                               YCX02170
C     ..........................................................                YCX02180
C     . STATE OF STRESS OUTSIDE LOADING SURFACE -PLASTIC BEHAVIOUR .            YCX02190
C     . DETERMINE THE PORTION OF STRAIN TAKEN ELASTICALLY          .            YCX02200
C     ..........................................................                YCX02210
C                                                                               YCX02220
300   IPELD=2                                                                   YCX02230
      IF (IPEL.EQ.3) IPPL=0                                                     YCX02240
      IF (IPEL.EQ.3) RATIO=0.                                                   YCX02250
      IF (IPEL.EQ.3.AND.RATIO.EQ.0.) GO TO 378                                  YCX02260
      IF (FTB.GT.0.) IPEL=3                                                     YCX02270
      IF (IPEL.EQ.2) RATIO=0.                                                   YCX02280
      IF (IPEL.EQ.2.AND.RATIO.EQ.0.) GO TO 303                                  YCX02290
      IF (IPEL.EQ.3) GO TO 315                                                  YCX02300
      AR=RA-(ALFA**2)*(DM**2)*9                                                 YCX02310
      BR=RB+(6*XKD*ALFA*DM)-(18*ALFA*ALFA*SM*DM)                                YCX02320
      DR=RD+(6*XKD*ALFA*SM)-(XKD*XKD)-(9*ALFA*ALFA*SM*SM)                       YCX02330
      GO TO 316                                                                 YCX02340
315   AR=RA-(ALC**2)*(DM**2)*9                                                  YCX02350
      BR=RB+6*UTT*ALC*DM-18*ALC*ALC*SM*DM                                       YCX02360
      DR=RD+6*UTT*ALC*SM-(UTT**2)-9*(ALC**2)*(SM**2)                            YCX02370
316   R=(BR**2)-4.*AR*DR                                                        YCX02380
      IF (R.LT.0.)GO TO 302                                                     YCX02390
      RZ=(-BR+DSQRT(R))/(2.*AR)                                                 YCX02400
      RW=(-BR-DSQRT(R))/(2.*AR)                                                 YCX02410
      IF (RZ.GE.0.AND.RZ.LE.1.) RATIO=RZ                                        YCX02420
      IF (RW.GE.0.AND.RW.LE.1.) GO TO 301                                       YCX02430
      RATIO=RZ                                                                  YCX02440
      IF (RATIO.LT.0.0) GO TO 302                                               YCX02450
      IF (RATIO.LT.1E-03) RATIO=0.                                              YCX02460
      GO TO  303                                                                YCX02470
301   IF (RZ.LT.0.) GO TO 304                                                   YCX02480
      IF (RZ.LT.RW) RATIO=RZ                                                    YCX02490
      IF (RW.LT.RZ) RATIO=RW                                                    YCX02500
      IF (RATIO.LE.1E-03) RATIO=0.                                              YCX02510
      GO TO 303                                                                 YCX02520
304   RATIO=RW                                                                  YCX02530
      IF (RATIO.LE.1E-03) RATIO=0.                                              YCX02540
      GO TO 303                                                                 YCX02550
302   WRITE(6,2200)                                                             YCX02560
      STOP                                                                      YCX02570
303   IF (IPEL.EQ.3.AND.RATIO.GT.0.) GO TO 317                                  YCX02580
      IF (IPEL.EQ.3.AND.RATIO.EQ.0.) GO TO 378                                  YCX02590
      DO 320 I=1,IST                                                            YCX02600
320   STRESS(I)=SIG(I)+RATIO*DELSIG(I)                                          YCX02610
      STRAIN(4)=EPS(4)+RATIO*D1*(DELEPS(1)+DELEPS(2))                           YCX02620
      GO TO 378                                                                 YCX02630
C     ..........................                                                YCX02640
C     . DETERMINE THE INCREMENT INTERVAL .                                      YCX02650
C     ..........................                                                YCX02660
317   INTER=25                                                                  YCX02670
      IPELD=2                                                                   YCX02680
      DO 312 I=1,IST                                                            YCX02690
312   STRESS(I)=SIG(I)                                                          YCX02700
```

```
      STRAIN(4)=EPS(4)                                                  YCX02710
      XM=RATIO/DFLOAT(INTER)                                            YCX02720
      GO TO 318                                                         YCX02730
378   INTER=25                                                          YCX02740
      IF (IPEL.EQ.3) IPELD=3                                            YCX02750
      IF (IPELD.NE.3) GO TO 313                                         YCX02760
      IF (RATIO.NE.0.) GO TO 313                                        YCX02770
      DO 314 I=1,IST                                                    YCX02780
314   STRESS(I)=SIG(I)                                                  YCX02790
      STRAIN(4)=EPS(4)                                                  YCX02800
313   XM=(1.-RATIO)/DFLOAT(INTER)                                       YCX02810
318   DO 380 I=1,ISR                                                    YCX02820
380   DEPS(I)=XM*DELEPS(I)                                              YCX02830
C                                                                       YCX02840
C     ***************************************                           YCX02850
C     * CALCULATION OF ELASTO-PLATIC STRESSES *                         YCX02860
C     ***************************************                           YCX02870
C                                                                       YCX02880
      DO 500 IN=1,INTER                                                 YCX02890
      IF(IN.GT.1) GO TO 419                                             YCX02900
      DELP(1)=A1*DEPS(1)+B1*DEPS(2)                                     YCX02910
      DELP(2)=B1*DEPS(1)+A1*DEPS(2)                                     YCX02920
      DELP(3)=C1*DEPS(3)                                                YCX02930
419   CALL MEDIP                                                        YCX02940
      DO 420 I=1,IST                                                    YCX02950
      DELP(I)=0.                                                        YCX02960
      DO 420 J=1,ISR                                                    YCX02970
      STRESS(I)=STRESS(I)+D(I,J)*DEPS(J)                                YCX02980
420   DELP(I)=DELP(I)+D(I,J)*DEPS(J)                                    YCX02990
      SM=(STRESS(1)+STRESS(2)+STRESS(4))/3.                             YCX03000
      SX=STRESS(1)-SM                                                   YCX03010
      SY=STRESS(2)-SM                                                   YCX03020
      SZ=STRESS(4)-SM                                                   YCX03030
C                                                                       YCX03040
500   CONTINUE                                                          YCX03050
      FTB=3.*ALC*SM+(DSQRT(.5*(SX**2+SY**2+SZ**2)+STRESS(3)**2))        YCX03060
      FTB=FTB - UTT                                                     YCX03070
      IF (IPEL.EQ.3.AND.IPELD.EQ.3) GO TO 502                           YCX03080
      IF (IPEL.EQ.3.AND.RATIO.GT.0.) GO TO 378                          YCX03090
      IF (FTB.LE.0.) GO TO 502                                          YCX03100
      IPPL=1                                                            YCX03110
      IPELD=3                                                           YCX03120
      DO 501 I=1,IST                                                    YCX03130
501   DELSIG(I)=STRESS(I)-SIG(I)                                        YCX03140
      GO TO 510                                                         YCX03150
502   IPEL=IPELD                                                        YCX03160
      IF (INDNL.NE.3) GO TO 600                                         YCX03170
      OMEGA=DISD(3)-DISD(4)                                             YCX03180
      STRESS(1)=STRESS(1)+OMEGA*SIG(3)                                  YCX03190
      STRESS(2)=STRESS(2)-OMEGA*SIG(3)                                  YCX03200
      STRESS(3)=STRESS(3)+.5*OMEGA*(SIG(2)-SIG(1))                      YCX03210
C                                                                       YCX03220
C     ********************                                            YCX03230
C     * UPDATE KAPPA(XK) *                                            YCX03240
C     ********************                                            YCX03250
```

```
600   IF (IPELD.EQ.3) GO TO 622                                          YCX03260
      IF (IPEL.EQ.3) GO TO 622                                           YCX03270
      IF (TMM.EQ.1) GO TO 601                                            YCX03280
      RD=.5*(SX**2+SY**2+SZ**2)+(STRESS(3)**2)                           YCX03290
      RT=(YF*(YKAP-DSQRT(RD))+XF*(YC-SM))                                YCX03300
      RTT=(RT**2)-4*XF*YF*(YKAP*(YC-SM)-YC*DSQRT(RD))                    YCX03310
      IF (RTT.LT.0.) RTT=0.                                              YCX03320
      IF (RTT.EQ.0.) GO TO 622                                           YCX03330
      RT=(DSQRT(RTT)-RT)/(2*XF*YF)                                       YCX03340
      IF (RT.GT.1.) GO TO 622                                            YCX03350
      XKDD=YKAP+RT*XF                                                    YCX03360
      IF (XKDD.LT.XK) GO TO 622                                          YCX03370
      XKD=XKDD                                                           YCX03380
      XALFA=(XKD/(YC+RT*YF))/3.                                          YCX03390
      GO TO 622                                                          YCX03400
601   XALFA=0.                                                           YCX03410
      XKDD=FTB+UTT                                                       YCX03420
      IF (XKDD.LT.XK) GO TO 622                                          YCX03430
      XKD=XKDD                                                           YCX03440
C                                                                        YCX03450
CC                                                                       YCX03460
CCC                                                                      YCX03470
C     ..................................                                 YCX03480
C     . UPDATING STRESSES,STRAINS ,KAPPA,IPEL .                          YCX03490
C     ..................................                                 YCX03500
C                                                                        YCX03510
622   IF (IUPDT.NE.0) GO TO 621                                          YCX03520
      XK=XKD                                                             YCX03530
      XXALFA=XALFA                                                       YCX03540
      IPEL=IPELD                                                         YCX03550
      DO 610 I=1,IST                                                     YCX03560
      SIG(I)=STRESS(I)                                                   YCX03570
610   EPS(I)=STRAIN(I)                                                   YCX03580
      EPS(4)=STRAIN(4)                                                   YCX03590
621   IF (KPRI.EQ.0) GO TO 700                                           YCX03600
      IF (ICOUNT.EQ.3) RETURN                                            YCX03610
C                                                                        YCX03620
C     ..........................................                         YCX03630
C     . FORM THE MATERIAL LAW                  .                         YCX03640
C     . IN DIVERGENCE REFORMATION (IEQREF=1),  .                         YCX03650
C     . ASSUME ELASTIC BEHAVIOUR               .                         YCX03660
C     ..........................................                         YCX03670
C                                                                        YCX03680
      IF (IEQREF.EQ.1) GO TO 623                                         YCX03690
      IF (IPELD.EQ.2) GO TO 650                                          YCX03700
      IF (IPELD.EQ.3) GO TO 650                                          YCX03710
623   DO 625 I=1,4                                                      YCX03720
      DO 625 J=1,4                                                       YCX03730
625   D(I,J)=0.                                                          YCX03740
      D(1,1)=A1                                                          YCX03750
      D(2,1)=B1                                                          YCX03760
      D(1,2)=B1                                                          YCX03770
      D(2,2)=A1                                                          YCX03780
      D(3,3)=C1                                                          YCX03790
      D(4,1)=0.                                                          YCX03800
```

```
      D(4,2)=0.                                                          YCX03810
      D(4,3)=0.                                                          YCX03820
      D(4,4)=0.                                                          YCX03830
      IF (IPELD.EQ.1) RETURN                                             YCX03840
      RETURN                                                             YCX03880
650   CALL MEDIP                                                         YCX03890
      RETURN                                                             YCX03900
C                                                                        YCX03910
C     ..........................                                         YCX03920
C     . PRINTING OF STRESSES   .                                         YCX03930
C     ..........................                                         YCX03940
C                                                                        YCX03950
700   DM=(STRESS(1)+STRESS(2)+STRESS(4))/3.                              YCX03960
      DX=STRESS(1)-DM                                                    YCX03970
      DY=STRESS(2)-DM                                                    YCX03980
      DZ=STRESS(4)-DM                                                    YCX03990
      DS=STRESS(3)                                                       YCX04000
      FTA=.5*(DX**2+DY**2+DZ**2)+DS**2                                   YCX04010
      FT=3*ALPA*DM+DSQRT(FTA)-YKAP                                       YCX04020
      IF (INDNL.NE.2) GO TO 800                                          YCX04030
      CALL CAUCHY                                                        YCX04040
800   IF (IPRI.NE.0) RETURN                                              YCX04050
      IF (INDNL.LE.2 .OR. ITYP2D.LT.2) GO TO 801                         YCX04060
      XBAR=THIC*DEXP(STRAIN(4))                                          YCX04070
801   IF (NG.NE.NGLAST) GO TO 802                                        YCX04080
      IF(NEL.GT.NELAST) GO TO 806                                        YCX04090
      IF (IPT-1) 809,808,809                                             YCX04100
802   NGLAST=NG                                                          YCX04110
808   IF (INDNL.EQ.3) GO TO 804                                          YCX04120
      WRITE(6,2002)                                                      YCX04130
      GO TO 806                                                          YCX04140
804   WRITE(6,2001)                                                      YCX04150
806   NELAST=NEL                                                         YCX04160
      WRITE(6,2004) NEL                                                  YCX04170
809   IF (IPELD.NE.3) GO TO 810                                          YCX04180
      WRITE(6,2221)                                                      YCX04190
810   CALL MAXMIN (STRESS,SX,SY,SM)                                      YCX04200
      IF (INDNL.EQ.3) GO TO 814                                          YCX04210
813   WRITE(6,2005) IPT,STATE(IPELD),(STRESS(I),I=1,IST),SX,SY,SM,FT     YCX04220
      GO TO 821                                                          YCX04230
814   WRITE(6,2007) IPT,STATE(IPELD),(STRESS(I),I=1,3),SX,SY,SM,FT,XBAR  YCX04240
821   WRITE(6,2006) (EPS(I),I=1,3),EPS(4)                                YCX04250
      RETURN                                                             YCX04260
2221  FORMAT(/T10,'THE MATERIAL HAS FAILED IN THIS REGION,STIFFNESS REDUYCX04270
     1CTION HAS OCCURED'//)                                              YCX04280
2001  FORMAT (90H ELEMENT  STRESS      STRESS-YY      STRESS-ZZ       STRESYCX04290
     1S-YZ       MAX STRESS     MIN STRESS,17X,10HEQUIVALENT/           YCX04300
     2         16H NUM/IPT   STATE,78X,5HANGLE,10X,6HSTRESS,5X,          YCX04310
     3         9HTHICKNESS/)                                            YCX04320
2002  FORMAT (90H ELEMENT STRESS      STRESS-YY      STRESS-ZZ       STRESYCX04330
     1S-YZ       MAX STRESS     MIN STRESS,17X,10HYELD FUNCT/           YCX04340
     2       16H NUM/IPT   STATE,78X,5HANGLE,10X,6HVALUE /)             YCX04350
2004  FORMAT(1I4/)                                                       YCX04360
2005  FORMAT(5X,I2,1X,A2,6HLASTIC,1X,3E14.6,3X,2E14.6,3X,F6.2,3X,E14.6)  YCX04370
2006  FORMAT(T10,'STRAINS',T20,'ST-YY  ',E14.7,'ST-ZZ  ',E14.7,'ST-YZ ',YCX04380
```

```
     1E14.7,'ST-XX ',E14.7/)                                                    YCX04390
2007  FORMAT(5X,I2,1X,A2,7HLASTIC ,3E14.6,3X,2E14.6,3X,F6.2,3X,2E14.6)          YCX04400
2200  FORMAT(T10,'INCORRECT VALUE FOR RATIO,STOP',3E14.7)                       YCX04410
      END                                                                       YCX04420
C                                                                               YCX04430
      SUBROUTINE MEDIP                                                          YCX04440
      IMPLICIT REAL*8 (A-H,O-Z)                                                 YCX04450
      COMMON /EL/ IND,ICOUNT,NPAR(20),NUMEG,NEGL,NEGNL,IMASS,IDAMP,ISTATYCX04460
     1,NDOF,KLIN,IEIG,IMASSM,IDAMPM                                             YCX04470
      COMMON /VMISES/ A1,B1,C1,D1,B2,BM,CEE,DEPS(4),EPS(4),                     YCX04480
     1          ISR,IST,ALPA,DV,ET,ST,FTB,IPELD,IPPL,RLIM,TMM,PPOT              YCX04490
      COMMON /DRUUK/ UTT,YKAP,ALC,YP,XP,YC,DELP(3),YM,SHL,EXPA,EXPB,            YCX04500
     1          ALFBAR,BET                                                      YCX04510
      COMMON/MATMOD/ STRESS(4),STRAIN(4),D(4,4),IPT,NEL,IPS                     YCX04520
      EQUIVALENCE (NPAR(5),ITYP2D)                                              YCX04530
      INTEGER PPOT,TMM                                                          YCX04540
      SM=(STRESS(1)+STRESS(2)+STRESS(4))/3.                                     YCX04550
      SX=STRESS(1)-SM                                                           YCX04560
      SY=STRESS(2)-SM                                                           YCX04570
      SZ=-SM                                                                    YCX04580
      SS=STRESS(3)                                                              YCX04590
      SM1=SM*3./2.                                                              YCX04600
      SM2=(((STRESS(1)-STRESS(2))/2.)**2)+SS**2                                 YCX04610
      PRST1=SM1+DSQRT(SM2)                                                      YCX04620
      PRST2=SM1-DSQRT(SM2)                                                      YCX04630
      PRS1=PRST1-SM                                                             YCX04640
      PRS2=PRST2-SM                                                             YCX04650
      DELM=(DELP(1)+DELP(2))/2.                                                 YCX04660
      DELM1=(((DELP(1)-DELP(2))/2.)**2)+DELP(3)**2                              YCX04670
      DELT1=DELM+DSQRT(DELM1)                                                   YCX04680
      DELT2=DELM-DSQRT(DELM1)                                                   YCX04690
      BET=.5*(SX**2+SY**2+SZ**2)+SS**2                                          YCX04700
      BET=2*DSQRT(BET)                                                          YCX04710
      IF (TMM.EQ.1) ALFT=0.                                                     YCX04720
      IF (TMM.EQ.1) ALC=0.                                                      YCX04730
C                                                                               YCX04740
CC    ***************************************                                   YCX04750
C     * FORM THE DP MATRIX-PLANE STRESS     *                                   YCX04760
CC    ***************************************                                   YCX04770
C                                                                               YCX04780
      IF (IPELD.EQ.3) ALFT=ALC                                                  YCX04790
      IF (IPELD.EQ.3) GO TO 1                                                   YCX04800
      IF (TMM.EQ.1) GO TO 2                                                     YCX04810
      RI=(YF*(YKAP-.5*BET)+XF*(YC-SM))                                          YCX04820
      RII=(RI**2)-4*XF*YF*(YKAP*(YC-SM)-YC*BET*0.5)                             YCX04830
      IF (RII.LT.0.) GO TO 3                                                    YCX04840
      RI=(DSQRT(RII)-RI)/(2*YF*XF)                                              YCX04850
      GO TO 3                                                                   YCX04860
2     RI=(.5*BET-YKAP)/XF                                                       YCX04870
      GO TO 4                                                                   YCX04880
3     IF (RII.LE.0.) RI=1E-03                                                   YCX04890
      ALFT=(YKAP+RI*XF)/((YC+RI*YF)*3.)                                         YCX04900
4     IF(RI.LT.0.) RI=1E-03                                                     YCX04910
1     DG=(DELT1*(ALFT+(PRS1/BET)))+(DELT2*(ALFT+(PRS2/BET)))                    YCX04920
```

```
      G=BET/(3*(PRS1*DELT1+PRS2*DELT2))                                    YCX04930
      IF(PPOT.EQ.2) GO TO   5                                              YCX04940
      G=G*2*((ALFT+(PRS1/BET))*PRST1+(ALFT+(PRS2/BET))*PRST2)              YCX04950
      G=G/BET                                                              YCX04960
C                                                                          YCX04970
5     IF (IPELD.EQ.3) EET=ET                                               YCX04980
      IF (IPELD.EQ.3) GO TO 6                                              YCX04990
      IF (RI.LE.RLIM) EET=YM+SHL*RI                                        YCX05000
      IF (RI.LE.RLIM) GO TO  6                                             YCX05010
      EET=EXPA*((2.71828183)**(EXPB*RI))                                   YCX05020
6     A2=YM*EET/(YM-EET)
      G=G*DG
      IF(PPOT.EQ.1) ALFBAR=ALFT
      IF (PPOT.EQ.2) ALFBAR=0.
      ARA=ALFT+(SX/BET)                                                    YCX05040
      ARB=ALFT+(SY/BET)                                                    YCX05050
      ARC=2*SS/BET                                                         YCX05060
      ARA1=ALFBAR+(SX/BET)                                                 YCX05070
      ARB1=ALFBAR+(SY/BET)                                                 YCX05080
      BAT=A2*G+A1*((ARA+PV*ARB)*ARA1+(PV*ARA+ARB)*ARB1+B2*(ARC**2))        YCX05140
      RLAMBD=BAT
      BAT=A1*A1/BAT                                                        YCX05150
C                                                                          YCX05160
      WP=SX*DEPS(1)+SY*DEPS(2)+SS*DEPS(3)                                  YCX05170
      IF (WP.LT.0.) BAT=0.                                                 YCX05180
C                                                                          YCX05190
      D(1,1)=A1-(BAT*((ARA1+PV*ARB1)*ARA+(ARA1+PV*ARB1)*PV*ARB))           YCX05200
      D(1,2)=B1-(BAT*(PV*(ARA1+PV*ARB1)*ARA+(ARA1+PV*ARB1)*ARB))           YCX05210
      D(1,3)=-BAT*ARC*(ARA1+PV*ARB1)*B2                                    YCX05220
      D(1,4)=0.                                                            YCX05230
      D(2,1)=B1-(BAT*(ARA*(PV*ARA1+ARB1)+PV*ARB*(PV*ARA1+ARB1)))           YCX05240
      D(2,2)=A1-(BAT*(PV*ARA*(PV*ARA1+ARB1)+ARB*(PV*ARA1+ARB1)))           YCX05250
      D(2,3)=-BAT*ARC*(ARB1+PV*ARA1)*B2                                    YCX05260
      D(2,4)=0.                                                            YCX05270
      D(3,1)=-BAT*ARC*B2*(ARA+PV*ARB)                                      YCX05280
      D(3,2)=-BAT*ARC*B2*(PV*ARA+ARB)                                      YCX05290
      D(3,3)=C1-BAT*(B2*B2*ARC*ARC)                                        YCX05300
      D(3,4)=0.                                                            YCX05310
      D(4,1)=0.                                                            YCX05320
      D(4,2)=0.                                                            YCX05330
      D(4,3)=0.                                                            YCX05340
      D(4,4)=0.                                                            YCX05350
C     ..................................................                   YCX05360
C     . REDUCE THE STIFFNESS IF THE ELEMENT HAS FAILED .                   YCX05370
C     ..................................................                   YCX05380
8     DO 10 I=1,4                                                          YCX05430
      DO 10 J=1,4                                                          YCX05440
10    IF ((DABS(D(I,J))).LT.1E-13) D(I,J)=0.                               YCX05450
      IF (WP.LE.0.) GO TO 11                                               YCX05460
      IF(PPOT.EQ.1) GO TO 12                                               YCX05470
      STRAIN(4)=STRAIN(4)-(DEPS(1)+DEPS(2))                                YCX05480
      STRAIN(4)=STRAIN(4)+((DELT1+DELT2)/BM)                               YCX05490
      RETURN                                                               YCX05500
12    RLMD=((ARA+ARB*PV)*DEPS(1)+(ARA*PV+ARB)*DEPS(2))*A1+ARC*C1*DEPS(3)
      RLAMBD=RLMD/RLAMBD
```

```
      SPL4=RLAMBD*(ALFT+(SZ/BET))                                        YCX05520
      STRAIN(4)=STRAIN(4)+SPL4*(DEPS(1)+DEPS(2))*D1                      YCX05530
      RETURN                                                             YCX05540
11    STRAIN(4)=STRAIN(4)+D1*(DEPS(1)+DEPS(2))                           YCX05550
      RETURN                                                             YCX05560
      END                                                                YCX05570
```

APPENDIX 4

PROPERTIES RELATING TO THE SHEAVE

A4.1 BEAM ELEMENT DIMENSIONS EMPLOYED IN THE PRELIMINARY ANALYSIS OF THE SHEAVE (Chapter 3)

The dimensions selected for representing the rim and spoke sections are illustrated in Fig A4.1. Owing to the naturally rectangular properties of the spoke, the dimensions represent the actual section. However the dimensions selected for the machined rim section (see Section A4.3) are based on representing the depth and second moment of area of the actual section. This approach was chosen since the significant stresses are induced by bending effects. The second moment of area and cross-sectional area of the above mentioned section is tabulated in Table A4.1.

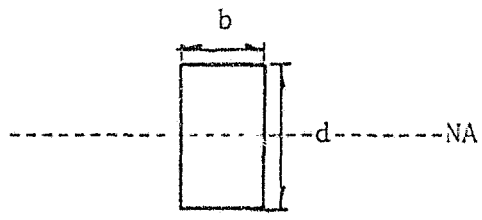

Figure 4.1 - Dimensions of the beam elements

TABLE A4.1 - DIMENSIONS OF THE BEAM ELEMENTS (RIM AND SPOKE)

	b	d	$I_{NA}(mm^3)$
Spoke	31	68	$812,2 \times 10^3$
Rim	37	48	340×10^3

A4.2 DIMENSIONS OF THE UNMACHINED SHEAVE

The dimensions of the unmachined sheave as used in the previous experiment conducted in 1981 are presented in Fig A4.2

A4.3 DIMENSIONS OF THE MACHINED SHEAVE

The dimensions of the machined sheave as employed in the present experiment are illustrated in Fig A4.3.

A4.4 CALCULATION OF THE SECOND MOMENT OF AREA OF THE RIM SECTION

The second moment of area, centroid and cross-sectional area were approximated by using the dimensions measured from the actual section. Owing to geometrical imperfections of the rim section introduced during the casting process, the internal and external radii of the section could not be measured accurately. This necessitated the simplification illustrated in Fig A4.4. Hence the calculation of the geometric properties was based on this section, which was divided into seven elements. These calculations are presented in Tables A4.2a and A4.2b, below Fig A4.4.

A4.5 GEOMETRIC PROPERTIES OF THE RIM SECTION EMPLOYED IN THE FINITE ELEMENT SIMULATION

As discussed in Chapter 5, the rim section was divided into eight elements, as illustrated in Fig A4.5. The dimensions of each element were selected so that the overall section would approximate the properties calculated in Section A4.4. These dimensions are illustrated in Fig A4.5. The calculation of the second moment of

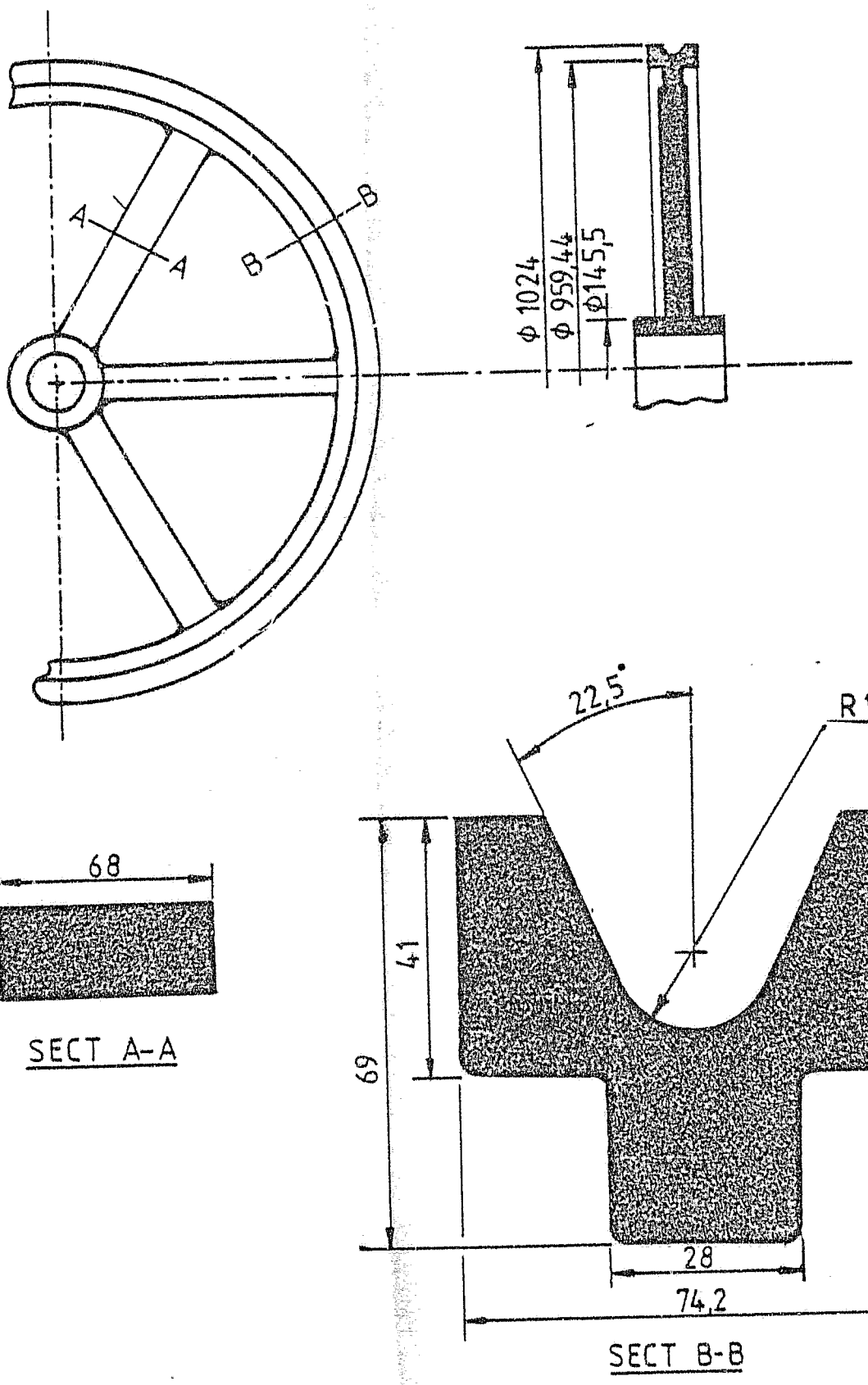

Figure A4.2 - Dimensions of the Unmachined Sheave

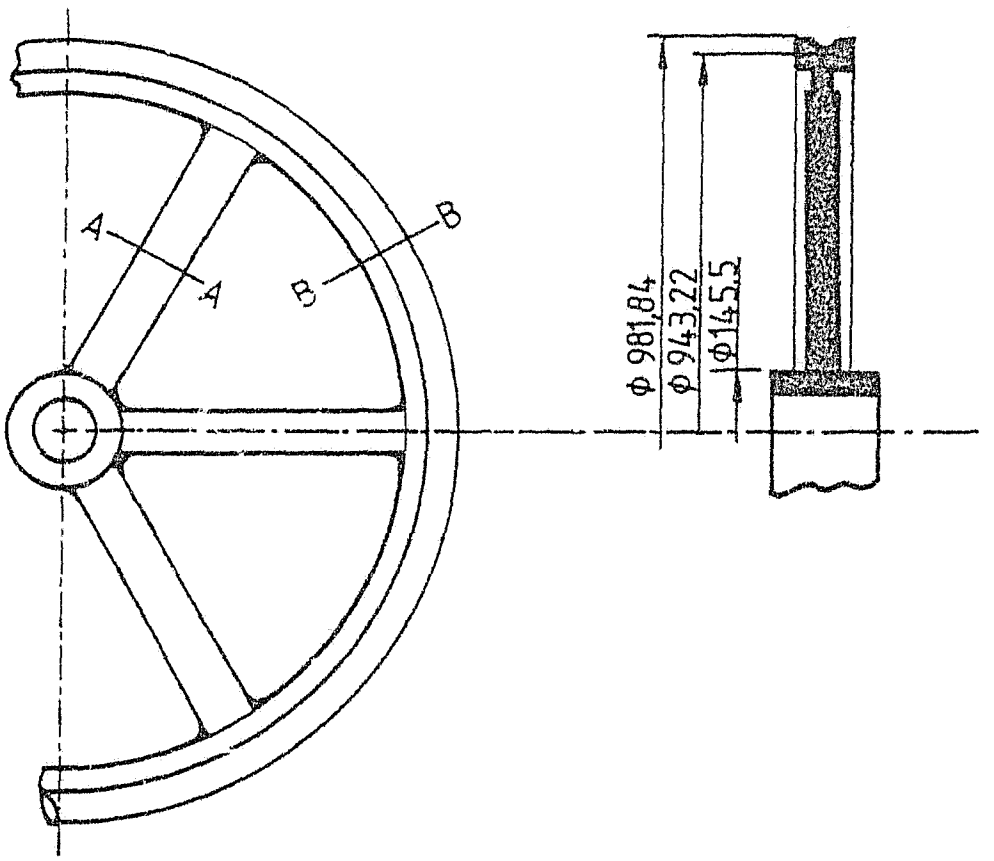

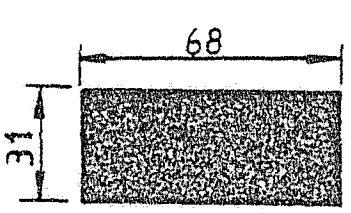

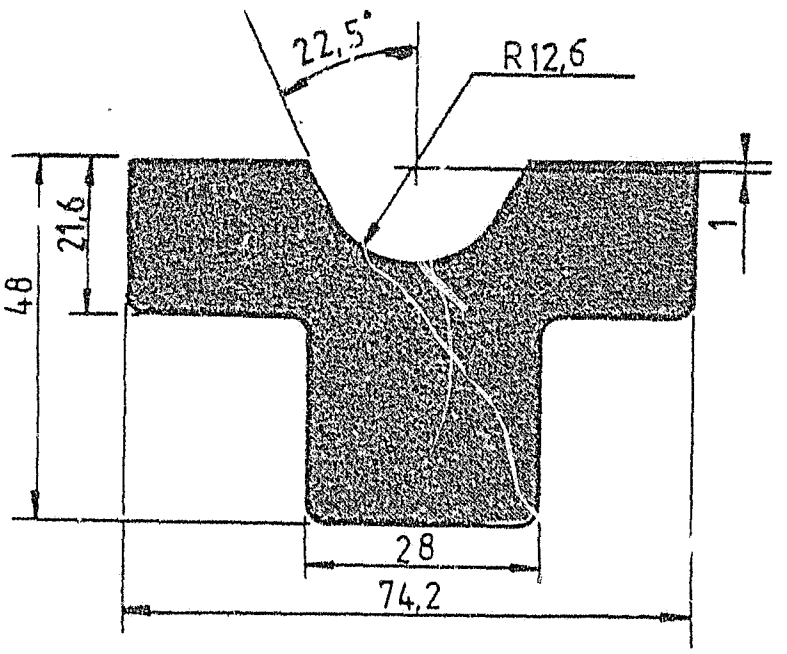

Figure A4.3 - Dimensions of the Machined Sheave

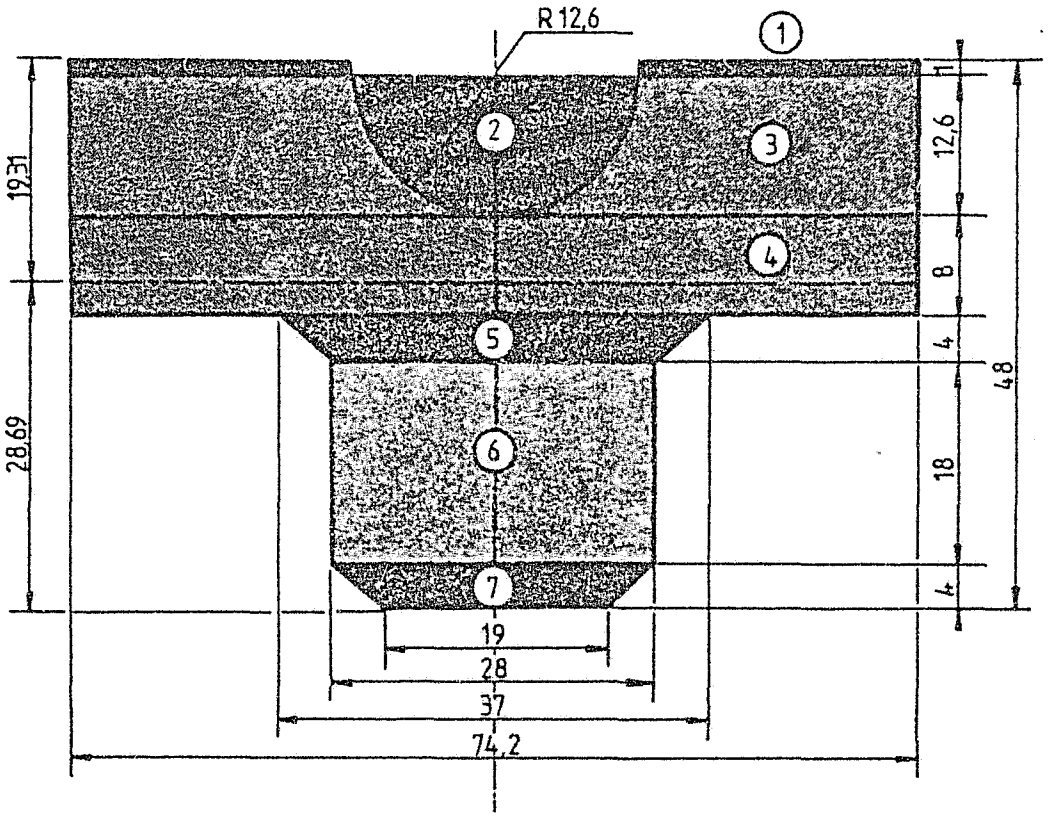

Figure A4.4 - Idealised Cross Section of the Rim

TABLE A4.2a - CALCULATION OF THE CENTROID OF THE SECTION

Element	A_e (mm^2)	$\bar{y}_e$ (mm)	$A\bar{y}_e$ ($\times 10^3$)
1	48,00	47,50	2,280
2	-249,37	41,75	-10,411
3	934,92	40,71	38,051
4	584,80	32,42	18,959
5	130,00	24,49	3,184
6	504,00	13,40	6,753
7	105,60	2,32	0,245
	2 057,45		59,060

$$\bar{y} = \frac{\Sigma A_e \bar{y}_e}{\Sigma A_e} = 28,69 \text{ mm}$$

TABLE A4.2b - CALCULATION OF THE MOMENT OF INERTIA

Element	$\bar{I}_e$ ($\times 10^3 mm^4$)	d(mm)	I_{NA} ($\times 10^3 mm^4$)
1	2 10⁻	18,801	16,968
2	-2,767	13,051	-45,241
3	12,368	12,011	147,243
4	3,118	3,721	11,215
5	0,172	- 4,208	2,473
6	13,608	-15,298	131,558
7	0,168	-26,376	73,633
			337,851

$$\bar{I}_{NA} \simeq 337,851 \times 10^3 mm^4$$

area, cross-sectional area and centroid area presented in Table A4.3, below Fig A4.5. It is evident that the second moment of area, centroid and cross-sectional area, compare well with those of the idealised section (Fig A4.5); the discrepancies are - 0,79%, 0,80% and 3,2% respectively. The larter discrepancy of modelling the cross-sectional area is not considered significant since the major effects are due to bending.

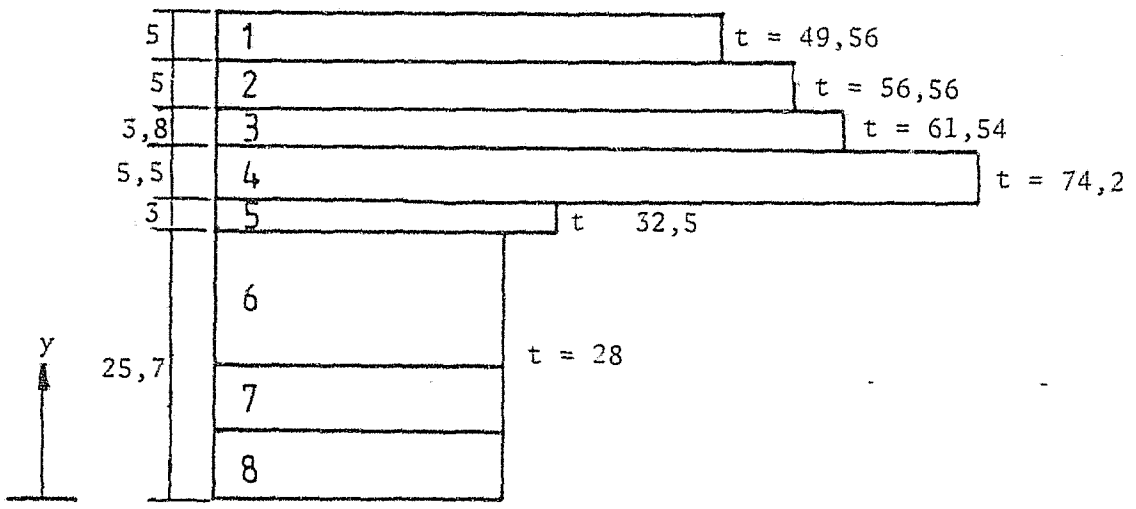

Figure A4.5 - Finite Element Simulation of the Rim Section

TABLE 4.3 - CENTROID, MOMENT OF INERTIA OF SIMULATED SECTION (FEM)

Element	A	$\bar{y}$	$A\bar{y}$	$\bar{I}$	d	I_{NA}
1	247,80	45,50	11 274,90	516,25	17,50	76 405,00
2	282,80	40,50	12 160,40	589,16	11,54	37 708,50
3	233,85	36,10	8 442,05	281,40	12,50	42 552,08
4	408,10	31,45	12 834,74	1 028,70	3,45	5 886,16
5	97,50	27,20	2 652,0	73,12	- 0,80	135,52
6,7,8	719,60	12,85	9 246,8	39 607,30	-15,15	204 771,70
	1 989,65		56 610,93			340 531,43

$\bar{y}$ = 28,452 7 mm $\qquad$ $\bar{I}_{NA}$ = 340 531,43 mm^4

A4.6 METHOD OF CONVERTING THE FINITE ELEMENT RESULTS

As discussed in Chapter 5, the strains predicted by the finite element coordinate analysis are output in terms of the global coordinate axes. The Mohr circle of strain was employed to convert these values to their local coordinate axes for direct comparison with the experimental results.

Fig A4.6 indicates the position of the gauges relative to the integration points and their rotation from the global y-axis. Formula A4.1 was employed to convert the ε_y, ε_z, γ_{yz} strains into into a reading tangential to the surface of the sheave

$$\varepsilon = \frac{\varepsilon_y+\varepsilon_z}{2} + \frac{\varepsilon_y-\varepsilon_z}{2}\cos 2\theta + \frac{\gamma_{yz}}{2}\sin 2\theta \quad \text{(gauges 1-15)} \qquad \text{(A4.1)}$$

$$\varepsilon = \frac{\varepsilon_y+\varepsilon_z}{2} + \frac{\varepsilon_y-\varepsilon_z}{2}(\cos 2(\theta+90) + \frac{\gamma_{yz}}{2}\sin 2(\theta+90) \quad \text{(gauges 20-23)}$$

In some cases the gauge was located between two elements and the reading was taken as the average of the strains of the relevant integration points. Table A4.4 tabulates the relationship between the gauges and the integration points employed in the calculation of the finite element values.

Tables A4.5a and A4.5b tabulate the converted readings from the above mentioned integration points for associated and non associated plastic simulations. These results formed the basis of the values used in Chapter 5.

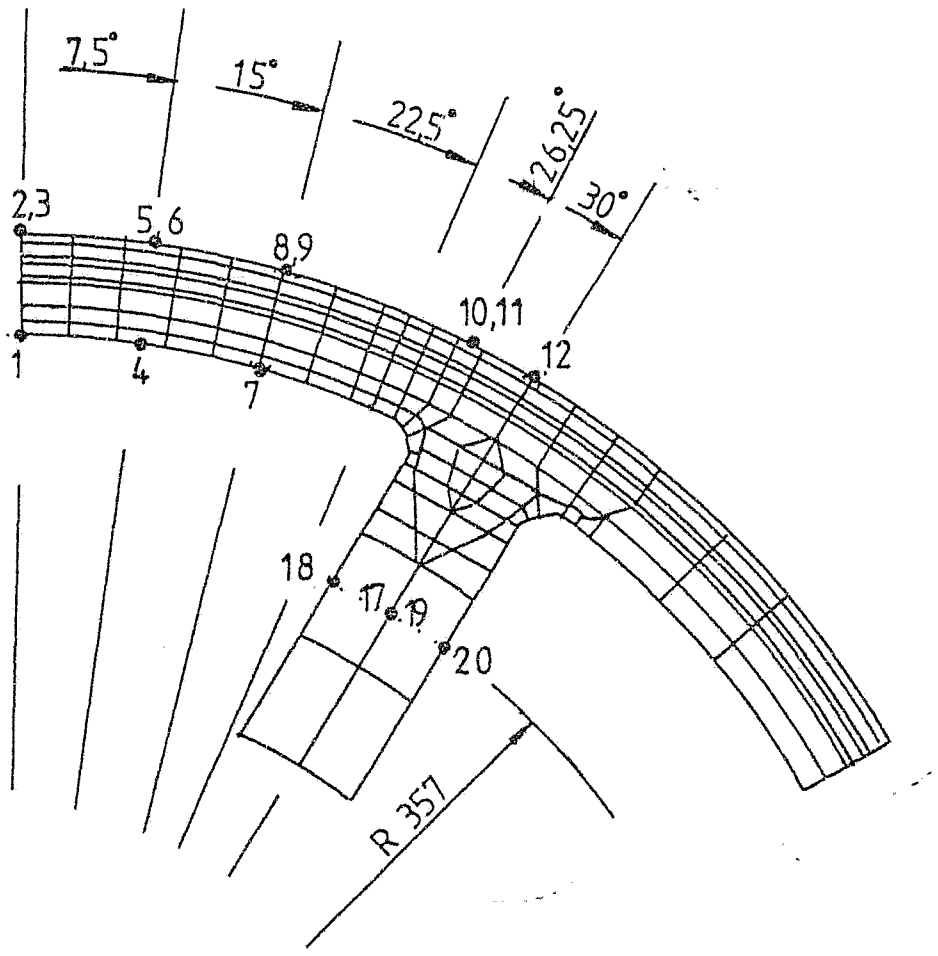

Figure A4.6 - Geometric Location of the Strain Gauges

TABLE A4.4 - ELEMENT/INTEGRATION POINT CORRESPONDING TO THE GAUGE LOCATION

Gauge	Element/Integration Point
1	104-7
2,3	16-9
4	106-4
5,6	16-6
7	109-7/108-1
8,9	11-9/12 - 3
10,11	6-6
12	4-9/5-3
18	134-7
17,19	137-8/134-2
20	137-2

TABLE A4.5a - Associated Plasticity

ROPE TENSION [KN]	ELEMENT/INTEGRATION NUMBER (DEG)							
	104.7 (0)	16.9 (0)	106.4 (7.5)	14.8 (7.5)	109.7 (15)	108.1 (15)	11.9 (15)	12.9 (15)
81.803	718.89	-578.1	551.18	-463.31	14.771	81.751	-120.8	-171.51
123.61	1515	-1178.8	1181.1	-932.98	26.975	180.41	-241.13	-342.24
185.41	2571	-1873.6	1776.4	-1420.1	20.383	220.86	-382.75	-513.94
247.21	4119.1	-2800.2	2589.5	-1993.6	22.734	289.24	-495.8	-692.44
309.02	6399.4	-4137.9	3849.8	-2704.7	-3.0949	319.23	-650.95	-897.32
370.82	8750.8	-6125	4991.3	-3810.5	-60.123	312.18	-892.2	-1095.1
432.62	13899	-8795.9	6798.2	-4917.2	-140.37	284.68	-1046.6	-1328

ROPE TENSION [KN]	ELEMENT/INTEGRATION NUMBER (DEG)						
	6.8 (26.25)	4.9 (30)	5.3 (30)	137.2 (30)	137.8 (30)	134.2 (30)	134.7 (30)
81.803	479.5	300.76	341.95	-23.983	-200.47	-250.56	-378.39
123.61	988.24	604.7	689.15	-47.372	-400.12	-500.27	-755.6
185.41	1834.4	911.75	1061.3	-88.07	-598.52	-746.65	-1127.3
247.21	2553.3	1235.7	1482.3	-79.929	-790.45	-992.79	-1490.3
309.02	3928.9	1576.5	1982.5	-71.348	-992.07	-1255.5	-1870
370.82	5874.8	1925	2536.3	-42.797	-1209.8	-1546.8	-2307.8
432.62	8351.3	2260.3	3187.8	-9.5024	-1452.1	-1873.9	-2704.6

TABLE A4.5b - Non Associated Plasticity

	ELEMENT/INTEGRATION NUMBER (DEG)							
ROPE TENSION [KN]	104.7 (0)	16.9 (0)	108.4 (7.5)	14.6 (7.5)	109.7 (15)	109.1 (15)	11.9 (15)	12.3 (15)
61.803	718.84	-578.1	551.18	-463.31	14.779	81.754	-120.8	-171.52
123.61	1512.5	-1178.9	1117.6	-932.17	28.372	180.41	-241.07	-342.18
185.41	2548.5	-1867.1	1778.2	-1427.8	31.285	231.91	-369.49	-514.17
247.21	4048.9	-2785.8	2598.7	-1995.6	22.528	289.58	-493.42	-690.71
309.02	6308.9	-4131.3	3697	-2707.9	.91098	318.18	-646.6	-884.97
370.82	9518.3	-6089.9	5111.5	-3815.9	-50.401	323.45	-817.6	-1084.8
432.62	13693	-8757.2	6872.2	-4768.6	-128.4	286	-1019	-1300.8

	ELEMENT/INTEGRATION NUMBER (DEG)						
ROPE TENSION [KN]	6.6 (26.25)	4.9 (30)	5.9 (30)	197.2 (90)	197.8 (30)	194.2 (90)	194.7 (30)
61.803	479.52	900.78	941.95	-29.883	-200.47	-250.58	-978.99
123.61	988.98	804.55	889.01	-47.977	-400.14	-500.91	-755.65
185.41	1619.7	912.42	1058.7	-68.6	-596.85	-748.92	-1127.9
247.21	2493.6	1242.2	1490.5	-78.142	-792.35	-995.24	-1492.6
309.02	3795.9	1592.4	1974.9	-70.747	-995.59	-1259.8	-1874
370.82	5552.9	1952.2	2552.4	-43.802	-1215.1	-1551.9	-2281.7
432.62	7810.6	2315.2	3291.5	-3.9499	-1481	-1883	-2709.8

A P P E N D I X 5

ADINA/ADINAT/ADINA-PLOT PROGRAMME EXECUTION

A5.1 PROGRAMME EXECUTION ON THE IBM 370

The procedure involved in the preparation and execution of the ADINA/ADINAT/ADINA-PLOT package is illustrated in the flow chart presented in Fig A5.1 below. The VMS/CMS commands employed in this procedure are presented in Table A5.1. The function of the ENGPAC, FADINA, ADINA 81, ADINAT, ADPLOT, will be discussed in the following section.

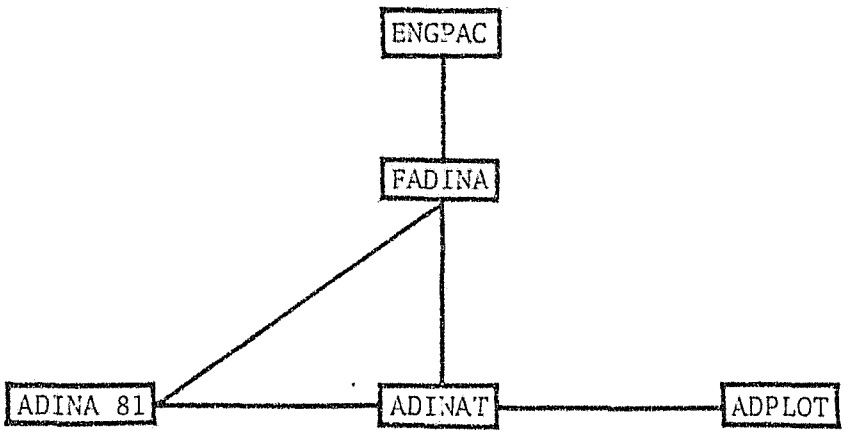

Figure A5.1 - Flow Chart Illustrating ADINA/ADINAT/ADINA-PLOT Execution Procedure

COMMAND	VMS/CMS RESPONSE
DEF STOR 2M I CMS	ENT STORAGE = 2M R = -----: ENT CMS
ENGPAC FADINA 20+	ENT FORMAT WILL ERASE ALL FILES ON DISK 'G(19F)'. DO YOU WISH TO CONTINUE)? (YES/NO). DMS FOR 605R ENTER DISK LABEL DMS FOR 733I FORMATTING DISK G.
ADINA PROGRAM: ADINA 81 FN FT FM* FN FT FM	ENT INPUT FILE? ENT OUTPUT FILE? EXECUTION BEGINS ------
ADINAT PROGRAM: ADINAT FN FT FM FN FT FM	ENT INPUT FILE? OUTPUT FILE? EXECUTION BEGINS -------
ADINA-PLOT PROGRAM: ADPLOT FN FT FM FN FT FM	ENT INPUT FILE? ENT OUTPUT FILE? ENT EXECUTION BEGINS -------

+ Number of temporary storage cylinder specified by the user

* FILE NAME FILE TYPE FILE MODE , eg INPUT DATA A1.

A5.2 BACKUP ROUTINES

The routines ENGPAC, FADINA, ADINA 81, ADINAT, ADPLOT, were implemented by W Leong of the computer science center. The purpose of these routines is summarised briefly below:

A5.2.1 ENGPAC+

This programme links the user to the disk containing the ADINA/ADINAT/ADINA-PLOT program texts, enabling these programs to be accessed for later use.

A5.2.2 FADINA+

This program creates temporary storage space and defines the logical read write units and the formatting options as required by the program for successful execution. These units provide the slow speed storage as required during execution.

A5.2.3 ADINA81/ADINAT/ADPLOT+

These routines load the respective programs for execution. They direct the input and output listing file as specified by the user.

A5.3 DEFINING TEMPORARY STORAGE SPACE ON THE READ/WRITE DISK FOR LARGE LISTING FILES

Analyses resulting in large output listing files require the definition of extra storage space if the user's available permanent storage allocation is not to be exceeded (±4 000 lines). The VMS/CMS commands

---

+The listings of the ENGPACK, FADINA, ADINA81, ADINAT, ADPLOT programs are included at the end of the appendix.

required to define such temporary storage are listed below.

DEF □ T3350 □ 195 □ 5 ENT

FORMAT □ 195 □ D ENT

ACC □ 191 □ C ENT

ACC □ 195 □ A ENT

Copy files from C disk to temporary A disk, ie

COPY □ FN □ FT □ FM □ FN □ FT □ A ENT

eg, Copy SHG DATA C SHG DATA A

After execution is complete and the listing file has been printed and sufficient plots obtained, all updated files must be copied to the C disk before signing off.

A5.4 REMOTE JOB EXECUTION

In cases where execution may take an extended period of time an option enabling remote execution is available allowing the user to return at a later time when execution is complete.

The commands required to utilise this facility are:

#CP SET RUN ON

#CP DISC

On issuing these commands the user has effectively terminated the session on the terminal without affecting program execution. The terminal may then be utilised by another user.

On reconnecting, the following command must be issued:

B

which notifies the computer that he is once again connected as an ordinary user.

```
FILE: ENGPAC    EXEC      Y2

&TRACE ERR
CP LINK ENG 196 19B RR STATS
ACCESS 19B B/A
```

```
FILE: FADINA    EXEC     B2

&TRACE ERR
&CYL = &1
&IF .&CYL ¬= . &GOTO -BR
&TYPE TYPE IN NUMBER OF CYLINDER FOR TEMPORARY DISK
&READ VAR &CYL
-BR &CONTINUE
CP DEFINE T3350 19F &CYL
&LABEL = &CONCAT OF TMP 19F
&STACK YES
&STACK &LABEL
FORMAT 19F G
FI   1 DISK W1 SCRATCH G (RECFM VBS BLOCK 4000  XTENT 790
FI   2 DISK W2 SCRATCH G
FI   3 DISK W3 SCRATCH G
FI   4 DISK W4 SCRATCH G
FI   7 DISK W7 SCRATCH G
FI   8 DISK W8 SCRATCH G
FI   9 DISK W9 SCRATCH G
FI  10 DISK W10 SCRATCH G
FI  11 DISK W11 SCRATCH G
FI  12 DISK W12 SCRATCH G
FI  13 DISK W13 SCRATCH G
FI  14 DISK W14 SCRATCH G
FI  15 DISK W15 SCRATCH G
FI  16 DISK W16 SCRATCH G
FI  17 DISK W17 SCRATCH G
FI  18 DISK W18 SCRATCH G
FI  19 DISK W19 SCRATCH G
FI  22 DISK W22 SCRATCH G
FI  23 DISK W23 SCRATCH G
FI  56 DISK W56 SCRATCH G
FI  59 DISK W59 SCRATCH G
FI  60 DISK PLOT DATA G
FI  61 DISK W61 SCRATCH G
FI  62 DISK W62 SCRATCH G
FI  63 DISK W63 SCRATCH G
```

```
FILE: ADINA81  EXEC     B1

&TRACE OFF
&TYPE     ENTER DATA FILE ID:
&READ VARS &INNAME &INTYPE &INMODE
&TYPE     ENTER OUTPUT FILE ID:
&READ VARS &OUTNAME &OUTTYPE &OUTMODE
GLOBAL TXTLIB CMSLIB FORTXLIB
LOAD ADINA81
FI 5 DISK &INNAME &INTYPE &INMODE
FI 6 DISK &OUTNAME &OUTTYPE &OUTMODE
START
&EXIT
```

```
FILE:  ADPLOT    EXEC     B1

&TRACE ERR
&TYPE     ENTER DATA FILE ID:
&READ VARS &INNAME &INTYPE &INMODE
&TYPE     ENTER OUTPUT FILE ID:
&READ VARS &OUTNAME &OUTTYPE &OUTMODE
-AGAIN &TYPE ENTER "N" OR "W" (N=NARROW PAPER(30CM), W=WIDE PAPER(83CM)):
&READ VARS &PAPER
&IF .&PAPER EQ .N &GOTO -PAPN
&IF .&PAPER EQ .W &GOTO -PAPW
&TYPE ' &PAPER ' IS AN INVALID ARGUMENT.
&GOTO -AGAIN
-PAPN &WIDTH = P
&GOTO -LIN
-PAPW &WIDTH = Q
-LIN CP LINK GRAPHICS 191 199 RR READ
AC 199 H
STACKID
&STACK &INNAME
X @ $ G (PROF @@@
GL TXTLIB
GL TXTLIB CMSLIB FORTXLIB GRAPHICS
LOAD ADPLOT
&RCC = &RC
&IF &RC NE 0 &GOTO -FAIL
FI FT01 001 CLEAR
FI FT05F001 CLEAR
FI FT06F001 CLEAR
FI FT18F001 CLEAR
FI FT19F001 CLEAR
FI FT50F001 CLEAR
FI FT60F001 CLEAR
FI 1 DISK DATA BASE G (RECFM F LRECL 2000 BLOCK 2000 DSORG DA XTENT 790
FI 5 DISK &INNAME &INTYPE &INMODE
FI 6 DISK &OUTNAME &OUTTYPE &OUTMODE
FI 18 DISK @ $ G
FI 19 DISK @ $$ G
FI 50 DISK &INNAME PLOT G (RECFM VS BLKSIZE 368
FI 60 DISK PLOT DATA G (RECFM VBS BLOCK 4000
START
&RCC = &RC
&IF &RC NE 0 &GOTO -FAIL
CP SP PU CALPLOT NOH NOC CL G CO 1 D &WIDTH
DISK DUMP &INNAME PLOT G
CP SP PU OFF CL A D OFF
-FAIL FI * CLEAR
GL TXTLIB
REL H (DET
&EXIT &RCC
```

```
FILE: ADPLOT   EXEC     B1


&TRACE ERR
&TYPE     ENTER DATA FILE ID:
&READ VARS &INNAME &INTYPE &INMODE
&TYPE     ENTER OUTPUT FILE ID:
&READ VARS &OUTNAME &OUTTYPE &OUTMODE
-AGAIN &TYPE ENTER "N" OR "W" (N=NARROW PAPER(30CM), W=WIDE PAPER(83CM)):
&READ VARS &PAPER
&IF .&PAPER EQ .N &GOTO -PAPN
&IF .&PAPER EQ .W &GOTO -PAPW
&TYPE ' &PAPER ' IS AN INVALID ARGUMENT.
&GOTO -AGAIN
-PAPN &WIDTH = P
&GOTO -LIN
-PAPW &WIDTH = Q
-LIN CP LINK GRAPHICS 191 199 RR READ
AC 199 H
STACKID
&STACK &INNAME
X @ $ G (PROP @@@
GL TXTLIB
GL TXTLIB CMSLIB FORTXLIB GRAPHICS
LOAD ADPLOT
&RCC = &RC
&IF &RC NE 0 &GOTO -FAIL
FI FT01F001 CLEAR
FI FT05F001 CLEAR
FI FT06F001 CLEAR
FI FT18F001 CLEAR
FI FT19F001 CLEAR
FI FT50F001 CLEAR
FI FT60F001 CLEAR
FI 1 DISK DATA BASE G (RECFM F LRECL 2000 BLOCK 2000 DSORG DA XTENT 790
FI 5 DISK &INNAME &INTYPE &INMODE
FI 6 DISK &OUTNAME &OUTTYPE &OUTMODE
FI 18 DISK @ $ G
FI 19 DISK @ $$ G
FI 50 DISK &INNAME PLOT G (RECFM VS BLKSIZE 368
FI 60 DISK PLOT DATA G (RECFM VBS BLOCK 4000
START
&RCC = &RC
&IF &RC NE 0 &GOTO -FAIL
CP SP PU CALPLOT NOH NOC CL G CO 1 D &WIDTH
DISK DUMP &INNAME PLOT G
CP SP PU OFF CL A D OFF
-FAIL FI * CLEAR
GL TXTLIB
REL H (DET
&EXIT &RCC
```

APPENDIX 6

UNDERGRADUATE PROJECTS (1982-83) RELEVANT TO THE DEVELOPMENT OF THE FINITE ELEMENT METHOD AT THE UNIVERSITY OF THE WITWATERSRAND

A6.1 REPLACING THE HUMAN KNEE JOINT: (G HACK, N LANE - BSc Design Report, Sept 1982. Supervisor, Dr H D Chandler)

This project consists of an overall view of knee prosthesis design with special reference to the van Reenen Knee. In order to assess the van Reenen knee prosthesis with regard to its tibial configuration a comparative study involving a finite element simulation of four different configurations (including that of the van Reenen knee) was undertaken.

The configurations examined were:

- The natural tibia.
- An all polyethylene tibial component (as used in the van Reenen knee).
- A polyethylene bearing surface supported by a metal tray.
- As above but with a pin attached to the lower surface of the metal tray.

The tibia was modelled with plain strain two-dimensional elements. The properties of the compact cancellous bone and the polyethylene/steel tray were accounted for by defining four material property sets applied to the relevant areas of the mesh indicated in Fig 6.1.

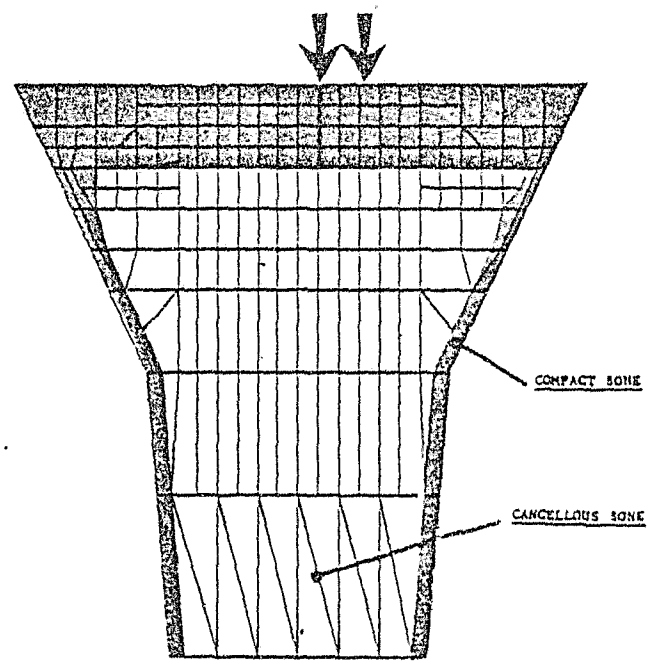

(a)

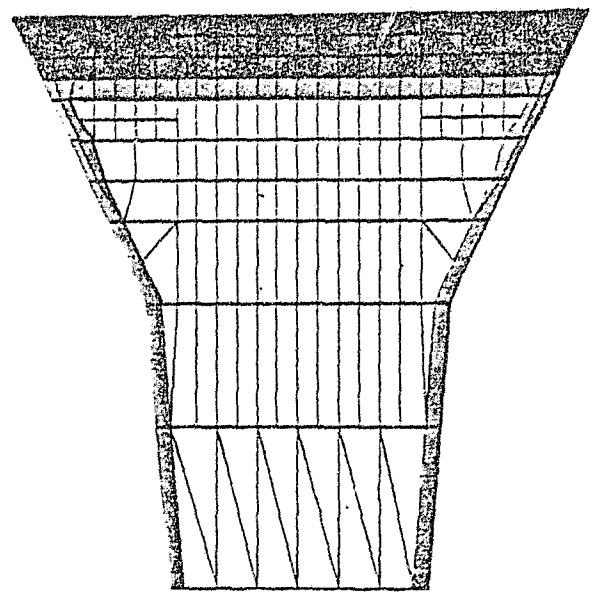

(b)

POLYETHYLENE STEEL TRAY

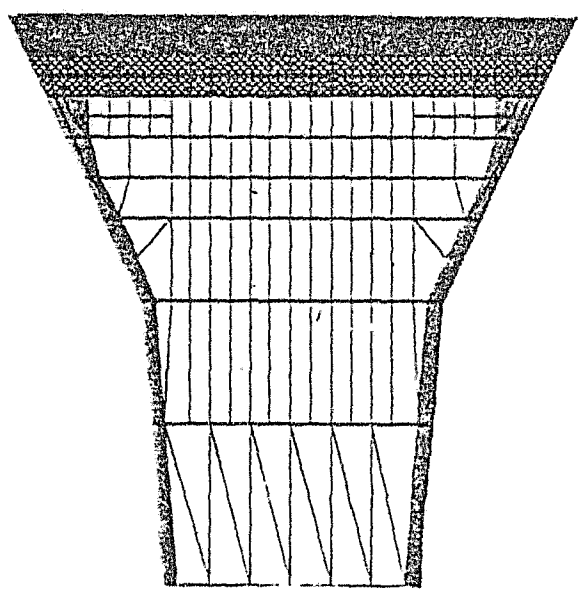

(c)

Steel tray

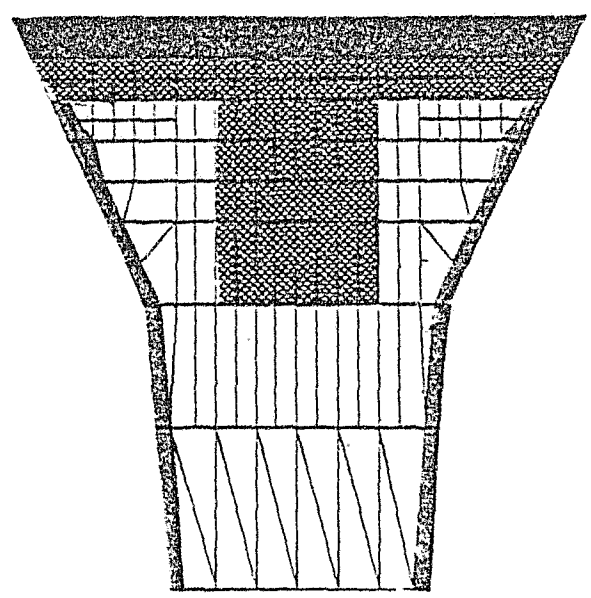

(d)

Steel tray with pin

(a) Tibia modelled with compact and cancellous bone only
(b) Polyethylene tibial component
(c) Pin attached to the lower surface of the metal tray

Figure 6.1 - Analysis of a Knee Joint Prosthesis

The results of this study indicate that improved performance of the van Reenen knee can be achieved by utilising a polyethelene bearing surface supported by a steel tray. This observation is drawn from a careful examination of the stresses induced in the above configuration which closely resembles those predicted in the analysis of the natural tibia. The writer acted as advisor in the use of ADINA.

A6.2 PREPROCESSOR PROGRAM: (S PAVLOVIC - BSc Design Report, Sept 1982. Supervisors: Prof C Dimitriou & Mr C Constancon

This project involved the preparation of a preprocessor programme capable of interactively structuring an input data file in the format required by the ADINA programme. At present the programme is partially complete, facilitating data preparation up to the beginning of element data input. Further work is required to complete this facility and to extend it to include data preparation for the ADINAT programme.

A6.3 FINITE ELEMENT ANALYSIS OF A THIN SQUARE PLATE: (A BIZOS - BSc Minilab Report, July 1983. Supervisors: Prof C Dimitriou & Mr C Constancon

This project involved utilising shell/plate shell elements to approximate the central deflection of a thin square plate subjected to a uniformly distributed pressure load normal to its surface. Small deflections were considered and the material was assumed isotropic; ie a linear elastic analysis was performed.

The performance of the two element types was assessed with regard to

(i) Shell elements:
- numerical integration order
- four, eight, nine, sixteen noded elements

- mesh refinement

(ii) Plate Shell elements:
- mesh refinement[1]

The results obtained were compared with a theoretical solution for the purpose of assessing the effect of the constraints listed above on the solution accuracy. In addition a geometrically nonlinear (total langrangian) analysis of the plate provided confirmation that the deflections imposed in the analyses were within the linear region.

The main purpose of this study was to introduce the pertinent aspects of the finite element method through the preparation of input data files, execution of the analyses and the interpretation of the results. This approach illustrated in a practical manner the importance of mesh refinement, element order, numerical integration order and the correct imposition of boundary conditions.

The results of the study confirmed that

- underintegration generally results in higher accuracy
- convergence to the true solution occurs with increasing mesh refinement and higher order elements
- the choice of mesh has to draw on finite element theory and past experience.

A preliminary assessment of the accuracy achieved in approximating the natural frequencies of plates by employing the two types of elements discussed indicated that the solutions were an order of magnitude different for similar meshes. This is not documented in

---

1. Plate shell elements are 3-noded elements which for a linear elastic analysis have a fixed numerical integration order of 2 x 2.

the report since a fuller investigation is required before conclusive statements can be made. This is likely to be the topic of future study.

A P P E N D I X 7

ADINA-PLOT, PROGRAM DESCRIPTION AND INSTALLATION

A7.1 PROGRAM DESCRIPTION

The ADINA-PLOT program constitutes a post-processing facility (ie after employing the ADINA package) enabling rapid interpretation of the results obtained from a finite element simulation. A flow chart illustrating its mode of operation in conjunction with the ADINA program is shown below in Fig A7.1.

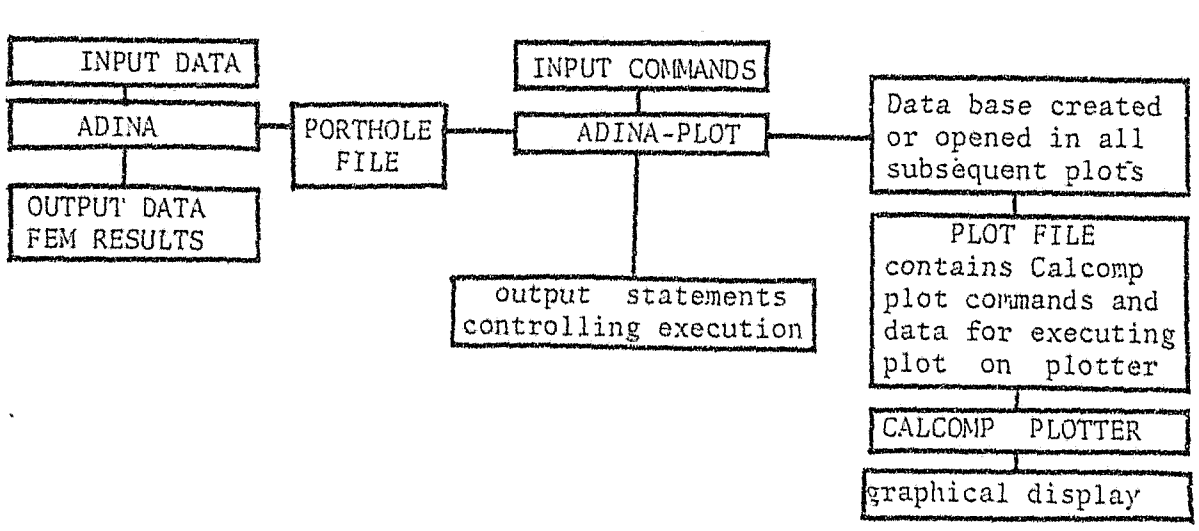

Figure A7.1 - Flow Chart Illustrating the Interaction between the ADINA/ADINA -PLOT PROGRAMS

A brief outline of the mode of operation is presented but a more detailed explanation can be found in the ADINA-PLOT user's manual [9]. The input and output data of a finite element simulation may be channelled by ADINA to a file called the porthole file. ADINA-PLOT reads this generated file in order to load a specifically designed data base which stores the data on a random access file for easy retrieval. Once the data base is loaded with data from an ADINA run it can be

accessed by ADINA-PLOT any number of times, hence the porthole file becomes redundant.

The input command file contains a command language which specifies the format and type of plot required. Default options are available which ensure that a satisfactory plot will be obtained with the minimum amount of input data.

Two types of error recovery are available to decide on a solution strategy when an error is encountered during execution. Either the execution can be terminated or it can be continued at the next command in the input file.

On successful execution, a plot file containing calcomp plotting commands is submitted directly to the calcomp plotter for a graphical output. Simultaneously, the output from the ADINA-PLOT can be directed to three print files: ECHO; LOG and LIST. The ECHO file contains an echo printing of the commands and parameters as they had been defined in the input file. The LOG file contains relevant diagnostic messages generated during the execution, whilst the LIST file contains selective data listings which can be requested by the user.

A7.2 INSTALLATION

ADINA-PLOT was installed on the IBM 370 in March 1983. The installation involved writing a backup routine ADPLOT which, prior to execution, defined the logical read write units used in the source as well as the location of the input command and output listing files. Ultimately this routine links the ADINA-PLOT program to the calcomp plotting library and directs the plot file created during execution to the calcomp plotter for a graphical output.

The test analysis supplied with the ADINA/ADINA-PLOT source[1] was

---

1. Dynamic analysis of an eight storey building

executed in order to verify that the program was operating correctly. Satisfactory execution was not achieved since the ADINA-PLOT program did not generate the required data base. Further attempts to achieve a satisfactory execution were unsuccessful and outside help was sought [26].

Errors were apparent in both the backup routine FADINA[2] and the source. It was evident that the logical write statement defining the format of the data base file was inconsistent for a random access file. In the original FADINA routine the following statement was used with no formatting options, ie

```
F I 1 DISK DATA G
```

For a random access file this should be defined as

```
F I  1 DISK DATA G (RECFM VBS BLOCK 4000)
```

By defining this logical write statement, the porthole file was created successfully. However in early test program runs it became apparent that the first statement in the input command file was not correctly executed by the program causing premature termination. This was overcome by placing a redundant statement at the beginning of the file and selecting the error recovery option which, upon the discovery of an error, proceeded to the next statement in the input file. Thus for future w :k, until this problem is rectified, the following statements should always be specified at the beginning of any input command file

```
FILE
CONTROL B = 0
.
.
.
END
```

---

2. A listing of the FADINA routine is presented in Appendix 5 together with a brief description.

Author Constancon C P
Name of thesis A study of the finite element method, with reference to the Adina finite element package 1983

PUBLISHER:
University of the Witwatersrand, Johannesburg
©2013

LEGAL NOTICES:

Copyright Notice: All materials on the University of the Witwatersrand, Johannesburg Library website are protected by South African copyright law and may not be distributed, transmitted, displayed, or otherwise published in any format, without the prior written permission of the copyright owner.

Disclaimer and Terms of Use: Provided that you maintain all copyright and other notices contained therein, you may download material (one machine readable copy and one print copy per page) for your personal and/or educational non-commercial use only.

The University of the Witwatersrand, Johannesburg, is not responsible for any errors or omissions and excludes any and all liability for any errors in or omissions from the information on the Library website.